

**Strategies for Peptide Backbone Modification in Protein Beta-Sheets**

by

George Andrew Lengyel

B.S. Chemistry, University of Pittsburgh, 2004

M.A.T. Secondary Science, University of Pittsburgh, 2005

M.S. Chemistry, University of Pittsburgh, 2011

Submitted to the Graduate Faculty of  
the Kenneth P. Dietrich School of Arts and Sciences in partial fulfillment  
of the requirements for the degree of  
Doctor of Philosophy

University of Pittsburgh

2014

UNIVERSITY OF PITTSBURGH  
DIETRICH SCHOOL OF ARTS AND SCIENCES

This dissertation was presented

by

George Lengyel

It was defended on

April 16, 2014

and approved by

Dr. Dennis Curran, Professor, Department of Chemistry

Dr. Steve Weber, Professor, Department of Chemistry

Dr. Ron Wetzel, Professor, Department of Structural Biology

Committee Chair: Dr. W. Seth Horne, Assistant Professor, Department of Chemistry

**STRATEGIES FOR PEPTIDE BACKBONE MODIFICATION IN PROTEIN BETA-SHEETS**

George Lengyel, PhD

University of Pittsburgh, 2014

Copyright © by George Lengyel

2014

## Strategies for Peptide Backbone Modification in Protein Beta-Sheets

George Lengyel, PhD

University of Pittsburgh, 2014

Design of foldamers, unnatural backbone oligomers that mimic the structure of proteins, is an important field of research as these species can bind to natural proteins but are resistant to proteolytic degradation. We have focused on developing strategies for the design of unnatural oligomers that adopt  $\beta$ -sheet secondary structures like those commonly found in protein tertiary folds. Our approach is to modify natural peptide sequences that encode for  $\beta$ -sheet folds with various unnatural amino acid building blocks to produce hybrid-backbone peptides that fold like the parent sequence in aqueous solution.

Through evaluation of  $\beta$ -hairpin model systems using multidimensional NMR, we have discovered several design strategies that may be applicable to mimicry of sheets found in larger protein tertiary structures and have ranked unnatural monomer types in order of increasing sheet propensity:  $\beta$ -amino acid < *N*-methyl- $\alpha$ -amino acid  $\leq$  vinylogous  $\gamma^4$ -amino acid < cyclic  $\gamma$ -amino acid. These substitutions require a 2:2 or 2:1  $\alpha$ - to  $\beta$ -residue substitution or 1:1  $\alpha$ - to  $\gamma$ - or  $\alpha$ - to *N*-methyl- $\alpha$ -residue substitution to maintain native-like folding behavior.

We applied these unnatural backbone substitutions to protein GB1, a 56 residue protein with a complex tertiary fold consisting of a four stranded  $\beta$ -sheet packed against an  $\alpha$ -helix. Using thermal denaturation melts and circular dichroism spectroscopy, we have determined that the trend of sheet propensity seen in the hairpin peptide is similar in a tertiary fold with the caveat that the position of the unnatural residues matters greatly. Substitution strategies that lengthen the strands of the  $\beta$ -sheet have varying effects on the stability of the folded structure depending on their placement; substitutions near the center of the strands are significantly more destabilizing than those placed near the termini. Use of *N*-methylated  $\alpha$ -amino acids is not limited in this fashion, but their positioning must be chosen so as to avoid disruption of inter-strand hydrogen bonding.

Overall, we have determined that several types of unnatural amino acids can be used to promote sheet formation with limited destabilization; these amino acids could potentially be used in other proteins with tertiary folded structures.

## TABLE OF CONTENTS

<b>1.0</b>	<b>INTRODUCTION TO BETA-SHEET FOLDAMERS.....</b>	<b>1</b>
<b>1.1</b>	<b>PEPTIDE THERAPEUTICS .....</b>	<b>1</b>
<b>1.2</b>	<b>FOLDAMERS AND SEQUENCE-BASED DESIGN .....</b>	<b>3</b>
<b>1.3</b>	<b>PROTEIN BETA-SHEETS .....</b>	<b>5</b>
<b>1.3.1</b>	<b>Beta-Hairpins .....</b>	<b>5</b>
<b>1.3.2</b>	<b>Amino Acid Identity and its Impact on Beta-Hairpin Formation .....</b>	<b>6</b>
<b>1.4</b>	<b>BETA-SHEET FOLDAMERS .....</b>	<b>8</b>
<b>1.4.1</b>	<b>Beta-Sheet Foldamers Derived from Cyclic Beta-Amino Acids .....</b>	<b>8</b>
<b>1.4.2</b>	<b>Beta-Sheet Foldamers Derived from Pyrrolinone-Based Scaffolds.....</b>	<b>9</b>
<b>1.4.3</b>	<b>Beta-Sheet Foldamers Templated by Methoxybenzamide .....</b>	<b>10</b>
<b>1.4.4</b>	<b>Beta-Sheet Foldamers Containing Alpha-Amino Acid Homologs.....</b>	<b>11</b>
<b>1.4.4.1</b>	<b>Beta-Sheet Foldamers Containing Beta-Amino Acids .....</b>	<b>11</b>
<b>1.4.4.2</b>	<b>Beta-Sheet Foldamers Containing Gamma-Amino Acids .....</b>	<b>12</b>
<b>1.5</b>	<b>SOLVENT CHOICE AND ITS EFFECT ON BETA-SHEET FORMATION.....</b>	<b>13</b>
<b>1.6</b>	<b>GOALS .....</b>	<b>14</b>
<b>1.6.1</b>	<b>Model System Selection .....</b>	<b>15</b>
<b>1.6.2</b>	<b>Outline.....</b>	<b>17</b>
<b>1.6.2.1</b>	<b>Analysis of <math>\alpha</math>- to <math>\beta</math>-Residue Substitution.....</b>	<b>17</b>
<b>1.6.2.2</b>	<b>Analysis of <math>\alpha</math>- to <math>\gamma</math>-Substitution and <i>N</i>-Methylation .....</b>	<b>18</b>
<b>1.6.2.3</b>	<b>Unnatural Residue Substitutions Applied to Protein GB 1 .....</b>	<b>18</b>

<b>2.0 IMPACT OF BETA-AMINO ACID INCORPORATION ON FOLDING OF BETA-HAIRPINS IN AQUEOUS SOLUTION.....</b>	<b>19</b>
<b>2.1 1:1 ALPHA- TO BETA-RESIDUE SUBSTITUTION.....</b>	<b>20</b>
2.1.1 Hairpin Peptide Design.....	20
2.1.2 Qualitative NMR Analysis.....	22
2.1.3 Structural Analysis by NMR.....	24
2.1.4 Analysis of 2:1 $\alpha$ - to $\beta$ -Residue Substitution Strategies .....	30
<b>2.2 2:1 OR 2:2 ALPHA- TO BETA-RESIDUE SUBSTITUTION.....</b>	<b>34</b>
2.2.1 Design of Alpha- to Beta-Residue Substitution Strategies .....	34
2.2.2 Selection of Hairpin Model System .....	35
2.2.3 Application of Beta-Residue Substitution Strategies to Model Hairpin System .	38
2.2.4 Structural Impact of 2:1 and 2:2 Alpha- to Beta-Residue Substitution.....	39
2.2.5 Thermodynamic Impact of 2:1 and 2:2 Alpha- to Beta-Residue Substitution ....	43
2.2.6 Conclusions .....	44
<b>2.3 EXPERIMENTAL.....</b>	<b>46</b>
2.3.1 Monomer Synthesis.....	46
2.3.1.1 General Information.....	46
2.3.1.2 Synthesis of Fmoc- $\beta^2$ -Monomers.....	47
2.3.1.3 Synthesis of <i>anti</i> Fmoc- $\beta^{2,3}$ -Monomers.....	53
2.3.1.4 Synthesis of <i>syn</i> Fmoc- $\beta^{2,3}$ -Monomers .....	57
2.3.1.5 Synthesis of <i>cis</i> Fmoc-ACPC Monomers .....	68
2.3.1.6 Synthesis of <i>cis</i> Fmoc-ACHC Monomers .....	71
2.3.2 Peptide Synthesis.....	74
Table 3. MALDI-TOF data for peptides 1a-17a and 1b-17b.....	76
2.3.3 NMR Sample Preparation and Data Collection .....	78
2.3.4 NMR Data Analysis and Structure Determination.....	79

2.3.5	Calculation of Folding Equilibria by NMR .....	80
3.0	GAMMA RESIDUES AND <i>N</i> -METHYL-ALPHA-RESIDUES IN HETEROGENEOUS BACKBONE HAIRPINS .....	82
3.1	1:1 ALPHA- TO GAMMA-RESIDUE SUBSTITUTION.....	83
3.1.1	Design of Alpha- to Gamma-Residue Substitution Strategies .....	83
3.1.2	Thermodynamic Analysis of 1:1 Alpha- to Gamma-Residue Substitution.....	84
3.1.3	Structural Analysis of 1:1 Alpha- to Gamma-Residue Substitution .....	86
3.1.4	Conclusions .....	91
3.2	<i>N</i> -METHYLATION OF SELECTED ALPHA-RESIDUES .....	92
3.2.1	<i>N</i> -Methylation Strategies Applied to a Model Hairpin Peptide.....	92
3.2.2	NMR Analysis of <i>N</i> -Methylated Hairpin Peptides.....	93
3.2.3	Conclusions .....	98
3.3	EXPERIMENTAL.....	99
3.3.1	Monomer Synthesis.....	99
3.3.1.1	General Information.....	99
3.3.1.2	Synthesis of Fmoc- <i>m</i> ABA-OH.....	100
3.3.1.3	Synthesis of Fmoc-Acc-OH .....	101
3.3.1.4	Synthesis of Fmoc- $\gamma^4$ -Ala-OH.....	102
3.3.2	Peptide Synthesis.....	103
3.3.3	NMR Sample Preparation and Data Collection .....	104
3.3.4	NMR Data Analysis and Structure Determination.....	105
3.3.5	Calculation of Folding Equilibria by NMR .....	105
4.0	UNNATURAL SHEET MODIFICATION APPLIED TO PROTEIN GB1 .....	106
4.1	UNNATURAL RESIDUE SUBSTITUTIONS IN PROTEIN GB1.....	107
4.1.1	<i>N</i> -Methyl Residue Substitution in Protein GB1 .....	108
4.1.2	Beta-Residue Substitution in Protein GB1 .....	112

4.1.3	Gamma-Residue Substitution in Protein GB1 .....	115
4.2	CONCLUSIONS.....	124
4.3	EXPERIMENTAL.....	126
4.3.1	Monomer Synthesis.....	126
4.3.1.1	General Information.....	126
4.3.1.2	Synthesis of Fmoc- $\beta^2$ -Monomers.....	126
4.3.1.3	Synthesis of Fmoc-Acc-OH.....	126
4.3.1.4	Synthesis of Vinylogous Fmoc- $\gamma^4$ -Monomers .....	127
4.3.2	Peptide Synthesis.....	131
4.3.3	CD Measurements.....	132
APPENDIX A	.....	133
APPENDIX B	.....	143
APPENDIX C	.....	181
APPENDIX D	.....	197
BIBLIOGRAPHY	.....	264

## LIST OF TABLES

Table 1. Folded populations of model peptides 19a-22a. ....	37
Table 2. Folded populations and $\Delta G_{\text{fold}}$ for peptide 22a and $\alpha/\beta$ -Hybrid Peptides 23a-26a.....	44
Table 3. MALDI-TOF data for peptides 1a-17a and 1b-17b. ....	76
Table 4. MALDI-TOF data for peptides 18-26 and their derivatives. ....	77
Table 5. Folded populations and $\Delta G_{\text{fold}}$ for parent peptide 22a and $\alpha/\gamma$ -hybrid peptides 73-75. ....	85
Table 6. Folded populations and $\Delta G_{\text{fold}}$ for peptide 22a and <i>N</i> -methyl peptides 77-80. ....	98
Table 7. MALDI-TOF masses of peptides 73-80. ....	104
Table 8. Normalized thermodynamic impacts of examined unnatural residue substitution strategies. ....	107
Table 9. Folding thermodynamics of proteins 81 and 82.....	112
Table 10. Folding thermodynamics for proteins 81, 85, and 86. ....	118
Table 11. Folding thermodynamics for proteins 81, 86, and 87. ....	120
Table 12. Folding thermodynamics for proteins 81, 86, and 88. ....	123
Table 13. Thermodynamic impacts of unnatural residue substitutions in $\beta$ -sheets. ....	125
Table 14. MALDI-TOF data for proteins 81-88. ....	132
Table 15. Backbone $^1\text{H}$ chemical shift assignments (in ppm) for oligomers 1a-17a and 1b-17b. ....	134
Table 16. Backbone chemical shift data for peptide 18. ....	135
Table 17. Backbone chemical shift data for peptide 19 its derivatives.....	135
Table 18. Backbone chemical shift data for peptide 20 its derivatives.....	136
Table 19. Backbone chemical shift data for peptide 22 its derivatives.....	136

Table 20. Backbone chemical shift data for peptide 23 its derivatives.....	137
Table 21. Backbone chemical shift data for peptide 24 its derivatives.....	137
Table 22. Backbone chemical shift data for peptide 25 its derivatives.....	138
Table 23. Backbone chemical shift data for peptide 26 its derivatives.....	138
Table 24. Backbone chemical shift data for peptide 73.....	139
Table 25. Backbone chemical shift data for peptide 74.....	139
Table 26. Backbone chemical shift data for peptide 75.....	140
Table 27. Backbone chemical shift data for peptide 76.....	140
Table 28. Backbone chemical shift data for peptide 77.....	141
Table 29. Backbone chemical shift data for peptide 78.....	141
Table 30. Backbone chemical shift data for peptide 79.....	142
Table 31. Backbone chemical shift data for peptide 80.....	142
Table 32. NOE distance restraints for peptide 1a.....	144
Table 33. NOE distance restraints for peptide 2a.....	147
Table 34. NOE distance restraints for peptide 8a.....	150
Table 35. NOE distance restraints for peptide 9a.....	154
Table 36. NOE Distance restraints for peptide 22a.....	158
Table 37. NOE Distance restraints for peptide 22b.....	161
Table 38. NOE Distance restraints for peptide 23b.....	164
Table 39. NOE Distance restraints for peptide 24b.....	167
Table 40. NOE Distance Restraints for Peptide 73.....	169
Table 41. NOE Distance Restraints for Peptide 74.....	174
Table 42. NOE Distance Restraints for Peptide 76.....	178

## LIST OF FIGURES

Figure 1. Cartoon of the HIV-1 protease dimer from PDB: 3HVP. ....	2
Figure 2. Cartoon of the six-helix bundle formed by gp41 during HIV infection from PDB: 1AIK. ....	3
Figure 3. $\beta$ -Hairpin structure with hydrogen bond contacts shown in red. ....	6
Figure 4. Hairpin structure of the C-terminal fragment of protein GB1. ....	7
Figure 5. An $\alpha$ -amino acid (yellow) and cyclic $\beta$ -amino acids <i>cis</i> -ACBC, <i>cis</i> -ACPC, and <i>trans</i> -ACPC (blue). ....	8
Figure 6. Tetramer conversion to a pyrrolinone-based scaffold. ....	9
Figure 7. Sheet formation templated by an oligourea scaffold. ....	10
Figure 8. Sheet-promoting backbones containing 5-amino-2-methoxybenzamide. ....	10
Figure 9. An $\alpha$ -amino acid (yellow) and several $\beta$ -amino acids (blue). ....	11
Figure 10. An $\alpha$ -amino acid (yellow) and several $\gamma$ -amino acids (green). ....	12
Figure 11. Cartoon structure and sequence of protein GB1. ....	15
Figure 12. Cartoon structure of protein GB1 with core packing residues displayed in grey. ....	16
Figure 13. Sequence and structure of the C-terminal fragment of protein GB1. ....	17
Figure 14. Sequence and NMR solution structure of hairpin peptide 1a. ....	20
Figure 15. Sequences of peptides 1a-17a and 1b-17b. ....	21
Figure 16. Glycine separation values for hybrid $\alpha/\beta$ -peptides 1a-17a. ....	23
Figure 17. Chemical shift deviation between unfolded and folded peptide pairs 1-17. ....	24
Figure 18. Cross-strand NOE's of peptides 1a, 2a, 8a, and 9a. ....	25
Figure 19. Ensembles of 20 lowest energy conformations of peptides 1a, 2a, 8a, and 9a. ....	27

Figure 20. Average structures of peptides 1a, 2a, 8a, and 9a.....	27
Figure 21. NMR solution structures of $\alpha$ -peptide 1a and $\alpha/\beta$ -hybrid peptides 2a, 8a, and 9a.....	29
Figure 22. Overlays of NMR solution structures of $\alpha$ -peptide 1a (white) with $\alpha/\beta$ -hybrid peptides 2a, 8a, and 9a (yellow). .....	29
Figure 23. Extended conformations of acyclic $\beta$ -residues and their resulting Newman projections.....	30
Figure 24. Bent conformations of acyclic $\beta$ -residues and their resulting Newman projections. ....	31
Figure 25. Two views of an $\alpha$ -residue, <i>trans</i> -ACPC, and <i>trans</i> -ACHC. ....	33
Figure 26. Front view of an $\alpha$ -residue, <i>cis</i> -ACPC, and <i>cis</i> -ACHC. ....	33
Figure 27. Possible $\alpha$ - to $\beta$ -residue substitution strategies.....	35
Figure 28. Sequence of GB1 C-terminal fragment, peptide 18.....	36
Figure 29. Model peptides 19a-22a and their derivatives (b-d). ....	36
Figure 30. Peptides 22a-26a and their derivatives (b-d). ....	39
Figure 31. Cross-strand NOE's displayed by peptides 22b-24b. ....	40
Figure 32. Glycine separation values of peptides 22b-26b. ....	41
Figure 33. NMR solution structures of peptides 22b-24b with hydrophobic side chains depicted as spheres. ....	42
Figure 34. Amide deletion experience with 2:1 $\alpha$ - to $\beta$ -residue substitution. ....	45
Figure 35. 1:1 $\alpha$ - to $\gamma$ -residue substitution resulting in backbone expansion.....	83
Figure 36. Backbone-constrained $\gamma$ -residues. ....	83
Figure 37. Model hairpin sequence 22a and $\alpha/\gamma$ -hybrid peptide sequences 73-75. ....	85
Figure 38. Sequence of cyclized $\alpha/\gamma$ -hybrid peptide 76.....	86
Figure 39. Cross-strand NOE's displayed by peptides 73, 74, and 76.....	87
Figure 40. NMR solution structures of $\alpha/\gamma$ -hybrid peptides 73, 74, and 76.....	88
Figure 41. Close-up view of the cyclic $\gamma$ -residues from the NMR solution structures of peptides 73 and 74. ....	90

Figure 42. Overlays of the NMR solution structures of peptides 73, 74, and 76 (yellow) with parent peptide 22a (white). .....	90
Figure 43. An $\alpha$ -residue and cyclic $\gamma$ -residues <i>m</i> ABA and Acc. ....	91
Figure 44. Sequences of model hairpin peptide 22a and <i>N</i> -methylated peptides 77-80. ....	93
Figure 45. Populations of <i>cis</i> and <i>trans</i> conformations of <i>N</i> -methylated peptides 77-80. ....	94
Figure 46. Close-up views of TOCSY spectra of peptide 80. ....	94
Figure 47. Predicted NOE signals with <i>trans</i> and <i>cis</i> <i>N</i> -Me amide configurations. ....	95
Figure 48. Comparison of side chain steric clash (red) seen in a <i>trans</i> vs <i>cis</i> <i>N</i> -Me amide conformation. ....	96
Figure 49. <i>trans</i> and <i>cis</i> conformers of peptide 80. ....	96
Figure 50. Folded populations of peptides 77-80. ....	97
Figure 51. X-ray crystal structure and sequence of protein GB1. ....	108
Figure 52. Sequences of parent protein 81 and <i>N</i> -methylated protein 82. ....	109
Figure 53. Model of GB1 variant 82 with positions of <i>N</i> -methyl residues highlighted pink. ....	109
Figure 54. CD scans of proteins 81 and 82. ....	110
Figure 55. Thermal denaturation melts of proteins 81 and 82. ....	111
Figure 56. Sequences parent protein 81 and $\alpha/\beta$ -hybrids proteins 83 and 84. ....	113
Figure 57. CD scans and melts of proteins 81, 83, and 84. ....	114
Figure 58. Sequences of parent protein 81 and $\alpha/\gamma$ -hybrid proteins 85 and 86. ....	115
Figure 59. CD scans and melts for proteins 81, 85, and 86. ....	116
Figure 60. CD scans of model hairpin peptide 22a and $\alpha/\gamma$ -hybrid peptides 74 and 75. ....	117
Figure 61. Side chain interactions of Acc-substituted positions (green) in protein 86. ....	118
Figure 62. Sequences of wild-type protein 81 and side chain mutant 87. ....	119
Figure 63. CD scans and melts of proteins 81, 86, and 87. ....	120
Figure 64. Crystal structure of GB1 highlighting helix packing residues (white) and Acc substitution sites (green). ....	121

Figure 65. Crystal structure of GB1 highlighting helix packing residues (white) and new Acc substitution sites (green).....	122
Figure 66. Sequences of parent protein 81 and Acc variants 86 and 88. ....	122
Figure 67. CD scans and melts of proteins 81, 86, and 88.....	123

## LIST OF SCHEMES

Scheme 2.1. Synthesis of Fmoc- $\beta^2$ -monomers. ....	47
Scheme 2.2. Synthesis of <i>anti</i> Fmoc- $\beta^{2,3}$ -monomers. ....	53
Scheme 2.3. Synthesis of <i>syn</i> Fmoc- $\beta^{2,3}$ -monomers. ....	57
Scheme 2.4. Synthesis of <i>cis</i> Fmoc-ACPC monomers. ....	68
Scheme 2.5. Synthesis of <i>cis</i> Fmoc-ACHC monomers.....	71
Scheme 3.1. Synthesis of Fmoc- <i>m</i> ABA-OH (81).....	100
Scheme 3.2. Synthesis of Fmoc-Acc-OH (83).....	101
Scheme 3.3. Synthesis of Fmoc- $\gamma^4$ -Ala-OH (86).....	102
Scheme 4.1. Synthesis of vinylogous Fmoc- $\gamma^4$ -monomers.....	127

## LIST OF ABBREVIATIONS

CNS	Crystallography & NMR System
COSY	Correlation spectroscopy
DIEA	<i>N,N</i> -diisopropylethylamine
DMF	Dimethylformamide
DMSO	Dimethylsulfoxide
DSS	4,4-dimethyl-4-silapentane-1-sulfonic acid
Fmoc-OSu	9-fluorenylmethyl <i>N</i> -succinimidyl carbonate
FPLC	Fast protein liquid chromatography
HPLC	High performance liquid chromatography
HRMS	High-resolution mass spectrometry
MALDI-TOF	Matrix assisted laser desorption ionization – time of flight
MD	Molecular dynamics
MS	Mass spectrometry
NOE	Nuclear Overhauser effect
NOESY	Nuclear Overhauser effect spectroscopy
NMR	Nuclear magnetic resonance
RMSD	Root-mean-square-deviation
TEM	Transmission electron microscopy
TOCSY	Total correlation spectroscopy
THF	Tetrahydrofuran

TFA

Trifluoroacetic acid

## ACKNOWLEDGEMENTS

There are many people who I would like to thank, for their help during the past five years has been instrumental in my success. Without a doubt, I would not have survived research without my advisor, Seth. I came into grad school knowing that my research wouldn't mean anything to me if it didn't go somewhere; I couldn't do organic synthesis just to do organic synthesis. Seth's work immediately appealed to me. Not only would I be making unnatural amino acids, I would actually get to the chance to incorporate them into peptides and then analyze the peptides themselves.

From the beginning, Seth has acted as the consummate professional and approachable mentor. I entered research knowing nothing of peptides, their synthesis, their purification, or their analysis. My fledgling knowledge was limited to only a small set of rusty organic synthesis skills garnered from my undergraduate research several years prior. During my first year in lab, I worked with Seth at a nearby hood (imagine that now), pestering him with questions as I fumbled about. The revisions of my early writing in the lab looked like a bloodbath of red pen after Seth looked over my work and I don't even want to think about how painful it must have been to sit through my early group meeting presentations (I didn't even use ChemDraw back then). Seth's dedication to me over the past five years has allowed me to become a productive member of the lab with a range of skills that I couldn't have dreamed of having coming in. Thank you, Seth, for all of your hard work.

I can't mention Seth without mentioning the other members of my lab group. Conor Haney has been with me since the beginning, and he has also had the privilege of witnessing my early group meeting presentations and attempts at scientific writing. Zach Reinert hasn't been far behind either, having joined the lab during the summer I really started delving into research. Over the years it has grown to the point

where I consider you two not only colleagues but as true friends. Of course Zach and Conor aren't the only members of the Horne group who have helped me along the way; I would like to thank Ken, Kaylyn, Nate, Halina, Will, Kelly and my pokémon (Geoff and Rebecca) for their support.

Over the past five years I've also had the support of other friends within the department. I would like to thank Kevin Bivona, Ben Hay, Laura Kocsis, and Everett Merling for supporting me through our first year and beyond. I would like that thank all of the members (past and present) of the Donut Wednesday crew and I hope that tradition carries on. Just remember, nothing good ever comes from a Donut Thursday.

Although many people have influenced me and supported me in my pursuit, I have to thank my parents; without them, I wouldn't have the work ethic it takes to succeed this far. My education has always been very important to me because of their influence and support. Mom, thank you for being there for me, even though you might not understand what I do (has to involve hamsters somehow though). I miss you, Dad.

Finally, and most importantly, I would like to thank my wife, Lorie, who has given me nothing but her strongest support during this entire process. When I was unsure whether or not to leave teaching to pursue my PhD, she was always behind me, encouraging me. She has endured my crazy schedule without complaint, although at times it's been hard either with sleepless nights with a baby or huge commutes to work to support us both. You've always lent me your support when I needed it. I love you and I am forever grateful for your support.

## **1.0 INTRODUCTION TO BETA-SHEET FOLDAMERS**

### **1.1 PEPTIDE THERAPEUTICS**

Proteins are responsible for a wide variety of natural processes within the body and malfunction of these processes is the root cause of many diseases.<sup>1</sup> Small molecules have been the focus of the majority of research in drug design, but these therapeutics are limited in their ability to target proteins with large surface areas.<sup>2</sup> Peptide therapeutics offer an attractive alternative to small-molecule drugs because they are often target-specific, do not elicit immune responses, and can bind to large surface areas.<sup>3</sup>

Design of peptide therapeutics relies on the ability of short peptide fragments to successfully mimic key structural features, such as turns, helices, or sheets, of well-folded proteins. One example of such structural mimicry is found in inhibition of HIV-1 protease (HIV-1 PR). Crystal structures of HIV-1 PR show that the sheet-like regions of the N-terminal and C-terminal domains of two monomer units associate, driving formation of a dimer (Figure 1).<sup>4</sup> Upon dimerization, HIV-1 PR acts as an aspartyl protease used for processing of polypeptide chains, a process necessary for viral infection.<sup>5</sup> Studies have shown that using a fragment of the C-terminal sheet can disrupt dimerization and prevent formation of the active site.<sup>6</sup>

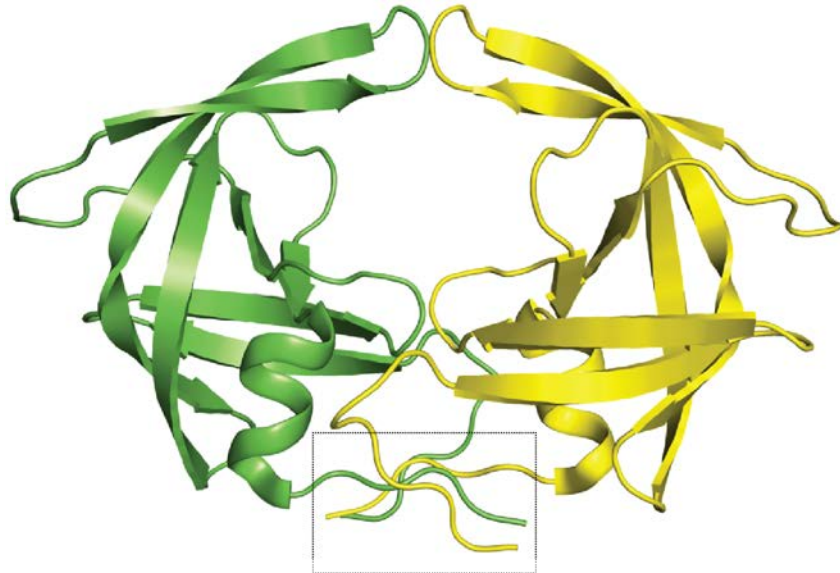


**Figure 1.** Cartoon of the HIV-1 protease dimer from PDB: 3HVP. Grey box highlights the N- and C-terminal sequences necessary for dimerization.

While the HIV-1 protease dimerization inhibitor described above uses a sheet-like structure,  $\alpha$ -helical structures have also seen wide applicability as peptide therapeutics. One example is enfuvirtide, a peptide that prevents HIV fusion between the virion and host cell.<sup>7</sup> When HIV virus binds to a target cell, the viral membrane protein gp41 undergoes a conformational change from an extended three-helix bundle to form a compact six-helix bundle (Figure 2).<sup>8</sup> This rearrangement brings the host cell and viral membrane into contact and creates a fusion pore, allowing viral infection of the host.<sup>9</sup> Enfuvirtide, a 36-residue fragment from the C-terminus of gp41, can disrupt this process by binding to the N-terminal three-helix bundle of gp41 and preventing formation of the six-helix bundle.

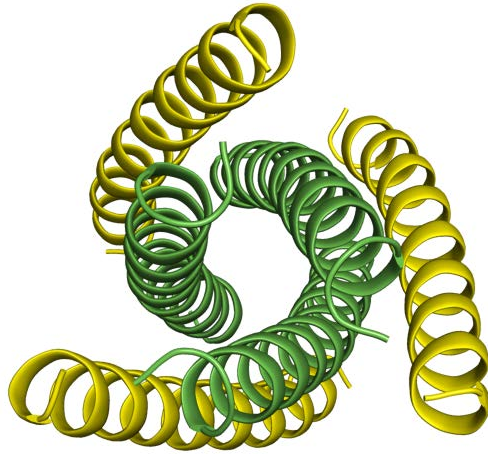


**Figure 2.** Cartoon of the six-helix bundle formed by gp41 during HIV infection from PDB: 1AIK. N- and C-terminal helices are shown as yellow and green, respectively.

A third example of secondary structure mimicry in peptides can be found with somatostatins. These peptides have a  $\beta$ -turn region necessary for binding to G-protein coupled receptors. Somatostatins are responsible for inhibition of endocrine secretion, a potential area for therapeutic exploitation for diseases such as diabetes.<sup>10</sup> Studies of SRIF-14, a 14-residue cyclic peptide found in the somatostatin family, show that it has a half-life less than three minutes in plasma.<sup>11</sup> The short life-span of this peptide highlights one of the key drawbacks of protein therapeutics: their rapid degradation by endogenous proteases.

## 1.2 FOLDAMERS AND SEQUENCE-BASED DESIGN

Small peptide and protein therapeutics, because of their hydrophilic nature and high solubility in aqueous media, are often cleared from the body during circulation through proteolysis by enzymes found dissolved in the blood or bound to cell membranes.<sup>12</sup> To circumvent the issue of proteolysis and to provide mimics of specific secondary structures, one direction of research has focused on design of

foldamers, defined as “polymers with a strong tendency to adopt a specific compact conformation.”<sup>13</sup> Foldamers, while able to mimic the structures of natural proteins, have backbones built using unnatural building blocks, thereby imparting resistance to proteolytic degradation and longer half-lives compared to natural backbone therapeutics.<sup>14-16</sup> Backbone homologation of an  $\alpha$ -peptide to a  $\beta$ -peptide, for example, can increase stability from degradation by a variety of proteases from <10 minutes to >48 hours.<sup>14</sup>

The source of proteolytic resistance of foldamers has been examined on several fronts. Studies of peptides containing fluorinated  $\alpha$ - and  $\beta$ -residues show that electronics do not affect proteolytic stability.<sup>17</sup> It has been suggested that changing the placement of amide bonds via inclusion of  $\beta$ - or  $\gamma$ -amino acids can prevent recognition by proteases.<sup>14</sup> *N*-Methylation of peptides provides a similar avenue of protection by providing steric disruption of potential recognition sites.<sup>18</sup> An alternative, and possibly additional, source of increased proteolytic stability of foldamers is their ability to manifest well-folded structures. Work with well-folded  $\beta$ -hairpin peptides has shown that as the folded stability of these peptides increases, they become less susceptible to proteolysis,<sup>19</sup> likely due to prevention of a single strand conformation necessary for enzyme recognition.<sup>20</sup> This finding suggests that if inclusion of unnatural backbones is able to promote a well-folded structure in a foldamer, it may prevent formation of an extended conformation necessary for amide cleavage. Similarly, if an unnatural backbone element is found in a larger disordered structure, it may be able to provide a degree of local protection to proteolysis by preorganizing nearby sections of the backbone to a specific fold.

Regardless of the cause of proteolytic stability, foldamers provide an interesting area of study for mimicry of structures found in nature. Early studies of foldamers focused largely on the design of mimics of  $\alpha$ -helices.<sup>13,21-24</sup> These studies have provided the foundation for design strategies that can be applied to the other secondary structures. One such strategy, sequence-based design, involves substitution of  $\alpha$ -residues with unnatural residues at carefully selected sites within a parent peptide sequence. Sequence dictates the secondary structures (helices, sheets, turns, loops) of peptide segments, judiciously applying substitutions to a sequence that dictates a specific type of fold can be a valuable tool for design of secondary structure mimics. Studies of helical systems have shown that sequence-based design incorporating  $\beta$ -amino acids,

backbone lengthened homologs of  $\alpha$ -amino acids, can be applied to generate  $\alpha/\beta$ -hybrid peptides that fold into discrete helical structures as well as more complex quaternary structure assemblies mimicking those formed by the parent  $\alpha$ -peptides.<sup>25-28</sup>

In some cases, peptides require only secondary structure, such as the helices described above, for activity, but most proteins require tertiary folds to function. Larger proteins have a more complex tertiary structure where several different secondary structures combine to form a folded structure, in turn dictating the function of the protein. Foldamer design has been focused almost exclusively on mimicry of secondary structures, thereby excluding the active folded conformations found in tertiary folds. Our goal is to provide strategies for mimicry of tertiary folds using unnatural backbones, but to mimic the tertiary structure of larger proteins, sequence-based design strategies for all secondary structure types need to be developed. While design strategies for design of  $\alpha$ -helical foldamers are well-established, similar strategies for mimicry of other secondary structure types, such as  $\beta$ -sheets, are not. Our research focuses on designing substitution strategies suitable for application in  $\beta$ -sheets and then applying these strategies to a tertiary fold.

## **1.3 PROTEIN BETA-SHEETS**

### **1.3.1 Beta-Hairpins**

The  $\beta$ -strand is a type of secondary structure where the amino acid backbone adopts an extended conformation.  $\beta$ -Sheets are formed as two or more  $\beta$ -strands associate with one another through inter-strand hydrogen bonds and contacts between hydrophobic side chains. Many investigations of  $\beta$ -sheet folding utilize smaller systems such as the  $\beta$ -hairpin, the simplest form of a  $\beta$ -sheet consisting of two anti-parallel strands connected by a tight turn (Figure 3).

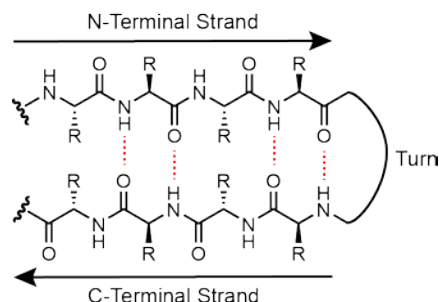


**Figure 3.**  $\beta$ -Hairpin structure with hydrogen bond contacts shown in red.

When removed from the context of an intact protein, many  $\beta$ -sheet peptides aggregate or lose all folded structure in solution. While limited in number, some examples of short sequences that encode sheets exist, such as the N-terminal hairpin fragment of the protein ubiquitin<sup>29,30</sup> and the C-terminal hairpin fragment of the protein GB1.<sup>31,32</sup> One drawback of these sequences is that their folds are also minimally stable in aqueous solution.

### 1.3.2 Amino Acid Identity and its Impact on Beta-Hairpin Formation

Because short peptide fragments are often unstable in terms of folded structure, studies have focused on how to improve the folded stability of these peptides, showing the identity of the residues involved in the hairpin plays an important role in the stability of the fold.<sup>33</sup>

A survey of various residue mutations in the C-terminal hairpin of GB1 suggests that the  $\beta$ -branching seen in amino acids such as threonine, valine, and isoleucine restrict the torsional preferences of the amino acid backbone and support sheet formation more than flexible amino acids such as alanine or glycine.<sup>34</sup> In addition to sheet propensity of amino acids, the side chains themselves can play an important role in sheet stability. The folding of the C-terminal fragment of GB1 is partially driven by packing of the side chains of four hydrophobic residues: valine, phenylalanine, tyrosine, and tryptophan (Figure 4).<sup>31</sup>

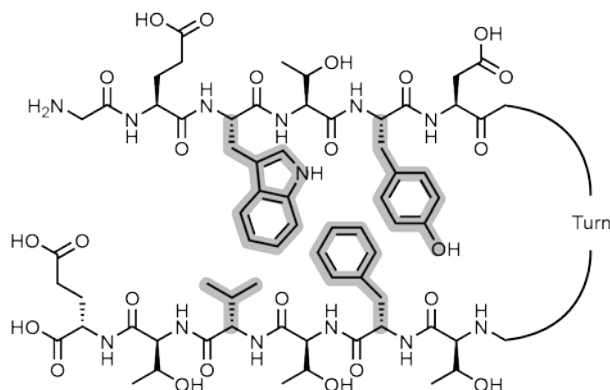


**Figure 4.** Hairpin structure of the C-terminal fragment of protein GB1. Side chains of hydrophobic packing residues are colored grey.

Mutation of valine to tryptophan results in a new side chain cross-strand pairing with the tryptophan residue naturally found in the parent, thereby significantly stabilizing the hairpin of the new “trpzip” mutant.<sup>35</sup> Removal of any of the three aromatic residues, tyrosine, phenylalanine, or tryptophan, in this fragment abolishes folding completely.<sup>36</sup>

Aside from stabilizing aromatic interactions, other side chain interactions can also promote sheet formation. Adding terminal salt-bridge interactions,<sup>37</sup> adding a Trp-Thr-Gly capping motif,<sup>38</sup> or creating a cation-pi interaction between tryptophan and *N*-methyl lysine residues<sup>39</sup> can also stabilize hairpin peptides.

The stability of hairpins is not only impacted by identity of strand residues but also by the residues involved in forming the turn. Replacing the turn segment of the C-terminal hairpin fragment of GB1 with D-Pro-Gly<sup>40</sup> or Asn-Pro-Ala-Thr-Gly-Lys<sup>41</sup> can pre-organize the peptide backbone with a well-defined turn region and dramatically improve the overall stability of the system. Turn mutations are not limited to natural residues either; other artificial loop designs such as Aib-Gly<sup>42</sup> have proven to be successful as sheet promoters.

## 1.4 BETA-SHEET FOLDAMERS

As described above, the folded stability of hairpin peptides can be increased by applying modifications in a variety of ways. While mutation of sequences with *naturally* occurring amino acids has been thoroughly investigated, our goal is to apply sequence-based design to a protein using *unnatural* amino acids. We surveyed the types of unnatural backbones previously examined in sheets to provide a basis for backbone modification in a tertiary fold.

### 1.4.1 Beta-Sheet Foldamers Derived from Cyclic Beta-Amino Acids

One of the original design strategies for  $\beta$ -sheet foldamers is use of a single unnatural amino acid building block in synthesis of a  $\beta$ -peptide. Studies have shown that three different types of cyclic  $\beta$ -amino acids can be used to generate sheets in this fashion (Figure 5).<sup>43-45</sup>

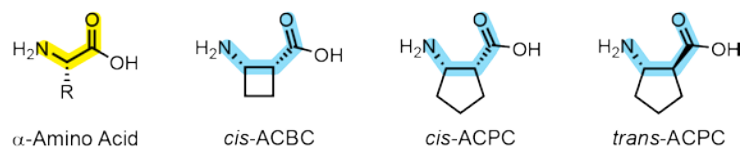


**Figure 5.** An  $\alpha$ -amino acid (yellow) and cyclic  $\beta$ -amino acids *cis*-ACBC, *cis*-ACPC, and *trans*-ACPC (blue).

A tetramer containing (1*R*,2*S*)-2-amino-cyclobutanecarboxylic acid (ACBC) assembles into sheet-like structures which form long fibrils visible by TEM.<sup>43</sup> Oligomers of (1*R*,2*S*)-2-amino-cyclopentanecarboxylic acid (*cis*-ACPC) form sheet structures in organic solvent<sup>44</sup> and alternating the two enantiomers of *trans*-ACPC in a hexamer also initiates formation of sheet-like fibrils.<sup>45</sup> While all three of these cyclic  $\beta$ -monomer types allow for formation of sheet-like structures, they lack the side chain

diversity of  $\alpha$ -residues. Because folded stability can be highly dependent on side chain interactions, removal of side chain functionality could significantly impact the folded stability of a hybrid peptide incorporating cyclic amino acids.

### 1.4.2 Beta-Sheet Foldamers Derived from Pyrrolinone-Based Scaffolds

One of the earliest investigations of sheet mimics bearing side chain functionality involved pyrrolinones.<sup>46</sup> In this work, a sequence of natural  $\alpha$ -amino acids was replaced with pyrrolinones with similar side chain functionalities (Figure 6) as a means to eliminate the amide bond cleaved by proteases while still maintaining side chain and carbonyl placement.

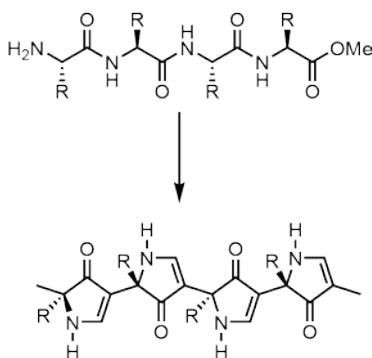
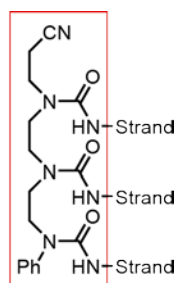


**Figure 6.** Tetramer conversion to a pyrrolinone-based scaffold.

Crystal structures of a compound with a pyrrolinone-based scaffold with alkyl side chains show that it is able to form sheets similar to those of the parent sequence.<sup>46</sup> Since this work was published, new synthetic routes have been developed to allow other side chain functionalities to be incorporated<sup>47</sup> and to allow for *N*-methylation backbone nitrogen atoms.<sup>48</sup> Using peptide therapeutics as templates for amide and side chain display, these pyrrolinone scaffolds have shown the ability to act as structural mimics.<sup>49,50</sup>

### 1.4.3 Beta-Sheet Foldamers Templated by Methoxybenzamide

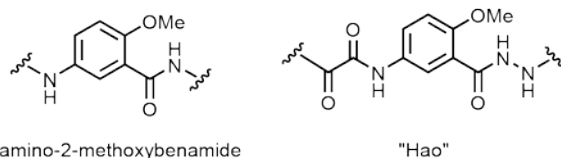
Rather than using a single unnatural amino acid type to template sheet formation, an alternative strategy is to use a sheet-forming scaffold while introducing unnatural backbone elements in a limited number of sites. Oligourea scaffolds (Figure 7) have shown utility in templating sheet formation.<sup>51,52</sup>



Oligourea Scaffold

**Figure 7.** Sheet formation templated by an oligourea scaffold.

Placing one or more unnatural sheet-promoting elements such as 5-amino-2-methoxybenzamide (Figure 8) on one of the strands of an oligourea scaffold can template  $\beta$ -sheet formation on its neighboring strand in organic solvent.<sup>53,54</sup>



5-amino-2-methoxybenzamide

"Hao"

**Figure 8.** Sheet-promoting backbones containing 5-amino-2-methoxybenzamide.

Combining 5-amino-2-methoxybenzamide with a hydrazine and oxalic acid generates an unnatural backbone unit which can mimic a tripeptide.<sup>55,56</sup> Use of the this unit in a two-strand scaffold can template sheet formation on the opposite strand while disrupting aggregation<sup>56,57</sup> and allowing mimicry of biologically relevant systems,<sup>58,59</sup> potentially leading to important discoveries regarding protein-protein interactions.

#### 1.4.4 Beta-Sheet Foldamers Containing Alpha-Amino Acid Homologs

The design strategies discussed above involve either repetition of unnatural amino acids or use of an unnatural scaffold to mimic natural sheets. While these strategies are effective for examining small systems, they do not allow for backbone modification in a larger protein. Incorporation of  $\alpha$ -amino acid homologs at a limited number of positions can limit the degree of unnatural character of the peptide backbone while adding enhanced proteolytic stability as inclusion of even a single unnatural amino acid in a peptide can protect nearby residues from proteolysis.<sup>60</sup>

##### 1.4.4.1 Beta-Sheet Foldamers Containing Beta-Amino Acids

One homolog of a natural  $\alpha$ -amino acid is a  $\beta$ -amino acid which incorporates an additional methylene carbon in the backbone. Side chain functionality can be introduced in various positions to generate  $\beta^2$ -,  $\beta^3$ -, or  $\beta^{2,3}$ -amino acids (Figure 9).

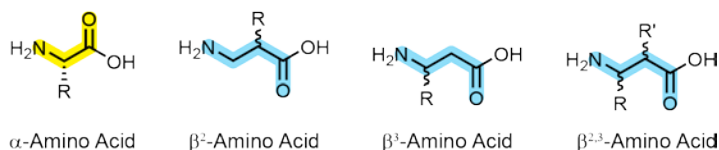


**Figure 9.** An  $\alpha$ -amino acid (yellow) and several  $\beta$ -amino acids (blue).

The first study reporting  $\beta$ -amino acids in a sheet-like fold compared the sheet-forming propensity of unsubstituted  $\beta$ -, monosubstituted  $\beta^3$ -, and disubstituted  $\beta^{2,3}$ -amino acids in a tetramer containing two  $\beta$ -residues linked by a D-Pro-Gly turn.<sup>61</sup> NMR studies in organic solvent (dichloromethane and methanol) as well as solid-state structures showed that  $\beta$ -residues are capable of forming a short hairpin, although eliminating substituents on the backbone destabilizes the structure. Further work with a tetramer consisting of a different short turn and  $\beta^{2,3}$ -residues formed a hairpin in methanol and in the solid state.<sup>62</sup> It was later demonstrated that a  $\beta$ -peptide hexamer consisting only of  $\beta^2$ -,  $\beta^3$ -, and  $\beta^{2,3}$ -residues is able to form a hairpin in methanol<sup>63</sup> and this structure was further supported by MD simulations.<sup>64</sup> Additionally, crystal structures of a hexamer with a D-Pro-Gly turn and two  $\beta$ -residues on either strand can adopt a sheet structure.<sup>65</sup>

With evidence of hairpin formation from turn units in combination with  $\beta$ -residues, further research was performed using mixed  $\alpha/\beta$ -hairpins. Crystal structures<sup>66-68</sup> and NMR in organic solvent,<sup>67,68</sup> showed that peptides containing a combination of  $\alpha$ - and  $\beta^3$ -residues can form hairpin structures.

#### 1.4.4.2 Beta-Sheet Foldamers Containing Gamma-Amino Acids

Study of  $\alpha$ -amino acid analogs is not limited in scope to  $\beta$ -amino acids;  $\gamma$ -amino acids (Figure 10) such as vinylogous  $\gamma^4$ -amino acids, (1*R*,3*S*)-3-aminocyclohexanecarboxylic acid (Acc), and *meta*-aminobenzoic acid (*m*ABA) have also shown the potential to template  $\beta$ -sheet formation.

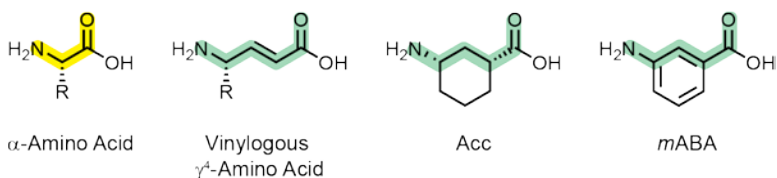


**Figure 10.** An  $\alpha$ -amino acid (yellow) and several  $\gamma$ -amino acids (green).

Crystal structures and NMR of short tetrapeptides containing two-residue turns attached to two vinylogous  $\gamma^4$ -residues have shown short hairpin structure formation.<sup>69</sup> A mixed  $\alpha/\gamma$ -hybrid peptide including vinylogous  $\gamma^4$ -amino acids has also been shown to form a hairpin structure in organic solvent, although it also shows removing the  $\alpha,\beta$ -unsaturation destabilizes the folded structure of the peptide.<sup>70</sup>

Using cyclic  $\gamma$ -amino acids in sheets can also be effective. NMR in organic solvent has shown that  $\alpha/\gamma$ -hybrid peptides containing *mABA* residues can form hairpins.<sup>71</sup> A saturated form of *mABA*, Acc, can also form sheet-like structures. Alternating D- $\alpha$ -residues and L- $\alpha$ -residues has been shown to promote formation of cyclic sheet structures.<sup>72</sup> Acc residues can be used in place of the natural L- $\alpha$ -residues to promote similar cyclic sheet structures.<sup>73-75</sup>

## 1.5 SOLVENT CHOICE AND ITS EFFECT ON BETA-SHEET FORMATION

As described above, a variety of backbone modification strategies can be applied to hairpin systems with minimal change in folded structure. A significant drawback of many studies, however, is the use of organic, rather than aqueous, solvent. Solvent choice can have a dramatic impact on the folded stability of peptides. Inclusion of trimethylamine *n*-oxide (TMAO) in aqueous solvent, for example, has been shown to increase the free energy of the unfolded state of proteins,<sup>76</sup> forcing equilibrium towards the folded state. Mechanistically, inclusion of TMAO co-solvent increases the number and strength of hydrogen bonds between water molecules,<sup>77</sup> preventing water from acting as a hydrogen bond donor or acceptor to the amides found in the protein backbone. When the amide bonds in a protein backbone are unaffected by solvent molecules, they can form the inter-residue hydrogen bonds necessary to stabilize folded structure.

Other solvents affect protein folding in a similar manner. 2,2,2-Trifluoroethanol (TFE) will surround a protein backbone, preventing water from accessing hydrogen bond sites.<sup>78</sup> The reverse is true

in the case of urea co-solvent; addition of urea provides a preferential hydrogen bond donor and acceptor relative to the backbone and allows solvation of the backbone amides.<sup>79</sup>

As shown above, the ability of the solvent to form hydrogen bonds with backbone amides within a protein plays a large role in the folded stability of a protein. Water, due to its ability to form hydrogen bonds, does not promote inter-residue hydrogen bonding in a protein.<sup>80</sup> Organic solvents, such as methanol or dimethylsulfoxide (DMSO), however, have weaker hydrogen bond capacity and can enhance folded stability relative to water.

## 1.6 GOALS

Many systems discussed above rely on artificial scaffolds that are difficult to synthesize or are impossible to incorporate into a protein with a complex folded structure. Additionally, the folded structures of hybrid peptides where unnatural amino acids are incorporated alongside natural  $\alpha$ -amino acids have only been examined in context of organic solvents. In cases where structural data is available, thermodynamic consequences of unnatural backbone modifications have not been evaluated. To design foldamers that mimic natural proteins, both the structural and thermodynamic impacts of such substitutions in a biologically relevant aqueous environment need to be examined. It is the goal of this work to develop general design rules for the incorporation of unnatural amino acids in natural sheet forming sequences to generate heterogeneous backbone mimics.



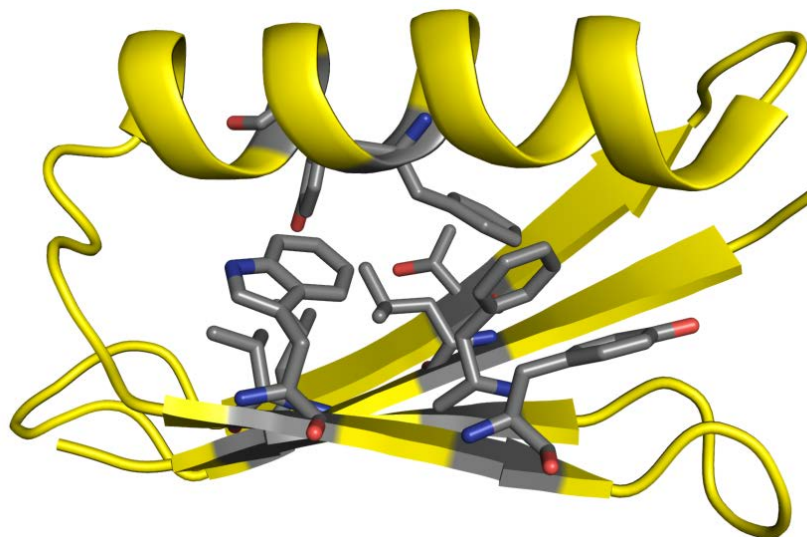


**Figure 12.** Cartoon structure of protein GB1 with core packing residues displayed in grey. Coordinates derived from PDB: 2QMT.

While GB1 can be used as a model protein for examining the structural and thermodynamic effects of backbone modification in tertiary systems, it is too large a system to be practical for initial screening of appropriate monomers for use in backbone modification. For these purposes, we have chosen to use a smaller model system, the C-terminal fragment of GB1 (Figure 13), shown to form a hairpin folded structure in water,<sup>32</sup> and several of its derivatives.

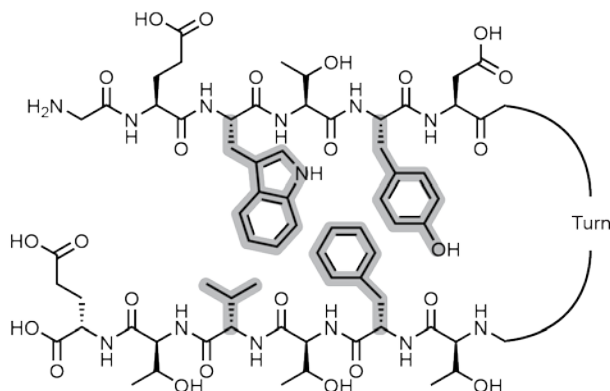


**Figure 13.** Sequence and structure of the C-terminal fragment of protein GB1. Side chains of hydrophobic packing residues are colored grey.

## 1.6.2 Outline

### 1.6.2.1 Analysis of $\alpha$ - to $\beta$ -Residue Substitution

This document is laid out into three chapters of data. The first details the structural and thermodynamic consequences of  $\beta$ -residue substitutions in derivatives of the C-terminal hairpin fragment of GB1. In this work, we first examined 1:1  $\alpha$ - to  $\beta$ -residue substitution by incorporating 16 different  $\beta$ -amino acids of varying side chain position, stereochemistry, and backbone ring constraint in a 12-residue hairpin peptide. Multidimensional NMR analysis revealed use of 1:1  $\alpha$ - to  $\beta$ -residue substitution leads to inversion of the hydrogen bond pattern and side chain display.

To prevent the inversion seen with 1:1 substitution, we next examined the effects of 2:1 or 2:2  $\alpha$ - to  $\beta$ -residue substitutions with a combination of  $\beta^2$ -,  $\beta^3$ -, and  $\beta^{2,3}$ -amino acids in a 16-residue hairpin peptide. Again using NMR analysis, we found that three of the substitution strategies applied can prevent inversion and maintain native-like folding of the hairpin, although at a significant cost to folded stability.

### 1.6.2.2 Analysis of $\alpha$ - to $\gamma$ -Substitution and *N*-Methylation

To find other monomer types that might allow native-like folding while not compromising the stability of the hairpin fold, we next examined the effects of 1:1  $\alpha$ - to  $\gamma$ -residue substitution using two types of cyclic  $\gamma$ -amino acids and a vinylogous  $\gamma^4$ -amino acid in the context of a 16-residue hairpin peptide. Unlike the case of 1:1  $\alpha$ - to  $\beta$ -residue substitution, use of  $\gamma$ -amino acids not only allows for native-like folding, but is also less destabilizing when vinylogous  $\gamma^4$ -amino acids are used. The hairpin fold is stabilized when cyclic  $\gamma$ -amino acid are used.

As an alternative to homologs of  $\alpha$ -residues, the impact of *N*-methylation of specific residues was also examined. We determined the individual effects of *N*-methylation on the four hydrophobic core residues of a 16-residue hairpin. This work showed that *N*-methylated residues can be used directly in place of  $\alpha$ -residues with varying degrees of destabilization. When substitution occurs away from the hairpin turn, this destabilization is decreased.

### 1.6.2.3 Unnatural Residue Substitutions Applied to Protein GB 1

In the final chapter, the various backbone modification strategies examined in chapters two and three are applied to the  $\beta$ -sheet of full-length protein GB1. Mutant analogs containing  $\beta$ -,  $\gamma$ -residues, and *N*-methyl amino acids were examined using circular dichroism spectroscopy and thermal denaturation melts to determine the thermodynamic effects of these substitutions on the stability of the folded structure. These experiments revealed that the sheet propensities of the unnatural amino acids predicted by the hairpin peptides can be applied to a larger protein with the caveat that the site of substitution plays an important role in the overall stability of the tertiary fold.

## 2.0 IMPACT OF BETA-AMINO ACID INCORPORATION ON FOLDING OF BETA-HAIRPINS IN AQUEOUS SOLUTION

The results detailed in this chapter have been published in:

1. Lengyel, G.A.; Frank, R.C.; Horne, W.S., “Hairpin Folding Behavior of Mixed  $\alpha/\beta$ -Peptides in Aqueous Solution,”; *Journal of the American Chemical Society*, **2011**, 4246-4249.
2. Lengyel, G.A.; Horne, W.S., “Design Strategies for the Sequence-Based Mimicry of Side-Chain Display in Protein  $\beta$ -Sheets by  $\alpha/\beta$  -Peptides,” *Journal of the American Chemical Society*, **2012**, 15906-15913.

As discussed in Chapter 1, work has been done investigating unnatural residue substitution in designed  $\beta$ -sheet peptides; however, guidelines for the use of such elements to mimic larger proteins have not been described. With an eventual goal of modifying a protein sheet in the context of a well-defined tertiary fold, we first sought to compare unnatural residue substitution strategies in the context of a minimal sheet model system: a hairpin peptide consisting of two anti-parallel  $\beta$ -strands connected by a tight turn.

## 2.1 1:1 ALPHA- TO BETA-RESIDUE SUBSTITUTION

### 2.1.1 Hairpin Peptide Design

To determine the structural impact of backbone modification in  $\beta$ -sheets, we first examined unnatural residue substitutions in peptide **1a**, derived from the C-terminal hairpin of protein GB1.<sup>85</sup> Peptide **1a** has two strands connected by a turn-promoting D-Pro-Gly sequence (Figure 14).<sup>86,87</sup> As in the case of the C-terminal hairpin fragment of GB1,<sup>32</sup> hydrophobic packing of core residues Trp<sub>3</sub>, Tyr<sub>5</sub>, Phe<sub>9</sub>, and Val<sub>11</sub> found in the strands of peptide **1a** drives the formation of a short hairpin structure in water. An approximate folded population of 61% at 275 K allows peptide **1a** to be a sensitive tool for measurement of either increases or decreases in folded population resulting from unnatural residue substitutions.

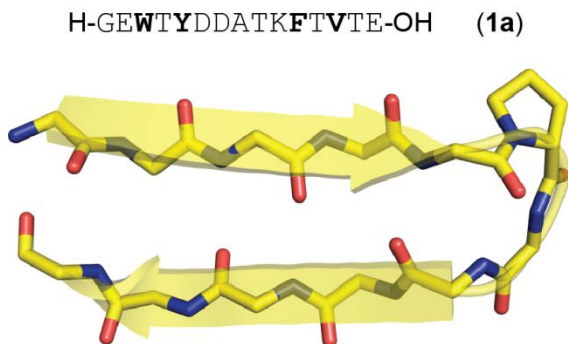


**Figure 14.** Sequence and NMR solution structure of hairpin peptide **1a**.

Based upon the utility of  $\beta$ -amino acid substitutions shown in prior work (see Chapter 1), we chose to use a 1:1  $\alpha$ - to  $\beta$ -residue substitution strategy. As  $\beta$ -amino acids contain an additional carbon atom in the backbone, they are generally more flexible than their shorter  $\alpha$ -amino acid analogs and can exhibit a wider range of conformations. To screen for specific amino acid types that might be

accommodated into a sheet structure in water, we examined sixteen different  $\alpha/\beta$ -hybrid peptides (peptides **2a-17a**) with  $\beta$ -residues incorporated in place of residues Gln<sub>3</sub> and Thr<sub>10</sub> of the  $\alpha$ -peptide sequence, **1a** (Figure 15). Positions 3 and 10 were chosen because they are found in the center of each strand in the hairpin and are not involved in the hydrophobic core of the hairpin structure. Compounds **1a-17a** were synthesized using standard Fmoc-protected solid-phase peptide synthesis techniques. Unnatural monomers were synthesized in Fmoc protected form by known routes<sup>28,88-106</sup> as detailed in Section 2.3. Compounds **1b-17b**, epimers of **1a-17a**, were also prepared; these incorporate L-Pro used in place of D-Pro at position 7 for use as unfolded control peptides in population analysis.

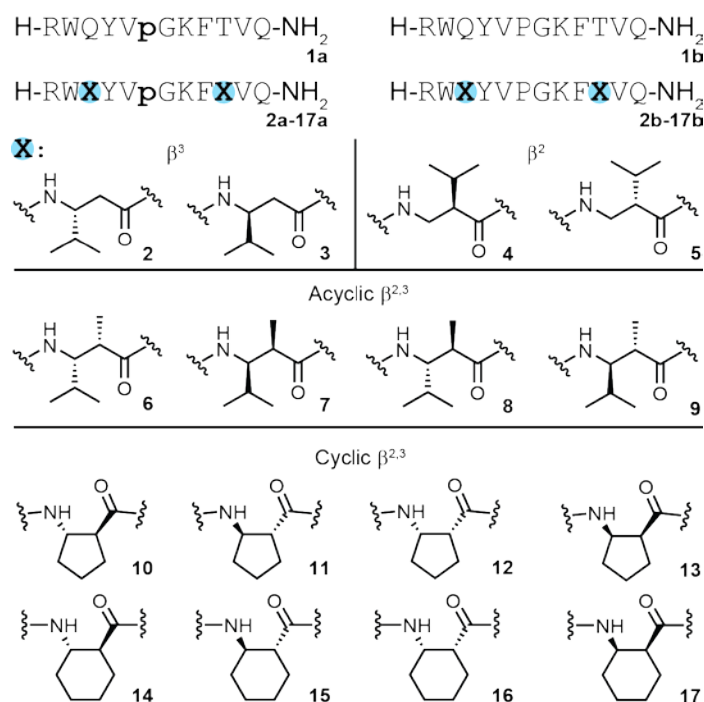


**Figure 15.** Sequences of peptides **1a-17a** and **1b-17b**. Locations of unnatural residues are highlighted blue.

The structures of the unnatural residues were systematically varied to evaluate the impact of side chain stereochemistry, backbone substitution pattern, and preorganization of backbone dihedrals by ring constraint in both five- and six-membered rings. The impact of side chain stereochemistry on folding was analyzed by incorporating each possible stereoisomer for each monomer class ( $\beta^2$ ,  $\beta^3$ , acyclic  $\beta^{2,3}$ , and cyclic  $\beta^{2,3}$ ) in oligomers **2a-17a**. Side chain substitution site within the unnatural residues was analyzed comparing  $\alpha/\beta^3$ -hybrid peptides (**2a, 3a**) to the corresponding  $\alpha/\beta^2$ -hybrid peptides (**4a, 5a**), each bearing an isopropyl side chain, or  $\alpha/\beta^{2,3}$ -hybrid peptides (**6a-9a**), functionalized with both an isopropyl and a methyl side chain. The effect of backbone preorganization on folding was measured using peptides with backbones including  $\beta$ -residues with five-membered (**10a-13a**) or six-membered (**14a-17a**) ring structures.

### 2.1.2 Qualitative NMR Analysis

Peptides **1a-17a** were analyzed using 2D  $^1\text{H-NMR}$  spectroscopy (TOCSY, NOESY, and COSY) at 278 K in aqueous buffer. From the NMR data, chemical shifts of backbone protons were assigned using sequential NOE analysis and the chemical shifts of the protons of Gly<sub>7</sub> were used as a measure of folding.<sup>107-110</sup> Glycine residues have two diastereotopic H <sub>$\alpha$</sub>  protons; when these protons are found in a well-folded environment, they resonate at distinct frequencies leading to separate peaks. There is a direct correlation between the separation of glycine resonances by NMR and hairpin folded population and glycine separation analysis has been used to gauge hairpin folded population.<sup>110</sup>

The separation of the Gly<sub>7</sub> H <sub>$\alpha$</sub>  protons ( $\Delta\delta$  Gly<sub>7</sub> H <sub>$\alpha/\alpha'$</sub> ) in peptides **1a-17a** was calculated to qualitatively measure the impact of unnatural residue substitution on folded stability (Figure 16). Values for hybrid peptides **2a-17a** ranged from 0.03 to 0.34 ppm compared to a value of 0.23 ppm for peptide **1a**. Of significance is that the glycine protons of peptides **8a** and **9a**, containing the two enantiomers of the *syn*  $\beta^{2,3}$ -residues, have the highest overall separation, even when compared to those found in parent peptide **1a**. Peptide **16a** shows a similar value to peptide **1a**, suggesting a similar folded population.

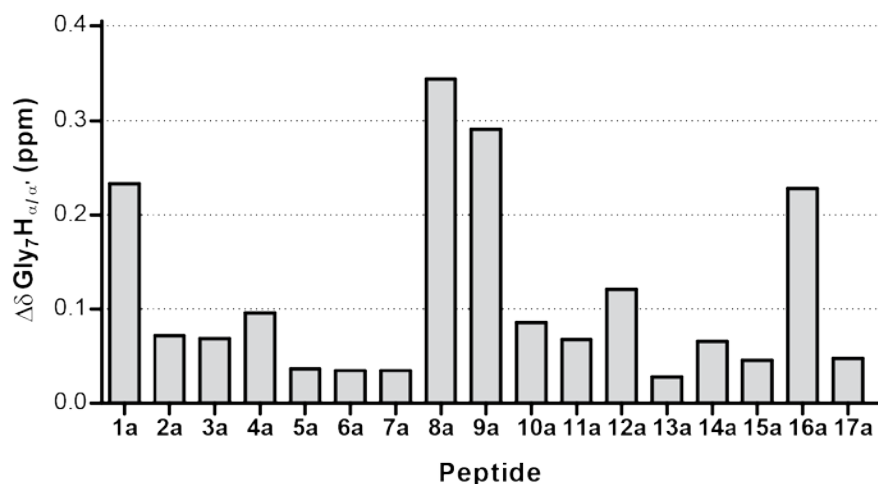


**Figure 16.** Glycine separation values for hybrid  $\alpha/\beta$ -peptides **1a-17a**.

As another means to gauge folded population, the chemical shift deviation (CSD) between peptides **1a-17a** and their unfolded analogs **1b-17b** was analyzed.<sup>30,32,110-112</sup> Peptides **1b-17b** served as unfolded controls as they contain a turn-abolishing L-Pro-Gly segment in place of turn-promoting D-Pro-Gly (Figure 17).<sup>40</sup> As in the case of the diastereotopic protons of glycine, the chemical shifts of backbone amide and  $\text{H}_{\alpha}$  protons change significantly when found in a folded hairpin conformation compared to an unfolded conformation; the larger the magnitude of the change, the larger the difference in folded population. The chemical shifts of the  $\alpha$ -protons ( $\text{H}_{\alpha}$ ) and amide protons ( $\text{H}_{\text{N}}$ ) for each residue except turn residues  $\text{Pro}_6$  and  $\text{Gly}_7$  were tabulated. The difference in  $\text{H}_{\alpha}$  or  $\text{H}_{\text{N}}$  chemical shifts between folded peptides **1a-17a** and unfolded peptides **1b-17b** were subtracted. The absolute values of these differences were summed to determine the total CSD values (Figure 17).

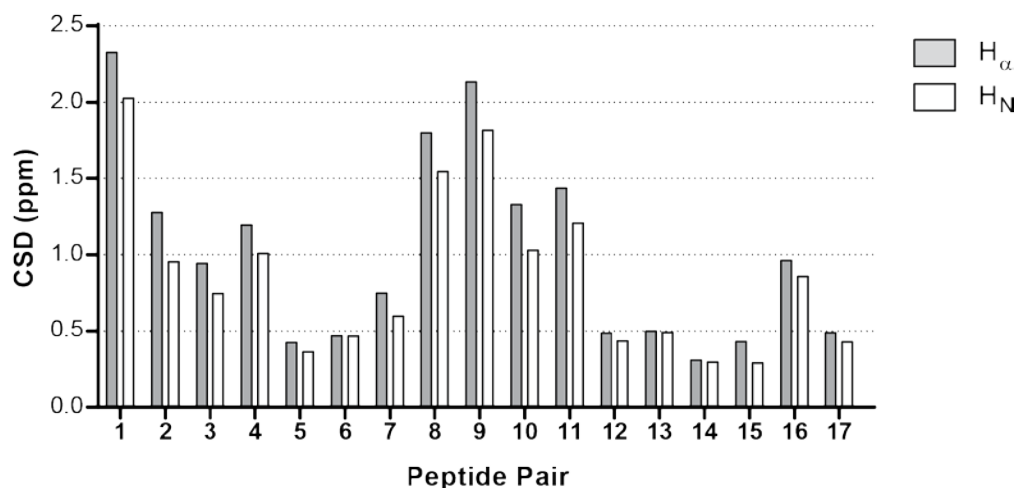


**Figure 17.** Chemical shift deviation between unfolded and folded peptide pairs 1-17.

From the CSD analysis, peptide pairs **8** and **9** show similar values to that of model hairpin peptide pair **1**, agreeing with the glycine separation data that also suggest peptides containing *syn*  $\beta^{2,3}$ -residues allow folding in a hairpin conformation. Peptide pair **16**, unlike in the case of glycine separation analysis, shows a much smaller CSD value than the parent peptide pair, suggesting the higher glycine separation in this case might not be indicative of a hairpin-like fold but the beginnings of an alternative folded structure.

### 2.1.3 Structural Analysis by NMR

With two peptides demonstrating potentially higher folded population than model peptide **1a**, each  $\alpha/\beta$ -hybrid peptide was analyzed using NOE analysis.<sup>30,31,113,114</sup> A well-folded hairpin will demonstrate inter-strand NOE's across the entire length of the backbone. When analyzed for cross-strand NOE signals, only peptides **1a**, **2a**, **8a**, and **9a** showed evidence of hairpin folding (Figure 18).

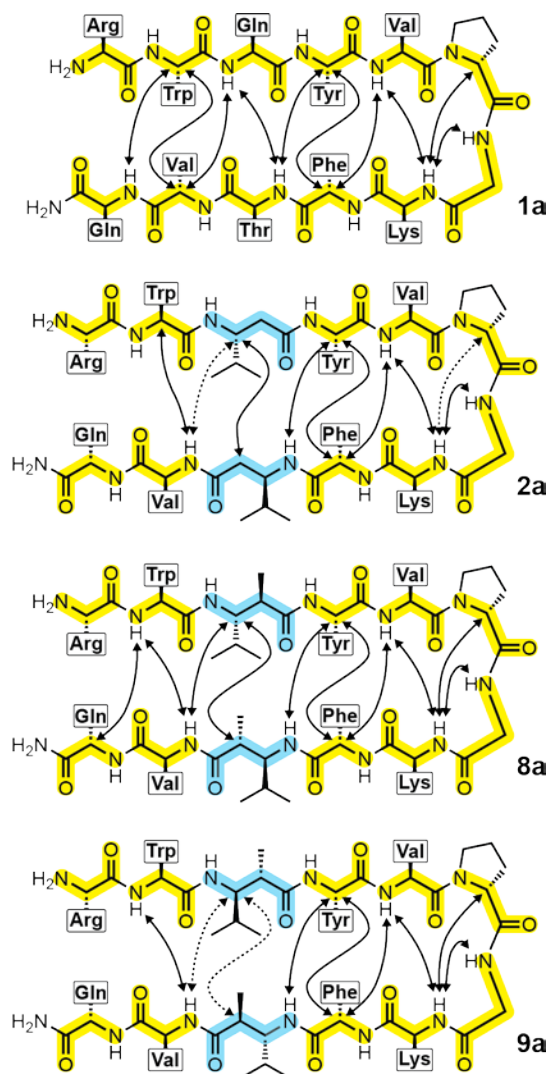


**Figure 18.** Cross-strand NOE's of peptides **1a**, **2a**, **8a**, and **9a**.

Ambiguous NOE's are shown as dotted lines.  $\alpha$ -Residues are colored yellow while  $\beta$ -residues are colored blue.

In each case, similar to parent peptide **1a**,  $\alpha/\beta$ -hybrid peptides **2a**, **8a**, and **9a** showed cross-strand NOE's along the entire length of the backbone. Of note, however, is the apparent inversion of both side chain and hydrogen bond display of any residues beyond the site of  $\beta$ -residue incorporation. This type of inversion has been seen previously,<sup>61,66</sup> but in the case of this peptide it is surprising that the hairpin maintains a folded structure in water. Inversion forces the Trp<sub>2</sub> and Val<sub>11</sub> side chains out of the hydrophobic core and likely decreases the energetic favorability of folding. One possible explanation of the hybrid peptides' ability to remain folded despite this disruption is the incorporation of the isopropyl group of the unnatural residue at position 3 into the hydrophobic core in place of the side chain of Trp<sub>2</sub>.

To further analyze the structural impact of  $\beta$ -residue substitution, 3D solution structures were generated using simulated annealing with NOE distance restraints using the CNS software package. The proton resonances of peptides **1a**, **2a**, **8a**, and **9a** were fully assigned and each peptide was examined for inter-residue NOE's which were tabulated and used as described in Section 2.3.4 to generate a list of NOE distance restraints. Simulated annealing was performed to arrive at the 20 lowest energy conformations (Figure 19) consistent with the experimental data and an average NMR structure (Figure 20) for each peptide. In each case, the average NMR structure of the  $\alpha/\beta$ -hybrid peptides closely resembles the hairpin structure of the parent peptide. As was suggested by cross-strand NOE analysis, the side chains of residues beyond unnatural residue insertion in hybrid peptides **2a**, **8a**, and **9a** are inverted relative to parent peptide **1a** (Figure 21).

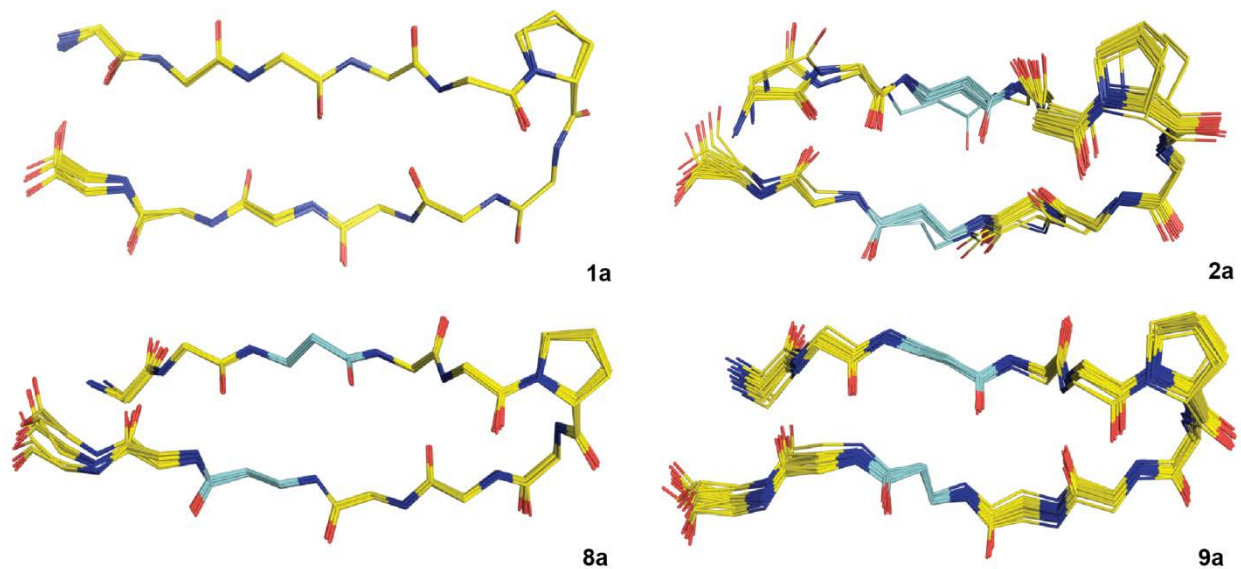


**Figure 19.** Ensembles of 20 lowest energy conformations of peptides **1a**, **2a**, **8a**, and **9a**. Structures calculated using NOE distance restraints from NMR. Samples consisted of ~1 mM solution of peptide and 0.1 M deuterated acetate buffer in 90% H<sub>2</sub>O/D<sub>2</sub>O, pH 3.8. Unnatural residues are shown in blue.

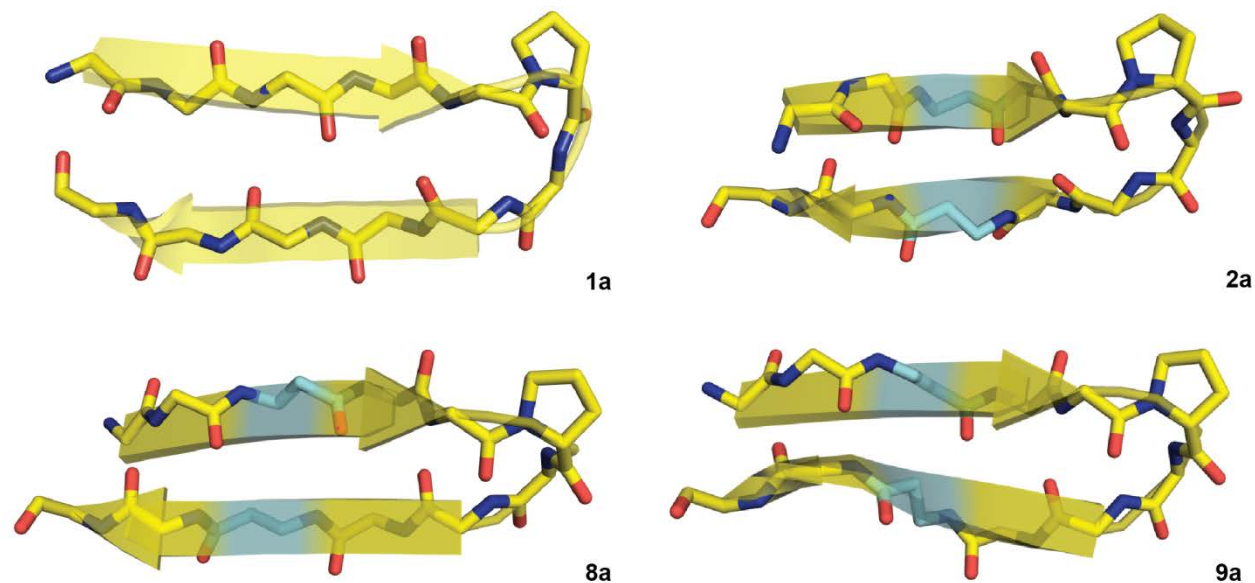


**Figure 20.** Average structures of peptides **1a**, **2a**, **8a**, and **9a**. Structures calculated from the average of 20 lowest energy conformations determined using NOE distance restraints from NMR. Samples consisted of ~1 mM solution of peptide and 0.1 M deuterated acetate buffer in 90% H<sub>2</sub>O/D<sub>2</sub>O, pH 3.8. Unnatural residues are shown in blue.

We overlaid the average coordinates of peptides **2a**, **8a**, and **9a** with **1a**, giving calculated RMSD values of 1.959, 1.540, and 1.740 Å, respectively (Figure 22). Peptide **2a**, relative to **1a**, has significant twisting of the backbone, likely due to the enhanced flexibility resulting from the unsubstituted methylene unit found in the  $\beta^3$ -residues. Introducing functionalization at this site, as in the case of an additional methyl group with the  $\beta^{2,3}$ -residues used (peptide **8a**), significantly decreases the RMSD of overlays as well as the twisting of the backbone, likely due to preorganization resulting from steric constraints of the  $C_\alpha$ - $C_\beta$  axis. Reversing the stereochemistry of the *syn*  $\beta^{2,3}$ -residue, as with the unnatural residue used in peptide **9a**, introduces a kink in the backbone, likely caused by a corresponding reversal in torsional preferences of the residue. Previous work has shown that incorporation of D- $\alpha$ -residues with similar stereochemistry to that of the monomer used in **9a** causes kinking in the backbone of  $\beta$ -sheets.<sup>115</sup>

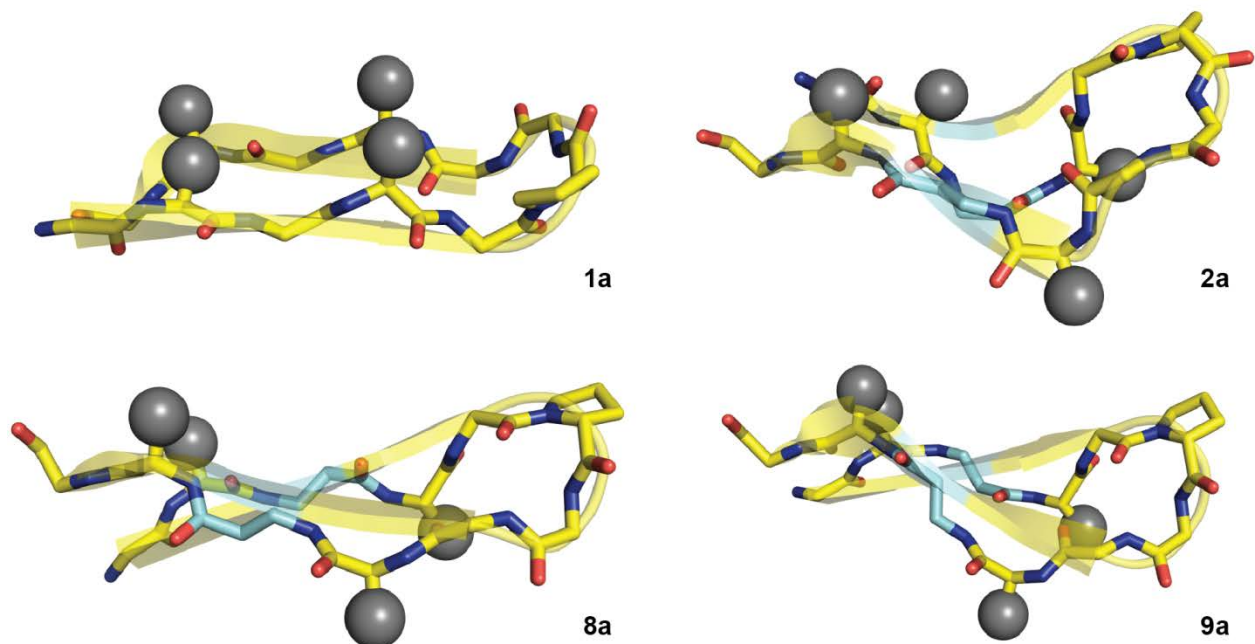


**Figure 21.** NMR solution structures of  $\alpha$ -peptide **1a** and  $\alpha/\beta$ -hybrid peptides **2a**, **8a**, and **9a**. Hydrophobic side chains are displayed as spheres.

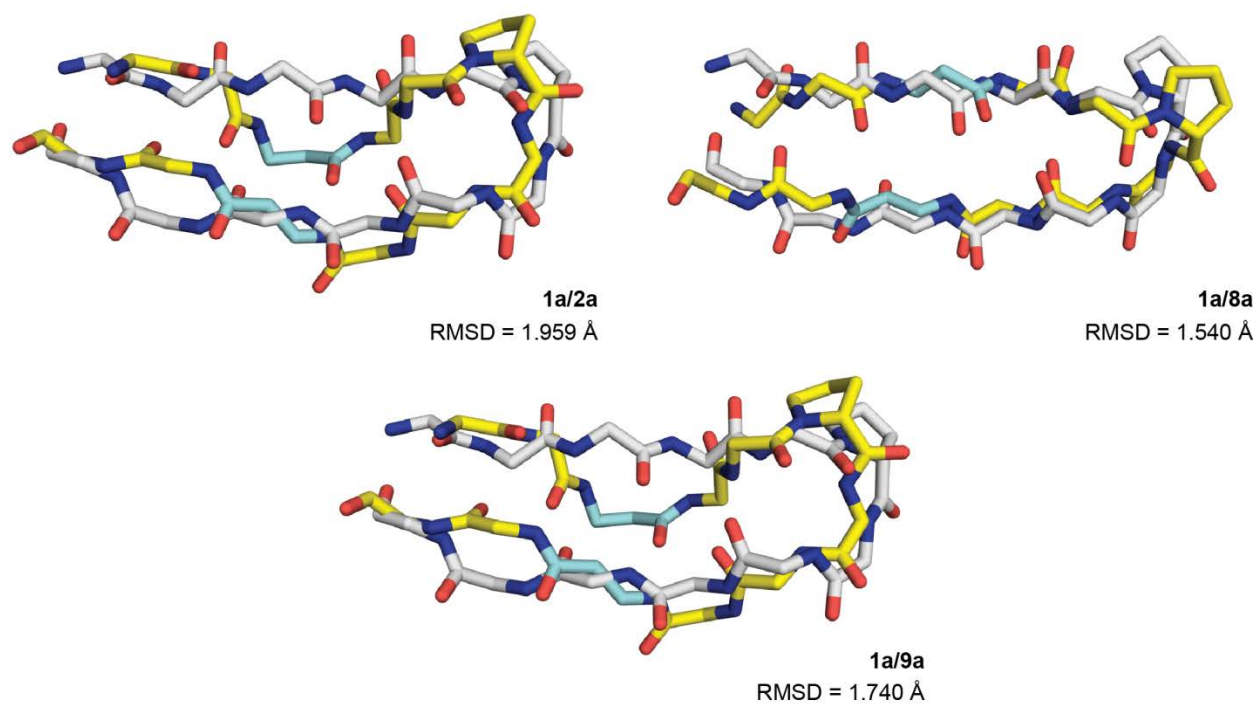


**Figure 22.** Overlays of NMR solution structures of  $\alpha$ -peptide **1a** (white) with  $\alpha/\beta$ -hybrid peptides **2a**, **8a**, and **9a** (yellow).

## 2.1.4 Analysis of 2:1 $\alpha$ - to $\beta$ -Residue Substitution Strategies

Based on the NOE analysis of the 16  $\alpha/\beta$ -hybrid peptides, three  $\beta$ -amino acids promoted folding: the  $\beta^3$ -amino acid with stereochemistry that mimics the natural L-configuration of  $\alpha$ -amino acids and both enantiomers of the *syn*  $\beta^{2,3}$ -amino acids used. Glycine separation and CSD analysis suggested that the two hybrids containing *syn*  $\beta^{2,3}$ -residues template hairpin formation most strongly and of the two, the peptide containing the monomer with a natural L-configuration most closely mimics the natural hairpin sequence.

These results suggest that the sheet propensities of acyclic  $\beta$ -amino acids are affected by the number of substituents in the  $\beta$ -residue backbone; functionalizing both carbon atoms in the backbone, as with an L-configured *syn*  $\beta^{2,3}$ -residue, increases the folded stability of the hairpin relative to a monosubstituted  $\beta^3$ -residue. The peptides including *anti*  $\beta^{2,3}$ -amino acids do not have hairpin folded structures, suggesting that in addition to number of substitutions, relative stereochemistry also plays an important role in the sheet propensity of  $\beta$ -residues. Backbone torsional preferences could be used to explain these differences in  $\beta$ -residue sheet propensities (Figure 23).

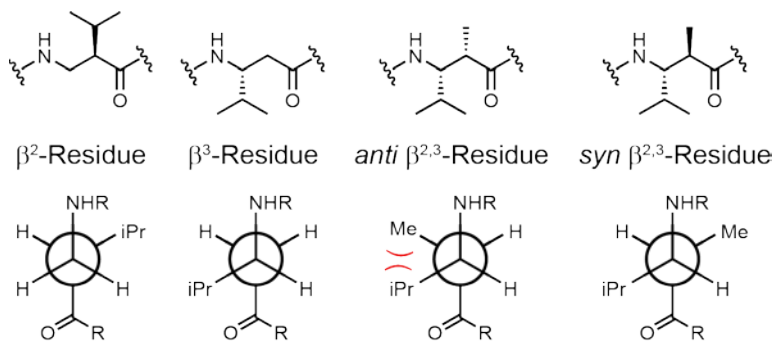


**Figure 23.** Extended conformations of acyclic  $\beta$ -residues and their resulting Newman projections. Newman projections are drawn along the C3-C2 bond.

Comparing the Newman projections of extended conformations (such as those found in a  $\beta$ -strand) along the C3-C2 bond of  $\beta^2$ - and  $\beta^3$ -residues shows only minor differences; both residues have

only one substituent and can therefore adopt extended conformations without creating gauche interactions, perhaps accounting for the low sheet propensity of these monomers. In the extended conformation, the position of the isopropyl moiety differs only in its position relative to the carbonyl carbon or amide nitrogen; the subtle change in steric repulsion between the isopropyl group and these two atoms may be enough to shift folded stability from marginally stable as with  $\beta^3$ -residue substitution to wholly unstable with  $\beta^2$ -residue substitution.

A less subtle difference is the folded stability of hairpins containing the *syn* versus *anti* configurations of  $\beta^{2,3}$ -residues. Newman projections show that to form an extended backbone conformation, *anti*  $\beta^{2,3}$ -residues force the isopropyl and methyl substituents gauche to one another. The *syn* configuration, however, allows these two substituents to orient in an anti relationship, thereby promoting an extended backbone conformation.

An important consequence of 1:1  $\alpha$ - to  $\beta$ -residue substitution with our chosen monomers is the inversion of the side chain and hydrogen bonding display of all residues beyond the site of unnatural residue insertion. This inversion is caused by the additional carbon atom found in the backbone of  $\beta$ -residues and can be seen when the backbones of these residues are found in an extended conformation. None of the acyclic  $\beta$ -residues were able to accommodate a conformation that would prevent an extended conformation and side chain inversion (Figure 24).

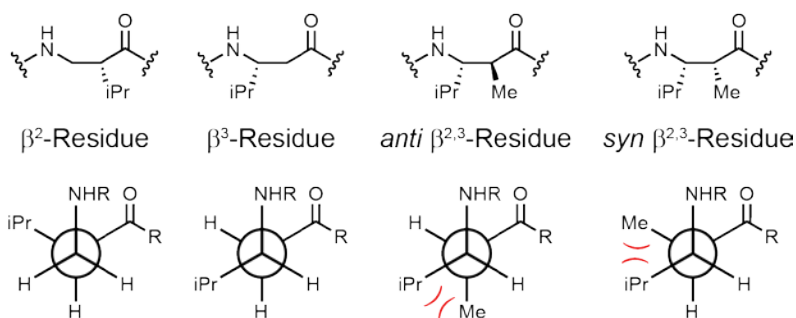


**Figure 24.** Bent conformations of acyclic  $\beta$ -residues and their resulting Newman projections. Newman projections are drawn along the C3-C2 bond.

Comparison of  $\beta^2$ - and  $\beta^3$ -residues once again shows a lack of any steric repulsion involving the isopropyl group. While these residues can adopt a “bent” conformation, they can also adopt the extended conformation described previously with less steric repulsion between the two R groups representing the peptide chain. Both the *syn* and *anti*  $\beta^{2,3}$ -residues experience significant steric hindrance in forming a bent conformation as the isopropyl and methyl groups are gauche in both cases. As the *syn*  $\beta^{2,3}$ -residue can adopt an extended conformation without this gauche interaction, an extended conformation is favored.

While close proximity of substituents in the case of  $\beta^{2,3}$ -residues can cause steric repulsion and prevent a bent conformation, it is not unreasonable to expect that restraining the side chain atoms in a ring could stabilize this conformation. It was somewhat unexpected, then, that none of the cyclic  $\beta$ -residues examined were able to promote hairpin formation. Upon closer examination, we saw that unlike  $\alpha$ -residues, the *trans* configuration of both ACPC and ACHC residues does not promote an extended conformation but instead acts similar to a turn promoter, forcing the two attached segments of the peptide chain closer together (Figure 25).  $\alpha/\beta$ -Residue hybrids containing *cis*-ACPC and *cis*-ACHC also discouraged hairpin formation. It is possible that the change in the directionality of the amide bonds connected to the unnatural residues disrupts sheet formation; relative to  $\alpha$ -residues, the amides found in *cis*-ACPC and *cis*-ACHC are forced closer together (Figure 26).

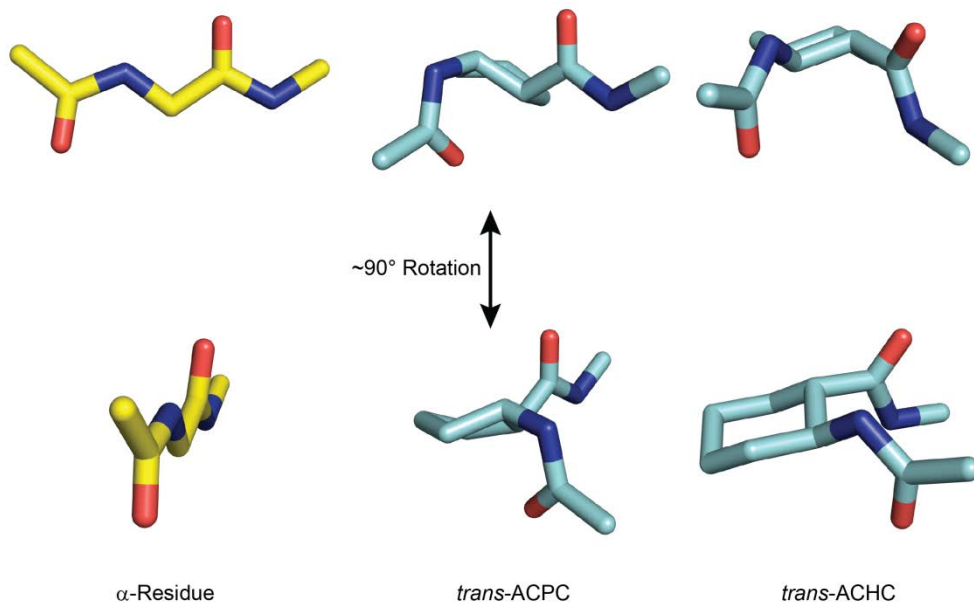


**Figure 25.** Two views of an  $\alpha$ -residue, *trans*-ACPC, and *trans*-ACHC.  $\alpha$ -Residues and  $\beta$ -residues are colored yellow and blue, respectively.

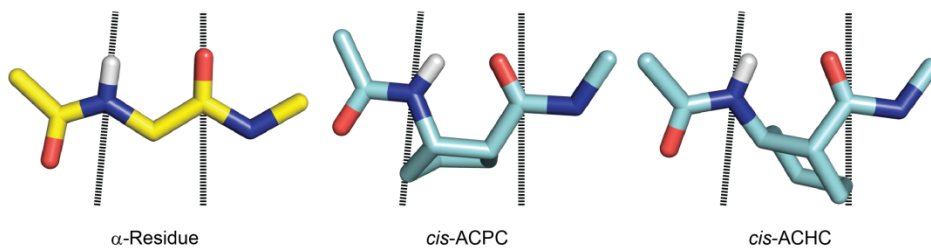


**Figure 26.** Front view of an  $\alpha$ -residue, *cis*-ACPC, and *cis*-ACHC.  $\alpha$ -Residues and  $\beta$ -residues are colored yellow and blue, respectively. Dotted lines highlight the deviation of cyclic  $\beta$ -residue amide directionality by showing the directionality found with  $\alpha$ -residues.

In summary, this work has shown that the backbone torsional preferences of  $\beta^3$ - or  $\beta^{2,3}$ -residues can promote hairpin formation in water, a solvent that does not typically support folded conformations of short peptides. This observation is however limited by a subtle change in side chain display.

## 2.2 2:1 OR 2:2 ALPHA- TO BETA-RESIDUE SUBSTITUTION

### 2.2.1 Design of Alpha- to Beta-Residue Substitution Strategies

As described in Chapter 2.1, application of a 1:1  $\alpha$ - to  $\beta$ -residue substitution strategy, while supportive of hairpin folding, caused inversion of hydrogen bonding and side chain display (Figure 27A). As this inversion could potentially disrupt the structure of larger proteins with more complex folding behavior, we sought alternative strategies for backbone modification. We hypothesized a 2:1  $\alpha$ - to  $\beta$ -residue substitution could be used (Figure 27B) without causing the inversion seen with a 1:1 substitution. This substitution strategy, essentially an amide deletion, would allow for retention of functionality from a single side chain with a  $\beta^2$ - or  $\beta^3$ -residue or both side chains with a  $\beta^{2,3}$ -residue substitution. Alternatively, the backbone could be lengthened using a 2:2  $\alpha$ - to  $\beta$ -residue substitution strategy (Figure 27C). Both side chain functionalities can be maintained using either a combination of  $\beta^2$ - and  $\beta^3$ - residues or a pair of *syn*  $\beta^{2,3}$ -residues. Use of *syn*  $\beta^{2,3}$ -residues in place of  $\beta^2$ - or  $\beta^3$ -residues allows incorporation of an extra methyl group, which should enforce an extended backbone conformation.

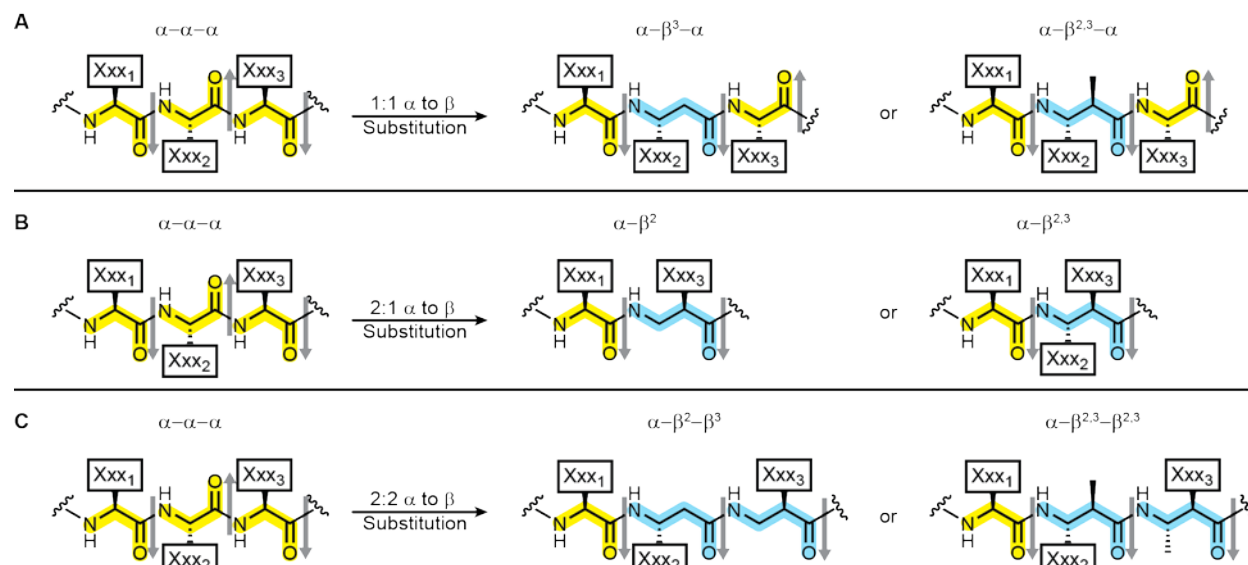


**Figure 27.** Possible  $\alpha$ - to  $\beta$ -residue substitution strategies.

A. 1:1  $\alpha$ - to  $\beta$ -residue substitution. B. 2:1  $\alpha$ - to  $\beta$ -residue substitution resulting in backbone contraction. C. 2:2  $\alpha$ - to  $\beta$ -residue substitution resulting in backbone expansion.

## 2.2.2 Selection of Hairpin Model System

Peptide **1a**, due to its small size and ease of synthesis, is useful for screens of unnatural backbone residues, but it is limited in several ways. While it is derived from the 16-residue C-terminal hairpin of GB1, peptide **1a** is a shorter 12-residue sequence; the natural Asp-Ala-Thr-Lys turn of peptide of GB1 is replaced by an unnatural D-Pro-Gly turn, modifying two residues while eliminating two more. D-Pro-Gly turns also display an increased glycine separation relative to what would be expected in natural turns as they enforce some degree of turn regardless of hairpin formation.<sup>109</sup> Because of these factors, a model system was sought after with several new requirements: 1) a length corresponding to that of the C-terminal hairpin of GB1, 2) a natural turn segment, and 3) a folded population of roughly 50% to accurately measure any thermodynamic changes affected by unnatural residue substitution.

The C-terminal hairpin fragment of GB1, peptide **18** (Figure 28), was synthesized and examined by NMR as it was previously reported to have a folded population of ~40% at 278 K.<sup>32</sup> We synthesized this peptide and collected NMR in aqueous buffer and found that, while meeting the guidelines for

selection as a model, this peptide demonstrated poor chemical shift dispersion of the threonine proton resonances, preventing their unambiguous assignment. As these signals are vital for determining folded population using CSD analysis, we were forced to look for a different model system.



**Figure 28.** Sequence of GB1 C-terminal fragment, peptide **18**.

We next analyzed peptide **19a** (Figure 29), a previously reported mutant of peptide **18** with a folded population of 86% at 298 K.<sup>41</sup> Additionally, we examined alanine mutant **20a**, where residues Thr<sub>4</sub> and Thr<sub>13</sub>, potential sites for backbone modification, were mutated to alanine to simplify monomer synthesis. As peptide **19a** has an innately high folded population, we also examined peptide **21a** with a reported folded population of 74% at 298 K,<sup>41</sup> and its alanine mutant, **22a**.

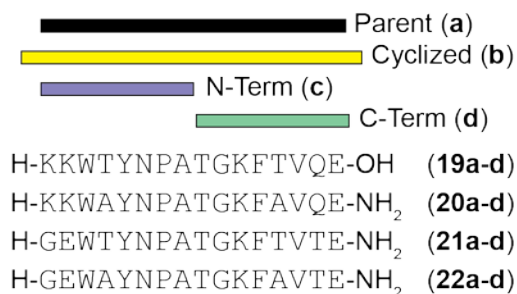


**Figure 29.** Model peptides **19a-22a** and their derivatives (**b-d**).

For each parent peptide (**a**), derivative **b** contains terminal cysteine residues connected via disulfide bridge, derivative **c** is an N-terminal fragment, and derivative **d** is a C-terminal fragment.

Unlike our previous study of single  $\alpha$ - to  $\beta$ -residue substitution, we wanted to quantify folded population. Both CSD and glycine separation analyses have been used to quantify population,<sup>110</sup> but both

of these methods require both fully-folded and fully-unfolded control peptides.<sup>111,112</sup> As folded control sequences, we modified peptides **19a-22a** to include terminal cysteine residues which were subsequently oxidized to create variants cyclized via a disulfide bond (**19b-22b**). Additionally, we prepared unfolded control peptides **19c-22c** and **19d-22d** by synthesizing 8-residue peptides derived from the N-terminal and C-terminal fragments, respectively, of the parent peptides.

We analyzed peptides **19-22** by NMR in aqueous buffer at 293 K and fully assigned the backbone proton chemical shifts. As detailed in Section 2.3.5, we used the chemical shifts for hydrogen-bonded residues remote from the turns to perform a CSD analysis and calculate folded populations (Table 1). Chemical shifts of non-hydrogen-bonded residues were not used as previous work has shown these chemical shifts are affected not only by folded structure, but also by side-chain interactions.<sup>112</sup> As each parent peptide also contained a glycine residue in the turn, glycine separation analysis was used separately to calculate folded populations.

**Table 1.** Folded populations of model peptides **19a-22a**.

Peptide	Folded Population	
	H <sub>α</sub> CSD	Gly H <sub>α</sub> /H <sub>α'</sub> Separation
<b>19a</b>	97 ± 6%	94 ± 6%
<b>20a</b>	66 ± 5%	68 ± 6%
<b>21a</b>	ND*	ND*
<b>22a</b>	55 ± 2%	64 ± 6%

\*Aggregation rendered this sample unfit for NMR analysis.

The folded populations determined by CSD and glycine separation analyses were identical within error. Peptide **19a** proved too well-folded for use as a model system for backbone modification. Peptide **21a** was also unfit for use as a model because aggregation-induced peak broadening in the NMR prevented population analysis. Both peptides **20a** and **22a** had similar folded populations within the range

we desired. We chose to use peptide **22a** for use as a model system as it exhibited more dispersion of chemical shift values due to a less homogeneous sequence than peptide **20a**.

### 2.2.3 Application of Beta-Residue Substitution Strategies to Model Hairpin System

In applying the design strategies discussed in Section 2.2.1 to peptide **20a**, two sites for  $\alpha$ - to  $\beta$ -residue substitution had to be selected. Three-residue sequences Trp<sub>3</sub>-Ala<sub>4</sub>-Tyr<sub>5</sub> and Phe<sub>12</sub>-Ala<sub>13</sub>-Val<sub>14</sub> were chosen as possible substitution sites as they are found in the center of each strand of the hairpin. Residues Ala<sub>4</sub> and Ala<sub>13</sub> are not found in the hydrophobic core and were therefore selected as the first mutation sites. Residue Tyr<sub>5</sub> was chosen for mutation over residue Trp<sub>3</sub> as the phenolic side-chain of tyrosine was more synthetically accessible than the indole containing side-chain of tryptophan. Phe<sub>12</sub>, the cross-strand partner of Tyr<sub>5</sub>, was chosen for the final site of mutation.

Four  $\alpha$ - to  $\beta$ -residue substitution strategies were applied using the four chosen sites described above to generate peptides **23a-26a** (Figure 30). A 2:1  $\alpha$ - to  $\beta$ -residue substitution was applied in Designs I and II while a 2:2  $\alpha$ - to  $\beta$ -residue substitution was applied in Designs III and IV. Design I eliminates the alanine side chain functionality found in Ala<sub>4</sub> and Ala<sub>13</sub> of the parent peptide while maintaining the side chains of hydrophobic core residues Tyr<sub>5</sub> and Phe<sub>12</sub>. Design II retains both the alanine and hydrophobic core side chain functionalities found in Ala<sub>4</sub>, Tyr<sub>5</sub>, Phe<sub>12</sub>, and Ala<sub>13</sub>. Design III maintains the presence of all four side chains while Design IV adds additional methyl groups to help promote an extended conformation. Once again, disulfide cyclized peptides (**23b-26b**) as well as N-terminal (**23c-26c**) and C-terminal (**23d-26d**) fragment peptides were synthesized for use as folded and unfolded controls, respectively. We synthesized each peptide using SPPS using Fmoc-protected monomers synthesized as described in Section 2.3.

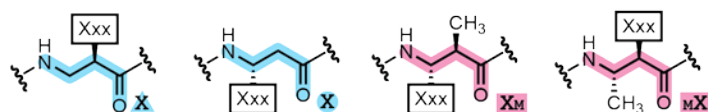
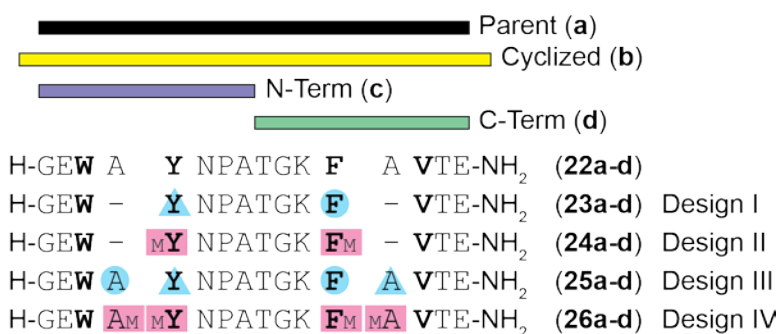


**Figure 30.** Peptides **22a-26a** and their derivatives (**b-d**).

For each parent peptide (**a**), derivative **b** contains terminal cysteine residues connected via disulfide bridge, derivative **c** is an N-terminal fragment, and derivative **d** is a C-terminal fragment.

#### 2.2.4 Structural Impact of 2:1 and 2:2 Alpha- to Beta-Residue Substitution

To determine if Designs I-IV were successful in preventing inversion of side chain and hydrogen-bond display in the hairpin peptides, cyclic peptides **22b-26b** were analyzed by 2D <sup>1</sup>H-NMR in aqueous buffer. Backbone H<sub>α</sub> and amide resonances were fully assigned for each peptide and cross-strand NOE's were examined (Figure 31).

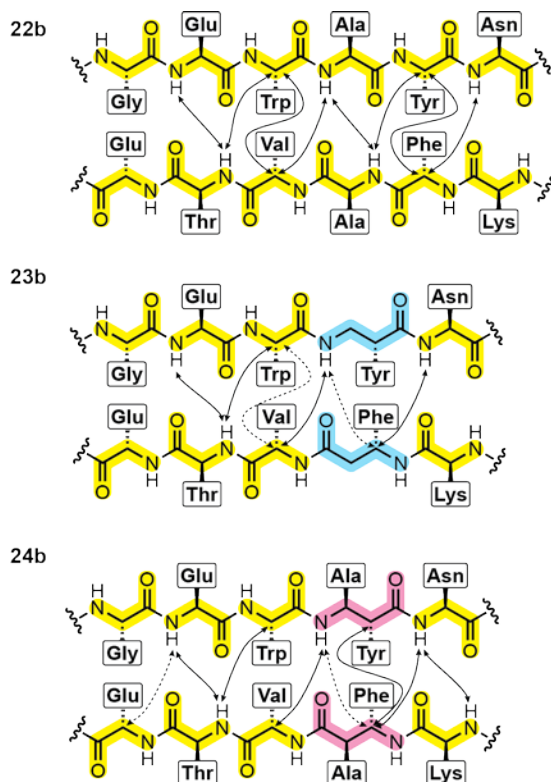


**Figure 31.** Cross-strand NOE's displayed by peptides **22b-24b**. Ambiguous assignments are shown as dotted lines. The termini and turns are removed for clarity.

Peptides **23b** and **24b**, like model peptide **22b**, displayed cross-strand NOE's across the backbone consistent with hairpin formation, suggesting Designs I and II are amenable to hairpin formation. Additionally, these cross-strand NOE's suggest that these designs can prevent inversion beyond the site of unnatural residue substitution. Design III, employed with peptide **25b**, showed no NOE's consistent with folding, leading us to believe the flexibility of the backbone imparted by use of two  $\beta^2$ - or  $\beta^3$ -residues in each strand significantly destabilizes the hairpin. Peptide **26b** was sparingly soluble in the pH 6.3 buffer solution used for analysis and did not have significant enough concentration to determine the presence of NOE's beyond sequential backbone NOE's.

As additional support for hairpin formation in peptides **23b** and **24b** and to determine if hairpin formation resulted with peptide **26b**, we performed glycine separation analysis of peptides **22b-26b** at 293 K in aqueous buffer (Figure 32).

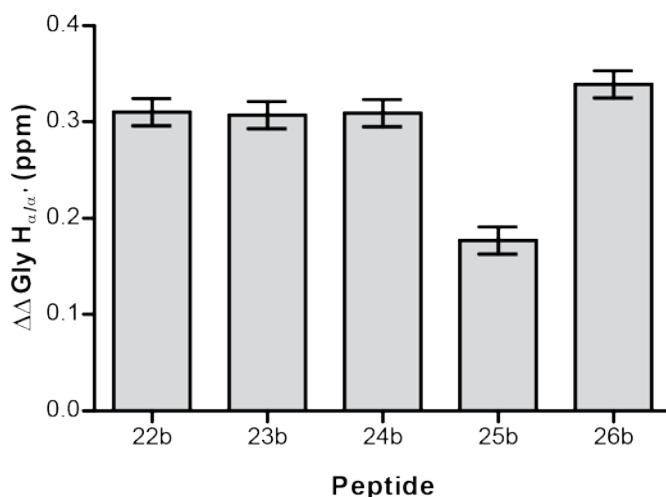


**Figure 32.** Glycine separation values of peptides **22b-26b**.

Peptides **22b-24b**, as expected from the NOE analysis, showed similar glycine separation values. Accordingly, peptide **25b**, which showed little NOE evidence of folding, showed a significantly decreased glycine separation value. Peptide **26b**, which was too dilute for NOE analysis, showed a similar glycine separation value to peptides **22b-26b**, suggesting it also has a hairpin formation. Based on these data, we concluded that Designs I, II, and IV could be used to foster hairpin formation.

Finally, to assess the full structural impact of these designs, we fully assigned the proton resonance for the peptides which showed NOE evidence of folding, **22b-24b**. As described in Section 2.3.4, NOE distance restraints were used in simulated annealing to generate low energy families of structures for each peptide. In the case of peptide **23b**, two families of structures, one depicting a hairpin structure, and the other a horseshoe shape with a significant kink in the backbone, were evident. We assigned the horseshoe conformation as a minor conformer brought upon by the presence of the disulfide linkage, not the presence of unnatural amino acid insertions. From the families of structures, average NMR structures for peptides **22b-24b** were generated (Figure 33).

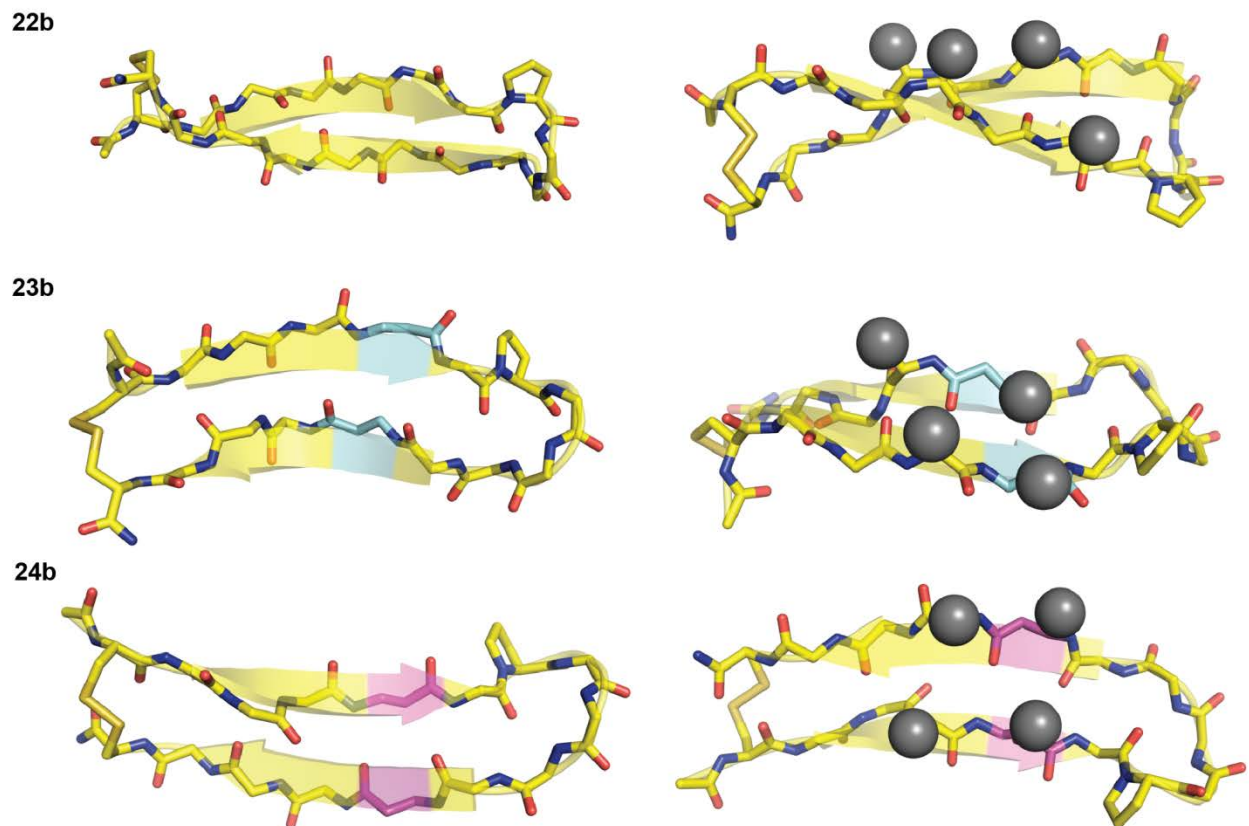


**Figure 33.** NMR solution structures of peptides **22b-24b** with hydrophobic side chains depicted as spheres. Structures calculated from the average of 10 lowest energy conformations determined using NOE distance restraints from NMR. Samples consisted of ~1 mM solution of peptide and 50 mM phosphate in 90% H<sub>2</sub>O/D<sub>2</sub>O, pH 6.3.  $\beta^2/\beta^3$ -Residues are colored cyan while  $\beta^{2,3}$ -residues are colored magenta.

In each case, hairpin structures can be clearly seen for peptides **22b-26b**. Overlays of the C<sub>α</sub> and C<sub>β</sub> atoms from the hydrophobic core residues of each peptide with those from the C-terminal hairpin of GB1 from which the sequence was derived gives RMSD values of 1.08, 1.03, and 1.80 Å for peptides **22b-24b**, respectively. These values suggest similar agreements in fit for the two hybrid peptides to the model peptide. The slightly better fit for **23b** relative to **24b** could arise from the increased flexibility in the backbone allowing the increased backbone length to be more easily accommodated into a more native-like fold. The side chains of the four hydrophobic core residues were displayed on the same face of the hairpin as well, suggesting Designs I and II can be used in sheets to prevent side chain inversion seen in 1:1 α- to β-residue substitutions.

### 2.2.5 Thermodynamic Impact of 2:1 and 2:2 Alpha- to Beta-Residue Substitution

Designs I, II, and IV suggested native-like folding behavior, so we sought to examine the thermodynamic impact of the backbone modification. Acyclic peptides **23a-26a** were synthesized and analyzed by NMR to determine the thermodynamic impact of Designs I-IV. As the folded populations calculated for peptides using CSD and glycine separation analysis were identical within error, glycine separation analysis was used to calculate folded populations for peptides **23a-26a** (Table 2). In this analysis, peptides **23b-26b** were used as folded controls while a value of 0 ppm was used for unfolded peptide glycine separation. From folded population data, values for  $\Delta G_{\text{fold}}$  were also calculated.

**Table 2.** Folded populations and  $\Delta G_{\text{fold}}$  for peptide **22a** and  $\alpha/\beta$ -Hybrid Peptides **23a-26a**.

Peptide	Folded Population (%)	$\Delta G_{\text{fold}}$ (kcal/mol)	$\Delta\Delta G_{\text{fold}}$ (kcal/mol) <sup>a</sup>
<b>22a</b>	$65 \pm 5$	$-0.35 \pm 0.13$	---
<b>23a</b>	$24 \pm 5$	$+0.65 \pm 0.15$	$+1.0 \pm 0.2$
<b>24a</b>	$17 \pm 5$	$+0.90 \pm 0.19$	$+1.4 \pm 0.2$
<b>25a</b>	<9	>1.3	>1.7
<b>26a</b>	$22 \pm 4$	$0.69 \pm 14$	$+1.0 \pm 0.2$

a. Values calculated versus  $\Delta G_{\text{fold}}$  of peptide **22a**.

Despite encouraging structural information from the cyclic variants, in each case, Designs I-IV destabilized the hairpin fold. Design III (**25a**) demonstrated minimal glycine separation, so a lower bound for the folded population based on the sensitivity on NMR measurements had to be used. Within error, the folded populations and relative values for  $\Delta\Delta G_{\text{fold}}$  of peptides **23a**, **24a**, and **26a** were identical. These data suggest Designs I, II, and IV are equally tolerated yet destabilizing in hairpin structures while Design III is not tolerated at all.

### 2.2.6 Conclusions

Of the four design strategies examined, three (a 2:1  $\alpha$ - to  $\beta^2/\beta^3$ -residue substitution, a 2:1  $\alpha$ - to  $\beta^{2,3}$ -residue substitution, and a 2:2  $\alpha$ - to  $\beta^{2,3}$ -residue substitution) were able to provide native-like folding behavior when applied to a model hairpin. Structurally, each of these strategies was able to prevent inversion seen when applying a 1:1  $\alpha$ - to  $\beta$ -residue substitution strategy, suggesting these strategies could be applied directly to a sheet in a larger tertiary fold.

Only one of the strategies assessed, a 2:2  $\alpha$ - to  $\beta^2/\beta^3$ -substitution, was unable to manifest native-like folding behavior. We attribute this instability to the lack of rigidity in the backbone that corresponds with  $\beta^2$ - and  $\beta^3$ -amino acids. While a single methylene unit can be tolerated in a hairpin (as with a 2:1  $\alpha$ - to  $\beta^2/\beta^3$ -residue substitution), adding an additional methylene unit in a 2:2 substitution abolishes folding.

Thermodynamically, the three strategies that allowed native-like folding behavior to occur were identical within error and each strategy resulted in destabilization of approximately 1 kcal/mol in total or 0.25 kcal/mol per  $\alpha$ -residue replaced. One potential cause for this destabilization is the amide deletion seen in the two 2:1  $\alpha$ - to  $\beta$ -residue substitution strategies which eliminates a hydrogen bond between the two strands (Figure 34).

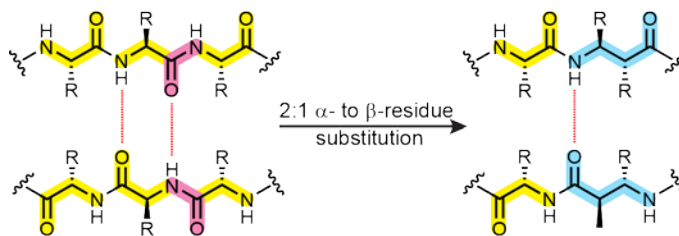


**Figure 34.** Amide deletion experience with 2:1  $\alpha$ - to  $\beta$ -residue substitution. Inter-strand hydrogen bonds are shown as red dotted lines.  $\alpha$ -Residues,  $\beta$ -residues, and deleted amide are shown as yellow, blue, and magenta, respectively.

The impact of hydrogen bond removal in a sheet depends on its location and the protein itself. One example shows that mutation of a hydrogen bond donor or acceptor in the peptide PIN WW, a three-stranded sheet, can decrease the folded stability by 1-5 kJ/mol, similar to the 1 kcal/mol decrease seen in our work.<sup>116</sup>

While the removal of a hydrogen bond can account for the destabilization with 2:1 substitution strategies, 2:2 substitution strategies maintain the same number of hydrogen bonds as the parent peptide. One alternative explanation for the destabilization seen in the 2:2  $\alpha$ - to  $\beta^{2,3}$ -residue substitution is the inclusion of a  $\beta^{2,3}$ -monomer with small methyl groups; perhaps increasing the bulk of the side chains would increase the steric hindrance to rotation and decrease the entropic penalty to folding.

Overall, unnatural residue substitution strategies utilizing 2:1  $\alpha$ - to  $\beta^2/\beta^3$ -residue substitution, 2:1  $\alpha$ - to  $\beta^{2,3}$ -residue substitution, or 2:2  $\alpha$ - to  $\beta^{2,3}$ -residue substitution may be useful for preventing inversion

in a protein with a larger tertiary fold, but in doing so could cause a significant destabilization of the folded structure.

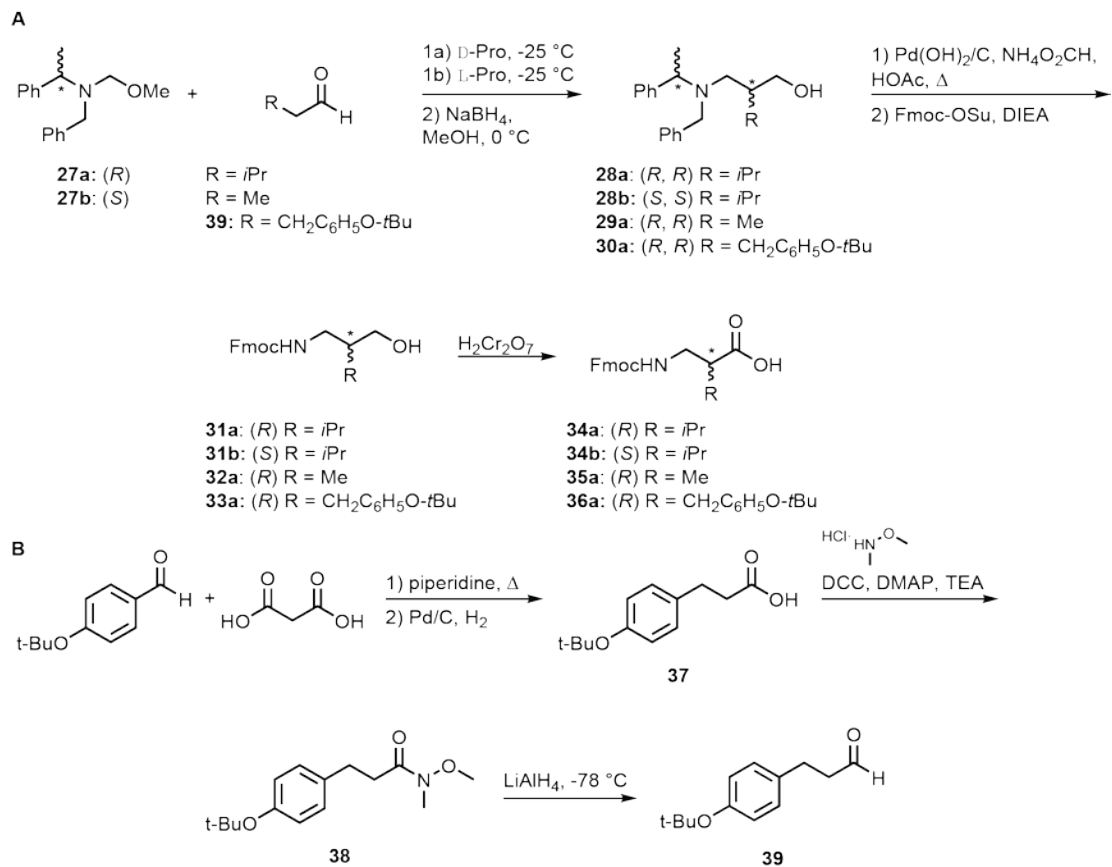
## 2.3 EXPERIMENTAL

### 2.3.1 Monomer Synthesis

#### 2.3.1.1 General Information

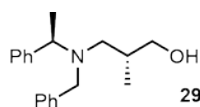
Optical rotations were measured on a Perkin-Elmer 241 digital polarimeter with a sodium lamp at ambient temperature. NMR spectra of synthetic intermediates and final monomer products were recorded on a Bruker Avance-300 or Bruker Avance-400 spectrometer. Anhydrous ether was distilled over solid sodium and benzophenone. Anhydrous dichloromethane was distilled over solid calcium hydride. Propionyl chloride was distilled prior to use. Lithium iodide was weighed out in a glove bag under nitrogen atmosphere and stored under nitrogen until use. Flash chromatography was performed using Silicycle SiliaFlash P60 (230-400 mesh) or SorbTech silica gel (60 Å, 40-63 µm). Both *trans* 2-amino-1-cyclopentanecarboxylic acid (ACPC) monomers,<sup>88</sup> *trans* 2-amino-1-cyclohexanecarboxylic acid (ACHC) monomers,<sup>89</sup> and *O*-trimethylsilylquinidine (TMS-quinidine) and *O*-trimethylsilylquinine (TMS-quinine),<sup>90</sup> were synthesized using a published route.

### 2.3.1.2 Synthesis of Fmoc-β<sup>2</sup>-Monomers



**Scheme 2.1.** Synthesis of Fmoc-β<sup>2</sup>-monomers.

Compounds **27a** and **27b** were synthesized from commercially available aldehydes using previously published protocols.<sup>91,92</sup> Compounds **30a**, **33a**, and **36a** were synthesized from precursor compound **39** using previously published protocols.<sup>91</sup>

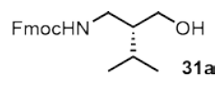


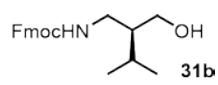
**(R,R)  $\beta^2$ -Ala Alcohol (29a):**<sup>91,92</sup> To 10 mL DMF under nitrogen was added 184 mg D-proline (1.59 mmol, 0.2 equiv). The solution was stirred 2 h and then cooled to  $-25$  °C. To this solution was added 1.15 mL propionaldehyde (16.0 mmol, 2 equiv) and the reaction was stirred 15 minutes, followed by addition of 1.969 g compound **27a** (7.71 mmol, 1 equiv) in 1 mL DMF. The reaction mixture was stirred 24 h at  $-25$  °C and then warmed to 0 °C. To the solution was added 918 mg sodium borohydride (24.3 mmol, 3 equiv) followed by slow addition of 10 mL methanol. The reaction was stirred for 30 minutes, quenched with 20 mL saturated aqueous ammonium chloride solution, and extracted three times with 50 mL diethyl ether. The organics were washed once with water, washed three times with brine, dried with magnesium sulfate, and then concentrated. The concentrate was purified using column chromatography (5% ethyl acetate in hexanes) and dried under vacuum to afford the product as a colorless oil (972 mg, 3.43 mmol, 43% yield).  $[\alpha]_D = -39.7$  ( $c = 1.00$ ,  $\text{CHCl}_3$ ).  $^1\text{H NMR}$  (400 MHz,  $\text{CDCl}_3$ )  $\delta$  7.23-7.38 (m, 10 H), 4.03 (q,  $J = 7.0$  Hz, 1 H), 3.95 (d,  $J = 13.2$  Hz, 1 H), 3.51 (m, 1 H), 3.38 (d,  $J = 13.1$  Hz, 1 H), 3.02 (dd,  $J = 10.5, 8.8$  Hz, 1 H), 2.47 (m, 2 H), 2.11 (m, 1 H), 1.36 (d,  $J = 6.8$  Hz, 3 H), 0.69 (d,  $J = 6.8$  Hz, 3 H);  $^{13}\text{C NMR}$  (100 MHz,  $\text{CDCl}_3$ )  $\delta$  142.7, 138.9, 129.4, 128.7, 128.3, 127.4, 127.2, 70.0, 56.3, 56.0, 55.1, 37.2, 15.3, 9.5). HRMS  $m/z$  calculated for  $\text{C}_{19}\text{H}_{26}\text{NO}$   $[\text{M}+\text{H}]^+$  284.2014; found 284.1987.

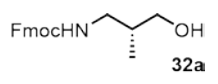
**Standard Procedure A.**<sup>92</sup> [This procedure was later optimized to improve the efficiency of the hydrogenolysis step. This updated procedure is detailed following this procedure.] To a stirred solution of alcohol precursor (1 equiv) in methanol (0.3 M) was added ammonium formate (10 equiv) and 10 wt% Pd/C (20% w/w). The solution was refluxed 5 h, filtered through Celite, and concentrated. The

concentrate was dissolved in dichloromethane (0.3 M) and to this solution was added Fmoc-OSu (1 equiv) and DIEA (1 equiv) with stirring. The reaction was stirred 1 h, then diluted with 100 mL ethyl acetate. The organics were washed with aqueous 5% sodium bisulfate, aqueous 5% sodium bicarbonate, and brine. The organic layer was dried with magnesium sulfate, concentrated, and purified using column chromatography to afford the product.

**Optimized hydrogenolysis:** To a stirred solution of alcohol (1 equiv) in methanol (0.1 M) was added ammonium formate (20 equiv), glacial acetic acid (1 equiv), and 20 wt% Pd(OH)<sub>2</sub>/C (20% w/w). The solution was refluxed overnight, filtered through Celite, and concentrated to afford the free amine.

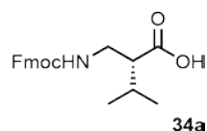
 **Fmoc-(R)- $\beta^2$ -Val Alcohol (31a):** Standard Procedure A was followed using 320 mg compound **28a** (1.03 mmol), 649 mg ammonium formate (10.3 mmol), 198 mg 10 wt% Pd/C, 179  $\mu$ L DIEA (1.03 mmol), and 347 mg Fmoc-OSu (1.03 mmol). Column chromatography (33% ethyl acetate in hexanes) provided a mixture of product and residual Fmoc-OSu which was used directly without further purification.

 **Fmoc-(S)- $\beta^2$ -Val Alcohol (31b):** Standard Procedure A was followed using 485 mg compound **28b** (1.56 mmol), 983 mg ammonium formate (15.6 mmol), 300 mg 10 wt% Pd/C, 271  $\mu$ L DIEA (1.56 mmol), and 526 mg Fmoc-OSu (1.56 mmol). Column chromatography (33% ethyl acetate in hexanes) provided a mixture of product and residual Fmoc-OSu which was used directly without further purification.

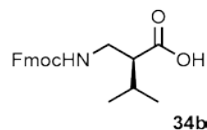
 **Fmoc-(R)- $\beta^2$ -Ala Alcohol (32a):** Standard Procedure A was followed using 972 mg compound **29a** (3.43 mmol), 2.149 g ammonium formate (34.1 mmol), 104 mg 10 wt% Pd/C, 590  $\mu$ L

DIEA (3.39 mmol), and 1.151 g Fmoc-OSu (3.41 mmol). For the hydrogenolysis, *t*-butanol was used in place of dichloromethane as solvent and the solution refluxed overnight. Column chromatography (33% → 50% ethyl acetate in hexanes) provided 367 mg (~1.18 mmol) of a mixture of product and 5% 9-fluorenemethanol byproduct which was used directly without further purification.

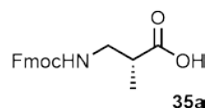
**Standard Procedure B.**<sup>92</sup> To a stirred solution of sodium dichromate in water (1 M) was added concentrated sulfuric acid to a final concentration of 4 M. The solution was then diluted with water to a final concentration of 0.5 M sodium dichromate and 2 M sulfuric acid. To a stirred solution of Fmoc-amino alcohol (1 equiv) in acetone (0.1 M) at 0°C was added Jones reagent solution (2 equiv) slowly. The solution was allowed to warm to room temperature and stirred for 2 h after which isopropanol was added and the reaction allowed to stir for an additional 2 h. The solution was then diluted with ethyl acetate and washed with aqueous 5% sodium bisulfate. The organics were dried with magnesium sulfate, concentrated, and purified using column chromatography to afford the product.



**Fmoc-(*R*)-β<sup>2</sup>-Val-OH (**34a**):** Standard Procedure B was followed using compound **31a** (~1.03 mmol), 10 mL acetone, and 4 mL Jones Reagent. Column chromatography (25% → 33% ethyl acetate in hexanes) afforded the product as a white solid (172 mg, 0.49 mmol, 47% yield over 3 steps). NMR data matched previously published results.<sup>6</sup>  $[\alpha]_D = -3.1$  ( $c = 1.00$ , CHCl<sub>3</sub>),  $[\alpha]_D = -17.1^\circ$  ( $c = 1.00$ , MeOH).

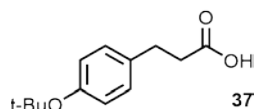


**Fmoc-(*S*)-β<sup>2</sup>-Val-OH (**34b**):** Standard Procedure B was followed using compound **31b** (~1.56 mmol), 10 mL acetone, and 4 mL Jones Reagent. Column chromatography (25% → 33% ethyl acetate in hexanes) afforded the product as a white solid (160 mg, 0.45 mmol, 29% yield over 3 steps). NMR data matched previously published results.<sup>6</sup>  $[\alpha]_D = +3.3$  ( $c = 1.00$ , CHCl<sub>3</sub>).



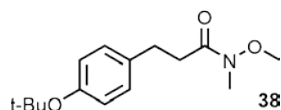
**Fmoc-(R)- $\beta^2$ -Ala-OH (35a):** Standard Procedure B was followed using compound

**32a** (~1.18 mmol), 12 mL acetone, and 4.7 mL Jones Reagent. Column chromatography (20%  $\rightarrow$  50%  $\rightarrow$  100% ethyl acetate in hexanes) afforded to product as a white solid (233 mg, 0.716 mmol, 21% yield over 3 steps). Spectra matched previously reported results.<sup>93</sup>  $[\alpha]_D = -10$  ( $c = 1.00$ ,  $\text{CHCl}_3$ ),  $[\alpha]_D = -5.6$  ( $c = 1.00$ ,  $\text{CH}_2\text{Cl}_2$ ),  $[\alpha]_{D, \text{Lit}} = -10.85$  ( $c = 0.273$ ,  $\text{CH}_2\text{Cl}_2$ ).  $[\alpha]_{D, \text{Lit}} = +9.6$  ( $c = 1.00$ ,  $\text{CHCl}_3$ ) for the enantiomer.<sup>94</sup>



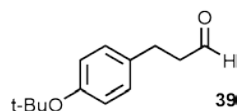
**3-(4-(*tert*-butoxy)phenyl)propanoic acid (37):**<sup>28</sup> To a solution of 4.89 mL 4-(*tert*-

butoxy)-benzaldehyde (28.1 mmol, 1 equiv) in 80 mL pyridine was added 4.38 g malonic acid (42.1 mmol, 1.5 equiv). 830  $\mu\text{L}$  piperidine (8.40 mmol, 0.3 eq) was added dropwise and the solution was refluxed for 3 h. The solution was then acidified with 1 M hydrochloric acid and extracted three times with ethyl acetate. The organics were combined, dried with magnesium sulfate, and concentrated under vacuum to yield the alkene addition product which was used directly. To a solution of alkene (28.1 mmol, 1 equiv) in 100 mL anhydrous THF was added 500 mg 10 wt% Pd/C (10% w/w). The reaction was stirred under a hydrogen balloon 16 h, filtered through Celite, washed with dichloromethane and methanol, and concentrated. The concentrate was purified using column chromatography (10%  $\rightarrow$  20%  $\rightarrow$  50% ethyl acetate in hexanes) and dried under vacuum to afford the product as a white solid (4.29 g, 19.3 mmol, 69% yield over two steps).  $^1\text{H}$  NMR (400 MHz,  $\text{DMSO-d}_6$ )  $\delta$  12.35 (s, 1 H), 7.11 (d,  $J = 8.3$  Hz, 2 H), 6.86 (d,  $J = 8.4$  Hz, 2 H), 2.76 (t,  $J = 7.8$  Hz, 2 H), 2.48 (t,  $J = 7.7$  Hz, 2 H), 1.26 (s, 9 H);  $^{13}\text{C}$  NMR (100 MHz,  $\text{CDCl}_3$ )  $\delta$  153.7, 135.3, 128.7, 124.4, 78.5, 36.2, 30.2, 28.9. HRMS  $m/z$  calculated for  $\text{C}_{13}\text{H}_{17}\text{O}_3$   $[\text{M}-\text{H}]^-$  221.1178; found 221.1167.



**3-(4-(*tert*-butoxy)phenyl)-*N*-methoxy-*N*-methylpropanamide (38):**<sup>95</sup> To a solution of 1.066 g compound **37** (4.796 mmol, 1 equiv) in 12 mL

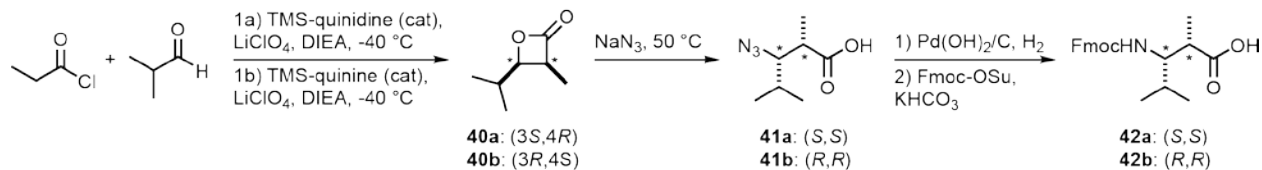
dichloromethane under nitrogen at 0 °C was added 657 mg *N,O*-dimethylhydroxylamine hydrochloride (6.74 mmol, 1.4 equiv), 940 μL triethylamine (6.74 mmol, 1.4 equiv), 824 mg 4-dimethylaminopyridine (6.74 mmol, 1.4 equiv), and 1.384 g *N,N'*-dicyclohexylcarbodiimide (6.708 mmol, 1.4 equiv). The solution was stirred for 16 h, and then filtered through Celite, eluting with ethyl acetate. The filtrate was washed sequentially with 1 M hydrochloric acid and saturated aqueous sodium bicarbonate. The organics were dried with magnesium sulfate and concentrated. The concentrate was purified using column chromatography (20% ethyl acetate in hexanes), and dried under vacuum to afford the product as a pale yellow oil (1.23 g, 4.64 mmol, 97% yield). <sup>1</sup>H NMR (400 MHz, CDCl<sub>3</sub>) δ 7.05 (d, *J* = 8.3 Hz, 2 H), 6.84 (d, *J* = 8.4 Hz, 2 H), 3.51 (s, 3 H), 3.10 (s, 3 H), 2.86 (t, *J* = 8.2 Hz, 2 H), 2.66 (t, *J* = 7.2 Hz, 2 H), 1.26 (s, 9 H); <sup>13</sup>C NMR (100 MHz, CDCl<sub>3</sub>) δ 173.5, 153.3, 135.9, 128.5, 124.0, 77.8, 60.9, 33.6, 31.9, 29.8, 28.6. HRMS *m/z* calculated for C<sub>15</sub>H<sub>24</sub>NO<sub>3</sub> [M+H]<sup>+</sup> 266.1576; found 266.1578.



**3-(4-(*tert*-butoxy)phenyl)propanal (39):**<sup>96</sup> To a solution of 4.969 g compound **38** (18.73 mmol, 1 equiv) in 75 mL anhydrous THF under nitrogen at -78 °C was

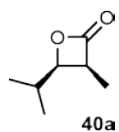
added 1.41 g lithium aluminum hydride (37.2 mmol, 2 equiv). The solution was stirred for 3 h and then quenched by pouring into a mixture of 200 mL water/ice. The mixture was filtered through Celite, eluting with dichloromethane. The filtrate was then extracted three times with dichloromethane. The organics were combined, dried with magnesium sulfate, and concentrated to yield the crude aldehyde which was used directly.

### 2.3.1.3 Synthesis of *anti* Fmoc- $\beta^{2,3}$ -Monomers

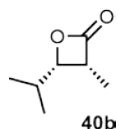


**Scheme 2.2.** Synthesis of *anti* Fmoc- $\beta^{2,3}$ -monomers.

**Standard Procedure C.**<sup>97</sup> To a stirred solution of 2.12 g lithium perchlorate (19.9 mmol, 2 equiv) in 10 mL anhydrous ether was added *O*-trimethylsilyl-quinine or *O*-trimethylsilyl-quinidine (400 mg, 1 mmol, 0.1 equiv) and 20 mL anhydrous dichloromethane. The reaction mixture was cooled to  $-40\text{ }^{\circ}\text{C}$  and 4.36 mL DIEA (25.0 mmol, 2.5 equiv) and 920  $\mu\text{L}$  isobutyraldehyde (10 mmol, 1 equiv) were added to the solution. A solution of 1.74 mL propionyl chloride (19.9 mmol, 2 equiv) in 5 mL anhydrous dichloromethane was added dropwise to the reaction over the course of 3 h after which time the reaction was allowed to stir at  $-40\text{ }^{\circ}\text{C}$  for 16 h. After this time, 20 mL of ether was added to the solution and the resulting mixture was filtered through a silica plug, washing with ether. The solution was concentrated at a light vacuum (as the product is volatile) and the concentrate was purified using column chromatography (10% ether in pentane).

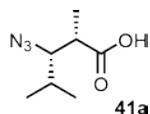


**(3*S*,4*R*)-4-isopropyl-3-methyloxetan-2-one (40a):** Standard Procedure C was employed using *O*-trimethylsilyl-quinidine to afford the product as a colorless oil (~4.56 mmol, 46% yield) which was used directly.  $^1\text{H NMR}$  (300 MHz,  $\text{CDCl}_3$ )  $\delta$  4.11 (dd,  $J = 6.07, 10.63$  Hz, 1 H), 3.73 (m, 1 H), 2.00 (m, 1 H), 1.34 (d,  $J = 7.97$  Hz, 3 H), 1.08 (d,  $J = 6.45$  Hz, 3 H), 0.93 ( $J = 6.83$  Hz, 3 H).

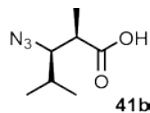


**(3R,4S)-4-isopropyl-3-methyloxetan-2-one (40b):** Standard Procedure C was employed using *O*-trimethylsilyl-quinine to afford the product as a colorless oil (~3.61 mmol, 36% yield) which was used directly.  $^1\text{H NMR}$  (300 MHz,  $\text{CDCl}_3$ )  $\delta$  4.12 (dd,  $J = 6.07, 10.63$  Hz, 1 H), 3.72 (m, 1 H), 2.00 (m, 1 H), 1.34 (d,  $J = 7.59$  Hz, 3 H), 1.08 (d,  $J = 6.45$  Hz, 3 H), 0.92 (d,  $J = 6.83$  Hz, 3 H).

**Standard Procedure D.**<sup>98</sup> To a stirred solution of sodium azide (2 equiv) in DMSO (0.6 M) was added lactone (1 equiv). The reaction mixture was stirred at 50 °C for 48 h, then allowed to cool to room temperature. 8 mL of saturated aqueous sodium bicarbonate was added to the solution, then water was added until all salts were dissolved. The aqueous layer was washed twice with ethyl acetate then acidified with 1 M hydrochloric acid. The acidified aqueous layer was then extracted three times with ethyl acetate. The organics were combined, washed twice with water, washed twice with brine, dried over sodium sulfate, concentrated, and dried under vacuum to afford the product.



**(2S,3S)-3-azido-2,4-dimethylpentanoic acid (41a):** Standard Procedure D was employed using 595 mg sodium azide (9.16 mmol) in 15.2 mL anhydrous DMSO and compound **40a** (~4.58 mmol). Drying under vacuum afforded the product as a colorless oil (523 mg, 3.06 mmol, 67% yield).  $[\alpha]_{\text{D}} = +11$  ( $c = 1.0$ ,  $\text{CHCl}_3$ ).  $^1\text{H NMR}$  (400 MHz,  $\text{CDCl}_3$ )  $\delta$  3.43 (dd,  $J = 4.52, 4.27, 9.03$  Hz, 1 H), 2.66 (m, 1 H), 2.01 (m, 1 H), 1.24 (d,  $J = 7.28$  Hz, 3 H), 1.09 (d,  $J = 6.78$  Hz, 3 H), 0.91 (d,  $J = 6.78$  Hz, 3 H);  $^{13}\text{C NMR}$  (100 MHz,  $\text{CDCl}_3$ )  $\delta$  180.0, 70.6, 42.4, 29.6, 20.6, 15.8, 14.6. HRMS  $m/z$  calculated for  $[\text{C}_7\text{H}_{13}\text{N}_3\text{O}_2]$  177.1008; found 171.1003.

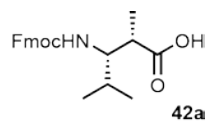


**(2R,3R)-3-azido-2,4-dimethylpentanoic acid (41b):** Standard Procedure D was employed using 468 mg sodium azide (7.20 mmol) in 12 mL anhydrous DMSO and compound **40b** (~3.61 mmol). Drying under vacuum afforded the product as a colorless oil (466 mg, 2.72 mmol, 75%

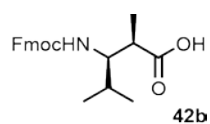
yield).  $[\alpha]_D = -12$  ( $c = 1.0$ ,  $\text{CHCl}_3$ ).  $^1\text{H NMR}$  (400 MHz,  $\text{CDCl}_3$ )  $\delta$  3.43(dd,  $J = 4.77, 4.27, 9.03$  Hz, 1 H), 2.66 (m, 1 H), 2.01 (m, 1 H), 1.24 (d,  $J = 7.03$  Hz, 3 H), 1.09 (d,  $J = 6.78$  Hz, 3 H), 0.91 (d,  $J = 6.78$  Hz, 3 H);  $^{13}\text{C NMR}$  (100 MHz,  $\text{CDCl}_3$ )  $\delta$  179.9, 70.6, 42.4, 29.6, 20.6, 15.8, 14.6. HRMS  $m/z$  calculated for  $[\text{C}_7\text{H}_{12}\text{N}_3\text{O}_2]$  170.0930; found 170.0938.

**Standard Procedure E.**<sup>98,99</sup> To a stirred solution of azido acid (1 equiv) in methanol (0.02 M) was added 20 wt%  $\text{Pd}(\text{OH})_2/\text{C}$  (25% w/w) under nitrogen. The vessel was evacuated, fitted with a hydrogen-filled balloon, and stirred for 24 h. The solution was then filtered through celite, washed with methanol, concentrated, and purified using column chromatography to afford the product.

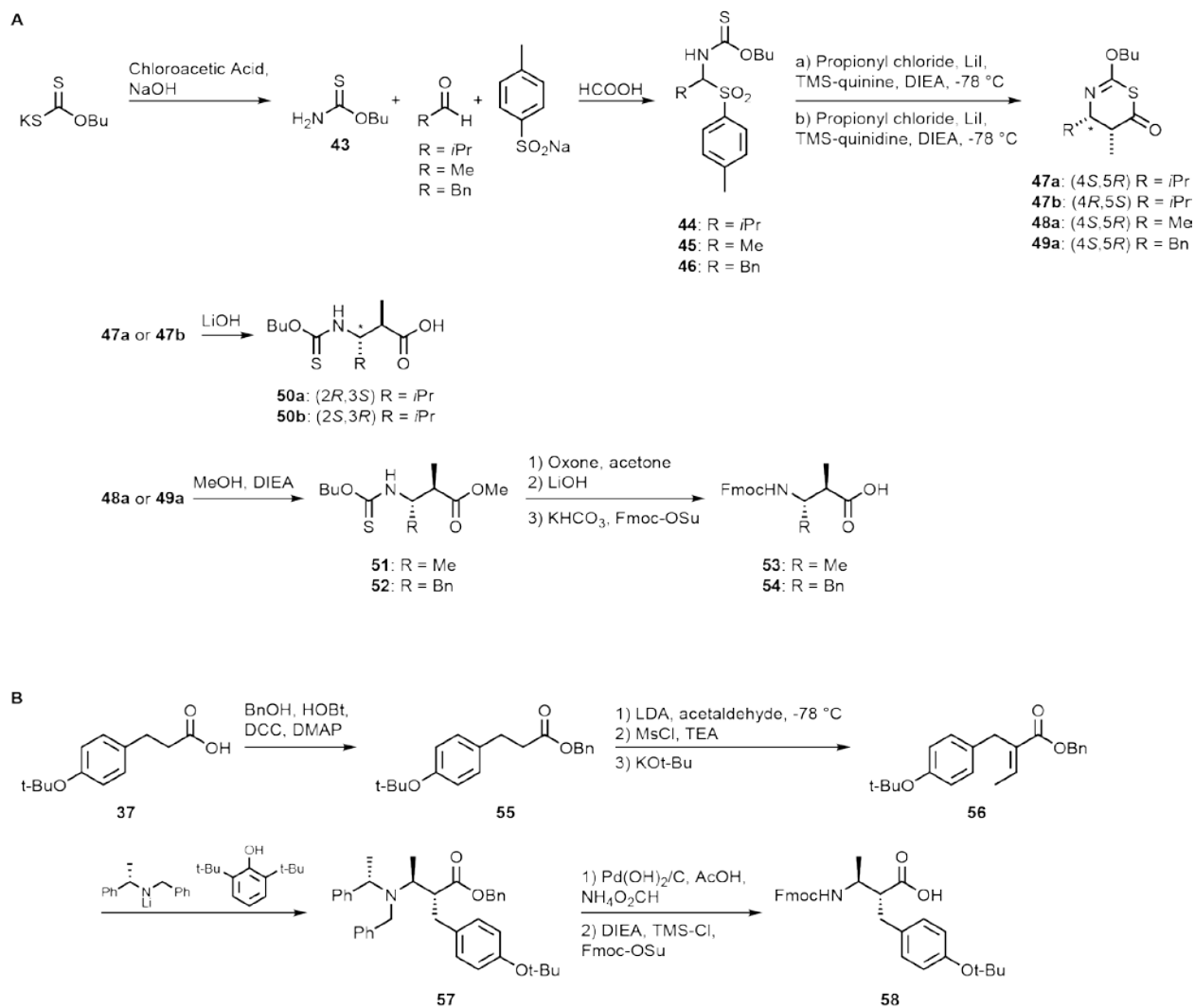
**Standard Procedure F.**<sup>99</sup> To a stirred solution of amine (1 equiv) in water (0.8 M) was added potassium bicarbonate (1 or 2 equiv) and Fmoc-OSu (1 equiv) solution in acetone (0.8 M). The reaction was stirred 48 h, then acidified 1 M hydrochloric acid. The mixture was then extracted three times with ethyl acetate. The organic layers were combined, dried with magnesium sulfate, and concentrated. The concentrate was purified using column chromatography and dried under vacuum to afford the product.

 **(2S,3S)-3-Fmoc-amino-2,4-dimethylpentanoic acid (42a):** Standard Procedure E was employed using 125 mg compound **41a** (0.73 mmol), 31 mL methanol, and 31 mg 20 wt%  $\text{Pd}(\text{OH})_2/\text{C}$ . Standard Procedure F was then employed using the resultant amino acid (0.73 mmol), 0.9 mL water, 100 mg sodium bicarbonate (0.73 mmol), 245 mg Fmoc-OSu (0.73 mmol), and 0.9 mL acetone. Column chromatography (10% ethyl acetate in hexanes  $\rightarrow$  33% ethyl acetate in hexanes with 1% acetic acid) afforded a mixture of 9-fluorenylmethanol and the product as a white foam (85 mg, 0.23 mmol, 32% yield over 2 steps).  $[\alpha]_D = -23$  ( $c = 1.0$ ,  $\text{CHCl}_3$ ). This compound exists as a series of conformers in slow exchange on the NMR timescale.  $^1\text{H NMR}$  of main conformer (400 MHz,  $\text{DMSO-d}_6$ )

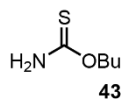
$\delta$  12.18 (s, 1 H), 7.89 (d,  $J = 7.53$  Hz, 2 H), 7.71 (t,  $J = 7.78$  Hz, 2 H), 7.41 (t,  $J = 7.53$  Hz, 2 H), 7.32 (qd,  $J = 7.52, 0.97$  Hz, 2 H), 7.03 (d,  $J = 9.79$  Hz, 1 H), 4.24 (m, 3 H), 3.55 (qd,  $J = 7.03, 2.76$  Hz, 1 H), 2.54 (m, 1 H), 1.81 (m, 1 H), 1.04 (d,  $J = 7.03$  Hz, 3 H), 0.84 (d,  $J = 6.78$  Hz, 3 H), 0.80 (d,  $J = 6.78$  Hz, 3 H);  $^{13}\text{C}$  NMR (100 MHz,  $\text{CDCl}_3$ )  $\delta$  176.65, 156.55, 144.45, 144.28, 141.17, 128.08, 127.55, 127.51, 125.83, 125.74, 120.57, 65.78, 58.24, 47.26, 42.07, 29.45, 20.49, 17.77, 14.76. HRMS  $m/z$  calculated for  $[\text{C}_{22}\text{H}_{24}\text{NO}_4]$  366.1705; found 366.1718.


**(2R,3R)-3-Fmoc-amino-2,4-dimethylpentanoic acid (42b):** Standard Procedure E was employed using 233 mg compound **41b** (1.36 mmol), 58 mL methanol, and 20 wt% 58 mg  $\text{Pd}(\text{OH})_2/\text{C}$ . Standard Procedure F was then employed using the resultant amino acid (1.36 mmol), 4 mL water, 136 mg sodium bicarbonate (1.36 mmol), 456 mg Fmoc-OSu (1.36 mmol), and 4 mL acetone. Column chromatography (10% ethyl acetate in hexanes  $\rightarrow$  33% ethyl acetate in hexanes with 1% acetic acid) afforded the product as a white foam (207 mg, 0.563 mmol, 41% yield over 2 steps).  $[\alpha]_D = +18$  ( $c = 1.0, \text{CHCl}_3$ ). This compound exists as a series of conformers in slow exchange on the NMR timescale.  $^1\text{H}$  NMR of main conformer (400 MHz,  $\text{DMSO-d}_6$ )  $\delta$  12.18 (s, 1 H), 7.89 (d,  $J = 6.04$  Hz, 2 H), 7.71 (t,  $J = 6.78$  Hz, 2 H), 7.41 (t,  $J = 7.20$  Hz, 2 H), 7.32 (qd,  $J = 6.78, 0.64$  Hz, 2 H), 7.02 (d,  $J = 10.06$  Hz, 1 H), 4.24 (m, 3 H), 3.55 (qd,  $J = 8.68, 1.87$  Hz, 1 H), 2.54 (m, 1 H), 1.81 (m, 1 H), 1.04 (d,  $J = 6.36$  Hz, 3 H), 0.84 (d,  $J = 6.83$  Hz, 3 H), 0.80 (d,  $J = 6.59$  Hz, 3 H);  $^{13}\text{C}$  NMR (100 MHz,  $\text{CDCl}_3$ )  $\delta$  178.18, 156.07, 143.96, 143.79, 140.69, 127.59, 127.06, 127.02, 125.35, 125.26, 120.08, 65.30, 57.75, 46.78, 41.59, 28.96, 20.00, 17.27, 14.26. HRMS  $m/z$  calculated for  $[\text{C}_{22}\text{H}_{24}\text{NO}_4]$  366.1739; found 366.1705.

### 2.3.1.4 Synthesis of *syn* Fmoc- $\beta^{2,3}$ -Monomers

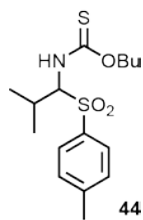


**Scheme 2.3.** Synthesis of *syn* Fmoc- $\beta^{2,3}$ -monomers.

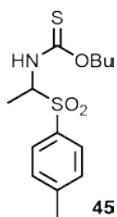


**O-butyl carbamothioate (43):**<sup>100</sup> To a stirred solution of 13.6 g chloroacetic acid (144 mmol, 1 equiv) in 130 mL water at 0 °C was added 5.76 g sodium hydroxide (144 mmol, 1 equiv). To this solution was added a solution of 27.1 g potassium butyl xanthate (144 mmol, 1 equiv) in 130 mL water and the reaction stirred overnight. After this time, 11.67 mL 28% aqueous ammonium hydroxide (173 mmol, 1.2 equiv) was added and the solution stirred overnight, then extracted five times with ether. The organic layers were combined, dried with magnesium sulfate, and concentrated afford the product as a colorless oil (17.129 g, 129 mmol, 89% yield). <sup>1</sup>H NMR (400 MHz, CDCl<sub>3</sub>) δ 7.08 (s, 1 H), 6.27 (s, 1 H), 4.34 (t, *J* = 6.78 Hz, 2 H), 1.62 (m, 2 H), 1.33 (m, 2 H), 0.88 (t, *J* = 7.53 Hz, 3H); <sup>13</sup>C NMR (100 MHz, CDCl<sub>3</sub>) δ 192.69, 71.61, 30.53, 18.95, 13.69. HRMS *m/z* calculated for [C<sub>10</sub>H<sub>23</sub>N<sub>2</sub>O<sub>2</sub>] (2M+H)<sup>+</sup> 267.1201; found 267.1225.

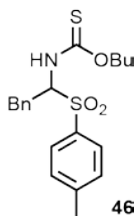
**Standard Procedure G:**<sup>101</sup> To a stirred solution of compound **43** (1 equiv) in water (0.9 M) was added sodium *para*-toluenesulfinate (1.2 equiv), aldehyde (1.2 equiv), and formic acid (6.9 equiv). This solution was allowed to stir for 48-72 h during which the product was formed as an oil or precipitate. The product was then isolated via extraction and concentrated under vacuum.



**Isopropyl Sulfone (44):** Standard Procedure G was employed using 7.0 g compound **43** (53 mmol), 60 mL water, 12.25 g sodium *para*-toluenesulfinate (63.1 mmol), 5.76 mL isobutyraldehyde (63.1 mmol), and 13.7 mL formic acid (362 mmol). After 48 h, the solution was diluted with 150 mL dichloromethane. The organics were washed twice with water, washed once with brine, dried over magnesium sulfate, and concentrated to afford the product as a white solid (16.173 g, 47.1 mmol, 90% yield). This compound exists as a series of conformers in slow exchange on the NMR time scale; NMR spectra are attached in Appendix D. HRMS *m/z* calculated for [C<sub>16</sub>H<sub>25</sub>NO<sub>3</sub>NaS<sub>2</sub>] 366.1198; found 366.1192.



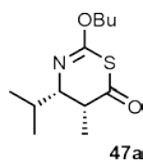
**Methyl Sulfone (45):** Standard Procedure G was employed using 2.66 g compound **43** (20.0 mmol), 23 mL water, 4.66 g sodium *para*-toluenesulfinate (24.0 mmol), 1.40 mL acetaldehyde (25.0 mmol), and 5.20 mL formic acid (138 mmol). The reaction was stirred for 48 h to afford the product as an oil. The product was dissolved in dichloromethane and washed twice with water and twice with brine. The organics were dried with magnesium sulfate, concentrated, and dried under vacuum to afford the product as a colorless oil (5.64 g, 17.9 mmol, 89% yield). This compound exists as a series of conformers in slow exchange on the NMR time scale; NMR spectra are attached in Appendix D. HRMS  $m/z$  calculated for  $C_{14}H_{21}NO_3NaS_2$   $[M+Na]^+$  338.0861; found 338.0870.



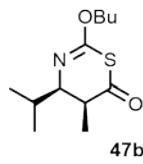
**Benzyl Sulfone (46):** Standard Procedure G was employed using 1.726 g compound **43** (12.96 mmol), 15 mL water, 3.00 g sodium *para*-toluenesulfinate (15.4 mmol), 1.80 mL phenylacetaldehyde (15.4 mmol), and 3.40 mL formic acid (90.1 mmol). The reaction was stirred for 72 h to afford the product as a white precipitate. The precipitate was filtered off, dissolved in ether, and washed nine times with water to remove excess aldehyde. The organics were dried with magnesium sulfate, concentrated, and dried under vacuum to afford the product as a pale yellow oil (2.15 g, 5.49 mmol, 42% yield). This compound exists as a series of conformers in slow exchange on the NMR time scale; NMR spectra are attached in Appendix D. HRMS  $m/z$  calculated for  $C_{20}H_{25}NO_3S_2K$   $[M+K]^+$  430.0913; found 430.0925.

**Standard Procedure H:**<sup>101</sup> To a stirred solution of sulfone (1 equiv) in anhydrous dichloromethane (0.1 M) under nitrogen was added TMS-quinine or TMS-quinidine (0.4 or 0.7 equiv). The solution was cooled to  $-78$  °C and DIEA (3.5 equiv) was added followed by addition of a solution of lithium iodide (0.7 equiv) in ether (0.2 M). A solution of propionyl chloride (0.5 equiv) in anhydrous dichloromethane (1.8 M) was added dropwise over 20 minutes after which the solution was allowed to stir 1 h. Addition of lithium iodide and propionyl chloride solutions followed by reaction time of 1 h was repeated an

additional four times after which the reaction was allowed to stir at  $-78\text{ }^{\circ}\text{C}$  for 16 h. The solution was then quenched with acetic acid in ether (10% v/v) and washed three times with saturated ammonium chloride solution. The aqueous washes were combined and extracted with ether. The ether and organic layers were combined, washed three times with brine, run through a silica plug, eluting with ether, and concentrated. The concentrate was purified using column chromatography and dried under vacuum.

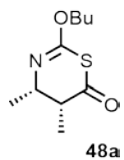


**(4S,5R) Isopropyl Thiazinone (47a):** Standard Procedure H was employed using 1.02 g compound **44** (2.96 mmol), 470 mg TMS-quinine (1.18 mmol, 0.4 equiv), 26 mL anhydrous dichloromethane, 188 mL DIEA (10.8 mmol), 1.25 g lithium iodide (9.35 mmol), 18 mL ether, and 650  $\mu\text{L}$  propionyl chloride (7.5 mmol). The crude reaction mixture was purified using column chromatography (0.5% ethyl ether in pentane) to afford a mixture of the product and ketene dimer. The impure mixture was dried under vacuum to eliminate any residual ketene dimer, affording the product as a yellow oil (67 mg, 0.28 mmol) that was used directly.  $^1\text{H}$  NMR (300 MHz,  $\text{CDCl}_3$ )  $\delta$  4.29 (t,  $J = 6.8$  Hz, 2 H), 3.03 (dd,  $J = 3.02, 9.63$  Hz, 1 H), 2.77 (qd,  $J = 2.83, 7.18$  Hz, 1H), 1.92 (m, 1 H), 1.70 (m, 2 H), 1.43 (m, 2 H), 1.11 (d,  $J = 6.61$  Hz, 3 H), 1.02 (d,  $J = 7.18$  Hz), 0.96 (t,  $J = 7.18$  Hz, 3 H), 0.95 (d,  $J = 6.61$  Hz, 3 H).

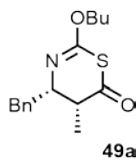


**(4R,5S) Isopropyl Thiazinone (47b):** Standard Procedure H was employed using 1.13 g compound **44** (3.28 mmol), 520 mg TMS-quinidine (1.31 mmol), 28 mL anhydrous dichloromethane, 2.08 mL DIEA (11.9 mmol), 1.25 g lithium iodide (9.35 mmol), 18 mL ether, and 720  $\mu\text{L}$  propionyl chloride (8.3 mmol). The crude reaction mixture was purified using column chromatography (0.5% ethyl ether in pentane) to afford a mixture of the product and ketene dimer. The impure mixture was dried under vacuum to eliminate any residual ketene dimer, affording the product as a yellow oil (160 mg, 0.66 mmol) that was used directly.  $^1\text{H}$  NMR (300 MHz,  $\text{CDCl}_3$ )  $\delta$  4.29 (t,  $J = 6.61$  Hz, 2 H), 3.03 (dd,  $J = 3.02, 9.63$  Hz, 1 H), 2.77 (qd,  $J = 2.83, 7.18$  Hz, 1H), 1.92 (m, 1 H), 1.70 (m, 2 H),

1.43 (m, 2 H), 1.11 (d,  $J = 6.61$  Hz, 3 H), 1.02 (d,  $J = 7.18$  Hz), 0.96 (t,  $J = 7.18$  Hz, 3 H), 0.95 (d,  $J = 6.61$  Hz, 3 H).

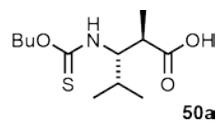


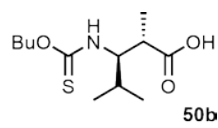
**(4S,5R) Isopropyl Thiazinone (48a):** Standard Procedure H was employed using 867 mg compound **45** (2.75 mmol), 500 mg TMS-quinine (1.26 mmol, 0.4 equiv), 100 mL dichloromethane, 1.70 mL DIEA (9.76 mmol), 1.25 g lithium iodide (9.33 mmol), and 600  $\mu$ L propionyl chloride (6.88 mmol). Column chromatography (1% diethyl ether in hexanes) afforded the product as a colorless oil (149 mg, 0.692 mmol, 25% yield).  $^1\text{H}$  NMR (400 MHz,  $\text{CDCl}_3$ )  $\delta$  4.20 (m, 2 H), 3.88 (m, 1 H), 2.62 (m, 1 H), 1.66 (m, 2 H), 1.39 (m, 2 H), 1.15 (d,  $J = 7.0$  Hz, 3 H), 1.10 (d,  $J = 7.0$  Hz, 3 H), 0.93 (t,  $J = 7.4$  Hz, 3 H);  $^{13}\text{C}$  NMR (100 MHz,  $\text{CDCl}_3$ )  $\delta$  199.7, 154.4, 68.4, 55.0, 46.0, 30.7, 19.2, 13.9, 10.5).  $[\alpha]_{\text{D}} = -31.3$  ( $c = 1.00$ ,  $\text{CHCl}_3$ ). HRMS  $m/z$  calculated for  $[\text{C}_{13}\text{H}_{24}\text{NO}_2\text{S}]$  258.1528; found 258.1538.



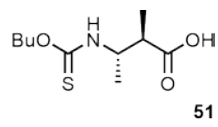
**(4S,5R) Benzyl Thiazinone (49a):** Standard Procedure H employed using 1.07 g compound **46** (2.73 mmol), 750 mg TMS-quinine (1.89 mmol, 0.7 equiv), 100 mL dichloromethane, 1.70 mL DIEA (9.76 mmol), 1.25 g lithium iodide (9.33 mmol), and 600  $\mu$ L propionyl chloride (6.88 mmol). Column chromatography (1% diethyl ether in hexanes) afforded a mixture of the product (~260 mg, 0.892 mmol) and a coeluting contaminant as a colorless oil which was used directly.

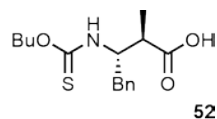
**General Procedure I:**<sup>102</sup> To a stirred solution of thiazinone (1 equiv) in THF (0.04 M) was added a solution of lithium hydroxide (3 equiv) in water. The reaction vessel was stirred overnight and then acidified to pH 2 with 1 M hydrochloric acid and extracted three times with dichloromethane. The organics were combined and washed twice with brine, dried over magnesium sulfate, and concentrated. The concentrate was purified using column chromatography (20% ethyl acetate in hexanes  $\rightarrow$  50% ethyl acetate in hexanes) to afford the product.


**(4*S*,5*R*) Isopropyl Thiocarbamate (50a):** Standard Procedure I was employed using 67 mg compound **47a** (0.28 mmol), 6.4 mL THF, 19 mg lithium hydroxide (0.82 mmol) and 3.2 mL water to afford the product as yellow crystals (58 mg, 0.22 mmol, 7.5% over two steps).  $[\alpha]_D = +20$  ( $c = 1.0$ ,  $\text{CHCl}_3$ ). This compound exists as a series of conformers in slow exchange on the NMR timescale; NMR spectra are attached in Appendix D. HRMS  $m/z$  calculated for  $[\text{C}_{12}\text{H}_{22}\text{NO}_3\text{S}]$  260.1320; found 260.1340.


**(4*R*,5*S*) Isopropyl Thiocarbamate (50b):** Standard Procedure I was employed using 160 mg compound **47b** (0.66 mmol), 15.6 mL THF, 46 mg lithium hydroxide (2.0 mmol) and 7.66 mL water to afford the product as yellow crystals (144 mg, 0.55 mmol, 17% over two steps).  $[\alpha]_D = -17$  ( $c = 1.0$ ,  $\text{CHCl}_3$ ). This compound exists as a series of conformers in slow exchange on the NMR timescale; NMR spectra are attached in Appendix D. HRMS  $m/z$  calculated for  $[\text{C}_{12}\text{H}_{22}\text{NO}_3\text{S}]$  260.1320; found 260.1328.

**Standard Procedure J:**<sup>101</sup> To a stirred solution of thiazinone (1 equiv) in methanol (0.1 M) under nitrogen was added DIEA (1.5 equiv). The reaction was stirred overnight then concentrated. The concentrate was purified using column chromatography and dried under vacuum to afford the product.

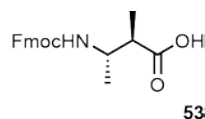

**(4*S*,5*R*) Methyl Thiocarbamate (51):** Standard Procedure J was employed using 149 mg compound **48a** (0.692 mmol), 7 mL methanol, and 182  $\mu\text{L}$  DIEA (1.04 mmol). Column chromatography (5% ethyl acetate in hexanes) afforded the product as a colorless oil. This compound exists as a series of conformers in slow exchange on the NMR time scale; NMR spectra are attached in Appendix D.  $[\alpha]_D = -37.1$  ( $c = 1.00$ ,  $\text{CHCl}_3$ ). HRMS  $m/z$  calculated for  $[\text{C}_{11}\text{H}_{21}\text{NO}_3\text{S}]$  270.1140; found 270.1162.



**(4S,5R) Benzyl Thiocarbamate (52):** Standard Procedure J was employed using

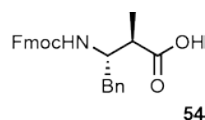
~260 mg compound **49a** (0.804 mmol), 9 mL methanol, and 230  $\mu$ L DIEA (1.35 mmol). Column chromatography (5% ethyl acetate in hexanes) afforded the product as a colorless oil (76 mg, 0.25 mmol, 9.1% yield over 2 steps). This compound exists as a series of conformers in slow exchange on the NMR time scale; NMR spectra are attached in Appendix D.  $[\alpha]_D = -27.8$  ( $c = 1.00$ ,  $\text{CHCl}_3$ ). HRMS  $m/z$  calculated for  $\text{C}_{17}\text{H}_{26}\text{NO}_3\text{S}$   $[\text{M}+\text{H}]^+$  324.1656; found 324.1633.

**Standard Procedure K:**<sup>101</sup> To a stirred solution of thiocarbamate (1 equiv) in 2:1:1 acetone/water/THF (0.25 M) under nitrogen at 0 °C was added Oxone (1.5 equiv). The reaction was stirred for 30 minutes at 0 °C, stirred at room temperature for 2.5 h, and then quenched by adjusting the pH to 11 using saturated aqueous sodium carbonate solution. The organics were removed under reduced pressure and the resulting aqueous solution was saturated using sodium chloride and extracted 6 times with chloroform. The organics were combined, dried with magnesium sulfate, and concentrated to afford the crude amino ester which was used directly. To a stirred solution of amino ester (1 equiv) in 1:1 THF/water (0.1 M) under nitrogen at 0 °C was added lithium hydroxide (2 equiv). The reaction was allowed to stir overnight at room temperature, and then acidified to pH 4 with 1 M hydrochloric acid. The organics were removed under reduced pressure to afford the crude amino acid salt in aqueous solution which was used directly. To a stirred solution of amino acid salt in 1:1 acetone/water (0.1 M) under nitrogen was added potassium bicarbonate (1 or 2 equiv), and Fmoc-OSu (1 equiv). The solution was stirred 48 h, acidified with 1 M hydrochloric acid, and extracted with three times ethyl acetate. The organics were combined, dried with magnesium sulfate, and concentrated. The concentrate was purified using column chromatography and dried under vacuum to afford the product.



**Fmoc-(2R,3S)-3-amino-2-methylbutanoic acid (53):** Standard Protocol K was

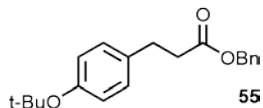
employed using 210 mg compound **51** (0.849 mmol), 6.4 mL 2:1:1 acetone/water/THF, 791 mg Oxone (1.28 mmol), 10 mL 1:1 THF/water, 40 mg lithium hydroxide (1.7 mmol), 14 mL 1:1 acetone/water, 83 mg potassium bicarbonate (0.85 mmol), and 287 mg Fmoc-OSu (0.851 mmol). Column chromatography (10% → 50% → 67% ethyl acetate in hexanes) afforded the product as a white solid (192 mg, 0.566 mmol, 67% yield over 3 steps). <sup>1</sup>H NMR (400 MHz, DMSO-d<sub>6</sub>) δ 12.24 (s, 1 H), 7.89 (d, *J* = 7.4 Hz, 2 H), 7.69 (d, *J* = 7.2 Hz, 2 H), 7.41 (t, *J* = 7.4 Hz, 2 H), 7.33 (t, *J* = 7.5 Hz, 2 H), 7.19 (d, *J* = 9.2 Hz, 1 H), 4.34 (m, 1 H), 4.25 (m, 2 H), 3.65 (m, 1 H), 2.32 (m, 1 H), 1.04 (d, *J* = 6.4 Hz, 3 H), 0.99 (d, *J* = 6.9 Hz, 3 H); <sup>13</sup>C NMR (100 MHz, DMSO-d<sub>6</sub>) δ 176.0, 156.7, 143.9, 140.7, 138.8, 127.6, 127.0, 125.2, 125.1, 120.1, 65.1, 48.6, 46.8, 45.0, 19.2, 14.2. [α]<sub>D</sub> = +2.3 (*c* = 0.50, acetone). HRMS *m/z* calculated for C<sub>20</sub>H<sub>22</sub>NO<sub>4</sub> [M+H]<sup>+</sup> 340.1549; found 340.1555.



**Fmoc-(2R,3S)-3-amino-2-methyl-4-phenylbutanoic acid (54):** Standard Procedure K

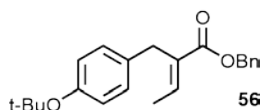
was employed using 221 mg compound **52** (0.683 mmol), 2.8 mL 2:1:1 acetone/water/THF, 655 mg Oxone (1.07 mmol), 8 mL 1:1 THF/water, 33 mg lithium hydroxide (1.4 mmol), 8 mL 1:1 acetone/water, 140 mg potassium bicarbonate (1.40 mmol), and 264 mg Fmoc-OSu (0.783 mmol). Column chromatography (20% → 50% ethyl acetate in hexanes) afforded a mixture of the product (178 mg, 0.41 mmol, 59% yield over 3 steps) and 9-fluorene-methanol (5 mol% by NMR) as a white solid. An analytically pure sample was obtained by dissolving the entire sample in 40 mL *tert*-butyl methyl ether. This solution was extracted four times with saturated aqueous sodium carbonate solution. The aqueous layers were combined and acidified using concentrated hydrochloric acid. The aqueous solution was then extracted 3 times with ethyl acetate. The organics were combined, dried with magnesium sulfate, and concentrated to yield the pure product as a white solid. <sup>1</sup>H NMR (400 MHz, DMSO-d<sub>6</sub>) δ 12.32 (s, 1 H), 7.88 (d, *J* = 7.5 Hz, 2 H), 7.61 (d, *J* = 7.4 Hz, 2 H), 7.40 (t, *J* = 7.40 Hz, 2 H), 7.30 (q, *J* = 7.7 Hz, 2 H), 7.18 (m, 5 H), 4.17 (m, 2 H), 4.10 (m, 1 H), 3.88 (m, 1 H), 2.67 (m, 2 H), 2.42 (m, 1 H), 1.04 (d, *J* = 7.0 Hz, 3 H); <sup>13</sup>C NMR (100 MHz, DMSO-d<sub>6</sub>) δ 176.1, 155.8, 143.8, 140.7, 138.8,

129.0, 128.1, 127.6, 127.0, 126.0, 125.2, 120.1, 65.1, 54.4, 46.7, 43.9, 38.5, 13.6.  $[\alpha]_D = -39.7$  ( $c = 1.00$ , acetone). HRMS  $m/z$  calculated for  $C_{26}H_{25}NO_4Na$   $[M+Na]^+$  438.1681; found 438.1678.



**Benzyl 3-(4-(*tert*-butoxy)phenyl)propanoate (55):** To a stirred solution of 4.966 g compound **37** (22.35 mmol), 1 equiv) in 50 mL dichloromethane under nitrogen

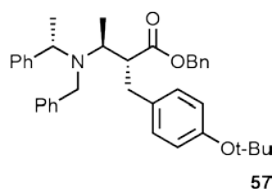
was added 6.885 g hydroxybenzotriazole monohydrate (45.00 mmol, 2 equiv), 4.66 mL benzyl alcohol (45.0 mmol, 2 equiv), and 2.771 g 4-dimethylaminopyridine (22.68 mmol, 1 equiv). The solution was cooled to 0 °C and 5.787 g *N,N'*-dicyclohexylcarbodiimide (28.05 mmol, 1.2 equiv) was added. The reaction was stirred for 3 h and run through a silica plug, eluting with ethyl acetate to remove dicyclohexylurea, and concentrated. The concentrate was purified using column chromatography (10% ethyl acetate in hexanes) and dried under vacuum to afford the product as a colorless oil (6.584 g, 21.07 mmol, 94% yield).  $^1H$  NMR (400 MHz,  $CDCl_3$ )  $\delta$  7.33 (m, 5 H), 7.07 (d,  $J = 8.3$  Hz, 2 H), 6.90 (d,  $J = 8.3$  Hz, 2 H), 5.12 (s, 2 H), 2.94 (t,  $J = 7.9$  Hz, 2 H), 2.67 (t,  $J = 7.5$  Hz, 2 H), 1.33 (s, 9 H);  $^{13}C$  NMR (100 MHz,  $CDCl_3$ )  $\delta$  172.9, 153.8, 136.1, 135.4, 128.7, 128.7, 128.3, 124.3, 77.8, 66.4, 36.1, 30.4, 29.0. HRMS  $m/z$  calculated for  $C_{20}H_{24}O_3$   $[M]^+$  312.1725; found 312.1766.



**(*E*)-benzyl 2-4-(*tert*-butoxy)benzyl)but-2-enoate (56):**<sup>103</sup> To a solution of 73 mL

anhydrous THF under nitrogen was added 23.4 mL LDA (1.8 M in heptane/THF/ethylbenzene, 42 mmol, 2 equiv). The solution was cooled to  $-78$  °C and 6.584 g compound **55** (21.07 mmol, 1 equiv) in 16 mL anhydrous THF was added to the LDA solution dropwise over 20 minutes then stirred for 1 h. After this time, 3.54 mL acetaldehyde (63.3 mmol, 3 equiv) in 22 mL anhydrous THF was added dropwise over 20 minutes then stirred 2 h. The reaction was quenched with saturated aqueous ammonium chloride, diluted with water, and extracted three times with ethyl acetate. The organics were combined, dried with magnesium sulfate, and concentrated. The concentrate was run through a silica plug, eluting with 50% ethyl acetate in hexanes, and then concentrated to afford the crude

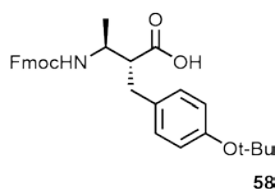
aldol product which was used directly. To a stirred solution of the aldol product (21.07 mmol, 1 equiv) in 34 mL 1:1 triethylamine/dichloromethane at 0 °C was added 2.45 mL methanesulfonyl chloride (31.2 mmol, 1.5 equiv) in 6 mL dichloromethane. The reaction was stirred 2 h at room temperature, then run through a silica plug, eluting with ethyl acetate and concentrated to afford the crude mesylate which was used directly. To a stirred solution of mesylate (21.07 mmol, 1 equiv) in 70 mL anhydrous THF at 0 °C was added 4.720 g potassium *tert*-butoxide. The reaction was stirred at room temperature overnight, quenched with 1 M hydrochloric acid, diluted with water, and extracted three times with ethyl acetate. The organics were combined, dried with magnesium sulfate, and concentrated to yield a crude mixture of product (83:17 *E/Z*). The concentrate was purified using column chromatography (5% → 10% diethyl ether in hexanes) to afford the product in a 94:6 *E/Z* ratio as a yellow oil (2.467 g, 7.289 mmol, 35% yield over 3 steps). <sup>1</sup>H NMR (400 MHz, CDCl<sub>3</sub>) δ 7.28 (m, 5 H), 7.08 (q, *J* = 7.2 Hz, 1 H), 7.04 (d, *J* = 8.3 Hz, 2 H), 6.86 (d, *J* = 8.4 Hz, 2 H), 5.13, (s, 2 H), 3.66 (s, 2 H), 1.89 (d, *J* = 7.2 Hz, 3 H), 1.31 (s, 9 H); <sup>13</sup>C NMR (100 MHz, CDCl<sub>3</sub>) δ 167.5, 153.5, 139.1, 136.3, 134.5, 132.3, 128.7, 128.5, 128.1, 128.0, 124.2, 78.2, 66.4, 31.5, 28.9, 14.8. HRMS *m/z* calculated for C<sub>22</sub>H<sub>26</sub>O<sub>3</sub>Na [M+Na]<sup>+</sup> 312.1780; found 312.1775.



**(2*R*,3*S*)-benzyl-3-benzyl((*S*)-1-phenylethyl)amino-2-(4-*tert*-butoxy)benzyl)butanoate (57):**<sup>103</sup> To a stirred solution of 2.44 mL (*S*)-(-)-*N*-benzyl- $\alpha$ -methylbenzylamine (11.7 mmol, 1.6 equiv) in 14.6 mL anhydrous

toluene under nitrogen at 0 °C was added 6.9 mL *n*-BuLi (1.6 M in hexanes, 11.0 mmol, 1.5 equiv). The reaction was cooled to -78 °C and stirred 15 minutes. To the reaction was added 2.467 g compound **56** (7.290 mmol, 1 equiv) in 7.3 mL anhydrous toluene dropwise and the reaction was stirred 1 h at -78 °C and 2 h at -30 °C. The reaction was cooled to -78 °C and diluted with 80 mL anhydrous THF. To the reaction was added 4.98 g 2,6-di-*tert*-butylphenol (24.1 mmol, 3 equiv) in 7 mL anhydrous THF dropwise. The reaction was stirred at room temperature for 2 h. The organic solvent was removed under reduced pressure, the concentrated solution was diluted with ethyl acetate, washed once with brine, dried with magnesium sulfate, and concentrated. The concentrate was run through a silica plug, eluting with

hexanes to remove excess 2,6-di-*tert*-butylphenol, then eluting with ethyl acetate to remove the product. The ethyl acetate fraction was concentrated, purified using column chromatography (2% → 5% → 10% diethyl ether in hexanes), and dried under vacuum to afford the product in a 94:6 (*2R,3S*: *2S,3R*) diastereomeric ratio as a yellow oil (1.812 g, 3.296 mmol, 45% yield).  $[\alpha]_D = -30.9$  ( $c = 1.00$ ,  $\text{CHCl}_3$ ).  $^1\text{H}$  NMR (400 MHz,  $\text{CDCl}_3$ )  $\delta$  7.45-7.05 (m, 15 H), 6.79 (s, 4 H), 4.87 (q,  $J = 12.4$  Hz, 2 H), 4.02 (q,  $J = 6.8$  Hz, 1 H), 3.88 (d,  $J = 13.9$  Hz, 1 H), 3.75 (d,  $J = 13.9$  Hz, 1 H), 3.13 (m, 1 Hz), 3.05 (d,  $J = 13.8, 3.6$ , Hz, 1 H), 2.65 (m, 1 H), 2.08 (m, 1 H), 1.43 (d,  $J = 6.9$  Hz, 3 H), 1.31 (s, 9 H), 1.13 (d,  $J = 6.7$  Hz, 3 H);  $^{13}\text{C}$  NMR (100 MHz,  $\text{CDCl}_3$ )  $\delta$  175.1, 153.5, 144.2, 141.1, 135.9, 135.1, 129.1, 129.1, 128.5, 128.3, 128.2, 128.1, 128.1, 127.1, 127.0, 124.1, 78.2, 66.0, 57.2, 54.1, 54.0, 50.4, 36.3, 29.0, 15.4, 15.0. HRMS  $m/z$  calculated for  $\text{C}_{37}\text{H}_{44}\text{NO}_3$   $[\text{M}+\text{H}]^+$  550.3321; found 550.3358.



**(2*R*, 3*S*)-3-amino-2-(4-(*tert*-butoxy)benzyl)butanoic acid (58):**<sup>92</sup> To a stirred

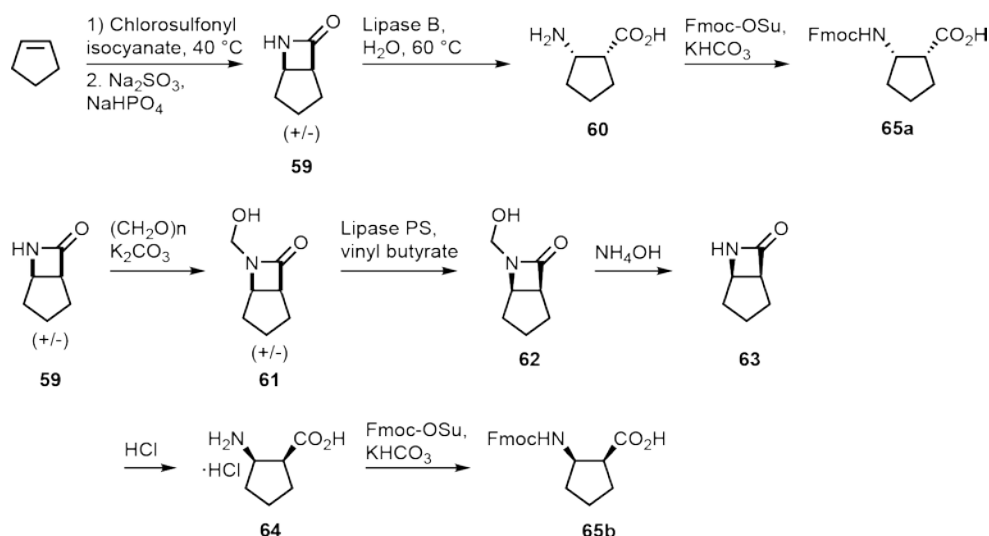
solution of 1.702 g compound **57** (3.096 mmol, 1 equiv) in 32 mL methanol was

added 177.5  $\mu\text{L}$  glacial acetic acid (3.101 mmol, 1 equiv), 3.899 g ammonium

formate (61.83 mmol, 20 equiv), and 341 mg 20 wt %  $\text{Pd}(\text{OH})_2/\text{C}$  (20% w/w). This solution was refluxed overnight under nitrogen, filtered through Celite, eluting with methanol, and concentrated to afford the crude amino acid which was used directly. To a stirred solution of amino acid (3.096 mmol, 1 equiv) in 31 mL anhydrous dichloromethane was added 2.16 mL DIEA (12.4 mmol, 4 equiv) and 786  $\mu\text{L}$  TMS-Cl (6.20 mmol, 2 equiv). After evolution of gas ceased, 1.150 g Fmoc-OSu (3.409 mmol, 1.1 equiv) was added and the reaction stirred overnight. The reaction mixture was washed with brine, dried with magnesium sulfate, and concentrated. The concentrate was purified using column chromatography (10% → 20% → 50% → 100% ethyl acetate in hexanes) and dried under vacuum to afford a mixture of the product (276 mg by NMR, 0.566 mmol, 18% yield over 2 steps) and 9-fluorenemethanol (~50% by NMR) which was used directly in peptide synthesis.  $[\alpha]_D = -3.5$  ( $c = 1.00$ ,  $\text{CHCl}_3$ ).  $^1\text{H}$  NMR (400 MHz,  $\text{DMSO-d}_6$ )  $\delta$  12.2 (s, 1 H), 7.88 (m, 2 H), 7.70 (d,  $J = 7.2$  Hz, 2 H), 7.39 (m, 3 H), 7.31 (m, 2 H), 7.03 (d,  $J = 8.3$  Hz, 2 H), 6.85 (d,  $J = 8.3$  Hz, 2 H), 4.40 (m, 1 H), 4.31 (m, 1 H), 4.23 (m, 1 H), 3.68 (q,  $J = 8.2$

Hz, 1 H), 2.75-2.56 (m, 3 H), 1.26 (s, 9 H), 1.07 (d,  $J = 6.7$  Hz, 3 H);  $^{13}\text{C}$  NMR (100 MHz,  $\text{CDCl}_3$ )  $\delta$  178.3, 155.8, 154.0, 144.0, 144.2, 133.5, 129.3, 127.8, 127.2, 125.2, 124.4, 120.1, 78.5, 66.8, 52.3, 48.2, 47.4, 34.2, 28.9, 17.6. HRMS  $m/z$  calculated for  $\text{C}_{30}\text{H}_{34}\text{NO}_5$   $[\text{M}+\text{H}]^+$  488.2437; found 488.2440.

### 2.3.1.5 Synthesis of *cis* Fmoc-ACPC Monomers

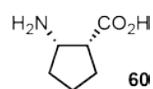


**Scheme 2.4.** Synthesis of *cis* Fmoc-ACPC monomers.

*N,O*-acetal **61**, lactam **63**, amino acid hydrochloride **64** were synthesized using published procedures.<sup>104,105</sup>

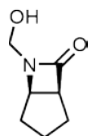
**Racemic *cis*-azabicyclo[3.2.0]heptan-7-one (59):**<sup>99</sup> To a stirred solution of 4.5 mL cyclopentene (51 mmol, 1 equiv) in 23 mL anhydrous dichloromethane at 0 °C under nitrogen **59** was added a solution of 4.3 mL chlorosulfonyl isocyanate (49 mmol, 1 equiv) in 7 mL anhydrous dichloromethane dropwise over 30 minutes. The reaction was then heated to 40 °C and stirred for 20 h.

The resulting solution was cooled to 0 °C, quenched with dropwise addition of water until bubbling ceased, and diluted with 120 mL chloroform. To this solution was added a solution of 15.8 g sodium sulfite (125 mmol, 2.5 equiv) and 35.1 g sodium biphosphate heptahydrate (125 mmol, 2.5 equiv) in 240 mL water and the combined solution stirred 36 h. After this time, the organic layer was collected and the aqueous layer was extracted with ethyl acetate. The organic layers were combined, dried with magnesium sulfate, and concentrated. The resulting solid was dissolved in ethyl acetate and recrystallized from pentane to afford the product as white crystals (3.232 g, 29.1 mmol, 58% yield). NMR spectra of the product matched previously published results.<sup>99</sup>

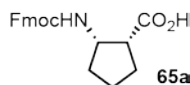


**(1R,2S)-2-aminocyclopentanecarboxylic acid (60):**<sup>106</sup> To a stirred solution of 1.006 g compound **59** (9.05 mmol, 1 equiv) in 180 mL diisopropyl ether was added 9.005 g Lipase B from *Candida antarctica* immobilized on Immobead 150 (50 mg/mL) and 162  $\mu$ L water (8.99 mmol, 1 equiv). The reaction was stirred under nitrogen at 60 °C for 10 days, then filtered and rinsed with diisopropyl ether. The enzyme solid was washed with water and the water layer was concentrated under vacuum. The resulting solid was dissolved in water and recrystallized using acetone to afford the product as a white solid (243 mg, 1.88 mmol, 21% yield). NMR spectra of the product matched previously published results.<sup>106</sup>

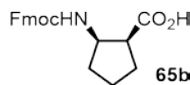
**Standard Procedure L:**<sup>104</sup> To a stirred suspension of 2.0 g Amano Lipase PS from *Burkholderia cepacia* and 1.2 g sucrose in 200 mL 20 mM Tris, pH 7.8 was added 6.8 g Celite. The suspension was concentrated to dryness to afford 20% w/w lipase on Celite. To a stirred solution of *N,O*-acetal (1 equiv) in anhydrous acetone was added vinyl butyrate (2 equiv) and 20% w/w Lipase PS (60% w/w). The solution was allowed to stir until the desired enzymatic resolution was obtained. The enzyme was filtered from the solution and washed with acetone. The organics were concentrated and purified using column chromatography to afford the desired product.



**(1S,5R)-6-(hydroxymethyl)-6-azabicyclo[3.2.0]heptan-7-one (62):** Standard Procedure L was employed using 533 mg compound **61** (3.78 mmol), 38.3 mL acetone, 960  $\mu$ L vinyl butyrate (7.6 mmol), and 1.89 g Lipase PS. The reaction was stirred for 36 h until NMR spectroscopy indicated 60% conversion. Column chromatography (50%  $\rightarrow$  75% ethyl acetate in hexanes) afforded the unreacted starting material as a colorless oil (143 mg, 1.01 mmol, 27% yield). NMR spectra for the product matched previously published results.<sup>104</sup>  $[\alpha]_D = -35$  ( $c = 1.0$ ,  $\text{CHCl}_3$ );  $[\alpha]_{D, \text{lit}} = -32.4$  ( $c = 1$ ,  $\text{CHCl}_3$ ).<sup>104</sup>

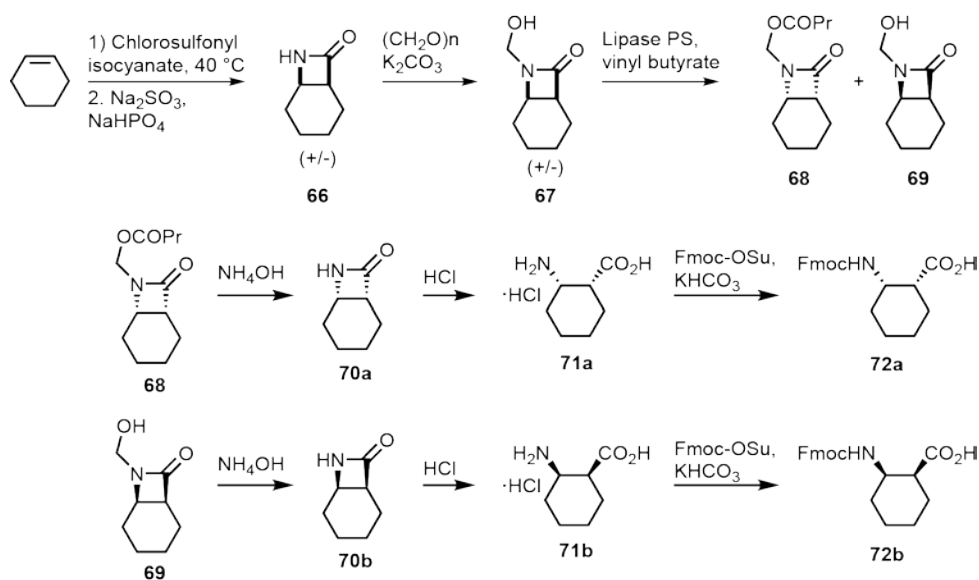


**(1R,2S)-2-Fmoc-aminocyclopentanecarboxylic acid (65a):** Standard Procedure F was employed using 94 mg compound **60** (0.73 mmol), 485  $\mu$ L water, 148 mg potassium bicarbonate (1.46 mmol) and 245 mg Fmoc-OSu (0.727 mmol). Column chromatography (20% ethyl acetate in hexanes  $\rightarrow$  50% ethyl acetate in hexanes) afforded the product as a white foam (139 mg, 0.396 mmol, 54% yield).  $[\alpha]_D = -29$  ( $c = 0.50$ ,  $\text{CHCl}_3$ ). NMR spectra for this product matched previously published results.<sup>99</sup> HRMS  $m/z$  calculated for  $\text{C}_{21}\text{H}_{21}\text{NO}_4\text{Na}$   $[\text{M}+\text{Na}]^+$  374.1368; found 374.1366.



**(1S,2R)-2-Fmoc-aminocyclopentanecarboxylic acid (65b):** Standard Procedure F was employed using 150 mg acid hydrochloride compound **64** (0.906 mmol), 1.10 mL water, 182 mg potassium bicarbonate (1.82 mmol) and 308 mg Fmoc-OSu (0.913 mmol). Column chromatography (20%  $\rightarrow$  50% ethyl acetate in hexanes) afforded the product as a white foam (243 mg, 0.692 mmol, 76% yield).  $[\alpha]_D = +29$  ( $c = 0.50$ ,  $\text{CHCl}_3$ ). NMR spectra for this product matched previously published results.<sup>99</sup> HRMS  $m/z$  calculated for  $\text{C}_{21}\text{H}_{21}\text{NO}_4\text{Na}$   $[\text{M}+\text{Na}]^+$  374.1368; found 374.1352.

### 2.3.1.6 Synthesis of *cis* Fmoc-ACHC Monomers

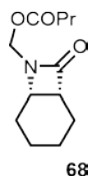


**Scheme 2.5.** Synthesis of *cis* Fmoc-ACHC monomers.

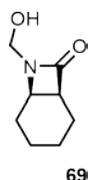
*N,O*-acetal **67**, amino acid hydrochloride **71a**, and amino acid hydrochloride **71b** were synthesized using published procedures.<sup>105</sup>

**Racemic *cis*-7-azabicyclo[4.2.0]octan-8-one (66):**<sup>99</sup> To a stirred solution of 10.1 mL cyclohexene (100 mmol, 1 equiv) in 45 mL anhydrous dichloromethane at 0 °C under nitrogen was added a solution of 8.6 mL chlorosulfonyl isocyanate (100 mmol, 1 equiv) in 15 mL anhydrous dichloromethane dropwise over 30 minutes. The reaction was allowed to warm to room temperature and stirred for 96 h, then cooled to 0 °C, quenched with dropwise addition of water until bubbling ceased, and diluted with 100 mL chloroform. To this solution was added a solution of 31.6 g sodium sulfite (250 mmol, 2.5 equiv) and 70.3 g sodium biphosphate heptahydrate (250 mmol, 2.5 equiv)

in 500 mL water. The solution was stirred 36 h, then the organic layer was collected and the aqueous layer was extracted with ethyl acetate. The organic layers were combined, dried with magnesium sulfate, and concentrated. The resulting yellow solid was re-dissolved in ethyl acetate and recrystallized using pentane to afford the product as white crystals (4.81 g, 38.4 mmol, 38% yield). NMR spectra matched for this product previously published results.<sup>105</sup>

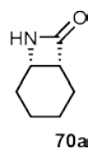


**((1R,6S)-8-oxo-7-azabicyclo[4.2.0]octan-7-yl)methyl butyrate (68):** Standard Procedure L was employed using 518 mg compound **67** (3.34 mmol), 34 mL acetone, 850  $\mu$ L vinyl butyrate (6.7 mmol), and 1.68 g Lipase PS. The reaction was stirred for 16 h when NMR spectroscopy indicated 40% conversion. Column chromatography (0%  $\rightarrow$  50% ethyl acetate in dichloromethane  $\rightarrow$  75% ethyl acetate in hexanes) afforded the product as a yellow oil (242 mg, 1.08 mmol, 32% yield). NMR spectra for this product matched previously published results.<sup>105</sup>  $[\alpha]_{\text{D}} -18$  ( $c = 1.0$ , MeOH);  $[\alpha]_{\text{D, lit}} = -15.5$  ( $c = 1$ , MeOH).<sup>105</sup>

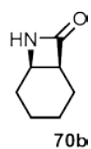


**(1S,6R)-7-(hydroxymethyl-7-azabicyclo[4.2.0]octan-8-one (69):** Standard Procedure L was employed using 518 mg compound **67** (3.34 mmol), 34 mL acetone, 0.85 mL vinyl butyrate (6.7 mmol), and 1.68 g Lipase PS. The reaction was stirred for 16 h when NMR spectroscopy indicated 40% conversion. Column chromatography (75% ethyl acetate in hexanes) afforded the unreacted starting material. Standard Procedure L was then employed again using 142 mg recovered starting material (0.915 mmol), 9.3 mL acetone, 230  $\mu$ L vinyl butyrate (1.8 mmol), and 463 mg Lipase PS. The reaction was stirred for 36 h when NMR spectroscopy indicated 60% conversion. Column chromatography (0%  $\rightarrow$  50%  $\rightarrow$  75% ethyl acetate in hexanes) afforded the unreacted starting material as a colorless oil (83 mg, 0.54 mmol, 16% yield). NMR spectra for this material matched previously published results.<sup>105</sup>  $[\alpha]_{\text{D}} = -33$  ( $c = 1.0$ , MeOH);  $[\alpha]_{\text{D, lit}} = -31.7$  ( $c = 1$ , MeOH).<sup>105</sup>

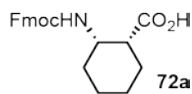
**Standard Procedure M: Acetal Hydrolysis:**<sup>105</sup> To a solution of *N,O*-acetal (1 equiv) in methanol was added concentrated aqueous ammonium hydroxide. The reaction mixture was stirred until TLC indicated full conversion to product. The solution was concentrated under vacuum to afford the product.



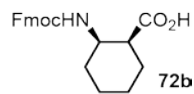
**(1R,6S)-7-azabicyclo[4.2.0]octan-8-one (70a):** Standard Procedure M was employed using 242 mg compound **68** (1.08 mmol), 15.8 mL methanol, and 1.6 mL concentrated aqueous ammonium hydroxide. The reaction was stirred for 3 days then concentrated to afford the product as white crystals (99 mg, 0.79 mmol, 73% yield). NMR spectra for this product matched previously published results.<sup>105</sup>



**(1S,6R)-7-azabicyclo[4.2.0]octan-8-one (70b):** Standard Procedure M was employed using 83 mg compound **69** (0.54 mmol), 8.3 mL methanol, and 0.8 mL concentrated aqueous ammonium hydroxide. The reaction was stirred 3 days then concentrated to afford the product as white crystals (62 mg, 0.50 mmol, 93% yield). NMR spectra matched previously published results.<sup>105</sup>



**(1R,2S)-2-Fmoc-amino-cyclohexanecarboxylic acid (72a):** Standard Procedure F was employed using 123 mg compound **71a** (0.684 mmol), 800  $\mu$ L water, 137 mg potassium bicarbonate (1.36 mmol), and 230 mg Fmoc-OSu (0.682 mmol). Column chromatography (20%  $\rightarrow$  50% ethyl acetate in hexanes ethyl acetate in hexanes) afforded the product as a white foam (115 mg, 0.315 mmol, 46% yield).  $[\alpha]_D = -12$  ( $c = 0.50$ ,  $\text{CHCl}_3$ ). NMR spectra for this product matched previously published results.<sup>99</sup> HRMS  $m/z$  calculated for  $\text{C}_{22}\text{H}_{23}\text{NO}_4\text{Na}$   $[\text{M}+\text{Na}]^+$  388.1525; found 388.1508.



**(1S,2R)-2-Fmoc-amino-cyclohexanecarboxylic acid (72b):** Standard Procedure F was employed using 76 mg compound **71b** (0.42 mmol), 510  $\mu$ L water, 84 mg potassium

bicarbonate (0.84 mmol), and 142 mg Fmoc-OSu (0.421 mmol). Column chromatography (20%  $\rightarrow$  50% ethyl acetate in hexanes) afforded the product as a white foam (97 mg, 0.27 mmol, 50% yield).  $[\alpha]_D = +13$  ( $c = 0.50$ ,  $\text{CHCl}_3$ ). NMR spectra matched previously published results.<sup>99</sup> HRMS  $m/z$  calculated for  $\text{C}_{22}\text{H}_{23}\text{NO}_4\text{Na}$   $[\text{M}+\text{Na}]^+$  388.1525; found 388.1521.

### 2.3.2 Peptide Synthesis

Peptides were synthesized using standard microwave-assisted Fmoc solid-phase synthesis techniques on a MARS microwave reactor (CEM). NovaPEG Rink Amide resin NovaPEG Rink Amide resin or H-Glu(*t*Bu) HMPB NovaPEG resin was used as the solid support. Couplings were carried out in NMP with a 2 min ramp to 70  $^\circ\text{C}$  and a 4 min hold at that temperature, using Fmoc-protected amino acid (4 equiv), HCTU (4 equiv), and DIEA (4 equiv). Deprotections were performed with a 2 min ramp to 80  $^\circ\text{C}$  followed by a 2 min hold at that temperature, using an excess of 20% 4-methylpiperidine in DMF. After each coupling or deprotection cycle, the resin was washed three times with DMF. Double coupling was performed at sequence positions following proline residues. N-terminal acetylation, when present, was carried out on resin by treatment with 8:2:1 v/v/v DMF:DIEA:Ac<sub>2</sub>O.

Peptides **8a**, **8b**, **9a**, and **9b** were synthesized using thiocarbamate-protected monomers. These monomers were coupled using standard microwave-assisted coupling procedures. For deprotection, the resin was first suspended in 1 mL dioxane. 1 mL of 0.04 M solution of Oxone in water was added to the suspension and stirred for 90 minutes. After this time, the solution was drained and the resin washed five times with 1:1 dioxane/water and washed three times with DMF.

Prior to cleavage from resin, peptides were washed three times each with DMF, dichloromethane, and methanol, and then dried. Peptide cleavage was performed using 95% trifluoroacetic acid (TFA), 2.5%

triisopropylsilane, and 2.5% water. Cysteine-containing peptides were purified, lyophilized, dissolved in 10 mM phosphate buffer (pH 8.9, 5% v/v DMSO), stirred until analytical HPLC and MS showed complete conversion to the cyclic disulfide (1-2 d), and then re-purified.

Peptides were purified by HPLC on a C<sub>18</sub> preparative column using gradients between 0.1% TFA in water and 0.1% TFA in acetonitrile. All peptides were >95% pure by analytical HPLC on a C<sub>18</sub> column. Identities of peptides were confirmed using a Voyager DE Pro MALDI-TOF instrument (Table 3 and Table 4).

**Table 3.** MALDI-TOF data for peptides **1a-17a** and **1b-17b**.

Peptide	[M+H] <sup>+</sup> <i>m/z</i>	
	Calculated	Observed
<b>1a</b>	1507.8	1508.3
<b>2a</b>	1504.9	1505.1
<b>3a</b>	1504.9	1505.0
<b>4a</b>	1504.9	1504.7
<b>5a</b>	1504.9	1504.4
<b>6a</b>	1532.9	1532.9
<b>7a</b>	1532.9	1532.9
<b>8a</b>	1532.9	1533.0
<b>9a</b>	1532.9	1533.0
<b>10a</b>	1500.8	1501.0
<b>11a</b>	1500.8	1501.0
<b>12a</b>	1500.8	1500.6
<b>13a</b>	1500.8	1500.6
<b>14a</b>	1528.9	1528.8
<b>15a</b>	1528.9	1528.8
<b>16a</b>	1528.9	1528.6
<b>17a</b>	1528.9	1528.5
<b>1b</b>	1507.8	1507.7
<b>2b</b>	1504.9	1504.6
<b>3b</b>	1504.9	1505.0
<b>4b</b>	1504.9	1504.7
<b>5b</b>	1504.9	1504.4
<b>6b</b>	1532.9	1532.9
<b>7b</b>	1532.9	1532.7
<b>8b</b>	1532.9	1533.0
<b>9b</b>	1532.9	1533.0
<b>10b</b>	1500.8	1500.5
<b>11b</b>	1500.8	1500.6
<b>12b</b>	1500.8	1500.6
<b>13b</b>	1500.8	1500.4
<b>14b</b>	1528.9	1528.5
<b>15b</b>	1528.9	1528.9
<b>16b</b>	1528.9	1528.5
<b>17b</b>	1528.9	1528.6

**Table 4.** MALDI-TOF data for peptides **18-26** and their derivatives.

Peptide	$[M+H]^+$ $m/z$	
	Calculated	Observed
<b>18</b>	1862.8	1862.7
<b>19a</b>	1897.0	1897.8
<b>19b</b>	2143.0	2143.8
<b>19c</b>	1006.5	1006.2
<b>19d</b>	951.5	951.1
<b>20a</b>	1837.0	1837.6
<b>20b</b>	2084.4	2084.8
<b>20c</b>	976.5	976.3
<b>20d</b>	921.5	921.2
<b>21a</b>	1798.9	1799.9
<b>22a</b>	1739.8	1739.2
<b>22b</b> *	2007.8	2008.3
<b>22c</b> *	928.4	928.2
<b>22d</b> *	915.5	916.0
<b>23a</b>	1625.8	1626.6
<b>23b</b>	1871.8	1871.3
<b>23c</b>	871.4	871.8
<b>23d</b>	836.5	837.1
<b>24a</b>	1653.8	1654.1
<b>24b</b>	1899.9	1900.2
<b>24c</b> *	863.4	855.2
<b>24d</b>	850.5	850.6
<b>25a</b>	1795.9	1796.1
<b>25b</b>	2041.9	2042.1
<b>25c</b>	934.4	934.6
<b>25d</b>	921.5	921.6
<b>26a</b>	1852.0	1852.1
<b>26b</b>	2098.0	2098.2
<b>26c</b>	984.5	984.6
<b>26d</b>	949.5	949.7

\* $[M+Na]^+$  Peak

### 2.3.3 NMR Sample Preparation and Data Collection

NMR samples were prepared by dissolving 2-3 mg peptide in 750-850  $\mu\text{L}$  de-gassed buffer solution to make 0.2–2 mM solutions. For peptides **1a-17a** and **1b-17b**, 0.1 M NaOAc- $\text{d}_3$ , 90%  $\text{H}_2\text{O}/\text{D}_2\text{O}$ , pH 3.8 (uncorrected for the presence of  $\text{D}_2\text{O}$ ) was used as the buffer system. For peptides **18-26** and their derivatives, 50 mM phosphate, 9:1  $\text{H}_2\text{O}/\text{D}_2\text{O}$ , pH 6.3, uncorrected, was used. 3-(Trimethylsilyl)-1-propanesulfonic acid sodium salt (DSS, 50 mM in water) was added to a final concentration of 0.2 mM DSS in the sample. Each solution was passed through a 0.2  $\mu\text{m}$  syringe filter, transferred to an NMR tube, and stored until analysis. The NMR tube headspace was purged with a stream of nitrogen prior to capping.

NMR spectra of peptides were recorded on a Bruker-Avance-600 or Bruker Avance-700 spectrometer. Chemical shifts are reported relative to DSS (0 ppm). TOCSY, NOESY, and COSY pulse programs used excitation-sculpted gradient-pulse solvent suppression. All experiments were obtained using 2048 data points in the direction dimension and 512 data points in the indirect dimension. TOCSY were acquired with a mixing time of 60 or 80 ms and NOESY were acquired with a mixing time of 200 ms.

For peptides **1a-17a** and **1b-17b**, NMR measurements were performed at 277 K. Other NMR measurements were performed at a temperature of 293 K unless otherwise noted. Linear hairpin peptides with unnatural backbones (**23a-26a**) were measured at 278 K to maximize folded population and facilitate comparison of folded stability. Natural backbone peptide **22a** was measured at both 278 K and 293 K. NMR data at 293 K were used for comparison among the  $\alpha$ -peptide series (**18**, **19a-22a**), while data at 278 K were used for comparison with the unnatural backbone series (**23a-26a**).

### 2.3.4 NMR Data Analysis and Structure Determination

The Sparky software package (T. D. Goddard and D. G. Kneller, SPARKY 3, University of California, San Francisco) was used to analyze 2D NMR data. Backbone chemical shift assignments were generated (Appendix A) and each peptide was analyzed for qualitative NOE's indicative of folding. Peptides that showed a high degree of folding were fully assigned and inter-residue NOE's were tabulated. NOE integration values were converted to distance restraints using equation 1:

$$(1) \quad I = cr^{-6}$$

where  $I$  is intensity,  $c$  is a constant (determined using resolved diastereotopic CH<sub>2</sub> groups),  $r$  is distance.<sup>117</sup> The distances were then classified as strong ( $\leq 2.7$  Å), medium ( $\leq 3.5$  Å), weak ( $\leq 4.5$  Å), or very weak ( $\leq 5.5$  Å) to generate distance restraints (Appendix B).

The Crystallography and NMR system (CNS) software package was used to generate 3D resolution structures.<sup>118,119</sup> Patches were written to accommodate  $\beta$ -residues. Distance restraints calculated above were used in 100 simulated annealing runs using default suggested parameters for protein NMR. Structures including any NOE distance-restraint violations ( $>0.5$  Å) were discarded and the 20 lowest energy structures were obtained. The minimum energy average of these 10 or 20 structures was inspected to identify H-bonding contacts. These contacts were then included in an additional restraint file and the annealing process repeated to generate an ensemble of 10 or 20 lowest energy structures and a minimized average structure for each peptide.

### 2.3.5 Calculation of Folding Equilibria by NMR

Fraction folded from chemical shift deviation ( $f_{H\alpha}$ ) was calculated using experimentally determined  $H_\alpha$  chemical shifts ( $\delta_{H\alpha}$ ) using equation 2:<sup>111</sup>

$$(2) \quad f_{H\alpha} = \frac{\delta_{H\alpha,observed} - \delta_{H\alpha,unfolded}}{\delta_{H\alpha,folded} - \delta_{H\alpha,unfolded}}$$

where  $\delta_{H\alpha,observed}$  is the chemical shift of a particular  $H_\alpha$  in the unknown peptide,  $\delta_{H\alpha,unfolded}$  its chemical shift in an N- or C-terminal fragment, and  $\delta_{H\alpha,folded}$  its chemical shift in a disulfide-bridged cyclic analog. Values of  $f$  reported are averages calculated using chemical shift data for residues 4, 11, and 13.

Fraction folded from separation of diastereotopic Gly  $H_\alpha$ 's ( $f_{Gly}$ ) was calculated using equation 3:

$$(3) \quad f_{Gly} = \frac{\Delta\delta_{H\alpha/H\alpha',observed}}{\Delta\delta_{H\alpha/H\alpha',folded}}$$

where  $\Delta\delta_{H\alpha/H\alpha',observed}$  is the chemical shift difference between Gly  $H_\alpha$ 's in an unknown peptide and  $\Delta\delta_{H\alpha/H\alpha',folded}$  the corresponding difference in a disulfide-bridged cyclic analogue.

The equilibrium constant for the folding equilibrium ( $K_{fold}$ ) and corresponding free energy of folding ( $\Delta G^\circ_{fold}$ ) were calculated from fraction folded using eq. 4 and eq. 5:

$$(4) \quad K_{fold} = \frac{f}{1-f}$$

$$(5) \quad \Delta G_{fold} = -RT \ln(K_{fold})$$

Experimental uncertainty for folded population determined by  $H_\alpha$  chemical shift deviation ( $f_{H\alpha}$ ) was estimated using the standard deviation of the mean for populations based on residues 4, 11, and 13. Error for folded population determined by Gly  $H_\alpha$  separation ( $f_{Gly}$ ) was estimated by assuming 0.01 ppm error in NMR peak assignment. The above values were used in standard error propagation based on eqs. 3, 4, and 5 to give uncertainties for  $f_{Gly}$ ,  $K_{fold}$ , and  $\Delta G_{fold}$ . A lower bound for the folded population of peptide **25a** was calculated using equation 3, an estimated minimum measurable glycine separation value

of 0.03 ppm, and an estimated value for the fully folded state of 0.322 ppm (average observed for peptides **22b**, **23b**, **24b**, and **26b**).

### 3.0 GAMMA RESIDUES AND N-METHYL-ALPHA-RESIDUES IN HETEROGENEOUS BACKBONE HAIRPINS

Some of the results detailed in this chapter have been published in:

1. Lengyel, G.A.; Eddinger, G.A.; Horne, W.S., "Introduction of Cyclically Constrained  $\gamma$ -Residues Stabilizes an  $\alpha$ -Peptide Hairpin in Aqueous Solution," *Organic Letters*, **2013**, 944-947.

Chapter 2 highlights the advantages and consequences of applying  $\beta$ -residue substitutions in hairpin-forming peptides. A 1:1  $\alpha$ - to  $\beta$ -residue substitution strategy inverts the display of side chains and hydrogen bonding pattern beyond the insertion site of the unnatural amino acids, but even with this inversion, hybrid  $\alpha/\beta$ -peptides can still fold into hairpin conformations in water. Utilizing 2:1 or 2:2  $\alpha$ - to  $\beta$ -residue substitution strategies prevents this inversion and allows native-like folding from the hybrid backbones, but significantly destabilizes the folded state. Because of this destabilization, we sought to investigate alternative monomer types which would both prevent side chain inversion and would have either a neutral or beneficial impact on folded stability.

## 3.1 1:1 ALPHA- TO GAMMA-RESIDUE SUBSTITUTION

### 3.1.1 Design of Alpha- to Gamma-Residue Substitution Strategies

Direct substitution of a single  $\alpha$ -amino acid in a strand with a  $\beta$ -amino acid causes side chain inversion due to the incorporation of an additional carbon unit in the backbone of the amino acid. Previous work has shown that incorporation of  $\gamma$ -amino acids, which increase the length of the amino acid backbone by two carbon atoms, can prevent inversion in extended strands (Figure 35).<sup>69</sup>

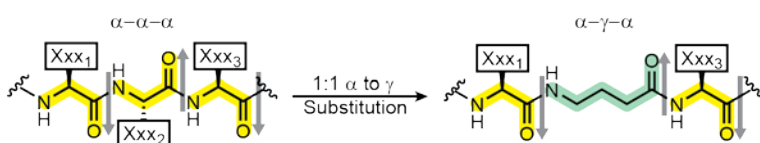


**Figure 35.** 1:1  $\alpha$ - to  $\gamma$ -residue substitution resulting in backbone expansion.

Additional work has shown that while  $\gamma$ -residues can prevent inversion of side chains without rigidifying the backbone of the  $\gamma$ -residue, the hairpin itself may become too flexible to form a discrete folded structure.<sup>70,120</sup> With these factors in mind, we selected three  $\gamma$ -residues with varying degrees of backbone constraint for use in a 1:1  $\alpha$ - to  $\gamma$ -residue substitution strategy (Figure 36).

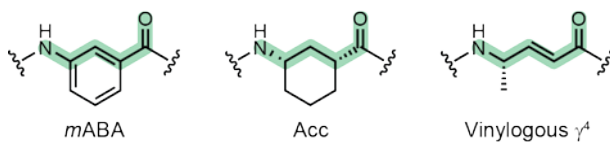


**Figure 36.** Backbone-constrained  $\gamma$ -residues.

Of the three  $\gamma$ -amino acids chosen, two have backbones incorporated into six-membered rings. *meta*-Aminobenzoic acid (*mABA*) has been successfully inserted into a hairpin peptide that folds in organic solvent<sup>71</sup> while substituted derivatives of this amino acid have been used in sheets to discourage sheet stacking and aggregation.<sup>53,59</sup> (1*R*,3*S*)-Aminocyclohexanecarboxylic acid (*Acc*) also has a ring-constrained backbone and can be used in place of L- $\alpha$ -amino acids<sup>72</sup> to form cyclic  $\beta$ -sheets in a nanotubular system.<sup>73,74</sup>

While both *mABA* and *Acc* have been shown as effective  $\alpha$ -amino acid replacements in sheets, use of these monomers eliminates any side chain functionality which may be essential to protein folding in larger proteins. To maintain side chain functionality while keeping a constrained backbone, we also examined vinylogous  $\gamma^4$ -amino acids in our studies. These  $\alpha,\beta$ -unsaturated acids, which have a backbone rigidified with one double bond paired with a side chain functionalized  $\gamma$ -carbon, have been used in both a small tetrapeptide sheet system<sup>69</sup> and a larger hairpin peptide.<sup>70</sup> In all of the studies mentioned above, only the structural impacts have been examined in organic solvent; there have been no examinations of the thermodynamic implications of  $\gamma$ -residue substitution or of structural impacts in aqueous media.

### 3.1.2 Thermodynamic Analysis of 1:1 Alpha- to Gamma-Residue Substitution

Using the same model hairpin peptide described in Section 2.2, we synthesized peptides **73**, **74**, and **75**, incorporating *mABA*, *Acc*, and vinylogous  $\gamma^4$ -alanine, respectively, in place of residues Ala<sub>4</sub> and Ala<sub>13</sub> of hairpin **22a** (Figure 37).

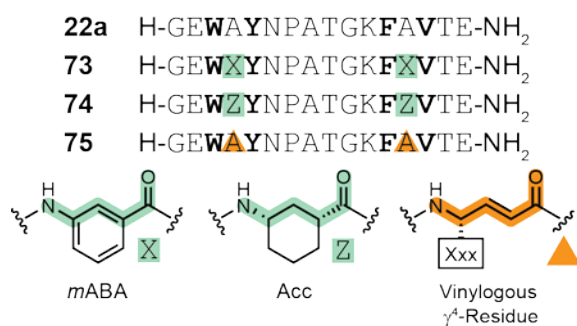


**Figure 37.** Model hairpin sequence **22a** and  $\alpha/\gamma$ -hybrid peptide sequences **73-75**.

Peptides **73**, **74**, and **75** were synthesized and analyzed at 278 K in aqueous phosphate buffer pH 6.3 using multidimensional NMR. The backbone H <sub>$\alpha$</sub>  and N<sub>H</sub> resonances of each peptide were fully assigned and glycine separation was measured (Table 5) using the same methodology described in Section 2.1.2. Using a value of 0.310 ppm (determined from cyclized parent peptide **22b**) as the maximum value of glycine H <sub>$\alpha$</sub>  separation for a fully-folded state, we determined the folded population of each peptide and the associated  $\Delta G_{\text{fold}}$ .

**Table 5.** Folded populations and  $\Delta G_{\text{fold}}$  for parent peptide **22a** and  $\alpha/\gamma$ -hybrid peptides **73-75**.

Peptide	Glycine Separation (ppm)	Folded Population (%)	$\Delta G_{\text{fold}}$ (kcal/mol)	$\Delta\Delta G_{\text{fold}}^{\text{a}}$ (kcal/mol)
<b>22a</b>	0.21 ± 0.01	66 ± 5	-0.35 ± 0.14	---
<b>73</b>	0.25 ± 0.01	79 ± 6	-0.74 ± 0.20	-0.4 ± 0.2
<b>74</b>	0.26 ± 0.01	83 ± 6	-0.88 ± 0.23	-0.5 ± 0.2
<b>75</b>	0.12 ± 0.01	39 ± 5	0.24 ± 0.11	+0.6 ± 0.2

a. Values calculated versus  $\Delta G_{\text{fold}}$  of peptide **22a**.

The folded populations of the hybrid peptides containing cyclic  $\gamma$ -residues (**73** and **74**) were both higher than the folded population of parent peptide **22a**. The corresponding  $\Delta\Delta G_{\text{fold}}$  for **73** and **74** relative to **22a** shows a stabilization of approximately 0.5 kcal/mol. Both *mABA* and *Acc* are significantly more stabilizing than the  $\beta$ -residue substitutions discussed in Section 2.2.5, where the most favorable case was a 1 kcal/mol *penalty* to folding from modifying two strands of the hairpin. Vinylogous  $\gamma^4$ -amino acid containing peptide **75**, with a  $\Delta\Delta G_{\text{fold}}$  of +0.6 kcal/mol, is not stabilized like peptides **73** and **74**, but is more stable than the peptides utilizing  $\beta$ -residue substitutions. The decreased stability of this system compared to the cyclic  $\gamma$ -residues most likely results from increased backbone flexibility.

### 3.1.3 Structural Analysis of 1:1 Alpha- to Gamma-Residue Substitution

Having accomplished the goal of finding amino acids that are more thermodynamically favored as  $\alpha$ -amino acid replacements than  $\beta$ -amino acids, we next sought to investigate the structural impacts of  $\gamma$ -residue substitution to the hairpin fold. As peptide **75** had a folded population less than 50%, we synthesized a cyclic variant, **76** (Figure 38), for structural analysis using a terminal disulfide bridge as discussed in Section 2.2.4.

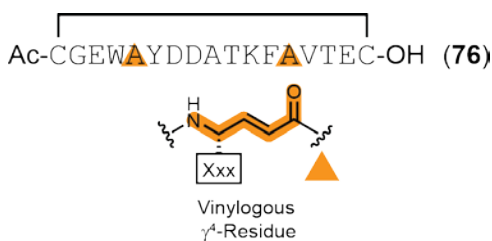


**Figure 38.** Sequence of cyclized  $\alpha/\gamma$ -hybrid peptide **76**.

The proton resonances of peptides **73**, **74**, and **76** were fully assigned, and the solution fold of these peptides investigated using NOE analysis (see Section 2.1.3 for details). In each case, as expected from our design principles, substitution of an  $\alpha$ -amino acid with a  $\gamma$ -amino acid prevented side chain inversion and NOE's were visible across the entire length of the backbone, suggesting hairpin-like structures (Figure 39).

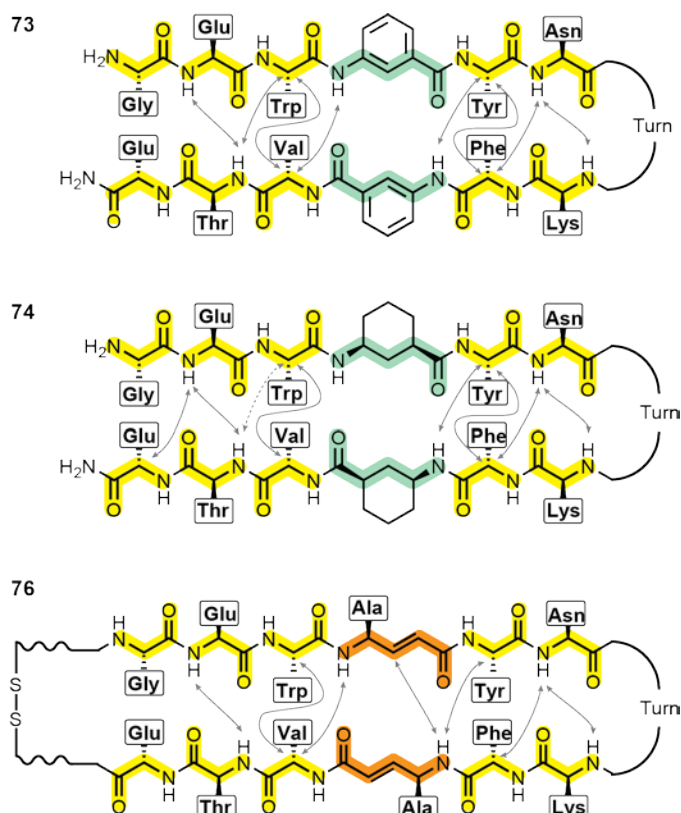


**Figure 39.** Cross-strand NOE's displayed by peptides **73**, **74**, and **76**. Ambiguous assignments are shown as dotted lines. Cyclic  $\gamma$ -residues are highlighted green while vinylogous  $\gamma^4$ -residues are highlighted orange.

With evidence of hairpin formation in hand, we generated NOE distance restraints and NMR structures of peptides **73**, **74**, and **76** as described in Section 3.3.4. We calculated the average structure for each compound using the 10 lowest energy structures for each (Figure 40). In the case of **74**, we saw a

minor conformer of a horseshoe shape in 2 of the 10 structures and calculated the average structure excluding the minor conformation.

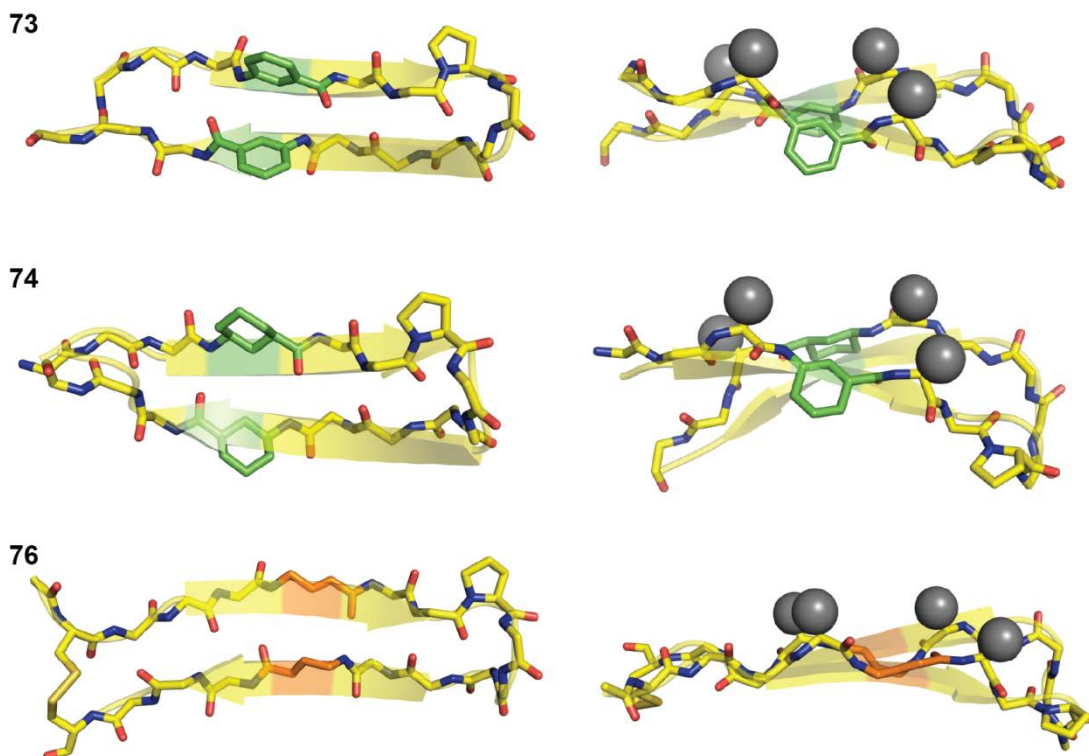


**Figure 40.** NMR solution structures of  $\alpha/\gamma$ -hybrid peptides **73**, **74**, and **76**. Structures calculated from the average of 10 lowest energy conformations determined using NOE distance restraints from NMR. Samples consisted of ~1 mM solution of peptide and 50 mM phosphate in 90% H<sub>2</sub>O/D<sub>2</sub>O, pH 6.3. Hydrophobic side chains displayed as spheres. *m*ABA and Acc residues are colored green while vinylogous  $\gamma^4$ -residues are colored orange.

Analysis of the 3D structures shows that each peptide forms a hairpin structure in aqueous solution. Peptide **74** experiences some twisting near the terminus, but the termini of hairpins are the least constrained section of the folded structure and are often subject to fraying. When viewed from the side, the four hydrophobic core residues of each hairpin are displayed on the same face, demonstrating no evidence of the inversion seen with 1:1  $\alpha$ - to  $\beta$ -residue substitution.

Closer examination of the two cyclic  $\gamma$ -residues used in peptides **73** and **74** shows a minor difference in the display of the amides on either end of the residues (Figure 41). The *m*ABA in peptide **73**, due to the planarity enforced by the conjugated ring, forces the adjacent amide N<sub>H</sub> and carbonyl groups closer together while the Acc monomer in **74** allows an extended backbone conformation that more closely mimics that of a natural sheet. However, in both cases, the amides are oriented in such a way as to allow for inter-sheet stacking without steric disruption from the backbones of the unnatural residues.

As a final point of comparison, peptides **73**, **74**, and **76** were overlaid with parent peptide **22a**. (Figure 42). In each case, measuring the RMSD values for the C, C <sub>$\alpha$</sub> , C <sub>$\beta$</sub> , N, and O atoms of residues Trp<sub>3</sub>, Tyr<sub>5</sub>, Phe<sub>12</sub>, and Val<sub>14</sub> between peptides **73**, **74**, and **76** versus **22a** gave values of 1.5 Å, 1.9 Å, and 1.5 Å, respectively. These values suggest that while 1:1  $\alpha$ - to  $\gamma$ -residue substitution changes the hairpin structure to a small degree, this substitution strategy using *m*ABA, Acc, and vinylogous  $\gamma^4$ -amino acids can be applied while still maintaining a native-like hairpin structure.

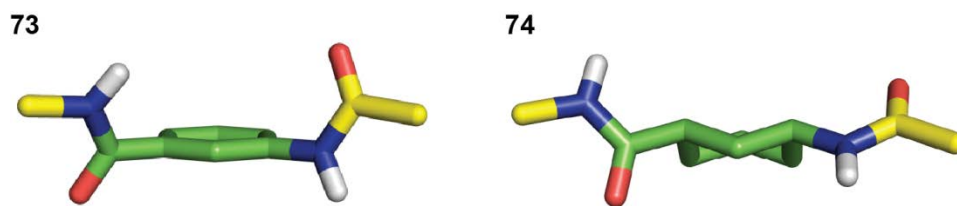


**Figure 41.** Close-up view of the cyclic  $\gamma$ -residues from the NMR solution structures of peptides **73** and **74**.

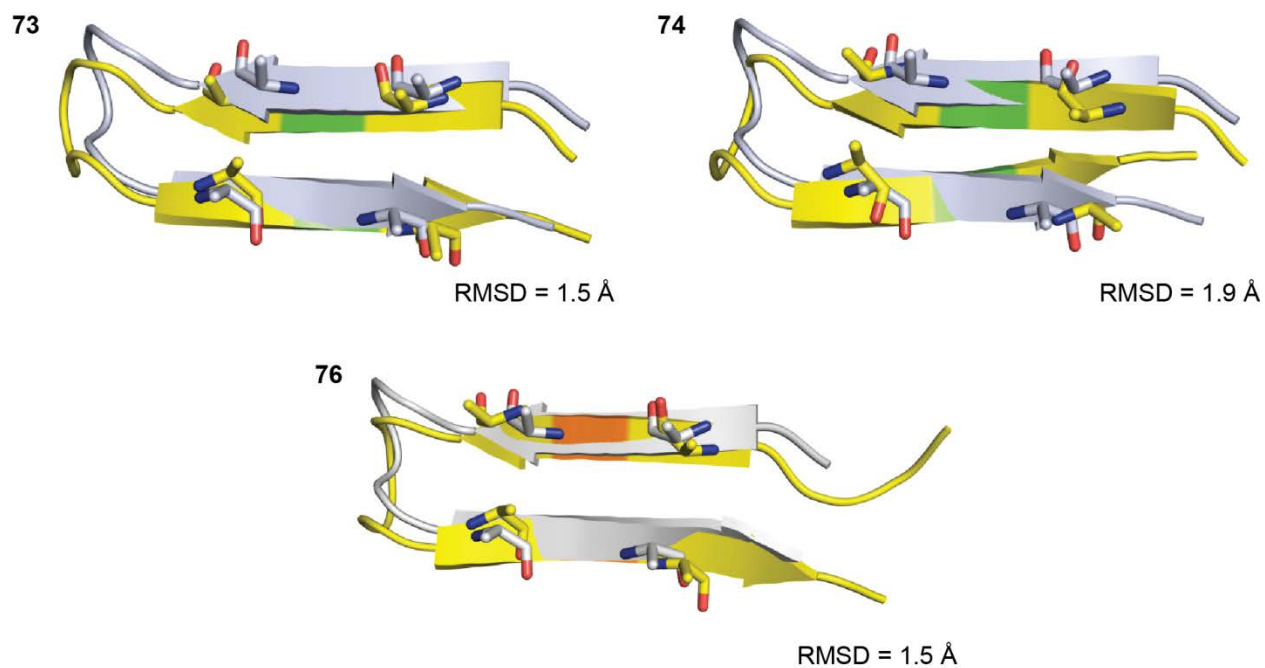


**Figure 42.** Overlays of the NMR solution structures of peptides **73**, **74**, and **76** (yellow) with parent peptide **22a** (white). *mABA* and *Acc* residues are colored green while vinylogous  $\gamma^4$ -residues are colored orange.

### 3.1.4 Conclusions

Unlike a 1:1  $\alpha$ - to  $\beta$ -residue substitution strategy which causes inversion of side chain display or 2:1 and 2:2  $\alpha$ - to  $\beta$ -residue substitution strategies which significantly destabilize the folded structure of small hairpin peptides, 1:1  $\alpha$ - to  $\gamma$ -residue substitution in each strand of a hairpin maintains native side chain display. Because  $\gamma$ -residues have an additional carbon atom in their backbones relative to  $\beta$ -residues, they can prevent the side chain inversion seen in  $\beta$ -residues.

Use of cyclic  $\gamma$ -amino acids *mABA* and *Acc* increases the stability of the folded structure by  $\sim 0.5$  kcal/mol. The enhanced stability of the hairpin arises from the ring constraint and backbone preorganization of cyclic  $\gamma$ -residues (Figure 43).

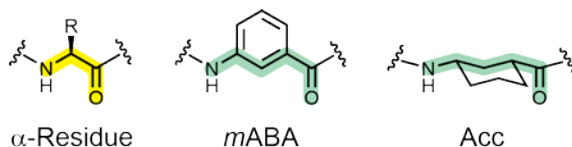


**Figure 43.** An  $\alpha$ -residue and cyclic  $\gamma$ -residues *mABA* and *Acc*.

The aromaticity of *mABA* residues enforces an extended chain geometry similar to that seen with an  $\alpha$ -residue. *Acc* residues, while not aromatic, also promote an extended chain in a similar fashion, enforced by a chair conformation equatorial substituents. Use of vinylogous  $\gamma^4$ -residues, on the other hand, slightly destabilizes the hairpin ( $\Delta\Delta G_{\text{fold}} = +0.6$  kcal/mol for two substitutions). Unlike the cyclic  $\gamma$ -residue variants, the backbones of vinylogous  $\gamma^4$ -residues are not as strongly constrained by aromaticity or a cyclohexane chair structure; instead, the  $\alpha,\beta$ -unsaturation is the sole source of backbone preorganization. While this double bond constrains rotation of the  $C_\alpha$ - $C_\beta$  bond, the  $N$ - $C_\gamma$  and  $C_\gamma$ - $C_\beta$  bonds are still relatively unconstrained and can freely rotate. The increased flexibility of the  $\gamma^4$ -residues relative

to cyclic  $\gamma$ -residues is likely the cause of the minor destabilization seen in the hairpin peptide. Unlike the cyclic residues, however, vinylogous  $\gamma^4$ -residues allow for retention of side chain functionality.

Overall, these data imply that 1:1  $\alpha$ - to  $\gamma$ -residue substitution could be applied to a sheet in a larger protein with a well-defined tertiary fold. Cyclic  $\gamma$ -residues can be used in place of  $\alpha$ -residues to when the side chain functionality is not critical. Vinylogous  $\gamma^4$ -residues can be used when a side chain functional group must be maintained, although with a slight penalty to overall stability.

## 3.2 N-METHYLATION OF SELECTED ALPHA-RESIDUES

While use of  $\gamma$ -residues in hairpin substitution strategies prevents inversion and can stabilize the folded structure, they also result in backbone lengthening which could impact the folded structure of larger proteins in unexpected ways. We chose to focus our next experiments on *N*-methylated  $\alpha$ -residues as these residues do not increase the length of the amino acid backbone and have been shown to impart enhanced proteolytic resistance<sup>121</sup> and increase bioavailability.<sup>122</sup> As with  $\gamma$ -residue substitution, the thermodynamic impact of *N*-methylation in peptide or protein  $\beta$ -sheets has not previously been examined.

### 3.2.1 *N*-Methylation Strategies Applied to a Model Hairpin Peptide

We first chose to individually substitute non-hydrogen bonding residues Trp<sub>3</sub>, Tyr<sub>5</sub>, Phe<sub>11</sub>, and Val<sub>13</sub> of peptide **22a** to generate peptides **77-80**, respectively (Figure 44). These four residues were individually substituted to determine the thermodynamic impact of *N*-methylation placement relative to the hairpin turn. Non-hydrogen-bonded positions were chosen as *N*-methylation has been shown to disrupt sheet stacking;<sup>74,123</sup> substitution at hydrogen-bonded positions would eliminate the possibility of the *N*-methyl residues disrupting inter-strand hydrogen-bonding.

**22a** H-GE**W**AYNPATGK**F**AVTE-NH<sub>2</sub>  
**77** H-GE**W**AYNPATGK**F**AVTE-NH<sub>2</sub>  
**78** H-GE**W**AYNPATGK**F**AVTE-NH<sub>2</sub>  
**79** H-GE**W**AYNPATGK**F**AVTE-NH<sub>2</sub>  
**80** H-GE**W**AYNPATGK**F**AVTE-NH<sub>2</sub>

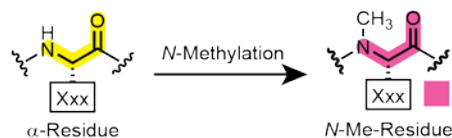


**Figure 44.** Sequences of model hairpin peptide **22a** and *N*-methylated peptides **77-80**.

### 3.2.2 NMR Analysis of *N*-Methylated Hairpin Peptides

Peptides **77-80** were synthesized by Fmoc solid-phase peptide synthesis methods and analyzed using multidimensional NMR as described in Section 3.3.4. Each *N*-methylated peptide showed evidence of two distinct conformations which we attributed to *cis* / *trans* isomerization about the tertiary amide at the site of *N*-methylation. We calculated the percentage of each conformation (Figure 45) by integration of the Asn<sub>6</sub> N<sub>H</sub>-H<sub>α</sub> and N<sub>H</sub>-H<sub>β</sub> TOCSY signals for each conformer. In this sequence, the protons of Asn<sub>6</sub> demonstrate clear dispersion from the resonances of other protons (Figure 46).

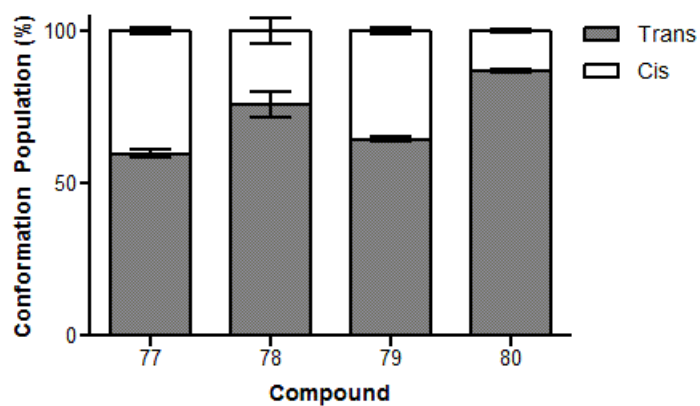


**Figure 45.** Populations of *cis* and *trans* conformations of *N*-methylated peptides **77-80**.

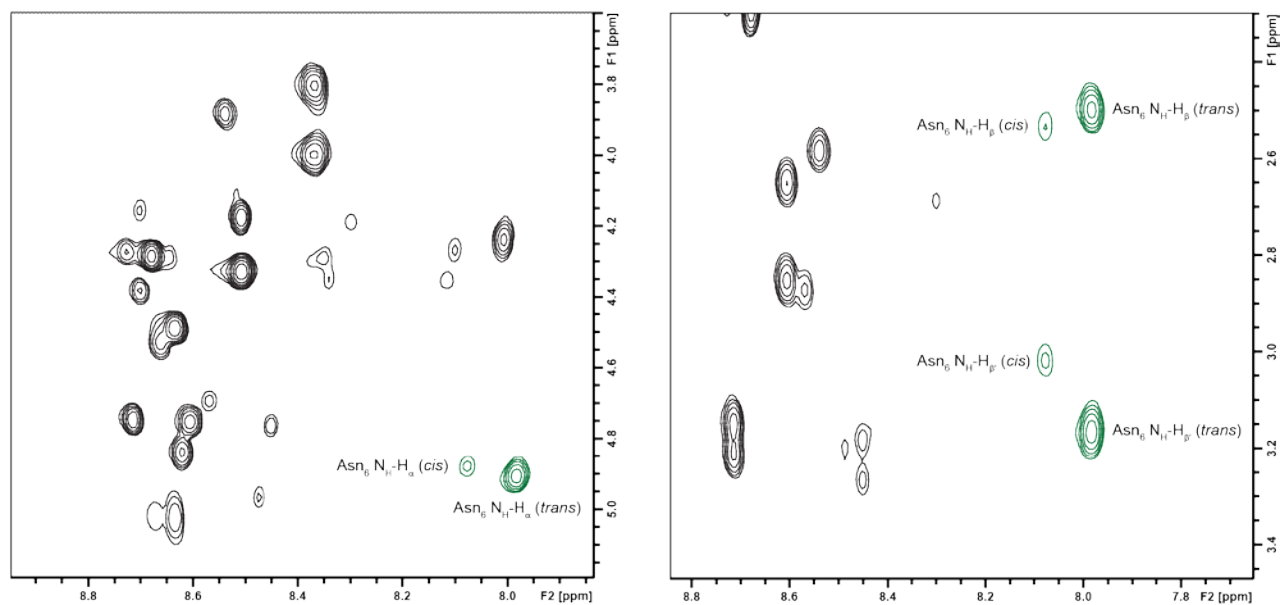


**Figure 46.** Close-up views of TOCSY spectra of peptide **80**.

$N_{H-\alpha}$  and  $N_{H-\beta}$  regions are displayed on the left and right, respectively.  $Asn_6$  cross-peaks are colored green.

Immediately apparent is the larger population of one conformation relative to the other. We assigned the predominant population as *trans* as this amide conformation has been shown to be the major conformer in peptide backbones. For all of the *N*-methyl peptides, NOE evidence verified this assignment as the *N*-Me protons had NOE contacts with both the side chain and H<sub>α</sub> protons of the preceding residue; these NOE's are consistent with the *trans* rather than the *cis* conformation (Figure 47). The *trans* amide population was roughly equal for peptides **77** and **79** while peptide **80** had a much higher population of *trans* conformer relative to the other peptides. The larger *trans* population of peptide **80** is consistent with published work showing that amino acids with β-branched side chains (such as valine) have a more destabilized *cis* conformation.<sup>124</sup> The *cis* amide conformation of an *N*-methyl amide forces the side chains of the *N*-Me and preceding residues closer together than in the *trans* conformation (Figure 48); introducing β-branching in the side chain of an *N*-Me residue creates additional steric clash, thereby destabilizing the *cis* conformation.

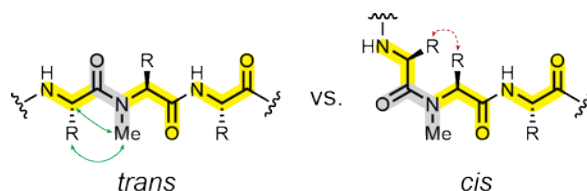


**Figure 47.** Predicted NOE signals with *trans* and *cis* *N*-Me amide configurations. Green arrows represent positive NOE contacts while red arrows represent NOE contacts not seen for the populations of *N*-Me peptides **77-80** assigned as *trans*.

Peptide **78** also has a larger population of *trans* conformer despite its lack of β-branching. In this peptide, the hydrophobic core side chains of Tyr<sub>5</sub>, Phe<sub>12</sub>, and Val<sub>14</sub> are found together in both *cis* and *trans* amide conformations (Figure 49); we hypothesized the increased *trans* population serves to draw Trp<sub>3</sub> into the hydrophobic core as well.



Using glycine separation analysis as in Section 2.1.2, we calculated the folded populations for both the *cis* and *trans* conformations of peptides **77-80** (Figure 50).

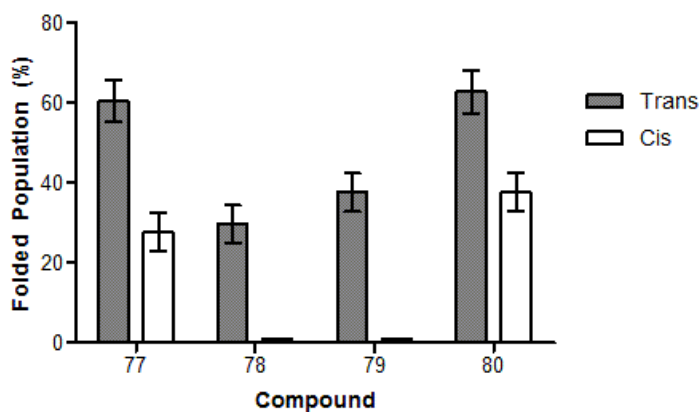


**Figure 50.** Folded populations of peptides **77-80**. Populations of *cis* and *trans* conformations were calculated using glycine separation analysis.

Peptides **77-80** each demonstrate a dramatic decrease in folded stability of the *cis* conformers relative to their respective *trans* conformers. This change is reasonable as the *cis* amide conformation redirects the peptide backbone, thereby disrupting the positioning of hydrophobic core residues necessary for maintaining the folded state. The magnitude of destabilization varies but is most significant when the *N*-methylation is found near the turn as in peptides **78** and **79**. As shown in peptides **77** and **80**, increasing the distance between the site of *N*-methylation and the turn of the hairpin decreases the degree of destabilization found with the *cis* conformer.

Analyzing the folded population of the *trans* conformers, we saw a decrease in folded stability when the site of *N*-methylation occurs near the turn. Computational studies have shown that *N*-methylation of  $\alpha$ -residues limits their energetically accessible conformations.<sup>125</sup> The region of the Ramachandran plot corresponding to dihedrals for extended conformations<sup>126</sup> becomes energetically

unfavorable for *N*-methyl residues, potentially leading to a change in backbone conformation and subsequent destabilization of folded structure.

To determine overall folded populations for peptides **77-80**, we multiplied the fraction of *trans* population by the folded population of the *trans* conformers (Table 6).

**Table 6.** Folded populations and  $\Delta G_{\text{fold}}$  for peptide **22a** and *N*-methyl peptides **77-80**.

Peptide	Folded Population (%)	$\Delta G_{\text{fold}}$ (kcal/mol)	$\Delta\Delta G_{\text{fold}}$ (kcal/mol)
<b>22a</b>	$66 \pm 5$	$-0.3 \pm 0.1$	---
<b>77</b>	$37 \pm 4$	$+0.3 \pm 0.1$	+0.6
<b>78</b>	$19 \pm 4$	$+0.8 \pm 0.2$	+1.1
<b>79</b>	$29 \pm 3$	$+0.5 \pm 0.2$	+0.8
<b>80</b>	$55 \pm 5$	$-0.1 \pm 0.1$	+0.2

*N*-methylation destabilizes the fold of a hairpin peptide by 0.2 – 0.6 kcal/mol when applied near the termini (peptides **77** and **80**) and ~1 kcal/mol when applied near the turn (peptides **78** and **79**). *N*-methylation of  $\beta$ -branched amino acids such as the valine used in peptide **80** can provide an increase in the *trans* population of the *N*-methyl amide and can increase folded stability.

### 3.2.3 Conclusions

Relative to the other monomer types discussed, *N*-methylation is less destabilizing than  $\beta$ -residue substitution but more destabilizing than  $\gamma$ -residue substitution. Unlike  $\beta$ -residue or vinylogous  $\gamma^4$ -residue substitution which can incorporate side chains required for folding or cyclic  $\gamma$ -residue substitution which can be applied at sites where side chain functionality is not required, choice of the location of *N*-

methylation is much more limited. Optimally, *N*-methylation would be restricted to sites with  $\beta$ -branched side chains. This decreases the population of the *cis* amide conformer, stabilizing the fold. Another important limitation is the need to restrict *N*-methylation to non-hydrogen bonded sites so as not to disrupt inter-strand contacts with the newly introduced backbone carbon. Additionally, *N*-methyl residues cannot be incorporated in the central strands of large sheet systems without disrupting hydrogen bonding. Overall, *N*-methylation can be used as a substitution strategy for  $\alpha$ -residues, but with some degree of destabilization and perhaps a limited selection of substitution sites.

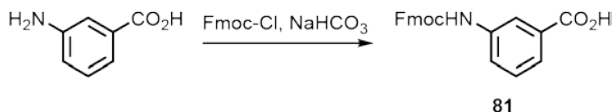
### 3.3 EXPERIMENTAL

#### 3.3.1 Monomer Synthesis

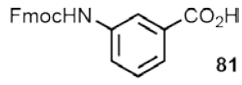
##### 3.3.1.1 General Information

Optical rotations were measured on a Perkin-Elmer 241 digital polarimeter with a sodium lamp at ambient temperature. NMR spectra of synthetic small molecules were recorded on a Bruker Avance-400 spectrometer. 2-(6-chloro-1H-benzotriazole-1-yl)-1,1,3,3-tetramethylammonium hexafluorophosphate (HCTU), NovaPEG Rink Amide Resin, 9-fluorenylmethyl *N*-succinimidyl carbonate (Fmoc-OSu), and Fmoc-protected  $\alpha$ -amino acids were purchased from Novabiochem. Solvents and all other reagents were purchased from Aldrich, Baker, Fisher, or TCI and used as received without further purification. Flash chromatography was performed using SorbTech silica gel (60 Å, 40-63  $\mu\text{m}$ ). Boc-(1*R*,3*S*)-3-aminocyclohexanecarboxylic acid (**82**) was synthesized from racemic *cis*-3-aminocyclohexanecarboxylic acid using a published protocol.<sup>127</sup> The Weinreb amide of Fmoc-Ala-OH (**84**) was synthesized using a published protocol.<sup>128</sup>

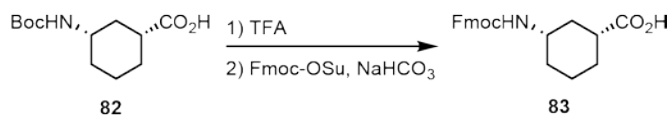
### 3.3.1.2 Synthesis of Fmoc-*m*ABA-OH



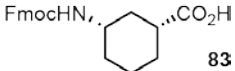
**Scheme 3.1.** Synthesis of Fmoc-*m*ABA-OH (**81**).

 **Fmoc-*m*-aminobenzoic acid (81):** To a solution of 501 mg *m*-aminobenzoic acid (3.65 mmol, 1 equiv) in 13 mL *p*-dioxane was added a solution of 1.53 g sodium bicarbonate (18.2 mmol, 5 equiv) in 5 mL of water followed by 1.04 g Fmoc chloride (4.02 mmol, 1.1 equiv). The reaction was allowed to stir overnight, then neutralized with 1 M hydrochloric acid and extracted three times with ethyl acetate. The organic layers were combined, dried with magnesium sulfate, and concentrated. The concentrate was purified using column chromatography (10% → 33% ethyl acetate in hexanes) and dried under vacuum to afford the product as a white solid (799 mg, 2.22 mmol, 61% yield). <sup>1</sup>H NMR matched previously reported spectral data.<sup>129</sup>

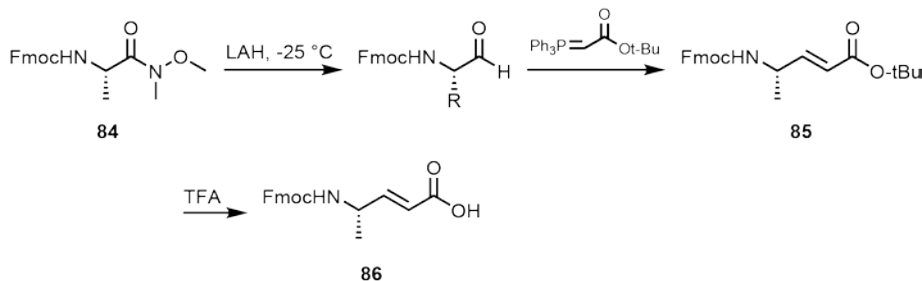
### 3.3.1.3 Synthesis of Fmoc-Acc-OH



**Scheme 3.2.** Synthesis of Fmoc-Acc-OH (**83**).

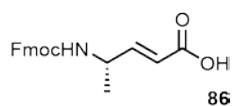
**Fmoc-(1R, 3S)-3-aminocyclohexanecarboxylic acid (83):** To a stirred solution of  **83** 1.116 g compound **82** (4.59 mmol, 1 equiv) in 4.6 mL dichloromethane was added 4.6 mL trifluoroacetic acid. The solution was stirred 2 h after which time it was concentrated and the solvent co-evaporated three times with chloroform to afford the amino acid TFA salt which was used directly. The concentrate (4.59 mmol, 1 equiv) was dissolved in 20 mL water and titrated to pH 7 with saturated aqueous sodium bicarbonate. To this solution was added 766 mg sodium bicarbonate (9.18 mmol, 2 equiv), 20 mL dioxane, and 1.548 g Fmoc-OSu (4.59 mmol, 1 equiv). The reaction was stirred overnight and then the organic solvent was removed under reduced pressure. The remaining aqueous solution was acidified with 1 M hydrochloric acid solution and extracted three times with ethyl acetate. The organics were dried with magnesium sulfate, concentrated, and purified using column chromatography (50% ethyl acetate in hexanes with 1% triethylamine → ethyl acetate → ethyl acetate with 1% acetic acid) to afford the product along with residual acetic acid. The acetic acid was removed via co-evaporation with heptane and the resulting residue was dried under vacuum to afford the product as a white solid (990 mg, 2.71 mmol, 59% yield).  $[\alpha]_D = -29$  ( $c = 0.50$ , MeOH);  $^1\text{H}$  NMR (400 MHz, DMSO- $d_6$ )  $\delta$  12.10 (s, 1 H), 7.88 (d,  $J = 7.4$  Hz, 2 H), 7.69 (d,  $J = 7.2$  Hz, 2 H), 7.41 (t,  $J = 7.3$  Hz, 2 H), 7.32 Hz (t,  $J = 7.4$  Hz, 2 H), 7.27 (d,  $J = 7.8$  Hz, 1 H), 4.30 (m, 2 H), 4.22 (d,  $J = 6.4$  Hz, 1 H), 3.31 (m, 1 H), 2.27 (t,  $J = 11.5$  Hz, 1 H), 2.00 (d,  $J = 11.7$  Hz, 1 H), 1.76 (m, 3 H), 1.26 (m, 2 H), 1.11 (m, 2 H);  $^{13}\text{C}$  NMR (100 MHz, DMSO- $d_6$ )  $\delta$  176.0, 155.3, 143.9, 140.7, 127.6, 127.0, 125.2, 120.1, 65.1, 49.0, 46.8, 41.7, 35.1, 32.0, 27.9, 23.8; HRMS  $m/z$  calculated for  $\text{C}_{22}\text{H}_{23}\text{NO}_4\text{Na}$   $[\text{M}+\text{Na}]^+$  388.1525; found 388.1502.

### 3.3.1.4 Synthesis of Fmoc- $\gamma^4$ -Ala-OH



**Scheme 3.3.** Synthesis of Fmoc- $\gamma^4$ -Ala-OH (**86**).

**Fmoc- $\gamma^4$ -Ala-OtBu (85).**<sup>130</sup> To a stirred solution of 673 mg compound **84** (1.90 mmol, 1 equiv) in 15 mL tetrahydrofuran at  $-25\text{ }^\circ\text{C}$  was added 79 mg lithium aluminum hydride (2.1 mmol, 1.1 equiv). The reaction was allowed to stir for 30 minutes, then quenched with 1 M hydrochloric acid, diluted with water, and extracted three times with ethyl acetate. The combined organics were washed with brine, dried with magnesium sulfate, and concentrated to afford the desired Fmoc-aldehyde which was used directly without purification. To a stirred solution of aldehyde (1.90 mmol, 1 equiv) in 10mL tetrahydrofuran was added 717 mg (*tert*-butoxycarbonylmethylene) triphenylphosphorane (1.90 mmol, 1 equiv). The reaction was stirred overnight, concentrated, and purified using column chromatography (20% ethyl acetate in hexanes) to afford the product as a white foam (426 mg, 1.08 mmol, 57% yield over 2 steps).  $[\alpha]_{\text{D}} = -13.2$  ( $c = 1.00$ ,  $\text{CHCl}_3$ ).  $^1\text{H NMR}$  (400 MHz,  $\text{CDCl}_3$ )  $\delta$  7.77 (d,  $J = 7.5$  Hz, 2 H), 7.59 (d,  $J = 7.3$  Hz, 2 H), 7.40 (t,  $J = 7.4$  Hz, 2 H), 7.32 (t,  $J = 7.3$  Hz, 2 H), 6.77 (dd,  $J = 4.6, 15.7$ , 1 H), 5.83 (d,  $J = 15.6$  Hz, 1 H), 4.78 (d,  $J = 6.8$  Hz, 1 H), 4.44 (m, 3 H), 4.22 (t,  $J = 6.7$  Hz, 1 H), 1.50 (s, 9 H), 1.30 (d,  $J = 6.4$  Hz, 3 H);  $^{13}\text{C NMR}$  (100 MHz,  $\text{CDCl}_3$ )  $\delta$  165.5, 155.4, 147.4, 143.8, 141.3, 127.7, 127.0, 125.0, 122.3, 120.0, 80.6, 66.7, 47.2, 28.1, 20.3. HRMS  $m/z$  calculated for  $\text{C}_{24}\text{H}_{28}\text{NO}_4$   $[\text{M}+\text{H}]^+$  394.2018; found 394.2014.



**Fmoc- $\gamma^4$ -Ala-OH (86).** To a stirred solution of 351 mg compound **85** (0.892 mmol, 1 equiv) in 5 mL dichloromethane was added 5 mL trifluoroacetic acid. The reaction

was stirred 4 h, concentrated, solvent-exchanged with chloroform three times, and purified using column chromatography (50% ethyl acetate in hexanes) to afford the product as a white solid (240 mg, 0.711 mmol, 80% yield).  $[\alpha]_D = -13$  ( $c = 0.50$ , DMSO- $d_6$ ).  $^1\text{H NMR}$  (400 MHz,  $\text{CDCl}_3$ )  $\delta$  12.33 (s, 1 H), 7.89 (d,  $J = 7.4$  Hz, 2 H), 7.71 (d,  $J = 7.3$  Hz, 2 H), 7.60 (d,  $J = 7.9$  Hz, 1 H), 7.41 (t,  $J = 7.4$  Hz, 2 H), 7.33 (t,  $J = 7.2$  Hz, 2 H), 6.67 (dd,  $J = 15.7$  Hz, 5.0 Hz, 1 H), 5.77 (d,  $J = 15.7$  Hz, 1 H), 4.32 (m, 2 H), 4.23 (m, 2 H), 1.19 (d,  $J = 6.8$  Hz, 3 H);  $^{13}\text{C NMR}$  (100 MHz,  $\text{CDCl}_3$ )  $\delta$  167.1, 155.4, 149.7, 143.9, 140.7, 127.6, 127.0, 125.2, 120.2, 120.1, 79.2, 65.4, 47.1, 46.7, 19.8. HRMS  $m/z$  calculated for  $\text{C}_{20}\text{H}_{20}\text{NO}_4$   $[\text{M}+\text{H}]^+$  338.1392; found 338.1382.

### 3.3.2 Peptide Synthesis

Peptides were synthesized using standard microwave-assisted (CEM MARS) Fmoc solid-phase synthesis techniques on NovaPEG Rink Amide resin. Couplings were carried out with a two minute ramp to 70 °C and a four minute hold at that temperature using 4 equiv Fmoc-protected amino acid, 4 equiv HCTU, and 6 equiv DIEA using *N*-methyl-2-pyrrolidone as the solvent. Deprotections were performed with a two minute ramp to 80 °C with a two minute hold at that temperature using an excess of 20% 4-methylpiperidine in DMF. After each coupling or deprotection cycle, the resin was washed three times with DMF. Residue Asn<sub>6</sub> and residues following *N*-methyl residues were double coupled and residues immediately following *m*ABA residues were triple coupled to prevent deletion products.

Prior to cleavage, the resin was washed three times with DMF, washed three times with dichloromethane, washed three times with methanol and dried under vacuum. Peptides were cleaved from resin by agitating in solution of 95% trifluoroacetic acid, 2.5% triisopropyl silane, and 2.5% water for 3 h.

Crude peptide was precipitated from the cleavage mixture by dilution with ether and purified by HPLC on a C<sub>18</sub> preparative column using gradients between 0.1% TFA in water and 0.1% TFA in acetonitrile

Cysteine-containing peptide **76** was purified, lyophilized, dissolved in 10 mM phosphate buffer (pH 8.9, 5% v/v DMSO), stirred until analytical HPLC and MS showed complete conversion to the cyclic disulfide (2 d), and then re-purified.

All peptides were >95% pure by analytical HPLC on a C<sub>18</sub> column. Identities were confirmed using a Voyager DE Pro MALDI-TOF instrument (Table 7).

**Table 7.** MALDI-TOF masses of peptides **73-80**.

Peptide	[M+H] <sup>+</sup> <i>m/z</i>	
	Calculated	Observed
<b>73</b>	1857.8	1857.9
<b>74</b>	1847.9	1847.8
<b>75</b>	1791.9	1791.4
<b>76</b>	2037.9	2037.5
<b>77</b>	1753.9	1753.8
<b>78</b>	1753.9	1753.8
<b>79</b>	1753.9	1753.7
<b>80</b>	1753.9	1752.8

### 3.3.3 NMR Sample Preparation and Data Collection

NMR samples were prepared by dissolving 2-3 mg peptide in 750-850  $\mu$ L de-gassed buffer solution (50 mM phosphate, 9:1 H<sub>2</sub>O/D<sub>2</sub>O, uncorrected pH 6.3) to make ~2 mM solutions. 3-(Trimethylsilyl)-1-propanesulfonic acid sodium salt (DSS, 50 mM in water) was added to a final concentration of ~0.2 mM DSS in the sample. Each solution was passed through a 0.2  $\mu$ m syringe filter, transferred to an NMR tube,

and stored until analysis. The NMR tube headspace was purged with a stream of nitrogen prior to capping.

NMR spectra of peptides were recorded on a Bruker Avance-700 spectrometer. Chemical shifts are reported relative to DSS (0 ppm). NMR spectra were measured at 278 K. TOCSY, NOESY, and COSY pulse programs used excitation-sculpted gradient-pulse solvent suppression. All experiments were obtained using 2048 data points in the direction dimension and 512 data points in the indirect dimension. TOCSY were acquired with a mixing time of 80 ms and NOESY were acquired with a mixing time of 200 ms.

### **3.3.4 NMR Data Analysis and Structure Determination**

NMR data was obtained and analyzed as detailed in Section 2.3.4. The ten lowest energy structures were used for calculating average structures of each peptide.

### **3.3.5 Calculation of Folding Equilibria by NMR**

Population analysis was performed as detailed in Section 2.3.5.

## 4.0 UNNATURAL SHEET MODIFICATION APPLIED TO PROTEIN GB1

Part of the results detailed in this chapter has been published in:

1. Reinert, Z.E.; Lengyel, G.A.; Horne, W.S., “Protein-like Tertiary Folding Behavior from Heterogeneous Backbones,” *Journal of the American Chemical Society*, **2013**, 12528-12531.

Previous chapters have detailed the structural and thermodynamic consequences of various unnatural residue substitution strategies in model  $\beta$ -hairpins. Application of a 1:1  $\alpha$ - to  $\beta$ -residue substitution disrupted the side chain and hydrogen bond display of the hairpin peptide model system (Section 2.1). All other strategies, 2:1 or 2:2  $\alpha$ - to  $\beta$ -residue substitution (Section 2.2), 1:1  $\alpha$ - to  $\gamma$ -residue substitution (Section 3.1), and *N*-methylation (Section 3.2), prevented this inversion while having varying impacts on the thermodynamics of folding.

To provide an overall comparison of the thermodynamic impact of each residue substitution strategy, the  $\Delta\Delta G_{\text{fold}}$  values for each substitution strategy tested were normalized to the number of  $\alpha$ -residues replaced (Table 8).

**Table 8.** Normalized thermodynamic impacts of examined unnatural residue substitution strategies.

Substitution Strategy	$\Delta\Delta G_{\text{fold}}$ per replacement (kcal/mol)
1:1 $\alpha$ to $\beta$	---
2:1 $\alpha$ to $\beta^2/\beta^3$	+0.5
2:1 $\alpha$ to $\beta^{2,3}$	+0.7
2:2 $\alpha$ to $\beta^2/\beta^3$	>0.9
2:2 $\alpha$ to $\beta^{2,3}$	+0.5
1:1 $\alpha$ to $\gamma$ ( <i>mABA</i> )	-0.2
1:1 $\alpha$ to $\gamma$ ( <i>Acc</i> )	-0.3
1:1 $\alpha$ to $\gamma$ (vinylogous $\gamma^4$ )	+0.3
<i>N</i> -methylation (turn)	+1.1
<i>N</i> -methylation (terminal)	+0.6
<i>N</i> -methylation (terminal, $\beta$ -branched)	+0.2

Overall, unnatural residue substitution had an accompanying  $\Delta\Delta G_{\text{fold}}$  ranging from +0.9 to -0.3 kcal/mol per  $\alpha$ -residue replaced. Because this data set is limited to a short hairpin peptide, conclusions that can be made for a larger protein with a more complex folded structure are limited. To gauge the utility of the successful unnatural residue substitutions examined in the hairpin peptide, we applied these strategies to a protein with a well-defined tertiary fold.

#### 4.1 UNNATURAL RESIDUE SUBSTITUTIONS IN PROTEIN GB1

As a model system, we chose protein GB1, from which the hairpin peptide used for our previous thermodynamic analysis is derived.<sup>41</sup> Protein GB1 is the 56 residue B1 domain of protein G, an immunoglobulin binding protein from *Streptococcus* bacteria.<sup>81</sup> GB1 has a compact tertiary fold with four  $\beta$ -strands packed against an  $\alpha$ -helix (Figure 51).<sup>82-84</sup>





Proteins **81** and **82** were synthesized using solid-phase peptide synthesis techniques and analyzed using CD in aqueous phosphate buffer, pH 7 (Figure 54). CD measures the differential absorbance of circularly polarized light by chiral molecules.<sup>134</sup> As peptides have chiral centers, they will demonstrate characteristic signatures depending on their secondary structure content.

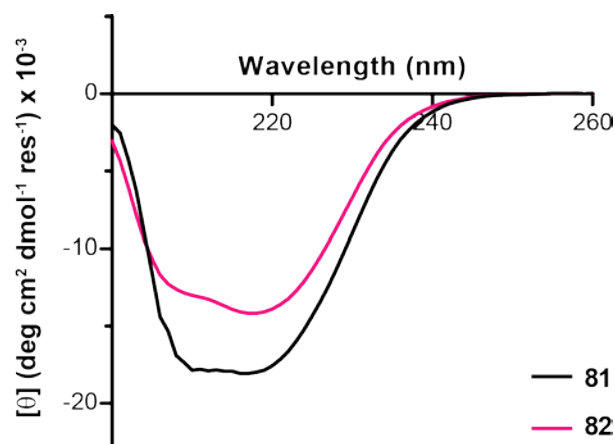


**Figure 54.** CD scans of proteins **81** and **82**.  
Samples consisted of 40  $\mu$ M protein in 20 mM sodium phosphate buffer, pH 7.0.

The CD scan of GB1, protein **81**, shows clear minima at 209 and 220 nm that are typical of a protein with combined  $\alpha$ -helical and  $\beta$ -sheet structures.<sup>135</sup> The scan of *N*-methyl variant **82** shows a similar shape, although the minima are less intense. The intensity of the minima at 209 and 220 nm are indicative of folded structure, suggesting protein **82** is not as well-folded as protein **81**. To quantify the degree of destabilization caused by *N*-methylation, we performed thermal denaturation experiments on proteins **81** and **82** (Figure 55).

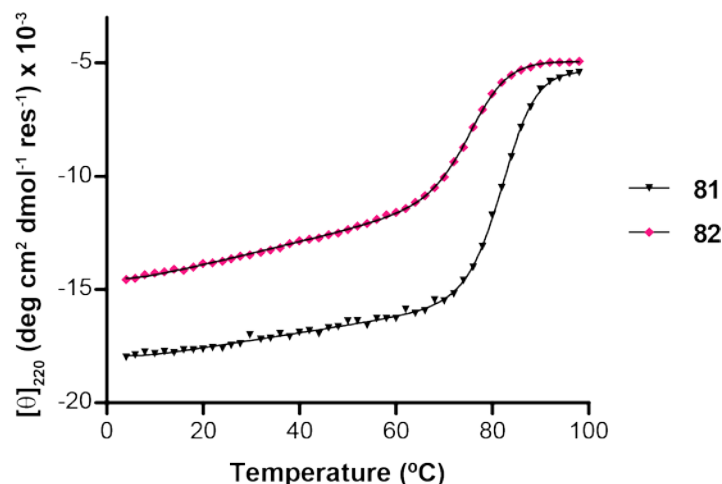


**Figure 55.** Thermal denaturation melts of proteins **81** and **82**. Samples consisted of 40  $\mu$ M protein in 20 mM sodium phosphate buffer, pH 7.0.

Thermal denaturation can be used as an assessment of folded structure stability; we monitored the CD signature of proteins **81** and **82** at 220 nm as a function of temperature. Both proteins **81** and **82** show a sigmoidal unfolding transition with a well-defined fully-folded baseline. A sigmoidal transition allows for measurement of a melting temperature ( $T_m$ ) and is indicative of cooperativity of folding; as one part of the protein begins to unfold, the entire protein unfolds. Using a two-state thermal denaturation model,<sup>136</sup> we calculated the midpoint of the melting transition for **81** and **82** (Table 9). From these  $T_m$  values and a  $\Delta H_{fold}$  value of  $-58.4$  kcal/mol for wild-type protein **81** found using differential scanning calorimetry,<sup>137</sup> we used equation 6 to estimate the  $\Delta\Delta G_{fold}$  for mutant protein **82**.<sup>138</sup>

$$(6) \quad \Delta\Delta G_{fold} = \Delta H_{fold} \frac{\Delta T_m}{T_m}$$

**Table 9.** Folding thermodynamics of proteins **81** and **82**.

<b>Protein</b>	<b>T<sub>m</sub> (°C)</b>	<b>ΔT<sub>m</sub> (°C)</b>	<b>ΔΔG<sub>fold</sub> (kcal/mol)</b>
<b>81</b>	82.1 ± 0.3	---	---
<b>82</b>	75.6 ± 0.2	-6.5	+1.1 ± 0.1

Protein **82** has a T<sub>m</sub> decrease of 6.5 °C relative to parent protein **81**. This value corresponds to an overall destabilization of roughly 1 kcal/mol or ~0.5 kcal/mol per α- to *N*-Me-α-residue substitution. This value is similar to the hairpin peptide value of ~0.4 kcal/mol per substitution for a non β-branched *N*-methyl residue found distant from the turn.

Overall, incorporation of *N*-methyl amino acids in the sheet of a protein is tolerated with a small amount of destabilization and folding similar to the parent protein. One significant limitation of this system, however, is the requirement of substitution of residues where the *N*-methyl group is facing away from the other strands found in a sheet so as not to disrupt inter-strand hydrogen bonding.

#### 4.1.2 Beta-Residue Substitution in Protein GB1

To move away from *N*-methyl amino acids, where substitution sites are limited by hydrogen bonding, we applied 2:1 (**83**) and 2:2 (**84**) α- to β-residue substitution strategies to a stripe of residues found in the central positions of each strand, similar to the positions selected in our work with β-hairpin peptides (Figure 56). As use of a combination of β<sup>2</sup>- and β<sup>3</sup>-amino acids or β<sup>2,3</sup>-amino acids had similar thermodynamic impacts in our hairpin studies, we chose to utilize β<sup>2</sup>- and β<sup>3</sup>-amino acids in this study for ease of monomer synthesis.

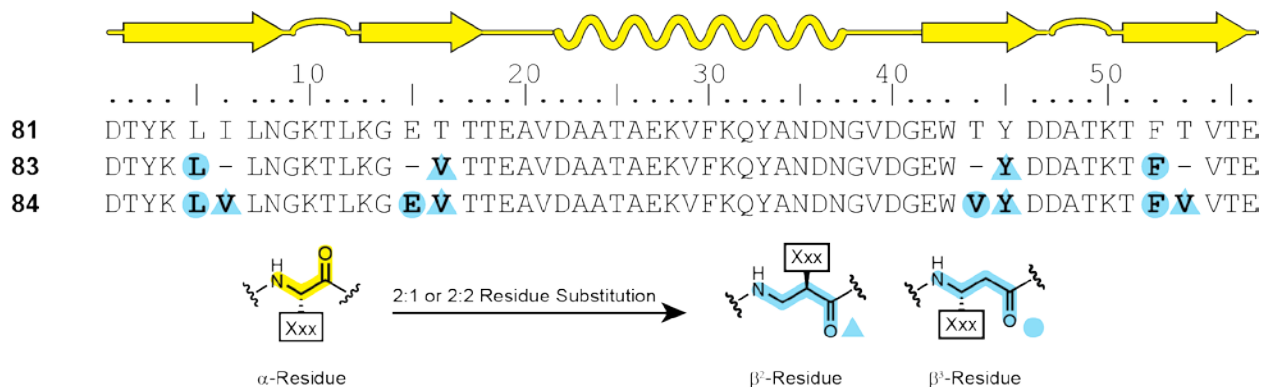


**Figure 56.** Sequences parent protein **81** and  $\alpha/\beta$ -hybrids proteins **83** and **84**.

A 2:1  $\alpha$ - to  $\beta$ -residue substitution strategy was applied with protein **83**. Use of a 2:1 substitution shortens the backbone by two atoms, essentially acting as an amide deletion while maintaining the backbone carbon atoms of the two  $\alpha$ -residues replaced. Residues Ile<sub>6</sub>, Glu<sub>15</sub>, Thr<sub>44</sub>, and Thr<sub>53</sub>, shown to have side chains oriented opposite the helix in the crystal structure of **81**, were removed. Hydrophobic packing residues Leu<sub>5</sub>, Val<sub>16</sub>, Tyr<sub>45</sub>, and Phe<sub>52</sub> were modified to either  $\beta^2$ - or  $\beta^3$ -residues, depending on the side chain display required to mimic the natural protein. Thr<sub>16</sub> was mutated to valine for ease of synthesis of the unnatural monomer. Valine is an isostere of threonine but lacks the alcohol functionality that requires an additional protecting group when used in SPPS.

A 2:2  $\alpha$ - to  $\beta$ -residue substitution strategy was applied to generate protein **84**, keeping the same four core side chains retained in protein **83**. Unlike 2:1 substitution which shortens the backbone by two atoms, 2:2 substitution *extends* the length of the backbone by two atoms. Ile<sub>6</sub>, Glu<sub>15</sub>, Thr<sub>44</sub>, and Thr<sub>53</sub> were also retained with mutations of the two threonine side chains to valine. Again,  $\beta^2$ - or  $\beta^3$ -amino acids were selected depending on the side chain display of parent protein **81**.

CD scans and thermal denaturation melts were obtained for proteins **81**, **83**, and **84** (Figure 57).

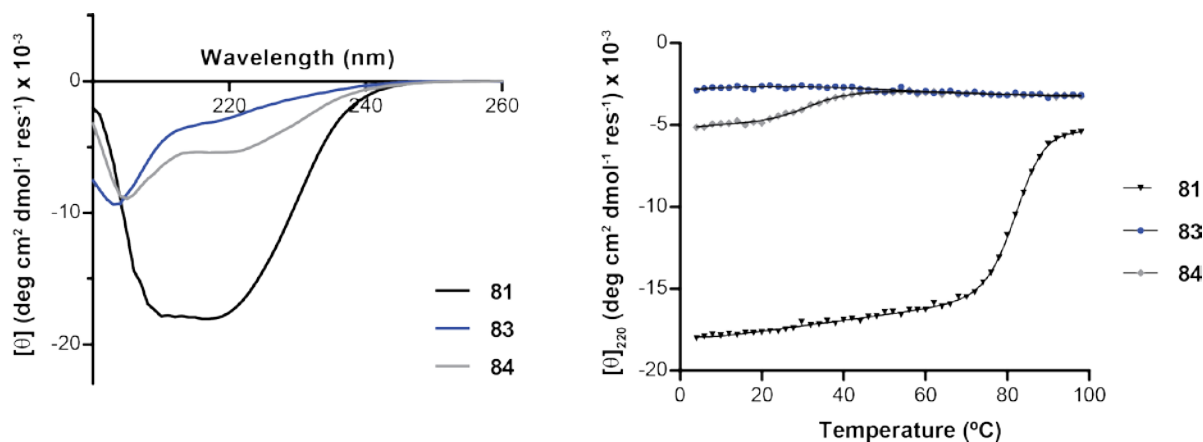


**Figure 57.** CD scans and melts of proteins **81**, **83**, and **84**.  
 Samples consisted of 40  $\mu\text{M}$  protein in 20 mM sodium phosphate buffer, pH 7.0.

In contrast to wild-type protein **81** which has a well-defined minima at 209 and 220 nm, the scans of **83** and **84** show a marked loss of minima at these two wavelengths and a new minimum near 200 nm, suggestive of random-coil structure. Counter to our work in the  $\beta$ -hairpin peptide which shows 2:2  $\alpha$ - to  $\beta^2/\beta^3$ -residue substitutions are the most destabilized, protein **84** demonstrates slightly more pronounced minima than protein **83** incorporating a 2:1 substitution. We hypothesize the added flexibility of two  $\beta$ -residues allows for accommodation of the lengthened backbone and formation of a more native-like fold, but the CD scan data suggest neither  $\beta$ -substituted proteins are stable enough to maintain an ordered folded tertiary structure.

Analysis of the melt data shows hybrid protein **83** undergoes no thermal transition while protein **84** undergoes a very minor transition near 35  $^{\circ}\text{C}$ . Based on these data combined with the results from the CD scans, it can be concluded that introducing  $\beta$ -amino acids into GB1 significantly destabilizes the folded structure or abolishes it completely.



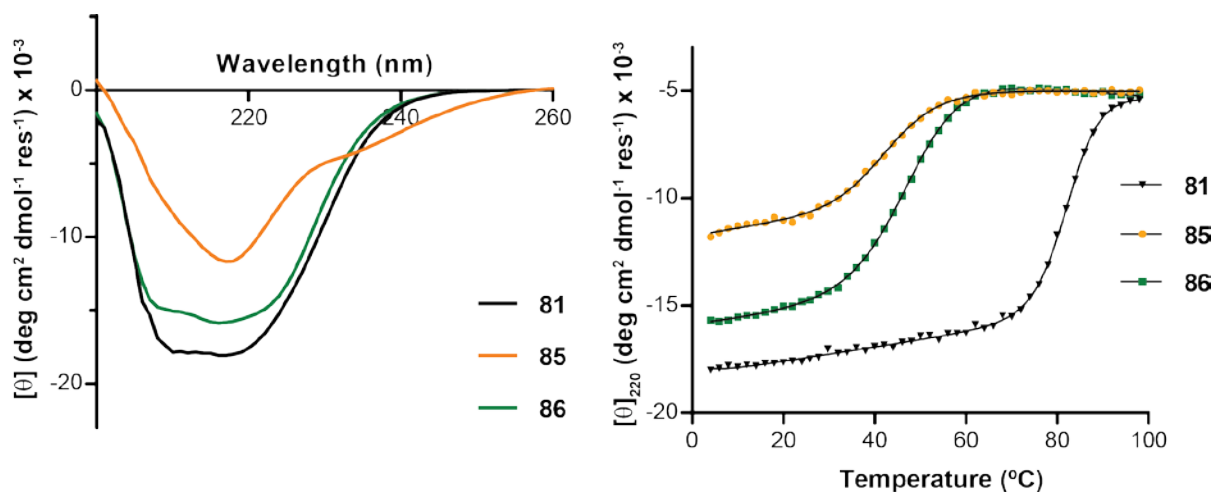


**Figure 59.** CD scans and melts for proteins **81**, **85**, and **86**. Samples consisted of 40  $\mu$ M protein in 20 mM sodium phosphate buffer, pH 7.0.

Analysis of the CD scans shows that, unlike the proteins with  $\beta$ -residue substitutions, Acc-substituted protein **86** has a similar shape to that of wild-type protein **81** with minima near 209 and 220 nm. Protein **85**, while having a distinct minimum around 218 nm, does not have the signature minimum at 209 nm. NMR structures showed that insertion of vinylogous  $\gamma^4$ -amino acids in our hairpin peptide did not significantly alter the shape of the  $\beta$ -sheet, so we theorized the change in CD signature results from the spectral character of the vinylogous  $\gamma^4$ -residue rather than a structural change of the protein. If this hypothesis is correct, CD scans of the hairpin peptide containing vinylogous  $\gamma^4$ -residues will also have a minimum shifted to 218 nm. We analyzed model hairpin peptide **22a** and hybrid hairpins **74** and **75** containing Acc and vinylogous  $\gamma^4$ -residues, respectively by CD (Figure 60).

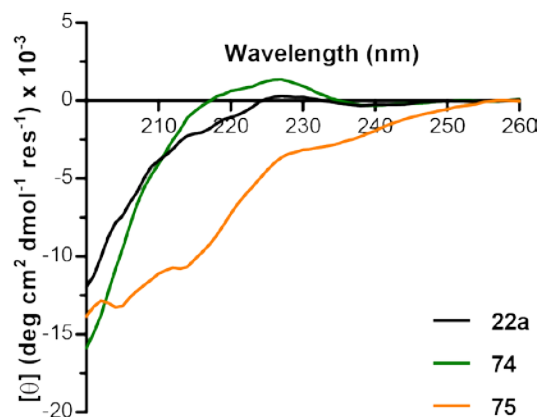


**Figure 60.** CD scans of model hairpin peptide **22a** and  $\alpha/\gamma$ -hybrid peptides **74** and **75**. Samples consisted of 40  $\mu$ M protein in 20 mM sodium phosphate buffer, pH 7.0.

CD scans of model peptide **22a** and Acc hybrid peptide **74** have similar shapes, suggesting Acc residues do not significantly alter the CD signature of a peptide. Vinylogous  $\gamma^4$ -hybrid peptide **75**, however, has a decreased signature near 218 nm relative to peptide **22a**. Also of note is a gradual tailing to a mean molar absorptivity of 0 in the range of 230 to 260 nm. Peptides **22a** and **74** have a signature near 0 along the same range. This data supports the hypothesis that the shift in CD signature of protein **85** relative to parent protein **81** may be a result of the change in signature from vinylogous  $\gamma^4$ -residues and not of a change in the folded structure of the protein.

We next compared the thermal denaturation melts for proteins **85** and **86** to protein **81**. Unlike  $\beta$ -residue containing proteins **83** and **84**, both proteins **85** and **86** have sigmoidal unfolding transitions, suggesting an ordered folded structure. Analysis of the melts gave  $T_m$  values of 43.5  $^{\circ}$ C and 46.7  $^{\circ}$ C for proteins **85** and **86**, respectively (Table 10). These two  $T_m$  values are significantly lower than the wild-type  $T_m$  of 82.1  $^{\circ}$ C, suggesting the inclusion of  $\gamma$ -amino acids in GB1 is significantly destabilizing. Calculating  $\Delta\Delta G_{\text{fold}}$  gave values near 6 kcal/mol or  $\sim 1.5$  kcal/mol per residue. Compared to the expected change of  $-0.3$  kcal/mol for Acc and  $+0.3$  kcal/mol for the vinylogous  $\gamma^4$ -residues in our hairpin model system, introduction of these amino acids in GB1 is significantly more destabilizing.

**Table 10.** Folding thermodynamics for proteins **81**, **85**, and **86**.

Protein	$T_m$ ( $^{\circ}\text{C}$ )	$\Delta T_m$ ( $^{\circ}\text{C}$ )	$\Delta\Delta G_{\text{fold}}$ (kcal/mol)
81	$82.1 \pm 0.3$	---	---
85	$43.5 \pm 0.9$	-38.6	$+6.3 \pm 0.2$
86	$46.5 \pm 0.5$	-35.6	$+5.9 \pm 0.1$

As  $\gamma$ -residue substitution was unpredictably destabilizing, we sought to further investigate the cause of this destabilization. Substitutions with Acc stabilized the hairpin peptide model system more than use of vinylogous  $\gamma^4$ -amino acids, so we focused on Acc substitution. Originally, positions for Acc substitution in protein **86** were chosen so as not to replace any of the hydrophobic residues that pack against the helix of GB1, but we did not take other stabilizing factors, such as salt-bridges or charge-charge interactions, into consideration. Looking at the crystal structure of wild-type GB1, we identified two sites where a stabilizing side chain interactions could be disrupted with Acc substitution (Figure 61).

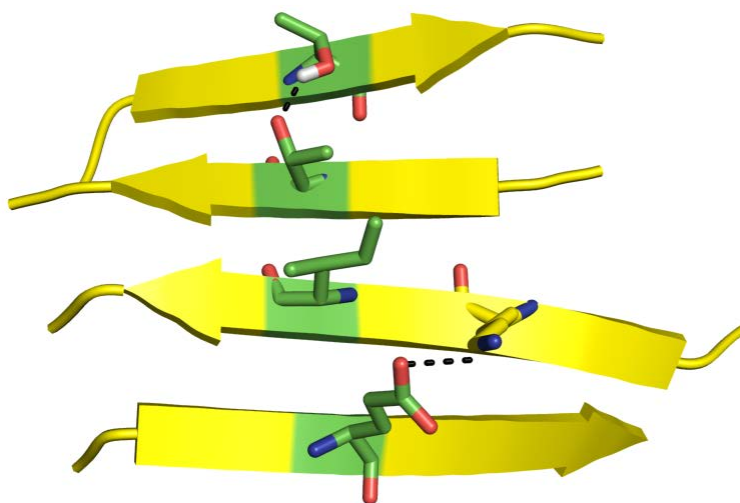


**Figure 61.** Side chain interactions of Acc-substituted positions (green) in protein **86**. Polar contacts are shown as black dotted lines. Coordinates based on PDB: 2QMT.

Acc-substituted position Glu<sub>15</sub> forms an inter-strand salt-bridge with Lys<sub>4</sub>. Additionally, the side chains of Thr<sub>44</sub> and Thr<sub>53</sub> have a hydrogen-bond interaction which would be lost with Acc substitution. To

determine the exact thermodynamic effects of losing these stabilizing interactions, we designed GB1 mutant **87** with an alanine mutation of Glu<sub>15</sub> and valine mutations of Thr<sub>44</sub> and Thr<sub>53</sub> (Figure 62). These mutations were chosen to eliminate any side-chain polar interactions while providing similar  $\beta$ -sheet propensities. We analyzed protein **87** using CD spectroscopy (Figure 63).

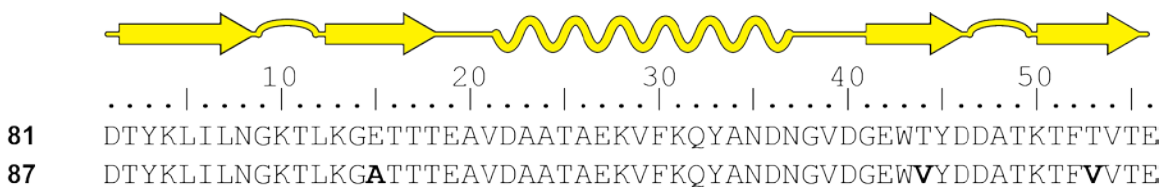


**Figure 62.** Sequences of wild-type protein **81** and side chain mutant **87**.

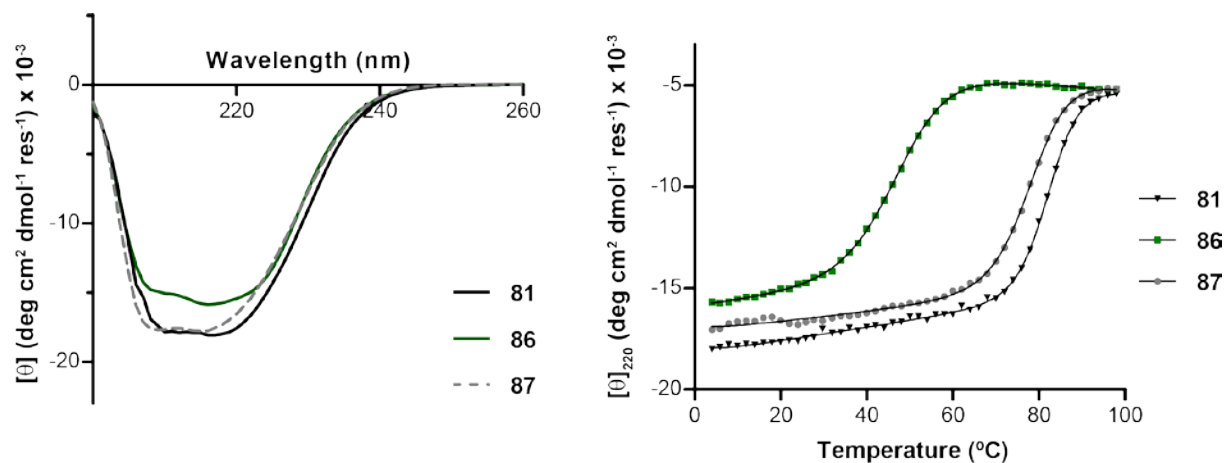


**Figure 63.** CD scans and melts of proteins **81**, **86**, and **87**. Samples consisted of 40  $\mu$ M protein in 20 mM sodium phosphate buffer, pH 7.0.

The scan of protein **87** has a very similar shape to wild-type protein **81**, suggesting a folded structure similar to the parent protein. The thermal denaturation melt also has a similar cooperativity and only a 4  $^{\circ}$ C shift in  $T_m$ . We calculated the  $\Delta\Delta G_{\text{fold}}$  for comparison purposes (Table 11).

**Table 11.** Folding thermodynamics for proteins **81**, **86**, and **87**.

Protein	$T_m$ ( $^{\circ}$ C)	$\Delta T_m$ ( $^{\circ}$ C)	$\Delta\Delta G_{\text{fold}}$ (kcal/mol)
<b>81</b>	$82.1 \pm 0.3$	---	---
<b>86</b>	$46.5 \pm 0.5$	-35.6	$+5.9 \pm 0.1$
<b>87</b>	$78.0 \pm 0.4$	-4.1	$+0.7 \pm 0.1$

Removal of the stabilizing salt-bridge and hydrogen bond by mutation of residues results in only a 0.7 kcal/mol destabilization, accounting for only a small portion of the 5.9 kcal/mol destabilization seen in protein **86** and suggesting the large destabilization resulted from a different source. We theorized the destabilization seen in  $\gamma$ -residue mutants of GB1 might result from increased backbone length as  $\gamma$ -

residues contain two additional carbon atoms in their backbones. To analyze how a change in strand length could impact folded stability, we once again examined the crystal structure of GB1 (Figure 64).

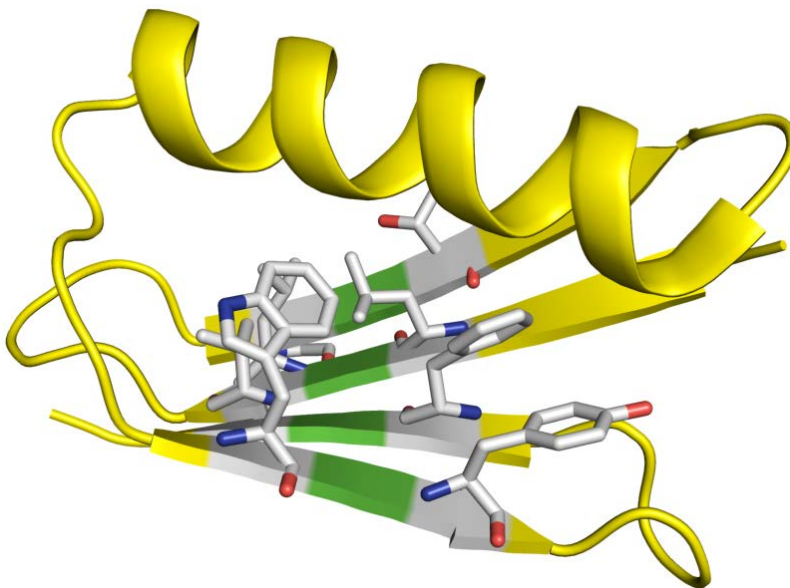


**Figure 64.** Crystal structure of GB1 highlighting helix packing residues (white) and Acc substitution sites (green). Coordinates based on PDB: 2QMT.

$\gamma$ -Residue substitution would extend the backbone length of the residues found between the helix packing residues, potentially forcing the hydrophobic side chains apart. While this increased length did not impact the stability of the small hairpin peptide, full length GB1 has a helix that packs against these residues in the tertiary fold. We hypothesized that shifting the position of the packing residues in the sheet may be the cause of the large destabilizing effect of  $\gamma$ -residue substitution in **81**. To test this hypothesis, we chose to shift the stripe of Acc substitution to residues Asn<sub>8</sub>, Lys<sub>13</sub>, Glu<sub>42</sub>, and Thr<sub>55</sub>, away from the center of the  $\beta$ -strands (Figure 65) to generate protein **88** (Figure 66).

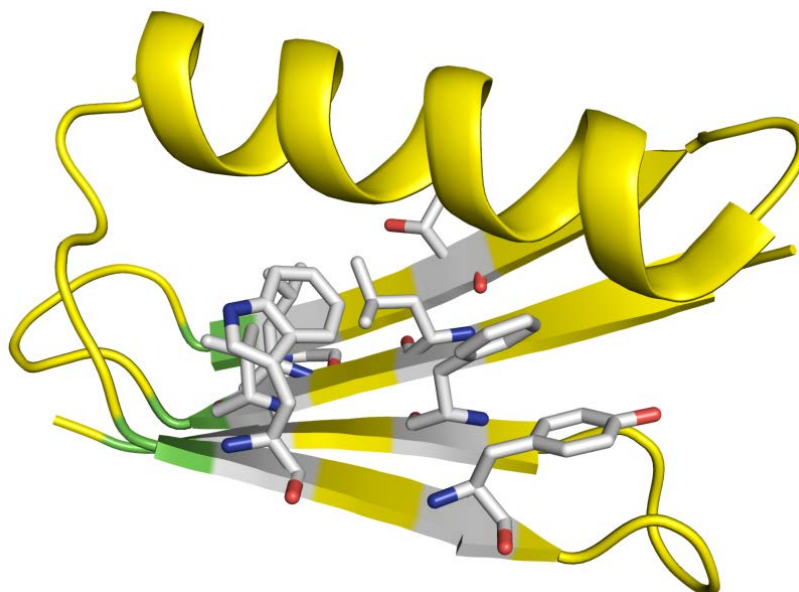


**Figure 65.** Crystal structure of GB1 highlighting helix packing residues (white) and new Acc substitution sites (green).  
Coordinates based on PDB: 2QMT.

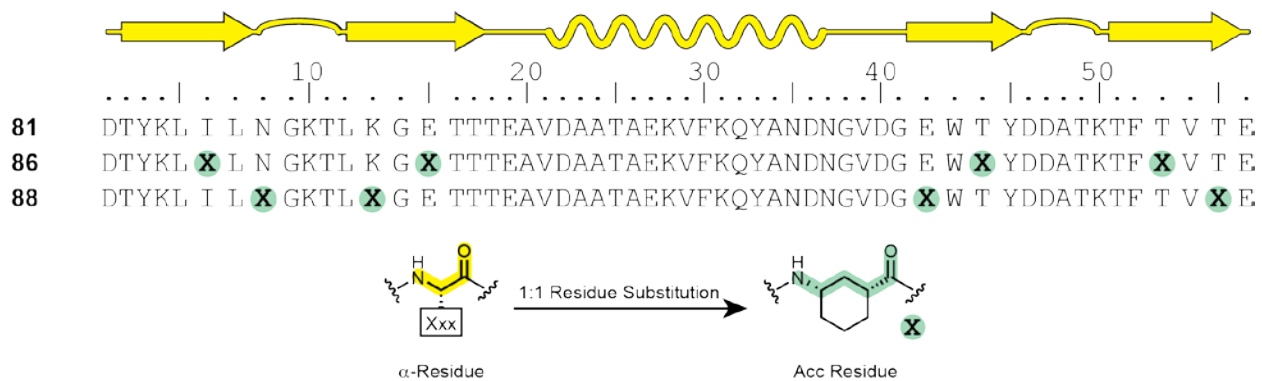


**Figure 66.** Sequences of parent protein **81** and Acc variants **86** and **88**.

We synthesized protein **88** and analyzed by CD (Figure 67).

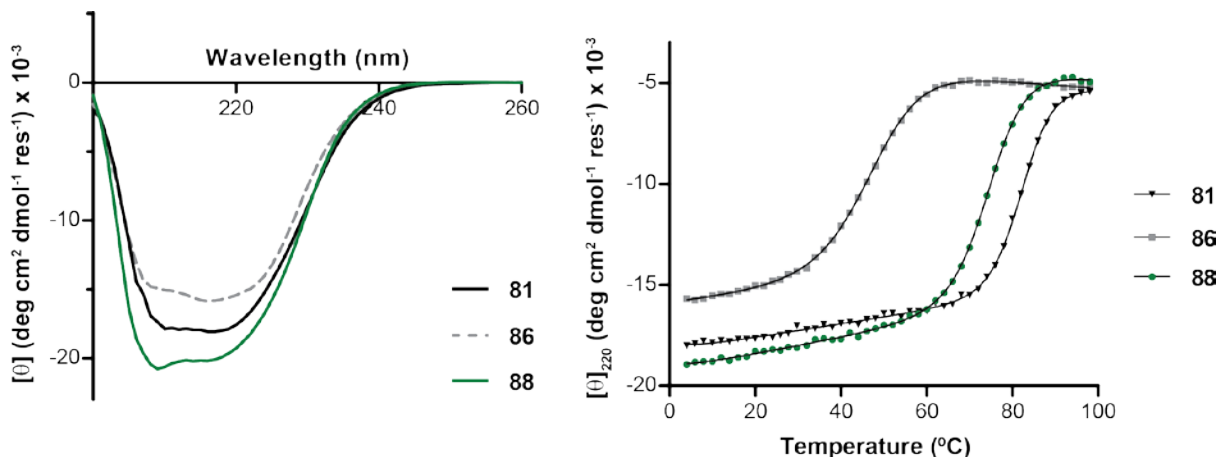


**Figure 67.** CD scans and melts of proteins **81**, **86**, and **88**.  
Samples consisted of 40  $\mu$ M protein in 20 mM sodium phosphate buffer, pH 7.0.

Gratifyingly, shifting the stripe of Acc away from the center of the strands in GB1 resulted in a dramatic shift in both the scan and melt of protein **88** relative to protein **86**. The CD scan shows stronger minima than those experienced by wild-type protein **81**, suggesting native-like folding behavior. More importantly, however, was the dramatic increase in the  $T_m$  from 46.5  $^{\circ}$ C to 74.4  $^{\circ}$ C. From these  $T_m$  data, we calculated  $\Delta\Delta G_{\text{fold}}$  (Table 12).

**Table 12.** Folding thermodynamics for proteins **81**, **86**, and **88**.

Protein	$T_m$ ( $^{\circ}$ C)	$\Delta T_m$ ( $^{\circ}$ C)	$\Delta\Delta G_{\text{fold}}$ (kcal/mol)
<b>81</b>	$82.1 \pm 0.3$	---	---
<b>86</b>	$46.5 \pm 0.5$	-35.6	$+5.9 \pm 0.1$
<b>88</b>	$74.4 \pm 0.2$	-7.7	$+1.3 \pm 0.1$

Protein **88** shows a decrease in  $T_m$  of  $\sim 8$   $^{\circ}$ C relative to wild-type protein **81**, corresponding to a loss of stability of 1.3 kcal/mol. This destabilization, while not predicted by our hairpin data, is

significantly minimized compared to protein **86**; there is a 4.6 kcal/mol increase in stability between the two Acc-hybrid proteins. Substitution of Acc in protein **88** is very well-tolerated with a  $\Delta\Delta G_{\text{fold}}$  of 0.3 kcal/mol per residue.

## 4.2 CONCLUSIONS

To compare the thermodynamic impact of unnatural residue substitution between our hairpin peptide and full-length protein GB1, we calculated the  $\Delta\Delta G_{\text{fold}}$  on a per residue basis (Table 13). We estimated a 4.6 kcal/mol destabilization for placement of  $\gamma$ -residues in the center of GB1's  $\beta$ -strands and used this to estimate a  $\Delta\Delta G_{\text{fold}}$  for vinylogous  $\gamma^4$ -residue substitution away from this location.

Some general conclusions can be drawn from comparison of the hairpin peptide and full-length protein. The hairpin seems to be an appropriate system to determine general trends in the stability of unnatural residue substitutions. Substitutions involving  $\beta$ -amino acids, for example, were significantly more destabilizing than the other substitution strategies in both systems. Ranking amino acid stability in the hairpin peptide shows  $\text{Acc} > \text{vinylogous } \gamma^4\text{-amino acids} \geq \text{N-methylated amino acid}$ . Assuming ideal positioning of substitutions, this same trend is observed, although less pronounced, in full-length GB1.

Although the hairpin could determine the relative sheet propensity of each monomer type, it could not predict the overall effect of backbone lengthening in the full-length protein. Larger proteins have much more complicated folded structures than those seen in short hairpin sequences and are therefore subject to more variables in predicting monomer suitability. Notably, positioning of the backbone-lengthened  $\gamma$ -residues had a significant effect on the stability of the overall fold evidenced by a dramatic increase in folded stability with just a minor shift in substitution position.

**Table 13.** Thermodynamic impacts of unnatural residue substitutions in  $\beta$ -sheets.

<b>Substitution Strategy</b>	<b>Hairpin <math>\Delta\Delta G_{\text{fold}}</math> per replacement (kcal/mol)</b>	<b>Protein <math>\Delta\Delta G_{\text{fold}}</math> per replacement (kcal/mol)</b>
1:1 $\alpha$ to $\beta$	---	---
2:1 $\alpha$ to $\beta^2/\beta^3$	+0.5	Significantly Destabilized
2:1 $\alpha$ to $\beta^{2,3}$	+0.7	---
2:2 $\alpha$ to $\beta^2/\beta^3$	>0.9	Significantly Destabilized
2:2 $\alpha$ to $\beta^{2,3}$	+0.5	---
1:1 $\alpha$ to $\gamma$ ( <i>mABA</i> )	-0.2	---
1:1 $\alpha$ to $\gamma$ (Acc)	-0.3	+1.5, +0.3 <sup>a</sup>
1:1 $\alpha$ to $\gamma$ (vinylogous $\gamma^4$ )	+0.3	+1.6, +0.5 <sup>b</sup>
<i>N</i> -methylation (turn)	+1.1	---
<i>N</i> -methylation (terminal)	+0.6	+0.6
<i>N</i> -methylation (terminal, $\beta$ -branched)	+0.2	---

a. Calculated from a shift in position of residues.

b. Estimated from 4.6 kcal/mol shift in stability as seen with Acc substitution.

Either vinylogous  $\gamma^4$ -residues or Acc can be directly substituted on a 1:1 basis for  $\alpha$ -residues with a minor change in the stability of the folded structure. However, substitution with  $\gamma$ -residues, while potentially effective in large proteins, requires careful positioning of the backbone-lengthened  $\gamma$ -residues. In the case where  $\gamma$ -residues will not be tolerated, *N*-methylation might be utilized as an appropriate substitute. However, positioning of the *N*-methyl functionality also has to be considered so as not to disrupt inter-strand hydrogen bonding. Folding in large proteins is too complex to define general rules for unnatural residue substitution in  $\beta$ -sheets, but with appropriate care in positioning of substitutions, we have found three unnatural residues which can be used as effective  $\alpha$ -residue substitutes in hybrid proteins. Future work applying the preferred substitution strategies discussed above will show whether or not the guidelines demonstrated in this work can be applicable to other protein systems.

## 4.3 EXPERIMENTAL

### 4.3.1 Monomer Synthesis

#### 4.3.1.1 General Information

Optical rotations were measured on a Perkin-Elmer 241 digital polarimeter with a sodium lamp at ambient temperature. NMR spectra of synthetic small molecules were recorded on a Bruker Avance-400 spectrometer. 2-(6-chloro-1H-benzotriazole-1-yl)-1,1,3,3-tetramethylammonium hexafluorophosphate (HCTU), NovaPEG Rink Amide Resin, 9-fluorenylmethyl N-succinimidyl carbonate (Fmoc-OSu), and Fmoc-protected  $\alpha$ -amino acids were purchased from Novabiochem. Solvents and all other reagents were purchased from Aldrich, Baker, Fisher, or TCI and used as received without further purification. Flash chromatography was performed using SorbTech silica gel (60 Å, 40-63  $\mu\text{m}$ ). The Weinreb amides of Fmoc-Ile-OH, Fmoc-Glu(tBu)-OH, and Fmoc-Thr(tBu)-OH were synthesized using a published protocol.<sup>128</sup>

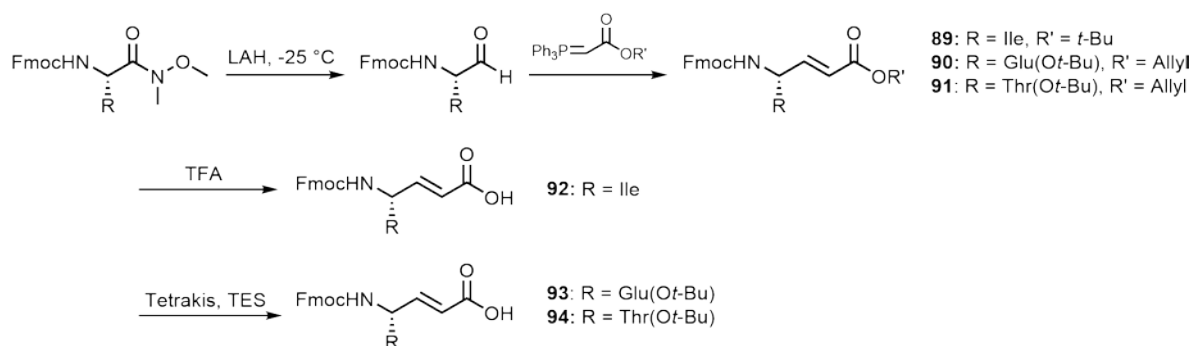
#### 4.3.1.2 Synthesis of Fmoc- $\beta^2$ -Monomers

Fmoc- $\beta^2$ -monomers were synthesized as detailed in Section 2.3.1.2.

#### 4.3.1.3 Synthesis of Fmoc-Acc-OH

Fmoc-Acc-OH was synthesized as detailed in Section 3.3.1.3.

#### 4.3.1.4 Synthesis of Vinylogous Fmoc- $\gamma^4$ -Monomers

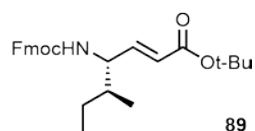


**Scheme 4.1.** Synthesis of vinylogous Fmoc- $\gamma^4$ -monomers.

**Standard Procedure N:** To a stirred solution of Fmoc-Weinreb amide (1 equiv) in tetrahydrofuran (0.1 M) at  $-25\text{ }^\circ\text{C}$  was added lithium aluminum hydride (1.1 equiv). The reaction was allowed to stir for 30 minutes and then quenched with 1 M hydrochloric acid, diluted with water, and extracted three times with ethyl acetate. The combined organics were washed with brine, dried with magnesium sulfate, and concentrated to afford the desired Fmoc-aldehyde which was used directly without purification.

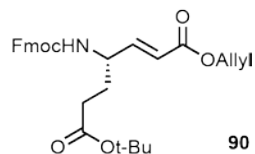
**Standard Procedure O:**<sup>130</sup> To a stirred solution of aldehyde (1 equiv) in tetrahydrofuran (0.2 M) was added (tert-butoxycarbonylmethylene) triphenylphosphorane (1 equiv). The reaction was stirred overnight, concentrated, and purified using column chromatography.

**Standard Procedure P:**<sup>139</sup> To a stirred solution of aldehyde (1 equiv) in toluene (0.1 M) at  $80\text{ }^\circ\text{C}$  was added (allyloxycarbonylmethyl)triphenylphosphonium iodide (1.6 equiv) and DIEA (1.4 equiv). The reaction was stirred 3 h. After this time, the reaction was washed with 0.1 M aqueous hydrochloric acid, saturated aqueous sodium bicarbonate solution, and brine. The organics were dried with magnesium sulfate, concentrated, and purified using column chromatography.



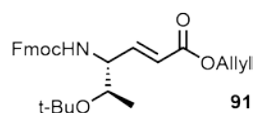
**Fmoc- $\gamma^4$ -Ile-OtBu (89):** Standard Procedure N was followed using 1.149 mg

Fmoc-Ile Weinreb amide (2.89 mmol), 23 mL tetrahydrofuran, and 124 mg lithium aluminum hydride (3.27 mmol). The resulting aldehyde was subjected to Standard Procedure O using 15 mL tetrahydrofuran and 1.092 g (tert-butoxycarbonylmethylene) triphenylphosphorane (2.90 mmol). The crude mixture was purified using column chromatography (20% ethyl acetate in hexanes) to afford the product as a white solid (815 mg, 1.87 mmol, 64% yield over 2 steps).  $[\alpha]_D = -3.4$  ( $c = 1.00$ ,  $\text{CHCl}_3$ ).  $^1\text{H}$  NMR (400 MHz,  $\text{CDCl}_3$ )  $\delta$  7.77 (d,  $J = 7.5$  Hz, 2 H), 7.60 (d,  $J = 7.3$  Hz, 2 H), 7.41 (t,  $J = 7.4$  Hz, 2 H), 7.32 (J = 7.3 Hz, 2 H), 6.76 (dd,  $J = 5.5, 15.6$  Hz, 1 H), 5.84 (d,  $J = 15.6$  Hz, 1 H), 4.82 (d,  $J = 9.0$  Hz, 1 H), 4.45 (m, 2 H), 4.30 (m, 1 H), 4.23 (t,  $J = 6.5$  Hz, 1 H), 1.63 (m, 1 H), 1.50 (s, 9 H), 1.46 (m, 1 H), 1.13 (m, 1 H), 0.91 (m, 6 H);  $^{13}\text{C}$  NMR (100 MHz,  $\text{CDCl}_3$ )  $\delta$  165.1, 155.4, 144.8, 143.5, 141.0, 127.4, 126.7, 124.6, 123.3, 119.6, 80.2, 66.3, 55.9, 47.0, 38.6, 27.8, 24.9, 14.9, 11.2. HRMS  $m/z$  calculated for  $\text{C}_{27}\text{H}_{34}\text{NO}_4$   $[\text{M}+\text{H}]^+$  436.2488; found 436.2488.



**Fmoc- $\gamma^4$ -Glu(tBu)-OAllyl (90):** Standard Procedure N was followed using 1.835 g

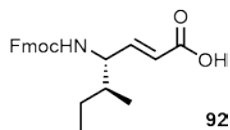
Fmoc-Glu(*t*Bu) Weinreb amide (3.92 mmol), 30 mL tetrahydrofuran, and 162 mg lithium aluminum hydride (4.27 mmol). Standard Procedure P was followed using 3.06 g phosphonium (6.27 mmol), 960  $\mu\text{L}$  DIEA (5.51 mmol), and 39 mL toluene. The crude mixture was purified using column chromatography (20% ethyl acetate in hexanes) to afford the product as a white solid (1.272 g, 2.59 mmol, 66% yield over 2 steps).  $[\alpha]_D = -6.7$  ( $c = 1.00$ ,  $\text{CHCl}_3$ ).  $^1\text{H}$  NMR (400 MHz,  $\text{CDCl}_3$ )  $\delta$  7.76 (d,  $J = 7.5$  Hz, 2 H), 7.59 (d,  $J = 7.3$  Hz, 2 H), 7.40 (t,  $J = 7.4$  Hz, 2 H), 7.31 (t,  $J = 7.3$  Hz, 2 H), 6.86 (dd,  $J = 5.3, 15.6$  Hz, 1 H), 5.94 (m, 2 H), 5.34 (dd,  $J = 1.4, 17.2$  Hz, 1 H), 5.26 (dd,  $J = 1.1, 10.4$  Hz, 1 H), 5.12 (d,  $J = 8.3$  Hz, 1 H), 4.64 (d,  $J = 5.7$  Hz, 2 H), 4.43 (m, 2 H), 4.36 (m, 1 H), 4.20 (t,  $J = 6.7$  Hz, 1 H), 2.32 (m, 2 H), 1.93 (m, 1 H), 1.83 (m, 1 H), 1.44 (s, 9 H);  $^{13}\text{C}$  NMR (100 MHz,  $\text{CDCl}_3$ )  $\delta$  172.3, 165.7, 155.7, 147.5, 143.8, 141.3, 132.0, 127.7, 127.1, 125.0, 121.1, 120.0, 118.4, 81.0, 66.7, 65.2, 51.8, 47.2, 31.7, 28.9, 28.0. HRMS  $m/z$  calculated for  $\text{C}_{27}\text{H}_{34}\text{NO}_6$   $[\text{M}+\text{H}]^+$  492.2386; found 492.2362.



**Fmoc- $\gamma^4$ -Thr(*t*Bu)-OAllyl (91):** Standard Procedure N was followed using 2.385 g

Fmoc-Glu(*t*Bu) Weinreb amide (5.41 mmol), 43 mL tetrahydrofuran, and 228 mg lithium aluminum hydride (6.00 mmol). Standard Procedure P was followed using 4.22 g phosphonium (8.64 mmol), 1.35 mL DIEA (7.75 mmol), and 54 mL toluene. The crude mixture was purified using column chromatography (20% ethyl acetate in hexanes) to afford the product as a colorless oil (1.652 g, 3.56 mmol, 66% yield over 2 steps).  $[\alpha]_D = +9.4$  ( $c = 1.00$ ,  $\text{CHCl}_3$ ).  $^1\text{H NMR}$ , Major Conformer (400 MHz,  $\text{CDCl}_3$ )  $\delta$  7.78 (d,  $J = 7.4$  Hz, 2 H), 7.62 (d,  $J = 7.2$  Hz, 2 H), 7.41 (t,  $J = 7.3$  Hz, 2 H), 7.33 (t,  $J = 6.8$  Hz, 2 H), 6.98 (dd,  $J = 4.9, 15.7$  Hz, 1 H), 5.96 (m, 2 H), 5.34 (dd,  $J = 1.3, 17.2$  Hz, 1 H), 5.24 (m, 2 H), 4.66 (d,  $J = 5.7$  Hz, 2 H), 4.45 (m, 2 H), 4.26 (m, 2 H), 3.82 (m, 1 H), 1.17 (m, 12 H);  $^{13}\text{C NMR}$  (100 MHz,  $\text{CDCl}_3$ )  $\delta$  165.7, 156.1, 147.7, 143.8, 141.3, 132.1, 127.7, 127.0, 125.0, 121.1, 119.9, 118.1, 74.11, 68.0, 66.8, 65.0, 57.4, 47.3, 28.5, 20.3. HRMS  $m/z$  calculated for  $\text{C}_{28}\text{H}_{33}\text{NO}_5\text{Na}$   $[\text{M}+\text{Na}]^+$  486.2256; found 486.2242.

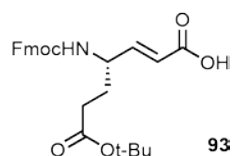
**Standard Procedure Q:** To a stirred solution of ester in 5 mL dichloromethane was added 5 mL trifluoroacetic acid. The reaction was stirred 4 h, concentrated, solvent-exchanged with chloroform three times, and purified using column chromatography.



**Fmoc- $\gamma^4$ -Ile-OH (92):** Standard procedure Q was followed using 815 mg compound

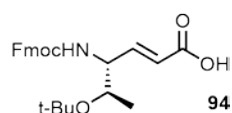
**89** (1.87 mmol). Column chromatography (50% ethyl acetate in hexanes) afforded the product as a white solid (659 mg, 1.74 mmol, 93% yield).  $[\alpha]_D = -7.6$  ( $c = 1.0$ ,  $\text{CHCl}_3$ ).  $^1\text{H NMR}$ , Major Conformer (400 MHz,  $\text{CDCl}_3$ )  $\delta$  10.04 (s, 1 H), 7.77 (d,  $J = 7.3$  Hz, 2 H), 7.60 (d,  $J = 7.3$  Hz, 2 H), 7.41 (t,  $J = 7.2$  Hz, 2 H), 7.33 (t,  $J = 6.7$  Hz, 2 H), 6.96 (dd,  $J = 15.6, 5.2$  Hz, 1 H), 5.91 (d,  $J = 15.6$  Hz, 1 H), 4.88 (d,  $J = 9.0$  Hz, 1 H), 4.48 (d,  $J = 6.4$  Hz, 2 H), 4.35 (m, 1 H), 4.22 (t,  $J = 6.3$  Hz, 1 H), 1.28-1.71 (m, 2 H), 1.13 (m, 1 H), 0.91 (m, 6 H);  $^{13}\text{C NMR}$  (100 MHz,  $\text{CDCl}_3$ )  $\delta$  170.9, 155.9, 149.0, 143.7, 141.3, 127.7, 127.1, 124.9, 121.2, 120.0, 66.6, 56.3, 47.3, 38.8, 25.2, 15.3, 11.5. HRMS  $m/z$  calculated for  $\text{C}_{23}\text{H}_{26}\text{NO}_4$   $[\text{M}+\text{H}]^+$  380.1862; found 380.1864.

**Standard Procedure R:** To a stirred solution of allyl ester (1 equiv) in dichloromethane (0.1 M) was added tetrakis(triphenylphosphine)palladium (0.1 equiv) and triethylsilane (5 equiv). The reaction was stirred 3 h, then diluted with ethyl acetate and washed once with 1 M HCl and twice with brine. The organics were dried with magnesium sulfate, concentrated, and purified using column chromatography.



**Fmoc- $\gamma^4$ -Glu(*t*Bu)-OH (93):** Standard Procedure R was followed using 71 mg compound **90** (0.14 mmol), 18 mg tetrakis (0.016 mmol), 115  $\mu$ L triethylsilane (0.72 mmol), and 1.4 mL dichloromethane. Column chromatography (50% ethyl acetate in

hexanes) afforded the product as a pale yellow solid (15 mg, 0.033 mmol, 23% yield).  $[\alpha]_D = -9.1$  ( $c = 1.0$ ,  $\text{CHCl}_3$ ).  $^1\text{H NMR}$ , Major Conformer (400 MHz,  $\text{CDCl}_3$ )  $\delta$  7.75 (d,  $J = 7.4$  Hz, 2 H), 7.59 (d,  $J = 7.0$  Hz, 2 H), 7.39 (t,  $J = 7.3$  Hz, 2 H), 7.31 (t,  $J = 7.2$  Hz, 2 H), 6.93 (dd,  $J = 15.7, 5.0$  Hz, 1 H), 5.92 (d,  $J = 15.6$  Hz, 1 H), 5.24 (d,  $J = 8.2$  Hz, 1 H), 4.43 (m, 3 H), 4.20 (t,  $J = 6.3$  Hz, 1 H), 2.31 (m, 2 H), 1.92 (m, 1 H), 1.83 (m, 1 H), 1.44 (s, 9 H),  $^{13}\text{C NMR}$  (100 MHz,  $\text{CDCl}_3$ )  $\delta$  172.2, 170.5, 155.8, 149.4, 143.7, 141.3, 127.7, 127.0, 124.9, 120.8, 119.9, 81.1, 66.7, 51.8, 47.2, 31.7, 28.9, 28.0. HRMS  $m/z$  calculated for  $\text{C}_{26}\text{H}_{30}\text{NO}_6$   $[\text{M}+\text{H}]^+$  452.2073; found 452.2070.



**Fmoc- $\gamma^4$ -Thr(*t*Bu)-OH (94):** Standard Procedure R was followed using 1.517 g compound **91** (3.27 mmol), 378 mg tetrakis (0.327 mmol), 2.6 mL triethylsilane (16

mmol), and 32 mL dichloromethane. Following a silica plug eluting with ethyl acetate, column chromatography (20%  $\rightarrow$  50% ethyl acetate in hexanes) afforded the product as a pale yellow solid (905 mg, 2.14 mmol, 65% yield).  $[\alpha]_D = +3.8$  ( $c = 1.0$ ,  $\text{CHCl}_3$ ).  $^1\text{H NMR}$ , Major Conformer (400 MHz,  $\text{CDCl}_3$ )  $\delta$  7.78 (d,  $J = 7.4$  Hz, 2 H), 7.62 (d,  $J = 7.0$  Hz, 2 H), 7.41 (t,  $J = 7.3$  Hz, 2 H), 7.33 (t,  $J = 7.0$  Hz, 2 H), 7.06 (dd,  $J = 15.7, 4.6$  Hz, 1 H), 5.92 (d,  $J = 15.7$  Hz, 1 H), 5.25 (d,  $J = 9.0$  Hz, 1 H), 4.47 (d,  $J = 6.8$  Hz, 2 H), 4.31 (m, 1 H), 4.25 (t,  $J = 6.7$  Hz, 1 H), 3.83 (m, 1 H), 1.17 (m, 12 H);  $^{13}\text{C NMR}$  (100 MHz,  $\text{CDCl}_3$ )  $\delta$  171.0, 156.2, 149.9, 143.8, 141.3, 127.7, 127.1, 125.0, 120.8, 120.0, 74.2, 68.0, 66.9, 57.4, 47.3, 28.5, 20.3. HRMS  $m/z$  calculated for  $\text{C}_{25}\text{H}_{28}\text{NO}_5$   $[\text{M}+\text{H}]^+$  422.1962; found 422.1976.

### 4.3.2 Peptide Synthesis

Modified GB1 proteins were synthesized with automated methods on a PTI Tribute synthesizer using NovaPEG Rink Amide resin (70  $\mu$ mol scale). Coupling reactions were performed by combining 3 mL of 0.4 M *N*-methylmorpholine in DMF with 7 equiv Fmoc-amino acid and 7 equiv HCTU. Following a two minute preactivation, the activated amino acid was added to the resin and vortexed for 45 min. Deprotection reactions were carried out twice with 3 mL of a 20% v/v solution of 4-methylpiperidine in DMF for 4 min. The resin was washed three times with 3 mL of DMF for 40 s between each cycle. After the final deprotection step, the resin was washed with 3 mL of dichloromethane followed by 3 mL of methanol. Resin was dried and subjected to cleavage by treatment with a solution of 94% TFA, 1% TIS, 2.5% water, and 2.5% ethanedithiol. Crude protein was precipitated by addition of cold diethyl ether. The solid was pelleted by centrifugation and dissolved in 6 M guanidinium chloride, 25 mM sodium phosphate, pH 6. This solution was subjected to purification by preparative C18 reverse-phase HPLC using gradients between 0.1% TFA in water and 0.1% TFA in acetonitrile. Each protein was subjected to a second purification by anion-exchange chromatography on a monoQ 5/50GL column (GE Healthcare) using 0.02 M Tris buffer at pH 8 and eluting with increasing concentrations of KCl.

All proteins were >95% pure as determined by analytical HPLC on a C18 column. Identities were confirmed by mass spectrometry using a Voyager DE Pro MALDI-TOF instrument (Table 14).

**Table 14.** MALDI-TOF data for proteins **81-88**.

Peptide	[M+H] <sup>+</sup> <i>m/z</i>	
	Calculated	Observed
<b>81</b>	6179.6	6178.6
<b>82</b>	6207.7	6207.5
<b>83</b>	5789.3	5791.5
<b>84</b>	6271.9	6274.6
<b>85</b>	6280.9	6281.8
<b>86</b>	6232.1	6231.1
<b>87</b>	6114.1	6113.6
<b>88</b>	6204.1	6204.5

### 4.3.3 CD Measurements

CD measurements were performed on an Olis DSM17 Circular Dichroism Spectrometer in 2 mm quartz cells. Samples consisted of 40  $\mu$ M protein in 20 mM sodium phosphate buffer, pH 7.0. Scans were carried out at 25 °C over the range of 200-260 nm with 1 nm increments and a 2 nm bandwidth. Scan data were smoothed by the Savitzky-Golay method. Melts were monitored at 220 nm over the range of 4 °C to 98 °C with 2 °C increments, a dead band of 0.5 °C, and a 2 min equilibration time at each temperature. All measurements were baseline corrected for blank buffer. Temperature-dependent CD data were fit to a two-state unfolding model to obtain melting temperature ( $T_m$ ). The change in free energy of folding for each mutant relative to wild-type ( $\Delta\Delta G_{\text{fold}}$ ) was estimated from the change in  $T_m$  ( $\Delta T_m$ ) using the enthalpy of folding determined for GB1 by differential scanning calorimetry.

## **APPENDIX A**

### **HAIRPIN PEPTIDE BACKBONE CHEMICAL SHIFTS**

**Table 15.** Backbone  $^1\text{H}$  chemical shift assignments (in ppm) for oligomers **1a-17a** and **1b-17b**.

#	R <sub>1</sub>	W <sub>2</sub>		X <sub>3</sub>					Y <sub>4</sub>		V <sub>5</sub>		P <sub>6</sub>	G <sub>7</sub>			K <sub>8</sub>		F <sub>9</sub>		X <sub>10</sub>					V <sub>11</sub>		Q <sub>12</sub>	
	H <sub>α</sub>	H	H <sub>α</sub>	H	H <sub>α</sub>	H <sub>α</sub> '	H <sub>β</sub>	H <sub>β</sub> '	H	H <sub>α</sub>	H	H <sub>α</sub>	H <sub>α</sub>	H	H <sub>α</sub>	H <sub>α</sub> '	H	H <sub>α</sub>	H	H <sub>α</sub>	H	H <sub>α</sub>	H <sub>α</sub> '	H <sub>β</sub>	H <sub>β</sub> '	H	H <sub>α</sub>	H	H <sub>α</sub>
<b>1a</b>	4.04	8.88	4.88	8.75	4.44	–	–	–	8.63	4.87	8.70	4.52	4.37	8.39	3.75	3.99	7.90	4.59	8.90	4.63	8.55	4.49	–	–	–	8.32	3.86	8.42	4.25
<b>1b</b>	4.05	8.94	4.62	8.04	4.15	–	–	–	8.22	4.20	8.01	4.21	4.22	8.50	3.89	3.92	8.20	4.27	8.48	4.74	8.20	4.34	–	–	–	8.42	4.07	8.63	4.24
<b>2a</b>	3.95	8.78	4.66	7.96	1.65	2.02	3.89	–	8.05	4.85	8.77	4.07	4.36	8.31	3.81	3.88	7.97	4.37	8.39	4.27	8.02	1.98	2.43	3.99	–	8.39	4.16	8.67	3.99
<b>2b</b>	3.91	8.72	4.66	8.15	1.83	2.11	3.88	–	8.14	4.59	8.21	3.74	4.21	8.45	3.82	3.85	8.06	4.19	8.21	4.56	8.13	2.31	2.54	4.03	–	8.28	4.15	8.60	3.88
<b>3a</b>	4.01	8.89	4.71	7.86	2.17	2.22	3.74	–	8.31	4.70	8.63	4.45	4.40	8.47	3.87	3.94	8.04	4.39	8.41	4.36	8.02	2.31	2.45	3.98	–	8.32	4.04	8.61	4.26
<b>3b</b>	4.01	8.90	4.70	7.95	2.22	2.30	3.78	–	8.34	4.52	8.13	4.26	4.23	8.53	3.90	3.94	8.17	4.25	8.28	4.62	8.14	2.39	2.52	4.06	–	8.30	4.06	8.63	4.29
<b>4a</b>	3.98	8.83	4.58	7.73	1.87	–	3.00	3.32	7.84	4.69	8.58	4.37	4.38	8.40	3.82	3.92	8.01	4.31	8.36	4.44	8.03	2.29	–	3.16	3.41	8.23	4.00	8.64	4.27
<b>4b</b>	3.98	8.89	4.63	8.11	1.93	–	3.07	3.48	7.99	4.44	8.02	4.18	4.16	8.46	3.87	3.90	8.12	4.22	8.30	4.60	8.16	2.32	–	3.31	3.44	8.34	4.01	8.66	4.28
<b>5a</b>	3.88	8.61	4.74	8.34	2.15	–	3.10	3.57	8.21	4.75	8.68	3.78	4.30	8.12	3.84	3.87	7.97	4.24	8.11	4.28	7.92	2.34	–	3.23	3.36	8.35	4.12	8.59	4.03
<b>5b</b>	3.89	8.60	4.74	8.33	2.18	–	3.16	3.54	8.28	4.67	8.29	3.72	4.19	8.44	3.82	3.86	8.11	4.22	8.16	4.49	8.06	2.38	–	3.33	3.37	8.35	4.13	8.55	4.04
<b>6a</b>	3.82	8.58	4.86	8.32	2.53	–	3.84	–	8.18	4.76	8.73	3.38	4.31	7.94	3.80	3.84	7.86	4.20	8.15	4.47	8.03	2.75	–	3.80	–	8.26	4.24	8.58	3.76
<b>6b</b>	3.82	8.59	4.84	8.32	2.53	–	3.82	–	8.19	4.69	8.32	3.38	4.18	8.42	3.78	3.82	7.96	4.15	8.19	4.62	8.15	2.75	–	3.87	–	8.27	4.23	8.60	3.68
<b>7a</b>	4.00	8.91	4.81	7.58	2.61	–	3.33	–	8.39	4.66	8.58	4.47	4.45	8.40	3.88	3.91	7.98	4.27	8.29	4.52	7.83	2.78	–	3.70	–	8.34	4.04	8.57	4.24
<b>7b</b>	3.98	8.89	4.80	7.69	2.62	–	3.47	–	8.32	4.56	8.18	4.32	4.29	8.55	3.91	3.94	8.13	4.26	8.30	4.66	7.94	2.75	–	3.80	–	8.33	4.00	8.60	4.29
<b>8a</b>	4.08	8.98	4.80	7.74	2.21	–	3.77	–	8.16	5.08	8.96	4.57	4.37	8.57	3.69	4.05	7.97	4.58	8.70	4.45	8.11	2.62	–	3.83	–	8.80	4.14	8.82	4.20
<b>8b</b>	4.00	8.96	4.75	7.88	2.18	–	3.61	–	8.43	4.64	8.24	4.31	4.30	8.56	3.90	3.93	8.14	4.23	8.50	4.66	7.95	2.55	–	3.82	–	8.52	3.98	8.69	4.28
<b>9a</b>	4.08	9.01	4.90	7.82	2.50	–	3.72	–	8.46	5.07	8.93	4.54	4.39	8.69	3.79	4.08	8.03	4.66	8.77	4.22	7.84	2.48	–	3.69	–	8.06	4.04	8.71	4.22
<b>9b</b>	4.05	8.98	4.86	7.79	2.39	–	3.64	–	8.57	4.51	8.09	4.23	4.20	8.50	3.88	3.93	8.17	4.25	8.53	4.70	7.96	2.59	–	3.82	–	8.53	4.06	8.67	4.28
<b>10a</b>	4.00	8.79	4.53	8.10	1.76	–	3.97	–	7.84	4.77	8.77	4.29	4.40	8.47	3.85	8.94	8.09	4.44	8.50	4.06	8.01	2.32	–	4.18	–	8.12	4.17	8.64	4.19
<b>10b</b>	4.00	8.75	4.55	8.22	1.85	–	4.07	–	8.04	4.59	8.28	3.99	4.23	8.48	3.87	3.92	8.21	4.22	8.25	4.51	8.04	2.50	–	4.19	–	8.29	4.17	8.62	4.16
<b>11a</b>	4.04	8.99	4.60	7.89	2.46	–	3.92	–	8.27	4.79	8.63	4.48	4.41	8.58	3.90	3.97	8.08	4.52	8.53	4.10	7.90	2.51	–	3.98	–	8.13	4.00	8.59	4.26
<b>11b</b>	4.02	8.94	4.55	7.87	2.43	–	3.90	–	8.30	4.55	8.17	4.24	4.23	8.52	3.90	3.94	8.18	4.29	8.35	4.50	8.14	2.58	–	4.14	–	8.33	4.05	8.67	4.28
<b>12a</b>	3.88	8.61	4.68	8.11	2.86	–	4.34	–	7.90	4.55	8.44	4.06	4.40	8.22	3.73	3.85	8.01	4.21	8.17	4.50	7.68	3.05	–	4.32	–	8.15	3.86	8.55	4.25
<b>12b</b>	3.91	8.70	4.70	8.14	2.87	–	4.35	–	8.12	4.30	7.88	4.11	4.18	8.44	3.84	3.87	8.06	4.19	8.24	4.60	7.76	3.06	–	4.39	–	8.16	3.88	8.59	4.25
<b>13a</b>	4.02	8.85	4.59	7.62	2.73	–	4.04	–	8.16	4.49	8.54	4.15	4.40	8.25	3.87	3.90	8.09	4.32	8.40	4.36	7.63	2.99	–	4.22	–	8.16	4.18	8.52	4.19
<b>13b</b>	4.10	8.85	4.66	7.70	2.78	–	4.11	–	8.25	4.43	8.13	4.14	4.27	8.45	3.90	3.95	8.21	4.24	8.39	4.47	7.60	3.02	–	4.23	–	8.12	4.17	8.53	4.18
<b>14a</b>	3.82	8.47	4.72	8.66	2.34	–	3.87	–	8.22	4.74	8.70	3.32	4.28	7.91	3.79	3.85	7.95	4.18	7.85	4.40	8.26	2.47	–	3.89	–	8.24	4.27	8.58	3.60
<b>14b</b>	3.82	8.44	4.71	8.64	2.35	–	3.86	–	8.21	4.68	8.29	3.30	4.14	8.38	3.80	3.84	8.03	4.15	7.99	4.53	8.34	2.46	–	3.88	–	8.28	4.24	8.60	3.62
<b>15a</b>	3.94	8.70	4.54	7.65	2.10	–	3.70	–	8.15	4.68	8.41	4.39	4.40	8.34	3.85	3.90	8.14	4.29	8.13	4.50	8.20	2.28	–	3.81	–	8.20	3.99	8.59	4.28
<b>15b</b>	3.97	8.78	4.60	7.75	2.11	–	3.68	–	8.17	4.54	8.13	4.25	4.24	8.52	3.91	3.95	8.22	4.28	8.17	4.50	8.20	2.26	–	3.82	–	8.22	3.99	8.59	4.29
<b>16a</b>	3.86	8.62	4.83	8.09	2.50	–	4.23	–	7.60	4.62	8.52	3.91	4.39	8.16	3.65	3.88	7.95	4.24	8.19	4.57	7.78	2.72	–	4.16	–	8.05	3.90	8.51	4.20
<b>16b</b>	3.95	8.72	4.76	7.97	2.37	–	4.12	–	7.80	4.33	7.96	4.01	4.21	8.46	3.85	3.88	8.09	4.22	8.25	4.67	7.90	2.70	–	4.28	–	8.05	3.94	8.57	4.18
<b>17a</b>	4.01	8.84	4.69	7.48	2.42	–	3.88	–	7.93	4.49	8.50	4.30	4.42	8.27	3.85	3.90	8.05	4.34	8.41	4.42	7.59	2.72	–	4.12	–	8.01	4.16	8.53	4.23
<b>17b</b>	4.09	8.85	4.70	7.55	2.47	–	3.99	–	7.95	4.44	8.23	4.23	4.29	8.48	3.93	3.96	8.22	4.29	8.39	4.52	7.65	2.74	–	4.13	–	8.00	4.13	8.54	4.24

**Table 16.** Backbone chemical shift data for peptide **18**.

Residue	Atom	$\delta$ (ppm)
G	H	---
G	H <sub><math>\alpha</math></sub>	3.710
G	H <sub><math>\alpha</math>'</sub>	3.827
E	H	8.655
E	H <sub><math>\alpha</math></sub>	4.395
W	H	8.623
W	H <sub><math>\alpha</math></sub>	4.927
T	H	8.459
T	H <sub><math>\alpha</math></sub>	4.331
Y	H	8.582
Y	H <sub><math>\alpha</math></sub>	4.311
D	H	8.159
D	H <sub><math>\alpha</math></sub>	4.58
D	H	8.445
D	H <sub><math>\alpha</math></sub>	4.293
A	H	8.389
A	H <sub><math>\alpha</math></sub>	4.242
T	H	7.768
T	H <sub><math>\alpha</math></sub>	4.246
K	H	8.098
K	H <sub><math>\alpha</math></sub>	4.055
T	H	7.653
T	H <sub><math>\alpha</math></sub>	4.478
F	H	8.607
F	H <sub><math>\alpha</math></sub>	4.965
T	H	8.634
T	H <sub><math>\alpha</math></sub>	4.498
V	H	8.467
V	H <sub><math>\alpha</math></sub>	4.173
T	H	8.450
T	H <sub><math>\alpha</math></sub>	4.356
E	H	8.611
E	H <sub><math>\alpha</math></sub>	4.255

**Table 17.** Backbone chemical shift data for peptide **19** its derivatives.

Residue	Atom	Chemical Shift (ppm)			
		<i>19a</i> (293 K)	<i>19b</i> (293 K)	<i>19c</i> (293 K)	<i>19d</i> (293 K)
C	H	---	8.454	---	---
C	H <sub><math>\alpha</math></sub>	---	4.513	---	---
K	H	---	a	---	---
K	H <sub><math>\alpha</math></sub>	4.057	a	a	---
K	H	8.708	8.566	8.076	---
K	H <sub><math>\alpha</math></sub>	4.625	4.594	4.348	---
W	H	8.755	8.695	8.52	---
W	H <sub><math>\alpha</math></sub>	5.181	5.233	4.66	---
T	H	9.195	9.175	7.902	---
T	H <sub><math>\alpha</math></sub>	4.761	4.749	4.192	---
Y	H	8.949	9.028	8.122	---
Y	H <sub><math>\alpha</math></sub>	4.174	4.085	4.358	---
N	H	7.636	7.598	8.320	---
N	H <sub><math>\alpha</math></sub>	5.013	5.01	4.854	---
P	H <sub><math>\alpha</math></sub>	3.986	3.961	4.249	---
A	H	7.888	7.861	8.079	---
A	H <sub><math>\alpha</math></sub>	4.226	4.208	4.254	---
T	H	7.07	7.005	---	8.292
T	H <sub><math>\alpha</math></sub>	4.409	4.398	---	4.304
G	H	8.358	8.349	---	8.553
G	H <sub><math>\alpha</math></sub>	3.745	3.729	---	3.920
G	H <sub><math>\alpha</math>'</sub>	4.054	4.059	---	---
K	H	7.314	7.264	---	8.088
K	H <sub><math>\alpha</math></sub>	4.692	4.714	---	4.261
F	H	8.866	8.894	---	8.322
F	H <sub><math>\alpha</math></sub>	5.271	5.269	---	4.723
T	H	9.041	9.071	---	8.121
T	H <sub><math>\alpha</math></sub>	4.743	4.711	---	4.321
V	H	8.467	8.423	---	8.264
V	H <sub><math>\alpha</math></sub>	4.175	4.338	---	4.095
Q	H	8.541	8.569	---	8.521
Q	H <sub><math>\alpha</math></sub>	4.491	4.621	---	4.363
E	H	8.306	8.654	---	8.176
E	H <sub><math>\alpha</math></sub>	4.053	4.443	---	4.128
C	H	---	8.41	---	---
C	H <sub><math>\alpha</math></sub>	---	4.351	---	---

a. Indicates an ambiguous assignment.

**Table 18.** Backbone chemical shift data for peptide **20** its derivatives.

Residue	Atom	$\delta$ (ppm)			
		20a (293 K)	20b (293 K)	20c (293 K)	20d (293 K)
C	H	---	a	---	---
C	H <sub><math>\alpha</math></sub>	---	a	---	---
K	H	---	a	---	---
K	H <sub><math>\alpha</math></sub>	a	a	a	---
K	H	a	a	8.066	---
K	H <sub><math>\alpha</math></sub>	a	a	4.338	---
W	H	8.537	8.46	8.438	---
W	H <sub><math>\alpha</math></sub>	4.818	5.06	4.593	---
A	H	8.602	8.737	8.094	---
A	H <sub><math>\alpha</math></sub>	4.540	4.691	4.223	---
Y	H	8.473	a	7.983	---
Y	H <sub><math>\alpha</math></sub>	4.088	a	4.377	---
N	H	7.997	7.744	8.301	---
N	H <sub><math>\alpha</math></sub>	4.940	4.975	4.857	---
P	H <sub><math>\alpha</math></sub>	4.114	3.997	4.251	---
A	H	8.002	7.848	8.066	---
A	H <sub><math>\alpha</math></sub>	4.260	4.218	4.254	---
T	H	7.382	7.064	---	8.292
T	H <sub><math>\alpha</math></sub>	4.377	4.408	---	4.321
G	H	8.339	8.317	---	8.572
G	H <sub><math>\alpha</math></sub>	3.805	3.732	---	3.922
G	H <sub><math>\alpha'</math></sub>	4.023	4.051	---	---
K	H	7.672	7.376	---	8.132
K	H <sub><math>\alpha</math></sub>	4.525	4.718	---	4.225
F	H	8.544	8.546	---	8.222
F	H <sub><math>\alpha</math></sub>	4.772	5.025	---	4.639
A	H	8.473	8.581	---	8.142
A	H <sub><math>\alpha</math></sub>	4.502	4.578	---	4.320
V	H	8.215	8.344	---	8.139
V	H <sub><math>\alpha</math></sub>	3.958	4.225	---	4.089
Q	H	8.542	8.787	---	8.512
Q	H <sub><math>\alpha</math></sub>	4.386	4.616	---	4.381
E	H	8.548	8.637	---	8.177
E	H <sub><math>\alpha</math></sub>	4.222	4.435	---	4.136
C	H	---	8.453	---	---
C	H <sub><math>\alpha</math></sub>	---	4.398	---	---

a. Indicates an ambiguous assignment.

**Table 19.** Backbone chemical shift data for peptide **22** its derivatives.

Residue	Atom	$\delta$ (ppm)			
		21a (278 K)	21b (293 K)	21c (293 K)	21d (293 K)
C	H	---	8.475	---	---
C	H <sub><math>\alpha</math></sub>	---	4.411	---	---
G	H	---	8.771	---	---
G	H <sub><math>\alpha</math></sub>	3.715	3.692	a	---
G	H <sub><math>\alpha'</math></sub>	3.829	4.11	---	---
E	H	8.648	7.853	8.612	---
E	H <sub><math>\alpha</math></sub>	4.471	4.554	4.285	---
W	H	8.718	8.77	8.364	---
W	H <sub><math>\alpha</math></sub>	4.790	4.646	4.636	---
A	H	8.633	8.733	8.066	---
A	H <sub><math>\alpha</math></sub>	4.556	4.716	4.219	---
Y	H	8.592	8.732	7.976	---
Y	H <sub><math>\alpha</math></sub>	3.896	3.726	4.367	---
N	H	7.966	7.784	8.260	---
N	H <sub><math>\alpha</math></sub>	4.919	4.967	4.857	---
P	H <sub><math>\alpha</math></sub>	4.078	4.001	4.251	---
A	H	8.016	7.891	8.060	---
A	H <sub><math>\alpha</math></sub>	4.244	4.221	4.255	---
T	H	7.334	7.087	---	8.291
T	H <sub><math>\alpha</math></sub>	4.379	4.398	---	4.320
G	H	8.383	8.347	---	8.573
G	H <sub><math>\alpha</math></sub>	3.802	3.741	---	3.920
G	H <sub><math>\alpha'</math></sub>	4.004	4.047	---	---
K	H	7.637	7.380	---	8.140
K	H <sub><math>\alpha</math></sub>	4.576	4.723	---	4.215
F	H	8.670	8.705	---	8.208
F	H <sub><math>\alpha</math></sub>	4.743	4.826	---	4.639
A	H	8.016	8.586	---	8.151
A	H <sub><math>\alpha</math></sub>	4.244	4.519	---	4.327
V	H	8.312	8.186	---	8.211
V	H <sub><math>\alpha</math></sub>	4.087	3.955	---	4.159
T	H	8.446	8.454	---	8.273
T	H <sub><math>\alpha</math></sub>	4.377	4.272	---	4.359
E	H	8.617	8.796	---	8.430
E	H <sub><math>\alpha</math></sub>	4.257	4.351	---	4.279
C	H	---	8.817	---	---
C	H <sub><math>\alpha</math></sub>	---	4.589	---	---

a. Indicates an ambiguous assignment.

**Table 20.** Backbone chemical shift data for peptide **23** its derivatives.

Residue	Atom	$\delta$ (ppm)			
		23a (278 K)	23b (293 K)	23c (293 K)	23d (293 K)
C	H	---	8.506	---	---
C	H <sub><math>\alpha</math></sub>	---	4.585	---	---
G	H	---	8.755	---	---
G	H <sub><math>\alpha</math></sub>	3.745	3.825	3.742	---
G	H <sub><math>\alpha</math>'</sub>	3.833	4.035	3.825	---
E	H	8.718	8.009	8.645	---
E	H <sub><math>\alpha</math></sub>	4.324	4.459	4.305	---
W	H	8.617	8.521	8.454	---
W	H <sub><math>\alpha</math></sub>	4.582	4.465	4.601	---
$\beta^2$ Y	H	8.129	8.141	7.998	---
$\beta^2$ Y	H <sub><math>\alpha</math></sub>	2.399	2.404	2.465	---
$\beta^2$ Y	H <sub><math>\beta</math></sub>	3.103	3.003	3.165	---
$\beta^2$ Y	H <sub><math>\beta</math>'</sub>	3.356	3.502	3.316	---
N	H	7.702	7.900	7.614	---
N	H <sub><math>\alpha</math></sub>	4.781	4.782	4.790	---
P	H <sub><math>\alpha</math></sub>	4.123	3.992	4.153	---
A	H	8.185	7.989	7.986	---
A	H <sub><math>\alpha</math></sub>	4.280	4.220	4.240	---
T	H	7.819	7.413	---	8.295
T	H <sub><math>\alpha</math></sub>	4.314	4.382	---	4.310
G	H	8.294	7.929	---	8.547
G	H <sub><math>\alpha</math></sub>	3.843	3.632	---	3.916
G	H <sub><math>\alpha</math>'</sub>	3.914	3.934	---	---
K	H	7.844	7.352	---	7.927
K	H <sub><math>\alpha</math></sub>	4.119	4.104	---	4.142
$\beta^3$ F	H	8.140	7.916	---	8.059
$\beta^3$ F	H <sub><math>\alpha</math></sub>	2.454	2.126	---	2.495
$\beta^3$ F	H <sub><math>\alpha</math>'</sub>	2.576	2.345	---	2.676
$\beta^3$ F	H <sub><math>\beta</math></sub>	4.397	4.204	---	4.455
V	H	8.336	8.085	---	8.265
V	H <sub><math>\alpha</math></sub>	4.132	4.221	---	4.104
T	H	8.398	8.336	---	8.266
T	H <sub><math>\alpha</math></sub>	4.327	4.206	---	4.356
E	H	8.536	8.628	---	8.433
E	H <sub><math>\alpha</math></sub>	4.240	4.319	---	4.268
C	H	---	8.702	---	---
C	H <sub><math>\alpha</math></sub>	---	4.587	---	---

**Table 21.** Backbone chemical shift data for peptide **24** its derivatives.

Residue	Atom	$\delta$ (ppm)			
		24a (278 K)	24b (293 K)	24c (293 K)	24d (293 K)
C	H	---	8.515	---	---
C	H <sub><math>\alpha</math></sub>	---	4.63	---	---
G	H	---	8.644	---	---
G	H <sub><math>\alpha</math></sub>	---	3.884	a	---
G	H <sub><math>\alpha</math>'</sub>	3.868	3.973	---	---
E	H	8.782	8.198	8.711	---
E	H <sub><math>\alpha</math></sub>	4.385	4.360	4.377	---
W	H	8.768	8.427	8.620	---
W	H <sub><math>\alpha</math></sub>	4.612	4.644	4.614	---
$\beta^{2,3}$ AY	H	8.047	7.949	7.933	---
$\beta^{2,3}$ AY	H <sub><math>\alpha</math></sub>	2.176	2.410	2.187	---
$\beta^{2,3}$ AY	H <sub><math>\beta</math></sub>	3.732	3.917	3.728	---
N	H	8.157	8.117	8.062	---
N	H <sub><math>\alpha</math></sub>	4.843	4.848	4.84	---
P	H <sub><math>\alpha</math></sub>	4.052	3.963	4.066	---
A	H	8.193	7.961	7.970	---
A	H <sub><math>\alpha</math></sub>	4.283	4.240	4.226	---
T	H	7.872	7.436	---	8.304
T	H <sub><math>\alpha</math></sub>	4.290	4.352	---	4.305
G	H	8.326	8.129	---	8.549
G	H <sub><math>\alpha</math></sub>	3.870	3.729	---	3.903
G	H <sub><math>\alpha</math>'</sub>	3.921	4.037	---	---
K	H	7.974	7.619	---	7.924
K	H <sub><math>\alpha</math></sub>	4.084	4.164	---	4.090
$\beta^{2,3}$ FA	H	8.018	7.891	---	7.942
$\beta^{2,3}$ FA	H <sub><math>\alpha</math></sub>	2.664	2.622	---	2.663
$\beta^{2,3}$ FA	H <sub><math>\beta</math></sub>	4.233	4.274	---	4.228
V	H	8.600	8.338	---	8.488
V	H <sub><math>\alpha</math></sub>	4.217	4.419	---	4.185
T	H	8.477	8.376	---	8.338
T	H <sub><math>\alpha</math></sub>	4.376	4.321	---	4.374
E	H	8.564	8.576	---	8.450
E	H <sub><math>\alpha</math></sub>	4.277	4.376	---	4.294
C	H	---	8.607	---	---
C	H <sub><math>\alpha</math></sub>	---	4.601	---	---

a. Indicates an ambiguous assignment.

**Table 22.** Backbone chemical shift data for peptide **25** its derivatives.

Residue	Atom	$\delta$ (ppm)			
		25a (278 K)	25b (293 K)	25c (293 K)	25d (293 K)
C	H	---	8.493	---	---
C	H <sub><math>\alpha</math></sub>	---	4.627	---	---
G	H	---	8.585	---	---
G	H <sub><math>\alpha</math></sub>	3.713	3.852	a	---
G	H <sub><math>\alpha'</math></sub>	3.824	3.877	---	---
E	H	8.704	8.254	8.614	---
E	H <sub><math>\alpha</math></sub>	4.289	4.198	4.292	---
W	H	8.496	8.081	8.352	---
W	H <sub><math>\alpha</math></sub>	4.513	4.511	4.528	---
$\beta^3$ A	H	7.954	7.588	7.834	---
$\beta^3$ A	H <sub><math>\alpha</math></sub>	1.901	2.103	1.948	---
$\beta^3$ A	H <sub><math>\beta</math></sub>	4.045	4.120	4.047	---
$\beta^2$ Y	H	7.989	7.988	7.887	---
$\beta^2$ Y	H <sub><math>\alpha</math></sub>	2.786	2.820	2.807	---
$\beta^2$ Y	H <sub><math>\beta</math></sub>	3.284	3.266	3.283	---
$\beta^2$ Y	H <sub><math>\beta'</math></sub>	---	3.403	---	---
N	H	8.284	8.165	8.209	---
N	H <sub><math>\alpha</math></sub>	4.825	4.832	4.854	---
P	H <sub><math>\alpha</math></sub>	4.131	4.068	4.149	---
A	H	8.190	8.03	7.988	---
A	H <sub><math>\alpha</math></sub>	4.292	4.266	4.239	---
T	H	7.850	7.572	---	8.299
T	H <sub><math>\alpha</math></sub>	4.290	4.307	---	4.299
G	H	8.353	8.198	---	8.56
G	H <sub><math>\alpha</math></sub>	3.870	3.798	---	3.913
G	H <sub><math>\alpha'</math></sub>	3.928	3.975	---	---
K	H	7.941	7.680	---	7.951
K	H <sub><math>\alpha</math></sub>	4.138	4.184	---	4.135
$\beta^3$ F	H	8.098	7.972	---	8.01
$\beta^3$ F	H <sub><math>\alpha</math></sub>	2.395	2.400	---	2.41
$\beta^3$ F	H <sub><math>\alpha'</math></sub>	2.508	2.491	---	2.521
$\beta^3$ F	H <sub><math>\beta</math></sub>	4.406	4.383	---	4.422
$\beta^2$ A	H	8.204	8.048	---	8.085
$\beta^2$ A	H <sub><math>\alpha</math></sub>	2.731	2.698	---	2.742
$\beta^2$ A	H <sub><math>\beta</math></sub>	3.099	3.084	---	3.126
$\beta^2$ A	H <sub><math>\beta'</math></sub>	3.361	3.232	---	3.379
V	H	8.368	8.199	---	8.254
V	H <sub><math>\alpha</math></sub>	4.100	4.110	---	4.121
T	H	8.366	8.183	---	8.249
T	H <sub><math>\alpha</math></sub>	4.340	4.299	---	4.355
E	H	8.533	8.462	---	8.419
E	H <sub><math>\alpha</math></sub>	4.261	4.339	---	4.282
C	H	---	8.501	---	---
C	H <sub><math>\alpha</math></sub>	---	4.617	---	---

a. Indicates an ambiguous assignment.

**Table 23.** Backbone chemical shift data for peptide **26** its derivatives.

Residue	Atom	$\delta$ (ppm)			
		26a (278 K)	26b (293 K)	26c (293 K)	26d (293 K)
C	H	---	8.478	---	---
C	H <sub><math>\alpha</math></sub>	---	4.595	---	---
G	H	---	8.655	---	---
G	H <sub><math>\alpha</math></sub>	3.743	3.819	a	---
G	H <sub><math>\alpha'</math></sub>	3.834	3.963	---	---
E	H	8.731	8.172	a	---
E	H <sub><math>\alpha</math></sub>	4.319	4.339	4.310	---
W	H	8.572	8.372	8.405	---
W	H <sub><math>\alpha</math></sub>	4.601	4.525	4.611	---
$\beta^{2,3}$ AA	H	7.949	7.407	7.846	---
$\beta^{2,3}$ AA	H <sub><math>\alpha</math></sub>	2.122	2.298	2.128	---
$\beta^{2,3}$ AA	H <sub><math>\beta</math></sub>	3.792	3.960	3.801	---
$\beta^{2,3}$ AY	H	8.293	8.251	8.155	---
$\beta^{2,3}$ AY	H <sub><math>\alpha</math></sub>	2.664	2.992	2.668	---
$\beta^{2,3}$ AY	H <sub><math>\beta</math></sub>	4.075	4.142	4.062	---
N	H	8.395	8.169	8.312	---
N	H <sub><math>\alpha</math></sub>	4.923	4.944	4.932	---
P	H <sub><math>\alpha</math></sub>	4.094	3.968	4.135	---
A	H	8.229	7.968	8.017	---
A	H <sub><math>\alpha</math></sub>	4.285	4.242	4.238	---
T	H	7.873	7.369	---	8.302
T	H <sub><math>\alpha</math></sub>	4.292	4.385	---	4.299
G	H	8.355	8.261	---	8.548
G	H <sub><math>\alpha</math></sub>	3.869	3.747	---	3.896
G	H <sub><math>\alpha'</math></sub>	3.944	4.086	---	---
K	H	7.970	7.581	---	7.930
K	H <sub><math>\alpha</math></sub>	4.108	4.271	---	4.088
$\beta^{2,3}$ FA	H	8.043	8.113	---	7.916
$\beta^{2,3}$ FA	H <sub><math>\alpha</math></sub>	2.507	2.451	---	2.538
$\beta^{2,3}$ FA	H <sub><math>\beta</math></sub>	4.204	4.208	---	4.210
$\beta^{2,3}$ AA	H	8.403	8.285	---	8.251
$\beta^{2,3}$ AA	H <sub><math>\alpha</math></sub>	2.564	2.439	---	2.583
$\beta^{2,3}$ AA	H <sub><math>\beta</math></sub>	4.109	4.132	---	4.098
V	H	8.512	8.260	---	8.378
V	H <sub><math>\alpha</math></sub>	4.148	4.266	---	4.146
T	H	8.456	8.444	---	8.319
T	H <sub><math>\alpha</math></sub>	4.361	4.318	---	4.370
E	H	8.568	8.638	---	8.442
E	H <sub><math>\alpha</math></sub>	4.265	4.353	---	4.283
C	H	---	8.686	---	---
C	H <sub><math>\alpha</math></sub>	---	4.603	---	---

a. Indicates an ambiguous assignment.

**Table 24.** Backbone chemical shift data for peptide **73.**

Residue	Atom	$\delta$ (ppm)
G1	H <sub><math>\alpha</math></sub>	3.762
G1	H <sub><math>\alpha'</math></sub>	3.850
E2	H	8.723
E2	H <sub><math>\alpha</math></sub>	4.471
W3	H	8.776
W3	H <sub><math>\alpha</math></sub>	4.671
X4	H	9.815
Y5	H	8.903
Y5	H <sub><math>\alpha</math></sub>	4.353
N6	H	8.082
N6	H <sub><math>\alpha</math></sub>	4.934
P7	H <sub><math>\alpha</math></sub>	4.154
A8	H	7.990
A8	H <sub><math>\alpha</math></sub>	4.258
T9	H	7.287
T9	H <sub><math>\alpha</math></sub>	4.406
G10	H	8.487
G10	H <sub><math>\alpha</math></sub>	3.810
G10	H <sub><math>\alpha'</math></sub>	4.062
K11	H	7.703
K11	H <sub><math>\alpha</math></sub>	4.642
F12	H	9.031
F12	H <sub><math>\alpha</math></sub>	4.525
X13	H	9.756
V14	H	8.421
V14	H <sub><math>\alpha</math></sub>	4.252
T15	H	8.513
T15	H <sub><math>\alpha</math></sub>	4.364
E16	H	8.523
E16	H <sub><math>\alpha</math></sub>	4.213

**Table 25.** Backbone chemical shift data for peptide **74.**

Residue	Atom	$\delta$ (ppm)
G1	H <sub><math>\alpha</math></sub>	3.772
G1	H <sub><math>\alpha'</math></sub>	3.852
E2	H	8.612
E2	H <sub><math>\alpha</math></sub>	4.639
W3	H	8.994
W3	H <sub><math>\alpha</math></sub>	4.229
X4	H	7.478
X4	H <sub><math>\alpha</math></sub>	2.379
X4	H <sub><math>\gamma</math></sub>	3.587
Y5	H	8.661
Y5	H <sub><math>\alpha</math></sub>	3.722
N6	H	7.906
N6	H <sub><math>\alpha</math></sub>	4.935
P7	H <sub><math>\alpha</math></sub>	4.033
A8	H	7.951
A8	H <sub><math>\alpha</math></sub>	4.220
T9	H	7.132
T9	H <sub><math>\alpha</math></sub>	4.399
G10	H	8.399
G10	H <sub><math>\alpha</math></sub>	3.778
G10	H <sub><math>\alpha'</math></sub>	4.036
K11	H	7.420
K11	H <sub><math>\alpha</math></sub>	4.739
F12	H	8.956
F12	H <sub><math>\alpha</math></sub>	4.338
X13	H	7.442
X13	H <sub><math>\alpha</math></sub>	2.064
X13	H <sub><math>\gamma</math></sub>	3.463
V14	H	8.303
V14	H <sub><math>\alpha</math></sub>	4.040
T15	H	8.454
T15	H <sub><math>\alpha</math></sub>	4.351
E16	H	8.660
E16	H <sub><math>\alpha</math></sub>	4.277

**Table 26.** Backbone chemical shift data for peptide 75.

Residue	Atom	$\delta$ (ppm)
G1	H <sub><math>\alpha</math></sub>	3.798
G1	H <sub><math>\alpha'</math></sub>	3.857
E2	H	8.767
E2	H <sub><math>\alpha</math></sub>	4.363
W3	H	8.669
W3	H <sub><math>\alpha</math></sub>	4.521
X4	H	8.114
X4	H <sub><math>\alpha</math></sub>	5.300
X4	H <sub><math>\beta</math></sub>	6.137
X4	H <sub><math>\gamma</math></sub>	4.333
Y5	H	8.216
Y5	H <sub><math>\alpha</math></sub>	4.487
N6	H	8.395
N6	H <sub><math>\alpha</math></sub>	4.990
P7	H <sub><math>\alpha</math></sub>	4.264
A8	H	8.221
A8	H <sub><math>\alpha</math></sub>	4.308
T9	H	7.697
T9	H <sub><math>\alpha</math></sub>	4.378
G10	H	8.474
G10	H <sub><math>\alpha</math></sub>	3.869
G10	H <sub><math>\alpha'</math></sub>	3.991
K11	H	7.993
K11	H <sub><math>\alpha</math></sub>	4.419
F12	H	8.698
F12	H <sub><math>\alpha</math></sub>	4.424
X13	H	8.104
X13	H <sub><math>\alpha</math></sub>	5.763
X13	H <sub><math>\beta</math></sub>	6.302
X13	H <sub><math>\gamma</math></sub>	4.421
V14	H	8.263
V14	H <sub><math>\alpha</math></sub>	4.238
T15	H	8.477
T15	H <sub><math>\alpha</math></sub>	4.378
E16	H	8.548
E16	H <sub><math>\alpha</math></sub>	4.251

**Table 27.** Backbone chemical shift data for peptide 76.

Residue	Atom	$\delta$ (ppm)
C1	H	8.478
C1	H <sub><math>\alpha</math></sub>	4.590
G2	H	8.544
G2	H <sub><math>\alpha</math></sub>	3.756
G2	H <sub><math>\alpha'</math></sub>	3.889
E3	H	8.257
E3	H <sub><math>\alpha</math></sub>	4.277
W4	H	8.184
W4	H <sub><math>\alpha</math></sub>	4.514
X5	H	7.780
X5	H <sub><math>\alpha</math></sub>	5.819
X5	H <sub><math>\beta</math></sub>	6.404
X5	H <sub><math>\gamma</math></sub>	4.460
Y6	H	8.542
Y6	H <sub><math>\alpha</math></sub>	4.271
N7	H	8.037
N7	H <sub><math>\alpha</math></sub>	5.009
P8	H <sub><math>\alpha</math></sub>	4.149
A9	H	7.993
A9	H <sub><math>\alpha</math></sub>	4.266
T10	H	7.284
T10	H <sub><math>\alpha</math></sub>	4.416
G11	H	8.410
G11	H <sub><math>\alpha</math></sub>	3.784
G11	H <sub><math>\alpha'</math></sub>	4.073
K12	H	7.568
K12	H <sub><math>\alpha</math></sub>	4.597
F13	H	8.755
F13	H <sub><math>\alpha</math></sub>	4.425
X14	H	7.955
X14	H <sub><math>\alpha</math></sub>	5.834
X14	H <sub><math>\beta</math></sub>	6.357
X14	H <sub><math>\gamma</math></sub>	4.489
V15	H	8.049
V15	H <sub><math>\alpha</math></sub>	4.192
T16	H	8.356
T16	H <sub><math>\alpha</math></sub>	4.260
E17	H	8.540
E17	H <sub><math>\alpha</math></sub>	4.349
C18	H	8.546
C18	H <sub><math>\alpha</math></sub>	4.620

**Table 28.** Backbone chemical shift data for peptide 77.

Residue	Atom	$\delta$ (ppm)	
		<i>trans</i>	<i>cis</i>
G1	H <sub><math>\alpha</math></sub>	3.599	a
G1	H <sub><math>\alpha'</math></sub>	3.794	a
E2	H	8.572	8.557
E2	H <sub><math>\alpha</math></sub>	4.791	4.807
W3	H <sub><math>\alpha</math></sub>	5.330	5.230
W3	H <sub>Me</sub>	3.118	2.902
A4	H	8.403	8.561
A4	H <sub><math>\alpha</math></sub>	4.524	4.407
Y5	H	8.637	8.612
Y5	H <sub><math>\alpha</math></sub>	4.117	4.508
N6	H	8.061	8.375
N6	H <sub><math>\alpha</math></sub>	4.948	4.961
P7	H <sub><math>\alpha</math></sub>	4.126	4.250
A8	H	8.061	8.219
A8	H <sub><math>\alpha</math></sub>	4.254	4.301
T9	H	7.409	7.752
T9	H <sub><math>\alpha</math></sub>	4.373	4.349
G10	H	8.400	8.426
G10	H <sub><math>\alpha</math></sub>	3.813	3.887
G10	H <sub><math>\alpha'</math></sub>	4.001	3.973
K11	H	7.697	8.028
K11	H <sub><math>\alpha</math></sub>	4.522	4.317
F12	H	8.618	8.427
F12	H <sub><math>\alpha</math></sub>	4.766	4.682
A13	H	8.480	8.319
A13	H <sub><math>\alpha</math></sub>	4.355	4.333
V14	H	8.204	8.353
V14	H <sub><math>\alpha</math></sub>	4.077	4.152
T15	H	8.362	8.350
T15	H <sub><math>\alpha</math></sub>	4.367	4.321
E16	H	8.572	8.534
E16	H <sub><math>\alpha</math></sub>	4.231	4.237

<sup>a</sup>Indicates an ambiguous assignment.**Table 29.** Backbone chemical shift data for peptide 78.

Residue	Atom	$\delta$ (ppm)	
		<i>trans</i>	<i>cis</i>
G1	H <sub><math>\alpha</math></sub>	3.724	3.707
G1	H <sub><math>\alpha'</math></sub>	3.814	3.804
E2	H	8.648	8.7
E2	H <sub><math>\alpha</math></sub>	4.356	4.334
W3	H	8.59	8.34
W3	H <sub><math>\alpha</math></sub>	4.696	4.656
A4	H	8.397	a
A4	H <sub><math>\alpha</math></sub>	4.809	a
Y5	H	4.769	4.879
Y5	H <sub>Me</sub>	2.989	2.930
N6	H	8.099	8.478
N6	H <sub><math>\alpha</math></sub>	4.923	4.594
P7	H <sub><math>\alpha</math></sub>	4.222	4.343
A8	H	8.258	8.287
A8	H <sub><math>\alpha</math></sub>	4.289	4.288
T9	H	7.707	7.992
T9	H <sub><math>\alpha</math></sub>	4.345	4.293
G10	H	8.366	8.394
G10	H <sub><math>\alpha</math></sub>	3.864	3.909
G10	H <sub><math>\alpha'</math></sub>	3.956	---
K11	H	7.905	8.197
K11	H <sub><math>\alpha</math></sub>	4.388	4.194
F12	H	8.487	8.300
F12	H <sub><math>\alpha</math></sub>	4.738	4.614
A13	H	8.476	8.218
A13	H <sub><math>\alpha</math></sub>	4.403	4.291
V14	H	8.329	8.335
V14	H <sub><math>\alpha</math></sub>	4.099	4.145
T15	H	8.404	a
T15	H <sub><math>\alpha</math></sub>	4.356	a
E16	H	8.576	8.546
E16	H <sub><math>\alpha</math></sub>	4.258	4.260

<sup>a</sup>Indicates an ambiguous assignment.

**Table 30.** Backbone chemical shift data for peptide **79**.

Residue	Atom	$\delta$ (ppm)	
		<i>trans</i>	<i>cis</i>
G1	H <sub><math>\alpha</math></sub>	3.708	3.703
G1	H <sub><math>\alpha'</math></sub>	3.817	3.806
E2	H	8.666	8.690
E2	H <sub><math>\alpha</math></sub>	4.371	4.275
W3	H	8.594	8.482
W3	H <sub><math>\alpha</math></sub>	4.709	4.625
A4	H	8.331	8.153
A4	H <sub><math>\alpha</math></sub>	4.292	4.212
Y5	H	8.182	8.099
Y5	H <sub><math>\alpha</math></sub>	4.072	4.346
N6	H	8.204	8.286
N6	H <sub><math>\alpha</math></sub>	4.878	4.831
P7	H <sub><math>\alpha</math></sub>	4.167	4.239
A8	H	8.125	8.227
A8	H <sub><math>\alpha</math></sub>	4.271	4.278
T9	H	7.645	7.815
T9	H <sub><math>\alpha</math></sub>	4.339	4.288
G10	H	8.387	8.352
G10	H <sub><math>\alpha</math></sub>	3.823	3.905
G10	H <sub><math>\alpha'</math></sub>	3.94	---
K11	H	7.786	8.138
K11	H <sub><math>\alpha</math></sub>	4.765	4.307
F12	H <sub><math>\alpha</math></sub>	5.204	5.050
F12	H <sub>Me</sub>	3.083	2.902
A13	H	8.27	8.386
A13	H <sub><math>\alpha</math></sub>	4.382	4.345
V14	H	8.386	8.474
V14	H <sub><math>\alpha</math></sub>	4.162	4.23
T15	H	8.453	8.431
T15	H <sub><math>\alpha</math></sub>	4.36	4.366
E16	H	8.589	8.557
E16	H <sub><math>\alpha</math></sub>	4.261	4.257

**Table 31.** Backbone chemical shift data for peptide **80**.

Residue	Atom	$\delta$ (ppm)	
		<i>trans</i>	<i>cis</i>
G1	H <sub><math>\alpha</math></sub>	3.683	a
G1	H <sub><math>\alpha'</math></sub>	3.831	a
E2	H	8.637	8.729
E2	H <sub><math>\alpha</math></sub>	4.492	4.282
W3	H	8.717	8.453
W3	H <sub><math>\alpha</math></sub>	4.754	4.771
A4	H	8.662	8.342
A4	H <sub><math>\alpha</math></sub>	4.541	4.354
Y5	H	8.543	8.302
Y5	H <sub><math>\alpha</math></sub>	3.888	4.196
N6	H	7.986	8.08
N6	H <sub><math>\alpha</math></sub>	4.912	4.885
P7	H <sub><math>\alpha</math></sub>	4.082	4.149
A8	H	8.01	8.101
A8	H <sub><math>\alpha</math></sub>	4.244	4.275
T9	H	7.364	7.556
T9	H <sub><math>\alpha</math></sub>	4.383	4.350
G10	H	8.37	8.357
G10	H <sub><math>\alpha</math></sub>	3.811	3.857
G10	H <sub><math>\alpha'</math></sub>	4.006	3.974
K11	H	7.663	7.808
K11	H <sub><math>\alpha</math></sub>	4.55	4.402
F12	H	8.61	8.573
F12	H <sub><math>\alpha</math></sub>	4.757	4.699
A13	H	8.625	8.477
A13	H <sub><math>\alpha</math></sub>	4.844	4.970
V14	H <sub><math>\alpha</math></sub>	4.668	4.675
V14	H <sub>Me</sub>	3.029	2.891
T15	H	8.513	a
T15	H <sub><math>\alpha</math></sub>	4.334	a
E16	H	8.682	a
E16	H <sub><math>\alpha</math></sub>	4.287	a

<sup>a</sup>Indicates an ambiguous assignment.

## **APPENDIX B**

### **NOE-DERIVED DISTANCE RESTRAINTS FOR SELECT HAIRPIN PEPTIDES**

**Table 32.** NOE distance restraints for peptide **1a**.

Residue		Proton	Residue		Proton	Distance
5	V	HA	6	P	QD	2.7
6	P	QD	5	V	HA	2.7
4	Y	HA	5	V	H	2.7
9	F	HA	10	T	H	2.7
2	W	HA	3	Q	H	2.7
8	K	HA	9	F	H	2.7
10	T	HA	11	V	H	2.7
11	V	H	10	T	HA	2.7
1	R	HA	2	W	H	2.7
11	V	HA	12	Q	H	2.7
4	Y	H	3	Q	HA	2.7
7	G	HA1	7	G	H	2.7
9	F	H	8	K	HA	2.7
3	Q	HA	4	Y	H	2.7
12	Q	H	11	V	HA	2.7
2	W	H	1	R	HA	2.7
10	T	H	9	F	HA	2.7
7	G	H	6	P	HA	2.7
6	P	HA	7	G	H	2.7
12	Q	HB1	12	Q	H	3.5
7	G	H	8	K	H	3.5
4	Y	HA	9	F	HA	3.5
2	W	HA	11	V	HA	3.5
8	K	H	7	G	H	3.5
1	R	QB	2	W	H	3.5
1	R	HA	2	W	HD1	3.5
7	G	HA1	8	K	H	3.5
7	G	HA2	8	K	H	3.5
5	V	H	8	K	H	3.5
11	V	H	10	T	HB	3.5
8	K	H	5	V	H	3.5
4	Y	H	3	Q	HB2	3.5
2	W	HB1	3	Q	H	3.5
4	Y	HB2	5	V	H	3.5
3	Q	H	2	W	HB2	3.5
9	F	H	8	K	HB2	3.5
8	K	HB2	9	F	H	3.5
8	K	H	7	G	HA1	3.5
4	Y	HA	10	T	H	3.5
4	Y	H	3	Q	HB1	3.5
4	Y	H	3	Q	HG1	3.5
10	T	H	3	Q	H	3.5

Residue		Proton	Residue		Proton	Distance
9	F	HB2	10	T	H	3.5
2	W	HB2	3	Q	H	3.5
5	V	H	4	Y	HB1	3.5
9	F	HA	5	V	H	3.5
3	Q	H	10	T	H	3.5
4	Y	HB1	5	V	H	3.5
11	V	HB	12	Q	H	3.5
8	K	H	7	G	HA2	3.5
10	T	H	9	F	HB2	3.5
8	K	HB1	9	F	H	3.5
5	V	QQXG	6	P	QD	4.5
12	Q	H	3	Q	H	4.5
4	Y	QE	9	F	HB1	4.5
8	K	HA	4	Y	QD	4.5
8	K	HA	4	Y	QE	4.5
2	W	H	1	R	QG	4.5
8	K	QG	9	F	H	4.5
2	W	HE3	3	Q	HA	4.5
10	T	QXGT	11	V	H	4.5
12	Q	H	11	V	QQXG	4.5
7	G	HA1	4	Y	QD	4.5
5	V	H	4	Y	QD	4.5
4	Y	HA	9	F	QD	4.5
9	F	QD	10	T	H	4.5
5	V	H	6	P	QD	4.5
10	T	H	9	F	QD	4.5
9	F	H	10	T	H	4.5
9	F	HB1	10	T	H	4.5
4	Y	QD	5	V	H	4.5
2	W	HE3	9	F	QD	4.5
10	T	H	11	V	H	4.5
9	F	H	8	K	H	4.5
2	W	HA	12	Q	H	4.5
10	T	H	9	F	HB1	4.5
11	V	H	10	T	H	4.5
4	Y	HB2	2	W	HE3	4.5
4	Y	HB1	9	F	QE	4.5
4	Y	HA	3	Q	HA	4.5
9	F	H	4	Y	QE	4.5
10	T	HA	2	W	HE3	4.5
8	K	H	6	P	HA	4.5
9	F	HA	4	Y	QD	4.5
3	Q	H	2	W	HE3	4.5

Residue		Proton	Residue		Proton	Distance
8	K	H	9	F	H	4.5
9	F	H	4	Y	QD	4.5
12	Q	HA	11	V	HA	4.5
10	T	H	9	F	H	4.5
5	V	HA	7	G	H	4.5
6	P	HA	8	K	H	4.5
7	G	H	5	V	H	4.5
2	W	HE3	10	T	H	4.5
2	W	HE3	10	T	HA	4.5
6	P	QB	7	G	H	4.5
2	W	HE3	3	Q	H	4.5
11	V	HA	3	Q	H	4.5
7	G	HA1	9	F	HB2	4.5
4	Y	QD	8	K	H	4.5
5	V	H	7	G	H	4.5
11	V	HA	2	W	HE3	4.5
2	W	HZ2	9	F	QD	4.5
10	T	H	2	W	HE3	4.5
3	Q	H	11	V	HA	4.5
10	T	HA	11	V	QQXG	4.5
7	G	H	6	P	QB	4.5
4	Y	HA	8	K	H	4.5
10	T	H	4	Y	QD	4.5
6	P	QD	5	V	H	4.5
4	Y	QE	9	F	H	4.5
3	Q	H	12	Q	H	4.5
3	Q	HA	2	W	HE3	4.5
11	V	HA	2	W	HD1	4.5
4	Y	H	3	Q	HG2	4.5
7	G	HA1	4	Y	QE	5.5
5	V	QQXG	4	Y	H	5.5
10	T	QXGT	12	Q	H	5.5
11	V	QQXG	9	F	QE	5.5
10	T	QXGT	5	V	H	5.5
4	Y	QE	7	G	HA1	5.5
8	K	QD	9	F	H	5.5
9	F	H	10	T	QXGT	5.5
5	V	HB	10	T	QXGT	5.5
11	V	QQXG	2	W	HD1	5.5

**Table 33.** NOE distance restraints for peptide **2a**.

Residue		Proton	Residue		Proton	Residue
2	W	HA	3	X	H	2.7
4	Y	HA	5	V	H	2.7
8	K	HA	9	F	H	2.7
5	V	HA	6	P	HD2	2.7
1	R	HA	2	W	H	2.7
11	V	HA	12	Q	H	2.7
5	V	HA	6	P	HD1	2.7
3	X	HA1	4	Y	H	2.7
6	P	HD2	5	V	HA	2.7
2	W	H	1	R	HA	2.7
12	Q	H	11	V	HA	2.7
6	P	HD1	5	V	HA	2.7
3	X	H	2	W	HA	2.7
9	F	HA	10	X	H	2.7
4	Y	H	3	X	HA2	2.7
10	X	H	9	F	HA	2.7
6	P	HA	7	G	H	2.7
7	G	HA2	8	K	H	2.7
3	X	HA2	4	Y	H	3.5
7	G	HA1	8	K	H	3.5
7	G	H	6	P	QG	3.5
6	P	QG	7	G	H	3.5
2	W	QB	3	X	H	3.5
3	X	H	2	W	QB	3.5
4	Y	HA	9	F	HA	3.5
8	K	H	7	G	H	3.5
8	K	H	7	G	HA1	3.5
7	G	H	8	K	H	3.5
12	Q	H	12	Q	HA	3.5
11	V	HB	12	Q	H	3.5
12	Q	H	11	V	HB	3.5
6	P	HD2	7	G	H	3.5
7	G	H	6	P	HD2	3.5
4	Y	HB2	5	V	H	3.5
9	F	H	8	K	H	3.5
5	V	H	4	Y	HB2	3.5
8	K	HA	9	F	QB	3.5
3	X	HB	10	X	HA2	3.5
5	V	QXG2	2	W	HD1	3.5
5	V	QXG1	6	P	HD1	3.5
11	V	HB	2	W	QB	3.5
9	F	QB	10	X	H	3.5

Residue		Proton	Residue		Proton	Residue
9	F	H	10	X	H	3.5
4	Y	HA	10	X	H	3.5
12	Q	H	11	V	QQXG	4.5
11	V	QQXG	12	Q	H	4.5
2	W	HA	3	X	HB	4.5
9	F	HA	4	Y	QD	4.5
5	V	HA	2	W	QB	4.5
5	V	QXG1	6	P	HD2	4.5
10	X	HA2	3	X	HB	4.5
3	X	QQXD	4	Y	H	4.5
1	R	QG	2	W	H	4.5
4	Y	QD	9	F	HA	4.5
1	R	HA	2	W	QB	4.5
4	Y	QE	9	F	QB	4.5
5	V	QXG2	6	P	HD1	4.5
2	W	QB	5	V	HA	4.5
4	Y	QD	5	V	H	4.5
7	G	HA1	6	P	HA	4.5
7	G	H	6	P	HD1	4.5
12	Q	H	11	V	H	4.5
7	G	HA2	6	P	HA	4.5
11	V	H	12	Q	H	4.5
3	X	HB	4	Y	H	4.5
6	P	HD1	7	G	H	4.5
5	V	HA	6	P	HA	4.5
6	P	HD2	5	V	H	4.5
4	Y	HB1	5	V	H	4.5
4	Y	HB2	7	G	H	4.5
6	P	QB	7	G	H	4.5
2	W	HA	11	V	H	4.5
4	Y	HB2	7	G	HA2	4.5
5	V	H	4	Y	HB1	4.5
4	Y	HB1	7	G	H	4.5
3	X	HB	2	W	HA	4.5
5	V	H	7	G	H	4.5
4	Y	HB1	7	G	HA1	4.5
6	P	HD1	5	V	H	4.5
9	F	QD	10	X	H	4.5
5	V	H	4	Y	H	4.5
7	G	H	4	Y	HB2	4.5
4	Y	H	5	V	H	4.5
7	G	HA1	4	Y	HB2	4.5
10	X	HA1	9	F	HA	4.5

Residue		Proton	Residue		Proton	Residue
3	X	HB	10	X	H	4.5
2	W	HE3	3	X	H	4.5
11	V	H	2	W	HA	4.5
3	X	HG	4	Y	H	4.5
11	V	H	2	W	H	4.5
9	F	HA	5	V	H	4.5
10	X	HB	9	F	HA	4.5
11	V	HB	2	W	H	4.5
3	X	QQXD	9	F	QE	4.5
5	V	QXG2	2	W	QB	4.5
5	V	QXG2	6	P	HD2	4.5
10	X	H	9	F	QD	4.5
5	V	HA	7	G	H	4.5
4	Y	QD	8	K	HA	4.5
3	X	HA2	2	W	HD1	4.5
7	G	H	5	V	HA	4.5
2	W	HA	1	R	HA	4.5
4	Y	HB1	8	K	H	4.5
11	V	QQXG	2	W	QB	5.5
3	X	QQXD	4	Y	QE	5.5
3	X	QQXD	4	Y	QD	5.5
3	X	QQXD	2	W	HA	5.5
2	W	QB	4	Y	H	5.5
5	V	QXG2	2	W	HE1	5.5
1	R	QD	2	W	HE1	5.5

**Table 34.** NOE distance restraints for peptide **8a**.

Residue		Proton	Residue		Proton	Residue
6	P	QD	5	V	HA	2.7
10	X	H	9	F	HA	2.7
9	F	HA	10	X	H	2.7
12	Q	H	11	V	HA	2.7
11	V	HA	12	Q	H	2.7
9	F	H	8	K	HA	2.7
8	K	HA	9	F	H	2.7
11	V	H	10	X	HA	2.7
10	X	HA	11	V	H	2.7
2	W	H	1	R	HA	2.7
1	R	HA	2	W	H	2.7
7	G	HA1	7	G	H	2.7
4	Y	HA	5	V	H	2.7
3	X	HB	10	X	HA	2.7
7	G	HA2	7	G	H	2.7
4	Y	H	3	X	QXE	3.5
3	X	QXE	4	Y	H	3.5
7	G	H	8	K	H	3.5
8	K	H	7	G	H	3.5
11	V	H	2	W	H	3.5
11	V	H	10	X	QXD1	3.5
10	X	QXD1	11	V	H	3.5
5	V	H	8	K	H	3.5
8	K	H	5	V	H	3.5
4	Y	HA	9	F	HA	3.5
7	G	HA1	8	K	H	3.5
1	R	QG	2	W	H	3.5
9	F	H	8	K	HB2	3.5
8	K	HB2	9	F	H	3.5
9	F	HA	4	Y	QD	3.5
5	V	H	4	Y	HB2	3.5
4	Y	HB2	5	V	H	3.5
3	X	HB	10	X	H	3.5
11	V	H	10	X	HB	3.5
10	X	HB	11	V	H	3.5
3	X	HB	4	Y	H	3.5
10	X	HG	11	V	H	3.5
3	X	HG	4	Y	H	3.5
9	F	H	8	K	HB1	3.5
8	K	HB1	9	F	H	3.5

Residue		Proton	Residue		Proton	Residue
11	V	H	3	X	HB	3.5
3	X	HB	11	V	H	3.5
9	F	HB1	8	K	HA	3.5
11	V	HA	10	X	HG	3.5
6	P	QD	5	V	QXG2	4.5
4	Y	QE	9	F	HB1	4.5
9	F	HB1	4	Y	QE	4.5
8	K	H	7	G	HA2	4.5
7	G	HA2	8	K	H	4.5
9	F	QD	3	X	HG	4.5
3	X	HG	9	F	QD	4.5
10	X	QXD1	5	V	HB	4.5
9	F	QD	10	X	QXE	4.5
10	X	QXE	9	F	QD	4.5
10	X	QXE	3	X	HB	4.5
3	X	QXE	2	W	HE1	4.5
2	W	HA	3	X	QXE	4.5
10	X	H	9	F	QD	4.5
9	F	QD	10	X	H	4.5
4	Y	QE	9	F	HB2	4.5
9	F	HB2	4	Y	QE	4.5
10	X	QXD1	9	F	HA	4.5
3	X	HG	10	X	QXE	4.5
10	X	QXE	9	F	HA	4.5
10	X	HA	3	X	QXE	4.5
3	X	QXE	10	X	HA	4.5
10	X	H	9	F	HB1	4.5
9	F	HB1	10	X	H	4.5
3	X	QXE	2	W	HB2	4.5
5	V	QXG2	6	P	HA	4.5
4	Y	QD	3	X	HG	4.5
3	X	HG	4	Y	QD	4.5
10	X	H	9	F	HB2	4.5
9	F	HB2	10	X	H	4.5
4	Y	QD	5	V	H	4.5
12	Q	HA	1	R	QG	4.5
1	R	QG	12	Q	HA	4.5
5	V	H	4	Y	HB1	4.5
4	Y	HB1	5	V	H	4.5
9	F	HA	10	X	HA	4.5
10	X	HA	9	F	HA	4.5

Residue		Proton	Residue		Proton	Residue
3	X	QXE	2	W	HZ2	4.5
8	K	H	6	P	HA	4.5
6	P	HA	8	K	H	4.5
3	X	HG	9	F	HA	4.5
5	V	H	6	P	QD	4.5
6	P	QD	5	V	H	4.5
9	F	HA	5	V	H	4.5
10	X	QXD1	2	W	HE3	4.5
9	F	H	10	X	H	4.5
10	X	H	9	F	H	4.5
9	F	H	8	K	HG1	4.5
8	K	HG1	9	F	H	4.5
10	X	QXE	9	F	HB1	4.5
9	F	H	8	K	H	4.5
8	K	H	9	F	H	4.5
5	V	H	4	Y	H	4.5
3	X	QXE	2	W	HB1	4.5
1	R	HE	12	Q	HA	4.5
9	F	HB2	8	K	HA	4.5
5	V	HB	8	K	H	4.5
3	X	QXE	2	W	HZ3	4.5
5	V	H	10	X	H	4.5
9	F	H	8	K	HG2	4.5
8	K	HG2	9	F	H	4.5
4	Y	HB2	5	V	HA	4.5
4	Y	QE	9	F	HA	4.5
3	X	HG	4	Y	QE	4.5
12	Q	HA	2	W	H	4.5
3	X	HG	10	X	H	4.5
11	V	H	10	X	H	4.5
10	X	H	11	V	H	4.5
3	X	HG	10	X	HA	4.5
11	V	H	2	W	HB1	4.5
11	V	H	2	W	HB2	4.5
2	W	HB2	11	V	H	4.5
2	W	HE3	11	V	H	4.5
8	K	H	4	Y	QD	4.5
4	Y	QD	8	K	H	4.5
1	R	HA	2	W	HB2	4.5
2	W	HB2	1	R	HA	4.5
8	K	H	4	Y	HB2	4.5

Residue		Proton	Residue		Proton	Residue
9	F	HA	4	Y	HB2	4.5
4	Y	HB2	9	F	HA	4.5
9	F	HA	4	Y	HB1	4.5
1	R	HE	2	W	H	4.5
8	K	HG2	6	P	HA	4.5
1	R	HE	12	Q	H	4.5
5	V	QXG1	2	W	HZ3	4.5
12	Q	HA	1	R	QB	4.5
1	R	QB	12	Q	HA	4.5
10	X	QXE	1	R	QD	5.5
3	X	QXE	10	X	H	5.5
10	X	QXE	11	V	HA	5.5
5	V	QXG1	2	W	HZ2	5.5
5	V	QXG1	4	Y	H	5.5
3	X	QXE	11	V	H	5.5
10	X	QXD1	11	V	HA	5.5
5	V	QXG1	10	X	H	5.5
3	X	QXE	4	Y	HB1	5.5
4	Y	QE	9	F	H	5.5
4	Y	HB2	6	P	QD	5.5
3	X	QXE	2	W	H	5.5
4	Y	QD	10	X	H	5.5
7	G	HA1	6	P	HA	5.5
3	X	QXE	5	V	H	5.5
6	P	QD	5	V	QXG1	5.5
5	V	QXG1	6	P	QD	5.5

**Table 35.** NOE distance restraints for peptide **9a**.

Residue		Proton	Residue		Proton	Residue
6	P	QD	5	V	HA	2.7
9	F	H	8	K	HA	2.7
8	K	HA	9	F	H	2.7
10	X	H	9	F	HA	2.7
11	V	H	10	X	HA	2.7
12	Q	H	11	V	HA	2.7
11	V	HA	12	Q	H	2.7
7	G	HA1	7	G	H	2.7
2	W	H	1	R	HA	2.7
4	Y	HA	5	V	H	2.7
7	G	HA2	7	G	H	2.7
3	X	HB	10	X	QXD1	3.5
7	G	H	6	P	HA	3.5
6	P	HA	7	G	H	3.5
10	X	QXE	5	V	HB	3.5
7	G	H	8	K	H	3.5
8	K	H	7	G	H	3.5
2	W	H	1	R	QB	3.5
5	V	H	8	K	H	3.5
8	K	H	5	V	H	3.5
3	X	H	2	W	QB	3.5
2	W	QB	3	X	H	3.5
4	Y	HA	9	F	HA	3.5
7	G	HA2	8	K	H	3.5
8	K	H	7	G	HA1	3.5
4	Y	H	3	X	HG	3.5
3	X	HG	4	Y	H	3.5
9	F	H	8	K	HB2	3.5
8	K	HB2	9	F	H	3.5
5	V	H	4	Y	HB1	3.5
11	V	H	10	X	HG	3.5
10	X	HG	11	V	H	3.5
4	Y	H	3	X	QXD2	4.5
3	X	QXD2	4	Y	H	4.5
3	X	QXD1	10	X	HA	4.5
3	X	HG	5	V	QXG1	4.5
5	V	QXG1	3	X	HG	4.5
11	V	H	10	X	QXE	4.5
10	X	QXE	11	V	H	4.5
3	X	HG	10	X	QXE	4.5
2	W	QB	11	V	HB	4.5
11	V	HB	2	W	QB	4.5

Residue		Proton	Residue		Proton	Residue
11	V	H	10	X	QXD1	4.5
10	X	QXD1	11	V	H	4.5
7	G	HA1	8	K	H	4.5
6	P	QD	5	V	HB	4.5
7	G	H	6	P	QD	4.5
6	P	QD	7	G	H	4.5
5	V	H	10	X	QXE	4.5
10	X	QXE	5	V	H	4.5
3	X	QXD1	2	W	QB	4.5
4	Y	HB1	5	V	H	4.5
11	V	H	3	X	QXD1	4.5
3	X	QXD1	11	V	H	4.5
11	V	QXG2	12	Q	H	4.5
10	X	QXD1	1	R	QD	4.5
10	X	QXD1	12	Q	HA	4.5
4	Y	H	3	X	HB	4.5
3	X	HB	4	Y	H	4.5
2	W	HA	3	X	HA	4.5
12	Q	H	11	V	H	4.5
11	V	H	12	Q	H	4.5
1	R	HA	2	W	QB	4.5
2	W	HA	3	X	QXD2	4.5
5	V	H	6	P	QD	4.5
6	P	QD	5	V	H	4.5
2	W	HD1	3	X	H	4.5
4	Y	HA	10	X	H	4.5
3	X	QXD2	2	W	HD1	4.5
10	X	QXD1	1	R	HG1	4.5
2	W	H	3	X	H	4.5
3	X	QXD1	4	Y	H	4.5
9	F	H	8	K	HB1	4.5
8	K	HB1	9	F	H	4.5
2	W	H	1	R	HG1	4.5
1	R	HG1	2	W	H	4.5
5	V	H	9	F	HA	4.5
9	F	HA	5	V	H	4.5
7	G	H	4	Y	HB1	4.5
4	Y	HB1	7	G	H	4.5
10	X	QXD2	12	Q	HA	4.5
3	X	HG	5	V	H	4.5
2	W	H	1	R	HG2	4.5
1	R	HG2	2	W	H	4.5
8	K	H	6	P	HA	4.5

Residue		Proton	Residue		Proton	Residue
6	P	HA	8	K	H	4.5
8	K	H	4	Y	HB1	4.5
6	P	HB2	7	G	H	4.5
8	K	HB1	5	V	H	4.5
7	G	H	5	V	HA	4.5
5	V	HA	7	G	H	4.5
9	F	H	4	Y	QE	4.5
4	Y	QE	9	F	H	4.5
8	K	HG2	9	F	H	4.5
9	F	H	8	K	H	4.5
8	K	H	9	F	H	4.5
5	V	H	4	Y	HB2	4.5
4	Y	HB2	5	V	H	4.5
7	G	HA2	6	P	HA	4.5
8	K	HG1	9	F	H	4.5
8	K	HA	4	Y	QE	4.5
5	V	H	4	Y	H	4.5
4	Y	H	5	V	H	4.5
10	X	H	9	F	H	4.5
2	W	H	11	V	H	4.5
11	V	H	2	W	H	4.5
7	G	H	4	Y	HB2	4.5
11	V	HB	2	W	HE3	4.5
10	X	HG	12	Q	H	4.5
10	X	H	5	V	H	4.5
8	K	H	4	Y	HB2	4.5
10	X	QXE	3	X	QXD1	5.5
10	X	QXE	8	K	QD	5.5
4	Y	HB1	8	K	H	5.5
11	V	QXG2	2	W	HE3	5.5
5	V	QXG1	10	X	H	5.5
3	X	QXD1	11	V	HB	5.5
10	X	QXD2	9	F	HB2	5.5
12	Q	H	11	V	QXG1	5.5
11	V	QXG1	12	Q	H	5.5
10	X	QXD1	1	R	HG2	5.5
11	V	QXG1	2	W	HE3	5.5
10	X	QXD1	2	W	H	5.5
3	X	QXD2	2	W	HE3	5.5
3	X	QXD1	2	W	HZ2	5.5
3	X	QXD2	2	W	HZ2	5.5
11	V	HA	10	X	QXD1	5.5
5	V	QXG1	4	Y	H	5.5

Residue		Proton	Residue		Proton	Residue
10	X	QXD2	9	F	HB1	5.5
8	K	QD	9	F	H	5.5
3	X	QXD1	2	W	HE3	5.5
4	Y	HB1	6	P	QD	5.5
10	X	QXD1	12	Q	H	5.5
11	V	H	10	X	QXD2	5.5
10	X	QXD2	11	V	H	5.5

**Table 36.** NOE Distance restraints for peptide **22a**.

Residue		Proton	Residue		Proton	Distance
2	E	HA	3	W	H	2.70
2	E	HB1	3	W	H	2.70
3	W	H	2	E	HA	2.70
4	A	HA	5	Y	H	2.70
5	Y	H	4	A	HA	2.70
5	Y	HA	6	N	H	2.70
6	N	H	5	Y	HA	2.70
6	N	HA	7	P	HD1	2.70
6	N	HA	7	P	HD2	2.70
8	A	H	9	T	H	2.70
9	T	H	8	A	H	2.70
9	T	H	10	G	H	2.70
10	G	H	9	T	H	2.70
11	K	HA	12	F	H	2.70
12	F	H	11	K	HA	2.70
13	A	HA	14	V	H	2.70
14	V	H	13	A	HA	2.70
14	V	HA	15	T	H	2.70
15	T	H	14	V	HA	2.70
15	T	HA	16	E	H	2.70
16	E	H	15	T	HA	2.70
1	G	HA1	2	E	H	3.50
1	G	HA2	2	E	H	3.50
2	E	HB2	3	W	H	3.50
3	W	H	2	E	HB2	3.50
3	W	HA	4	A	H	3.50
3	W	HA	14	V	HA	3.50
3	W	HA	15	T	H	3.50
4	A	H	3	W	HA	3.50
4	A	H	3	W	HB2	3.50
4	A	QXB	5	Y	H	3.50
5	Y	H	6	N	H	3.50
5	Y	HA	12	F	HA	3.50
5	Y	QD	7	P	HB2	3.50
6	N	H	5	Y	H	3.50
6	N	H	11	K	H	3.50
6	N	H	13	A	H	3.50
6	N	HA	8	A	H	3.50
6	N	HB2	11	K	H	3.50
7	P	HA	5	Y	QD	3.50
7	P	HA	8	A	H	3.50
7	P	HB2	5	Y	QD	3.50

Residue		Proton	Residue		Proton	Distance
7	P	HB2	8	A	H	3.50
7	P	HD1	8	A	H	3.50
7	P	HD2	6	N	H	3.50
7	P	HD2	8	A	H	3.50
7	P	QG	8	A	H	3.50
8	A	H	7	P	HA	3.50
8	A	H	7	P	HD1	3.50
8	A	H	7	P	HD2	3.50
8	A	H	7	P	QG	3.50
8	A	HA	9	T	H	3.50
8	A	HA	10	G	H	3.50
9	T	H	8	A	HA	3.50
9	T	HA	10	G	H	3.50
10	G	H	8	A	HA	3.50
10	G	H	9	T	HA	3.50
10	G	H	11	K	H	3.50
10	G	HA1	11	K	H	3.50
10	G	HA2	11	K	H	3.50
11	K	H	6	N	H	3.50
11	K	H	10	G	H	3.50
11	K	H	10	G	HA1	3.50
11	K	H	10	G	HA2	3.50
11	K	H	12	F	H	3.50
11	K	HB2	12	F	H	3.50
11	K	HG1	12	F	H	3.50
12	F	H	11	K	HB2	3.50
12	F	HA	5	Y	HA	3.50
12	F	HA	6	N	H	3.50
12	F	HA	13	A	H	3.50
12	F	HB1	13	A	H	3.50
13	A	H	12	F	HA	3.50
13	A	H	12	F	HB1	3.50
13	A	QXB	14	V	H	3.50
14	V	HA	3	W	HA	3.50
14	V	HA	4	A	H	3.50
14	V	HB	15	T	H	3.50
15	T	H	14	V	HB	3.50
15	T	HB	16	E	H	3.50
16	E	H	15	T	HB	3.50
4	A	H	3	W	HB1	4.50
4	A	HA	5	Y	QB	4.50
4	A	QXB	5	Y	QB	4.50
5	Y	HA	13	A	H	4.50

Residue		Proton	Residue		Proton	Distance
5	Y	QB	4	A	HA	4.50
5	Y	QB	6	N	H	4.50
5	Y	QB	12	F	QD	4.50
5	Y	QD	7	P	QG	4.50
5	Y	QE	6	N	H	4.50
6	N	H	5	Y	QB	4.50
6	N	HA	7	P	QG	4.50
6	N	HB2	10	G	H	4.50
7	P	HA	5	Y	QE	4.50
7	P	HB2	5	Y	QE	4.50
7	P	QG	5	Y	QD	4.50
7	P	QG	5	Y	QE	4.50
8	A	H	10	G	H	4.50
8	A	QXB	9	T	HA	4.50
10	G	H	8	A	H	4.50
12	F	HA	5	Y	QB	4.50
12	F	HB1	3	W	HE1	4.50
12	F	HB2	3	W	HE1	4.50
12	F	HB2	13	A	H	4.50
12	F	QD	5	Y	HA	4.50
13	A	H	5	Y	HA	4.50
13	A	H	12	F	HB2	4.50
13	A	HA	14	V	HA	4.50
13	A	QXB	15	T	H	4.50
14	V	QXG2	15	T	H	4.50
15	T	H	14	V	QXG2	4.50
3	W	HH2	14	V	QXG2	5.50
4	A	QXB	6	N	HD2	5.50
8	A	QXB	6	N	HD2	5.50
8	A	QXB	10	G	H	5.50
14	V	QXG1	15	T	H	5.50
15	T	H	14	V	QXG1	5.50

**Table 37.** NOE Distance restraints for peptide **22b**.

Residue		Proton	Residue		Proton	Distance
6	Y	HA	7	N	H	2.70
7	N	H	6	Y	HA	2.70
7	N	HA	8	P	QD	2.70
9	A	H	10	T	H	2.70
10	T	H	9	A	H	2.70
10	T	H	11	G	H	2.70
11	G	H	10	T	H	2.70
12	K	HA	13	F	H	2.70
13	F	HA	6	Y	HA	2.70
13	F	HA	14	A	H	2.70
14	A	HA	15	V	H	2.70
15	V	H	14	A	HA	2.70
15	V	HA	16	T	H	2.70
16	T	H	15	V	HA	2.70
16	T	HB	17	E	H	2.70
17	E	H	16	T	HB	2.70
17	E	HA	18	C	H	2.70
17	E	HB2	1	C	H	2.70
18	C	H	17	E	HA	2.70
2	G	HA1	3	E	H	3.50
3	E	H	2	G	HA1	3.50
3	E	H	2	G	HA2	3.50
3	E	H	16	T	HA	3.50
4	W	HA	16	T	H	3.50
6	Y	QE	8	P	HA	3.50
7	N	HB2	12	K	H	3.50
8	P	HA	6	Y	QE	3.50
8	P	HG1	9	A	H	3.50
8	P	HG2	6	Y	QE	3.50
8	P	HG2	9	A	H	3.50
8	P	QD	7	N	HB1	3.50
8	P	QD	9	A	H	3.50
9	A	H	8	P	QD	3.50
9	A	HA	10	T	H	3.50
10	T	HA	11	G	H	3.50
11	G	H	8	P	HA	3.50
11	G	H	10	T	HA	3.50
11	G	H	12	K	H	3.50
12	K	H	7	N	H	3.50
12	K	H	11	G	H	3.50
12	K	H	11	G	HA1	3.50
12	K	HB2	13	F	H	3.50

Residue		Proton	Residue		Proton	Distance
13	F	H	12	K	HB2	3.50
13	F	HA	7	N	H	3.50
14	A	H	13	F	HB1	3.50
14	A	QXB	15	V	H	3.50
15	V	H	14	A	QXB	3.50
16	T	H	3	E	H	3.50
16	T	HA	3	E	H	3.50
16	T	HA	17	E	H	3.50
17	E	H	16	T	HA	3.50
2	G	HA1	15	V	QXG2	4.50
2	G	HA2	3	E	H	4.50
3	E	H	16	T	H	4.50
4	W	HA	15	V	HA	4.50
4	W	HA	15	V	QXG1	4.50
4	W	QB	13	F	HB1	4.50
4	W	QB	13	F	QD	4.50
5	A	H	15	V	HA	4.50
6	Y	QD	7	N	H	4.50
6	Y	QD	8	P	HA	4.50
6	Y	QD	8	P	HG2	4.50
6	Y	QD	8	P	QD	4.50
7	N	H	6	Y	QD	4.50
7	N	H	6	Y	QE	4.50
7	N	H	12	K	H	4.50
7	N	HA	9	A	H	4.50
7	N	HB2	11	G	H	4.50
8	P	HA	6	Y	QD	4.50
8	P	HA	9	A	H	4.50
8	P	HG2	6	Y	QD	4.50
8	P	QD	6	Y	QD	4.50
8	P	QD	6	Y	QE	4.50
8	P	QD	7	N	H	4.50
9	A	H	8	P	HA	4.50
9	A	H	11	G	H	4.50
9	A	QXB	10	T	H	4.50
10	T	HB	12	K	H	4.50
11	G	H	9	A	H	4.50
12	K	HA	13	F	QD	4.50
12	K	HB1	13	F	H	4.50
13	F	HA	6	Y	QD	4.50
13	F	HB1	4	W	QB	4.50
13	F	HB1	14	A	H	4.50
13	F	HB2	14	A	H	4.50

Residue		Proton	Residue		Proton	Distance
13	F	QD	4	W	QB	4.50
14	A	HA	15	V	QXG1	4.50
15	V	HA	4	W	HA	4.50
15	V	HA	5	A	H	4.50
15	V	HB	16	T	H	4.50
15	V	QXG1	16	T	H	4.50
15	V	QXG2	2	G	HA1	4.50
16	T	H	15	V	QXG1	4.50
16	T	H	15	V	QXG2	4.50
16	T	QXGT	17	E	H	4.50
17	E	H	16	T	QXGT	4.50
6	Y	QD	13	F	QD	5.50
9	A	QXB	10	T	HA	5.50
13	F	QD	6	Y	QD	5.50
15	V	QXG1	4	W	QB	5.50
15	V	QXG2	16	T	H	5.50

**Table 38.** NOE Distance restraints for peptide **23b**.

Residue		Proton	Residue		Proton	Distance
4	W	HA	5	BY	H	2.70
4	W	HA	13	V	HA	2.70
5	BY	H	4	W	HA	2.70
5	BY	HA	6	N	H	2.70
6	N	H	5	BY	HA	2.70
11	K	HA	12	BF	H	2.70
12	BF	H	11	K	HA	2.70
12	BF	HA2	13	V	H	2.70
13	V	H	12	BF	HA2	2.70
13	V	HA	14	T	H	2.70
14	T	H	13	V	HA	2.70
14	T	HA	15	E	H	2.70
15	E	HA	16	C	H	2.70
16	C	H	15	E	HA	2.70
1	C	HA	2	G	H	3.50
2	G	H	1	C	HA	3.50
2	G	H	1	C	HB1	3.50
2	G	HA1	3	E	H	3.50
3	E	H	2	G	H	3.50
3	E	H	2	G	HA1	3.50
3	E	H	2	G	HA2	3.50
4	W	H	5	BY	H	3.50
5	BY	H	13	V	HA	3.50
5	BY	HG1	4	W	QB	3.50
6	N	HA	7	P	QD	3.50
6	N	HB2	11	K	H	3.50
8	A	H	7	P	HA	3.50
8	A	H	9	T	H	3.50
8	A	HA	9	T	H	3.50
9	T	H	7	P	HA	3.50
9	T	H	8	A	H	3.50
9	T	H	8	A	HA	3.50
9	T	H	10	G	H	3.50
9	T	HA	10	G	H	3.50
9	T	QXGT	11	K	HA	3.50
10	G	H	9	T	H	3.50
10	G	H	9	T	HA	3.50
10	G	H	11	K	H	3.50
10	G	HA2	11	K	H	3.50
11	K	H	10	G	H	3.50
11	K	H	10	G	HA1	3.50
12	BF	HA1	5	BY	H	3.50

Residue		Proton	Residue		Proton	Distance
12	BF	HA1	13	V	H	3.50
13	V	HA	5	BY	H	3.50
13	V	HB	14	T	H	3.50
14	T	H	13	V	HB	3.50
15	E	HB2	16	C	H	3.50
1	C	H	2	G	H	4.50
2	G	H	1	C	H	4.50
2	G	H	1	C	HB2	4.50
2	G	HA2	3	E	H	4.50
3	E	H	4	W	H	4.50
3	E	H	14	T	H	4.50
3	E	HB1	4	W	H	4.50
4	W	H	3	E	H	4.50
4	W	HA	13	V	QXG1	4.50
4	W	HA	13	V	QXG2	4.50
4	W	HE3	14	T	H	4.50
4	W	HE3	5	BY	H	4.50
4	W	HE3	12	BF	QE	4.50
4	W	QB	13	V	QXG2	4.50
5	BY	H	5	BY	H	4.50
5	BY	H	4	W	HE3	4.50
5	BY	HA	4	W	QB	4.50
5	BY	HB1	12	BF	QE	4.50
6	N	H	6	N	H	4.50
6	N	H	5	BY	HB1	4.50
6	N	HA	5	BY	HB2	4.50
6	N	HB2	8	A	H	4.50
6	N	HB2	9	T	H	4.50
7	P	QD	12	BF	QE	4.50
8	A	QXB	8	A	H	4.50
9	T	H	9	T	H	4.50
9	T	QXGT	8	A	QXB	4.50
9	T	QXGT	10	G	H	4.50
10	G	HA1	11	K	H	4.50
11	K	HA	11	K	H	4.50
12	BF	HA1	12	BF	QE	4.50
12	BF	HA1	4	W	HE3	4.50
12	BF	HA1	4	W	HE3	4.50
12	BF	HA2	4	W	HZ3	4.50
12	BF	HB	4	W	HE3	4.50
12	BF	HG1	5	BY	HA	4.50
12	BF	HG2	13	V	H	4.50
13	V	H	4	W	HZ3	4.50

Residue		Proton	Residue		Proton	Distance
13	V	H	12	BF	HG2	4.50
13	V	HA	14	T	H	4.50
13	V	HB	4	W	HE3	4.50
13	V	QXG1	4	W	HE3	4.50
13	V	QXG1	4	W	HA	4.50
13	V	QXG1	4	W	HE3	4.50
13	V	QXG2	14	T	H	4.50
13	V	QXG2	4	W	HA	4.50
14	T	H	4	W	HE3	4.50
14	T	H	4	W	HE3	4.50
14	T	H	13	V	H	4.50
14	T	H	13	V	QXG1	4.50
15	E	H	15	E	H	4.50
15	E	H	14	T	H	4.50
15	E	HA	14	T	QXGT	4.50
15	E	HB1	2	G	H	4.50
1	C	HB1	16	C	H	4.50
1	C	HB2	2	G	H	5.50
4	W	HH2	2	G	H	5.50
8	A	QXB	13	V	QXG2	5.50
8	A	QXB	9	T	HA	5.50
9	T	QXGT	12	BF	QE	5.50
12	BF	HA2	12	BF	QE	5.50
12	BF	HG2	4	W	HE3	5.50
12	BF	HG2	13	V	H	5.50
12	BF	HG2	13	V	QXG1	5.50
12	BF	QE	13	V	QXG2	5.50
12	BF	QE	4	W	HE3	5.50
13	V	QXG1	2	G	H	5.50
13	V	QXG1	3	E	H	5.50
13	V	QXG1	15	E	H	5.50
13	V	QXG2	4	W	HZ2	5.50
13	V	QXG2	5	BY	H	5.50
13	V	QXG2	12	BF	QE	5.50
13	V	QXG2	14	T	H	5.50
14	T	H	13	V	QXG2	5.50
14	T	QXGT	2	G	H	5.50
14	T	QXGT	15	E	H	5.50
15	E	QG	16	C	H	5.50

**Table 39.** NOE Distance restraints for peptide **24b**.

Residue		Proton	Residue		Proton	Distance
3	E	HA	4	W	H	2.70
4	W	H	3	E	HA	2.70
4	W	HA	5	BAY	H	2.70
5	BAY	HA	6	N	H	2.70
6	N	H	5	BAY	HA	2.70
11	K	HA	12	BFA	H	2.70
12	BFA	H	11	K	HA	2.70
12	BFA	HA	13	V	H	2.70
13	V	H	12	BFA	HA	2.70
13	V	HA	14	T	H	2.70
15	E	HA	16	C	H	2.70
1	C	HA	2	G	H	3.50
2	G	HA1	3	E	H	3.50
2	G	HA1	16	C	H	3.50
2	G	HA2	3	E	H	3.50
3	E	H	2	G	HA1	3.50
3	E	H	2	G	HA2	3.50
3	E	HB2	4	W	H	3.50
4	W	HA	3	E	H	3.50
4	W	HA	14	T	H	3.50
4	W	QB	14	T	H	3.50
5	BAY	HA	12	BFA	HB	3.50
5	BAY	QE	4	W	HE1	3.50
5	BAY	QE	7	P	HA	3.50
7	P	HA	8	A	H	3.50
7	P	HG2	8	A	H	3.50
8	A	H	9	T	H	3.50
9	T	H	8	A	H	3.50
9	T	H	10	G	H	3.50
10	G	H	9	T	H	3.50
10	G	H	9	T	HA	3.50
10	G	H	11	K	H	3.50
10	G	HA1	11	K	H	3.50
10	G	HA2	11	K	H	3.50
11	K	H	12	BFA	H	3.50
11	K	HB1	12	BFA	H	3.50
12	BFA	HB	6	N	H	3.50
12	BFA	QXG	13	V	H	3.50
13	V	H	12	BFA	QXG	3.50
14	T	HA	15	E	H	3.50
15	E	H	14	T	HA	3.50
15	E	QG	2	G	HA2	3.50

Residue		Proton	Residue		Proton	Distance
1	C	H	2	G	H	4.50
2	G	H	1	C	H	4.50
2	G	H	3	E	H	4.50
3	E	H	2	G	H	4.50
3	E	H	4	W	H	4.50
3	E	H	14	T	H	4.50
3	E	HB1	4	W	H	4.50
4	W	H	3	E	H	4.50
4	W	H	5	BAY	H	4.50
5	BAY	H	4	W	H	4.50
5	BAY	H	13	V	HA	4.50
5	BAY	HG1	4	W	HD1	4.50
5	BAY	QE	4	W	HZ2	4.50
5	BAY	QE	6	N	H	4.50
5	BAY	QE	12	BFA	HD2	4.50
5	BAY	QE	12	BFA	QH	4.50
5	BAY	QE	12	BFA	QZ	4.50
5	BAY	QXI	6	N	H	4.50
6	N	H	5	BAY	QXI	4.50
7	P	QD	8	A	H	4.50
8	A	HA	9	T	H	4.50
8	A	QXB	9	T	H	4.50
9	T	H	8	A	HA	4.50
11	K	H	10	G	H	4.50
11	K	HB2	12	BFA	H	4.50
12	BFA	H	11	K	HB1	4.50
12	BFA	HB	5	BAY	H	4.50
13	V	H	14	T	QXGT	4.50
13	V	HA	5	BAY	H	4.50
13	V	QQXG	12	BFA	HD2	4.50
13	V	QQXG	14	T	H	4.50
14	T	H	3	E	H	4.50
14	T	HB	15	E	H	4.50
14	T	QXGT	15	E	H	4.50
15	E	H	14	T	H	4.50
15	E	H	14	T	HB	4.50
16	C	H	1	C	H	4.50
11	K	H	6	N	H	5.50
12	BFA	HB	5	BAY	HA	5.50
12	BFA	QZ	5	BAY	QZ	5.50
13	V	QQXG	4	W	HD1	5.50
13	V	QQXG	12	BFA	QZ	5.50

**Table 40.** NOE Distance Restraints for Peptide 73.

Residue		Proton	Residue		Proton	Distance
2	E	HA	2	E	HB1	2.7
2	E	HA	3	W	H	2.7
3	W	H	2	E	HA	2.7
5	Y	HA	6	N	H	2.7
5	Y	HA	12	F	HA	2.7
6	N	H	5	Y	HA	2.7
6	N	HA	7	P	QD	2.7
7	P	HB1	8	A	H	2.7
8	A	H	7	P	HB1	2.7
8	A	H	9	T	H	2.7
8	A	H	9	T	HB	2.7
9	T	H	8	A	H	2.7
9	T	H	10	G	H	2.7
9	T	HB	8	A	H	2.7
10	G	H	9	T	H	2.7
10	G	H	11	K	H	2.7
11	K	H	10	G	H	2.7
12	F	HA	5	Y	HA	2.7
12	F	HA	13	X	H	2.7
13	X	H	12	F	HA	2.7
14	V	HA	15	T	H	2.7
15	T	H	14	V	HA	2.7
15	T	HA	16	E	H	2.7
16	E	H	15	T	HA	2.7
1	G	HA1	2	E	H	3.5
1	G	HA2	2	E	H	3.5
2	E	H	1	G	HA1	3.5
2	E	H	1	G	HA2	3.5
2	E	HB1	3	W	H	3.5
2	E	HB2	3	W	H	3.5
3	W	H	2	E	HB1	3.5
3	W	H	2	E	HB2	3.5
3	W	H	3	W	HA	3.5
3	W	HA	4	X	H	3.5
3	W	HA	14	V	HA	3.5
3	W	HB1	4	X	H	3.5
3	W	HB2	4	X	H	3.5
4	X	H	3	W	HA	3.5
4	X	H	3	W	HB1	3.5
4	X	H	3	W	HB2	3.5
5	Y	H	12	F	HB1	3.5
5	Y	HA	13	X	H	3.5

Residue		Proton	Residue		Proton	Distance
5	Y	HB2	6	N	H	3.5
5	Y	QD	7	P	HB1	3.5
5	Y	QD	12	F	HB2	3.5
5	Y	QE	7	P	HA	3.5
5	Y	QE	7	P	HB1	3.5
5	Y	QE	7	P	HB2	3.5
6	N	H	11	K	H	3.5
6	N	H	12	F	HA	3.5
6	N	HA	8	A	H	3.5
6	N	HB2	9	T	H	3.5
6	N	HB2	10	G	H	3.5
6	N	HB2	11	K	H	3.5
7	P	HA	5	Y	QE	3.5
7	P	HA	8	A	H	3.5
7	P	HB1	5	Y	QD	3.5
7	P	HB1	5	Y	QE	3.5
7	P	HB2	5	Y	QE	3.5
7	P	QD	8	A	H	3.5
8	A	H	7	P	HA	3.5
8	A	H	7	P	QD	3.5
8	A	QXB	7	P	HB1	3.5
8	A	QXB	9	T	H	3.5
9	T	H	8	A	QXB	3.5
9	T	H	10	G	HA1	3.5
9	T	HA	10	G	H	3.5
9	T	HB	11	K	H	3.5
10	G	H	9	T	HA	3.5
10	G	HA1	5	Y	QD	3.5
10	G	HA1	5	Y	QE	3.5
10	G	HA1	9	T	H	3.5
10	G	HA1	11	K	H	3.5
10	G	HA2	5	Y	QE	3.5
10	G	HA2	11	K	H	3.5
11	K	H	6	N	H	3.5
11	K	H	9	T	HA	3.5
11	K	H	10	G	HA1	3.5
11	K	H	10	G	HA2	3.5
11	K	HA	12	F	H	3.5
11	K	QB	12	F	H	3.5
11	K	QD	12	F	H	3.5
12	F	H	11	K	HA	3.5
12	F	H	11	K	QB	3.5
12	F	H	11	K	QD	3.5

Residue		Proton	Residue		Proton	Distance
12	F	HA	5	Y	QD	3.5
12	F	HA	6	N	H	3.5
12	F	HB1	13	X	H	3.5
12	F	HB2	5	Y	QD	3.5
12	F	HB2	13	X	H	3.5
12	F	QD	5	Y	HB1	3.5
12	F	QD	13	X	H	3.5
13	X	H	5	Y	HA	3.5
13	X	H	12	F	HB1	3.5
13	X	H	12	F	HB2	3.5
14	V	HA	3	W	HA	3.5
14	V	HA	15	T	QXGT	3.5
14	V	QXXG	15	T	H	3.5
15	T	H	2	E	H	3.5
2	E	HA	3	W	HD1	4.5
2	E	QG	3	W	H	4.5
3	W	H	4	X	H	4.5
3	W	HA	14	V	QXXG	4.5
3	W	HA	15	T	H	4.5
3	W	HD1	4	X	H	4.5
4	X	H	3	W	H	4.5
4	X	H	14	V	HA	4.5
4	X	H	15	T	H	4.5
5	Y	HB1	6	N	H	4.5
5	Y	QD	6	N	H	4.5
5	Y	QD	7	P	HA	4.5
5	Y	QD	7	P	HB2	4.5
5	Y	QD	13	X	H	4.5
5	Y	QE	6	N	H	4.5
5	Y	QE	10	G	H	4.5
6	N	H	5	Y	HB1	4.5
6	N	H	5	Y	QD	4.5
6	N	H	13	X	H	4.5
6	N	HA	8	A	QXB	4.5
6	N	HB2	8	A	H	4.5
6	N	HB2	9	T	QXGT	4.5
7	P	HA	5	Y	QD	4.5
7	P	HA	9	T	H	4.5
7	P	HA	9	T	QXGT	4.5
7	P	HB2	5	Y	QD	4.5
7	P	HB2	8	A	H	4.5
7	P	QD	6	N	H	4.5
8	A	H	9	T	HA	4.5

Residue		Proton	Residue		Proton	Distance
8	A	H	9	T	QXGT	4.5
8	A	H	10	G	H	4.5
8	A	QXB	9	T	HA	4.5
8	A	QXB	9	T	QXGT	4.5
8	A	QXB	10	G	H	4.5
9	T	H	7	P	HA	4.5
9	T	HA	8	A	H	4.5
9	T	HA	8	A	QXB	4.5
9	T	HA	10	G	HA2	4.5
9	T	QXGT	8	A	H	4.5
9	T	QXGT	8	A	QXB	4.5
9	T	QXGT	10	G	H	4.5
9	T	QXGT	11	K	QD	4.5
10	G	H	5	Y	QE	4.5
10	G	H	6	N	H	4.5
10	G	H	8	A	H	4.5
10	G	H	8	A	QXB	4.5
10	G	H	9	T	QXGT	4.5
10	G	HA2	5	Y	QD	4.5
10	G	HA2	9	T	H	4.5
11	K	H	9	T	QXGT	4.5
11	K	H	12	F	H	4.5
11	K	HA	5	Y	QE	4.5
11	K	QD	10	G	H	4.5
11	K	QG	12	F	H	4.5
12	F	H	11	K	H	4.5
12	F	H	11	K	QG	4.5
12	F	H	13	X	H	4.5
12	F	HA	5	Y	QE	4.5
12	F	HB2	5	Y	QE	4.5
13	X	H	12	F	H	4.5
14	V	HA	3	W	HD1	4.5
14	V	HA	4	X	H	4.5
15	T	H	3	W	HA	4.5
1	G	HA1	14	V	QQXG	5.5
1	G	HA2	14	V	QQXG	5.5
7	P	HA	8	A	QXB	5.5
8	A	QXB	7	P	HA	5.5
11	K	HA	10	G	H	5.5
14	V	QQXG	1	G	HA1	5.5
14	V	QQXG	15	T	HA	5.5
15	T	HA	14	V	QQXG	5.5
15	T	HA	15	T	H	5.5

Residue		Proton	Residue		Proton	Distance
15	T	HB	14	V	QQXG	5.5

**Table 41.** NOE Distance Restraints for Peptide 74.

Residue		Proton	Residue		Proton	Distance
2	E	H	1	G	HA2	2.7
3	W	HA	4	X	H	2.7
3	W	HA	14	V	HA	2.7
4	X	H	3	W	HA	2.7
4	X	HA	5	Y	H	2.7
5	Y	H	4	X	HA	2.7
5	Y	HA	6	N	H	2.7
6	N	H	5	Y	HA	2.7
8	A	H	9	T	H	2.7
10	G	H	9	T	H	2.7
10	G	H	11	K	H	2.7
11	K	HA	12	F	H	2.7
12	F	HA	5	Y	HA	2.7
12	F	HA	13	X	H	2.7
13	X	H	12	F	HA	2.7
14	V	H	13	X	HA	2.7
14	V	HA	3	W	HA	2.7
14	V	HA	15	T	H	2.7
15	T	HA	16	E	H	2.7
1	G	HA1	2	E	H	3.5
1	G	HA2	2	E	H	3.5
2	E	H	1	G	HA1	3.5
2	E	H	3	W	H	3.5
2	E	H	15	T	H	3.5
2	E	HA	3	W	H	3.5
2	E	HB1	3	W	H	3.5
2	E	HB2	3	W	H	3.5
3	W	H	2	E	HA	3.5
3	W	H	2	E	HB1	3.5
3	W	H	2	E	HB2	3.5
3	W	HA	15	T	H	3.5
3	W	HE3	14	V	H	3.5
3	W	HZ3	13	X	HA	3.5
5	Y	H	6	N	H	3.5
5	Y	HA	13	X	H	3.5
5	Y	HB2	6	N	H	3.5
6	N	H	12	F	HA	3.5
7	P	HA	8	A	H	3.5
7	P	HG2	8	A	H	3.5
7	P	QD	8	A	H	3.5
8	A	H	7	P	HA	3.5
8	A	H	7	P	HG2	3.5

Residue		Proton	Residue		Proton	Distance
8	A	H	7	P	QD	3.5
8	A	H	10	G	H	3.5
8	A	HA	9	T	H	3.5
9	T	H	8	A	H	3.5
9	T	H	10	G	H	3.5
9	T	HB	11	K	HG1	3.5
10	G	H	8	A	H	3.5
10	G	H	9	T	HA	3.5
10	G	HA1	11	K	H	3.5
10	G	HA2	9	T	H	3.5
10	G	HA2	11	K	H	3.5
11	K	H	6	N	HB2	3.5
11	K	H	10	G	H	3.5
11	K	H	10	G	HA1	3.5
11	K	HG2	12	F	H	3.5
12	F	HA	6	N	H	3.5
12	F	HB1	3	W	HE1	3.5
12	F	HB1	5	Y	HA	3.5
13	X	H	6	N	H	3.5
13	X	H	12	F	HB1	3.5
13	X	HA	5	Y	QE	3.5
13	X	HA	14	V	H	3.5
14	V	HA	4	X	H	3.5
14	V	HB	15	T	H	3.5
14	V	QXG2	3	W	HE3	3.5
14	V	QXG2	13	X	H	3.5
14	V	QXG2	13	X	HG	3.5
15	T	H	2	E	H	3.5
15	T	HB	16	E	H	3.5
16	E	H	15	T	HB	3.5
2	E	QG	3	W	H	4.5
3	W	HA	14	V	H	4.5
3	W	HD1	14	V	H	4.5
3	W	HD1	14	V	QXG2	4.5
3	W	HE3	14	V	QXG1	4.5
3	W	HZ3	14	V	H	4.5
3	W	HZ3	14	V	QXG2	4.5
4	X	H	15	T	H	4.5
4	X	HA	12	F	QE	4.5
4	X	HG	3	W	HD1	4.5
4	X	HG	5	Y	H	4.5
5	Y	H	4	X	HG	4.5
5	Y	HB2	12	F	HA	4.5

Residue		Proton	Residue		Proton	Distance
5	Y	HB2	12	F	QE	4.5
5	Y	QD	6	N	H	4.5
5	Y	QD	10	G	H	4.5
5	Y	QD	12	F	H	4.5
5	Y	QE	6	N	H	4.5
5	Y	QE	12	F	H	4.5
5	Y	QE	12	F	HA	4.5
6	N	H	5	Y	HB2	4.5
6	N	H	11	K	H	4.5
6	N	HB2	8	A	H	4.5
6	N	HB2	9	T	H	4.5
6	N	HB2	10	G	H	4.5
6	N	HB2	11	K	H	4.5
7	P	HG1	8	A	H	4.5
7	P	QB	8	A	H	4.5
7	P	QB	10	G	H	4.5
7	P	QD	6	N	H	4.5
8	A	H	7	P	HG1	4.5
8	A	QXB	9	T	H	4.5
9	T	H	6	N	H	4.5
9	T	H	6	N	HB2	4.5
9	T	H	7	P	QD	4.5
9	T	H	8	A	QXB	4.5
9	T	HA	10	G	H	4.5
9	T	HB	11	K	HD1	4.5
9	T	HB	11	K	QB	4.5
9	T	QXGT	8	A	H	4.5
9	T	QXGT	10	G	H	4.5
10	G	H	6	N	HB2	4.5
10	G	HA1	9	T	H	4.5
11	K	H	6	N	H	4.5
11	K	H	6	N	HB1	4.5
11	K	HD1	12	F	H	4.5
11	K	HG1	12	F	H	4.5
11	K	QB	12	F	H	4.5
12	F	H	11	K	HG1	4.5
12	F	H	11	K	QB	4.5
12	F	HA	5	Y	HB2	4.5
12	F	HB1	13	X	H	4.5
12	F	QE	4	X	HA	4.5
12	F	QE	5	Y	HB2	4.5
13	X	H	5	Y	HA	4.5
13	X	HA	3	W	HZ2	4.5

Residue		Proton	Residue		Proton	Distance
13	X	HA	5	Y	QD	4.5
13	X	HG	14	V	H	4.5
14	V	HA	2	E	H	4.5
14	V	HA	3	W	HE3	4.5
14	V	HB	3	W	HE3	4.5
14	V	QXG1	1	G	HA2	4.5
14	V	QXG1	2	E	H	4.5
14	V	QXG1	3	W	HE3	4.5
14	V	QXG1	15	T	H	4.5
14	V	QXG2	3	W	HD1	4.5
14	V	QXG2	3	W	HZ3	4.5
14	V	QXG2	15	T	H	4.5
15	T	H	4	X	H	4.5
15	T	H	14	V	HB	4.5
15	T	H	14	V	QXG1	4.5
15	T	H	14	V	QXG2	4.5
15	T	HB	2	E	H	4.5
15	T	QXGT	16	E	H	4.5
16	E	H	15	T	QXGT	4.5
3	W	HE3	14	V	HB	5.5
5	Y	HB1	12	F	HA	5.5
6	N	H	5	Y	HB1	5.5
6	N	H	10	G	H	5.5
8	A	QXB	7	P	QD	5.5
8	A	QXB	9	T	HA	5.5
8	A	QXB	10	G	H	5.5
9	T	HA	8	A	QXB	5.5
12	F	QE	5	Y	HB1	5.5
14	V	QXG1	3	W	H	5.5
14	V	QXG2	3	W	H	5.5
15	T	QXGT	2	E	H	5.5
15	T	QXGT	16	E	HE2	5.5

**Table 42.** NOE Distance Restraints for Peptide 76.

Residue		Proton	Residue		Proton	Distance
1	C	HA	2	G	H	2.70
3	E	HA	4	W	H	2.70
3	E	HB1	3	E	H	2.70
4	W	H	3	E	HA	2.70
5	$\gamma^4$	HA	6	Y	H	2.70
6	Y	H	5	$\gamma^4$	HA	2.70
6	Y	HA	7	N	H	2.70
7	N	H	6	Y	HA	2.70
7	N	HA	8	P	QD	2.70
10	T	H	11	G	H	2.70
11	G	H	10	T	H	2.70
14	$\gamma^4$	HA	15	V	H	2.70
15	V	H	14	$\gamma^4$	HA	2.70
15	V	HA	15	T	H	2.70
16	T	H	15	V	HA	2.70
16	T	HA	17	E	H	2.70
17	E	H	16	T	HA	2.70
2	G	H	3	E	H	3.50
2	G	HA1	3	E	H	3.50
2	G	HA2	3	E	H	3.50
3	E	H	2	G	H	3.50
3	E	H	2	G	HA1	3.50
3	E	H	2	G	HA2	3.50
3	E	HB2	4	W	H	3.50
4	W	H	5	$\gamma^4$	H	3.50
4	W	HA	5	$\gamma^4$	H	3.50
4	W	HA	15	V	HA	3.50
5	$\gamma^4$	H	4	W	H	3.50
5	$\gamma^4$	H	4	W	HA	3.50
5	$\gamma^4$	HA	13	F	QD	3.50
5	$\gamma^4$	HB	14	$\gamma^4$	H	3.50
6	Y	HA	13	F	QD	3.50
6	Y	HA	14	$\gamma^4$	H	3.50
6	Y	HB2	7	N	H	3.50
6	Y	QE	7	P	HA	3.50
7	P	HA	6	Y	QE	3.50
7	P	HA	9	A	H	3.50
7	P	QB	6	Y	QE	3.50
7	P	QD	9	A	H	3.50
7	P	QG	9	A	H	3.50
9	A	H	8	P	HA	3.50
9	A	H	8	P	QD	3.50

Residue		Proton	Residue		Proton	Distance
9	A	H	10	T	H	3.50
9	A	HA	9	A	H	3.50
9	A	HA	10	T	H	3.50
10	T	H	9	A	H	3.50
10	T	H	9	A	HA	3.50
10	T	H	9	A	QXB	3.50
10	T	HA	6	Y	QD	3.50
10	T	QXGT	10	T	HA	3.50
10	T	QXGT	10	T	HB	3.50
11	G	H	12	K	H	3.50
11	G	HA1	12	K	H	3.50
11	G	HA2	12	K	H	3.50
12	K	H	11	G	H	3.50
12	K	QB	13	F	H	3.50
13	F	H	12	K	QB	3.50
13	F	HA	7	N	H	3.50
13	F	HA	14	$\gamma^4$	H	3.50
14	$\gamma^4$	H	5	$\gamma^4$	HB	3.50
14	$\gamma^4$	H	13	F	HA	3.50
14	$\gamma^4$	H	13	F	QB	3.50
15	V	H	14	$\gamma^4$	HB	3.50
15	V	HB	16	T	H	3.50
16	T	H	15	V	H	3.50
16	T	H	15	V	QXG2	3.50
16	T	H	17	E	H	3.50
17	E	H	16	T	H	3.50
17	E	H	17	E	HA	3.50
18	C	H	17	E	HA	3.50
3	E	HB1	4	W	H	4.50
4	W	HH2	16	T	QXGT	4.50
4	W	HZ3	5	$\gamma^4$	H	4.50
4	W	QB	5	$\gamma^4$	H	4.50
5	$\gamma^4$	H	15	V	HA	4.50
5	$\gamma^4$	HA	13	F	QE	4.50
6	Y	HB1	7	N	H	4.50
6	Y	HB2	13	F	QD	4.50
6	Y	HB2	13	F	QE	4.50
6	Y	QD	7	N	H	4.50
6	Y	QD	8	P	QD	4.50
6	Y	QD	13	F	QD	4.50
7	N	H	6	Y	H	4.50
7	N	H	6	Y	QD	4.50
7	N	H	6	Y	QE	4.50

Residue		Proton	Residue		Proton	Distance
7	N	H	12	K	H	4.50
7	N	HA	9	A	H	4.50
8	P	HA	6	Y	QD	4.50
8	P	QB	6	Y	QD	4.50
8	P	QG	6	Y	QE	4.50
9	A	H	11	G	H	4.50
9	A	QXB	10	T	H	4.50
10	T	H	12	K	H	4.50
10	T	HA	11	G	H	4.50
10	T	HB	12	K	H	4.50
10	T	QXGT	9	A	HA	4.50
11	G	H	10	T	HA	4.50
11	G	HA1	6	Y	QD	4.50
11	G	HA1	6	Y	QE	4.50
12	K	H	7	N	H	4.50
12	K	H	10	T	H	4.50
12	K	HA	6	Y	QD	4.50
12	K	HA	6	Y	QE	4.50
12	K	HA	13	F	H	4.50
13	F	H	12	K	HA	4.50
13	F	H	12	K	QD	4.50
13	F	QD	6	Y	QD	4.50
13	F	QD	14	$\gamma^4$	H	4.50
14	$\gamma^4$	QXD	5	$\gamma^4$	HB	4.50
15	V	H	14	$\gamma^4$	QXD	4.50
15	V	HA	5	$\gamma^4$	H	4.50
15	V	QXG1	4	W	HZ3	4.50
15	V	QXG2	2	G	HA1	4.50
15	V	QXG2	2	G	HA2	4.50
15	V	QXG2	16	T	H	4.50
16	T	H	3	E	H	4.50
16	T	H	15	V	QXG1	4.50
16	T	QXGT	15	V	H	4.50
16	T	QXGT	17	E	H	4.50
5	$\gamma^4$	QXD	6	Y	H	5.50
8	P	QD	6	Y	QD	5.50
14	$\gamma^4$	HB	5	$\gamma^4$	H	5.50
15	V	QXG1	16	T	H	5.50

## **APPENDIX C**

### **CNS SOFTWARE PATCHES FOR UNNATURAL RESIDUES**

Parameters for B3F

```

ANGLE      CH2E CH1E CH2E      500.00 {sd= 0.031}--      109.5000
IMPRoper   HA   NH1  CH2E CH2E      500.00 {sd= 0.031}      0      70.0000
!-----

```

Parameters for B3V and beta linkages

```

ANGLE      CH2E C    NH1      500.00 {sd= 0.031}      116.1998
IMPRoper   HA   HA   C    CH1E      500.00 {sd= 0.031}      0      -70.0000
IMPRoper   HA   NH1  CH2E CH1E      500.00 {sd= 0.031}      0      70.0000
IMPRoper   CH1E NH1  C    CH2E      500.00 {sd= 0.031}      0      180.0000
IMPRoper   C    CH2E NH1  O      500.00 {sd= 0.031}      0      0.0000
IMPRoper   NH1  C    CH2E H      500.00 {sd= 0.031}      0      0.0000
!-----

```

Parameters for B2Y

```

ANGLE      CH1E CH2E NH1      500.00 {sd= 0.031}      111.4875
DIHEdral   CH2E CH1E CH2E CY      2.00      3      0.0000
IMPRoper   HA   CH2E C    CH2E      500.00 {sd= 0.031}      0      65.9907
IMPRoper   CH2E NH1  C    CH1E      500.00 {sd= 0.031}      0      180.0000
!-----

```

Parameters for BAY

```

IMPRoper   HA   NH1  CH1E CH3E      500.00 {sd= 0.031}      0      70.0000
IMPRoper   HA   CH2E C    CH1E      500.00 {sd= 0.031}      0      -70.0000
!-----

```

Parameters for BFA

```

IMPRoper   HA   NH1  CH1E CH2E      500.00 {sd= 0.031}      0      70.0000
!-----

```

Parameters for BVA

```

ANGLE      CH1E CH1E CH1E      500.00 {sd= 0.031}      109.5000
IMPRoper   HA   CH3E C    CH1E      500.00 {sd= 0.031}      0      -70.0000
IMPRoper   HA   NH1  CH1E CH1E      500.00 {sd= 0.031}      0      70.0000
IMPRoper   HA   C    CH3E CH1E      500.00 {sd= 0.031}      0      -70.0000
IMPRoper   HA   CH1E NH1  CH1E      500.00 {sd= 0.031}      0      70.0000
!-----

```

Parameters for ACC and Linkages

BOND	CC1E	NH1		1000.000	{sd= 0.001}		1.458
BOND	CC1E	CC2E		1000.000	{sd= 0.001}		1.530
BOND	CC2E	CC2E		1000.000	{sd= 0.001}		1.520
BOND	CC2E	HAA		1000.000	{sd= 0.001}		1.080
BOND	CC2E	HAE		1000.000	{sd= 0.001}		1.080
BOND	CC1E	HAA		1000.000	{sd= 0.001}		1.080
BOND	C	CC1E		1000.000	{sd= 0.001}		1.525
ANGLE	H	NH1	CC1E	500.00	{sd= 0.031}		125.5
ANGLE	NH1	CC1E	HAA	500.00	{sd= 0.031}		107.0
ANGLE	NH1	CC1E	CC2E	500.00	{sd= 0.031}		110.0
ANGLE	HAA	CC1E	CC2E	500.00	{sd= 0.031}		109.4
ANGLE	CC1E	CC2E	CC1E	500.00	{sd= 0.031}		111.0
ANGLE	CC1E	CC2E	CC2E	500.00	{sd= 0.031}		111.0
ANGLE	CC2E	CC2E	CC2E	500.00	{sd= 0.031}		111.0
ANGLE	CC1E	CC2E	HAA	500.00	{sd= 0.031}		109.4
ANGLE	CC2E	CC2E	HAA	500.00	{sd= 0.031}		109.4
ANGLE	CC1E	CC2E	HAE	500.00	{sd= 0.031}		111.0
ANGLE	CC2E	CC2E	HAE	500.00	{sd= 0.031}		111.0
ANGLE	CC2E	CC1E	CC2E	500.00	{sd= 0.031}		111.0
ANGLE	CC2E	CC1E	C	500.00	{sd= 0.031}		110.0
ANGLE	HAA	CC2E	HAE	500.00	{sd= 0.031}		107.0
ANGLE	HAA	CC1E	C	500.00	{sd= 0.031}		107.0
ANGLE	CC1E	C	O	500.00	{sd= 0.031}		123.9
ANGLE	C	NH1	CC1E	500.00	{sd= 0.031}		120
ANGLE	CC1E	C	NH1	500.00	{sd= 0.031}		120
NONBonded	CC1E			0.0903	3.2072		0.0903 3.2072
NONBonded	CC2E			0.0903	3.2072		0.0903 3.2072
NONBonded	HAA			0.0045	2.6157		0.0045 2.6157
NONBonded	HAE			0.0045	2.6157		0.0045 2.6157
IMPRoper	NH1	CC1E	CC2E	CC1E	500.00	{sd= 0.031}	0 180
IMPRoper	C	CC1E	CC2E	CC1E	500.00	{sd= 0.031}	0 180
IMPRoper	HAA	CC1E	CC2E	HAA	500.00	{sd= 0.031}	0 180
IMPRoper	HAA	CC2E	CC2E	HAA	500.00	{sd= 0.031}	0 180
IMPRoper	O	C	NH1	H	500.00	{sd= 0.031}	0 180
IMPRoper	CC1E	C	NH1	CH1E	500.00	{sd= 0.031}	0 180
IMPRoper	CH1E	C	NH1	CC1E	500.00	{sd= 0.031}	0 180
IMPRoper	O	C	NH1	CH1E	500.00	{sd= 0.031}	0 0

!-----

## Parameters for G4A

BOND	CH1E	CD1E		1000.000	{sd= 0.001}	1.516	
BOND	CD1E	CD1E		1000.000	{sd= 0.001}	1.34	
BOND	CD1E	C		1000.000	{sd= 0.001}	1.516	
BOND	CD1E	HA		1000.000	{sd= 0.001}	1.080	
ANGLE	NH1	CH1E	CD1E	500.00	{sd= 0.031}	109.5000	
ANGLE	HA	CH1E	CD1E	500.00	{sd= 0.031}	109.5000	
ANGLE	CD1E	CH1E	CH3E	500.00	{sd= 0.031}	109.5000	
ANGLE	CH1E	CD1E	CD1E	500.00	{sd= 0.031}	120.0000	
ANGLE	CH1E	CD1E	HA	500.00	{sd= 0.031}	120.0000	
ANGLE	CD1E	CD1E	HA	500.00	{sd= 0.031}	120.0000	
ANGLE	CD1E	CD1E	C	500.00	{sd= 0.031}	120.0000	
ANGLE	C	CD1E	HA	500.00	{sd= 0.031}	120.000	
ANGLE	CD1E	C	O	500.00	{sd= 0.031}	120.000	
ANGLE	CD1E	C	NH1	500.00	{sd= 0.031}	120.000	
IMPRoper	HA	CD1E	C	CH1E	500.00	{sd= 0.031}	0 0
IMPRoper	C	CD1E	NH1	O	500.00	{sd= 0.031}	0 0
IMPRoper	CD1E	C	NH1	CH1E	500.00	{sd= 0.031}	0 180
IMPRoper	HA	NH1	CH3E	CD1E	500.00	{sd= 0.031}	0 70.0000

!-----

## Parameters for MABA

BOND	NH1	CF		1000.000	{sd= 0.001}	1.373	
BOND	CF	C		1000.000	{sd= 0.001}	1.373	
ANGLE	H	NH1	CF	500.00	{sd= 0.031}	119.9118	
ANGLE	NH1	CF	CR1E	500.00	{sd= 0.031}	119.9118	
ANGLE	CR1E	CF	C	500.00	{sd= 0.031}	119.9118	
ANGLE	CF	CR1E	CF	500.00	{sd= 0.031}	119.9118	
ANGLE	C	CF	CR1E	500.00	{sd= 0.031}	119.9118	
ANGLE	CF	C	O	500.00	{sd= 0.031}	119.9118	
ANGLE	C	NH1	CF	500.00	{sd= 0.031}	119.9118	
ANGLE	CF	C	NH1	500.00	{sd= 0.031}	119.9118	
IMPRoper	CF	CR1E	CF	CR1E	500.00	{sd= 0.031}	0 0.0000
IMPRoper	CR1E	CF	CR1E	CF	500.00	{sd= 0.031}	0 0.0000
IMPRoper	NH1	C	CF	H	500.00	{sd= 0.031}	0 0.0000
IMPRoper	CH2G	C	NH1	CF	500.00	{sd= 0.031}	0 0.0000
IMPRoper	C	CF	NH1	O	500.00	{sd= 0.031}	0 0.0000

!-----

## Topologies

residue ACC

group

atom N	type=NH1	charge=-0.600	end
atom HN	type=H	charge= 0.400	end
atom CRA	type=CC1E	charge= 0.000	end
atom HA	type=HAA	charge= 0.000	end
atom CRB	type=CC2E	charge= 0.000	end
atom HB1	type=HAA	charge= 0.000	end
atom HB2	type=HAE	charge= 0.000	end
atom CRG	type=CC1E	charge= 0.000	end
atom HG	type=HAA	charge= 0.000	end
atom CRD	type=CC2E	charge= 0.000	end
atom HD1	type=HAA	charge= 0.000	end
atom HD2	type=HAE	charge= 0.000	end
atom CRE	type=CC2E	charge= 0.000	end
atom HE1	type=HAA	charge= 0.000	end
atom HE2	type=HAE	charge= 0.000	end
atom CRZ	type=CC2E	charge= 0.000	end
atom HZ1	type=HAA	charge= 0.000	end
atom HZ2	type=HAE	charge= 0.000	end
atom C	type=C	charge= 0.500	end
atom O	type=O	charge=-0.500	end

bond N	HN				
bond N	CRG	bond CRG	HG	bond CRG	CRB
bond CRB	CRA	bond CRB	HB1	bond CRB	HB2
bond CRA	CRZ	bond CRA	HA		
bond CRZ	CRE	bond CRZ	HZ1	bond CRZ	HZ2
bond CRE	CRD	bond CRE	HE1	bond CRE	HE2
bond CRD	CRG	bond CRD	HD1	bond CRD	HD2
bond CRA	C				
bond C	O				

improper N CRG CRB CRA

improper C CRA CRB CRG

!Ring Improvers

improper HG CRG CRB HB1  
improper HB1 CRB CRA HA  
improper HA CRA CRZ HZ1  
improper HZ1 CRZ CRE HE1  
improper HE1 CRE CRD HD1  
improper HD1 CRD CRG HG

DONO	HN	N
ACCE	O	C

End

!-----

residue B3F

group

```
atom N      type=NH1      charge=-0.600 end
atom HN     type=H        charge= 0.400 end
atom CA     type=CH2E     charge= 0.000 end
atom HA1    type=HA       charge= 0.000 end
atom HA2    type=HA       charge= 0.000 end
atom CB     type=CH1E     charge= 0.000 end
atom HB     type=HA       charge= 0.000 end
atom CG     type=CH2E     charge= 0.000 end
atom HG1    type=HA       charge= 0.000 end
atom HG2    type=HA       charge= 0.000 end
atom CD     type=CF       charge= 0.000 exclude=(CH) end
atom CE1    type=CR1E     charge= 0.000 exclude=(CZ2) end
atom HE1    type=HA       charge= 0.000 end
atom CE2    type=CR1E     charge= 0.000 exclude=(CZ1) end
atom HE2    type=HA       charge= 0.000 end
atom CZ1    type=CR1E     charge= 0.000 exclude=(CE2) end
atom HZ1    type=HA       charge= 0.000 end
atom CZ2    type=CR1E     charge= 0.000 exclude=(CE1) end
atom HZ2    type=HA       charge= 0.000 end
atom CH     type=CR1E     charge= 0.000 exclude=(CD) end
atom HH     type=HA       charge= 0.000 end
atom C      type=C        charge= 0.500 end
atom O      type=O        charge=-0.500 end
```

```
bond N      HN
bond N      CB      bond CB  HB
bond CB     CG      bond CG  HG1      bond CG  HG2
bond CG     CD
bond CD     CE1     bond CE1 HE1
bond CD     CE2     bond CE2 HE2
bond CE1    CZ1     bond CZ1 HZ1
bond CZ1    CH
bond CZ2    CH
bond CE2    CZ2     bond CZ2 HZ2
bond CH     HH
bond CB     CA      bond CA  HA1      bond CA  HA2
bond CA     C
bond C      O
```

```
improper HB  N      CA  CG      !chirality CB
improper HG1 HG2    CB  CD      !stereo CG
```

! Hs and CG around the ring

```
improper HE2 CE2 CZ2 CH
improper HZ2 CZ2 CH  CZ1
improper HH  CH  CZ1 CE1
improper HZ1 CZ1 CE1 CD
improper HE1 CE1 CD  CE2
improper CG  CD  CE2 CZ2
```

```

! around the ring
improper CD  CE1 CZ1 CH
improper CE1 CZ1 CH  CZ2
improper CZ1 CH  CZ2 CE2
improper CH  CZ2 CE2 CD
improper CZ2 CE2 CD  CE1
improper CE2 CD  CE1 CZ1

dihedral N    CB  CA  C
dihedral CD  CG  CB  N
dihedral CE1 CD  CG  CB

DONO HN      N
ACCE O       C
end
!-----

residue B3V
group
  atom N      type=NH1      charge=-0.600 end
  atom HN     type=H        charge= 0.400 end
  atom CA     type=CH2E     charge= 0.000 end
  atom HA1    type=HA        charge= 0.000 end
  atom HA2    type=HA        charge= 0.000 end
  atom CB     type=CH1E     charge= 0.000 end
  atom HB     type=HA        charge= 0.000 end
  atom CG     type=CH1E     charge= 0.000 end
  atom HG     type=HA        charge= 0.000 end
  atom CD1    type=CH3E     charge= 0.000 end
  atom HD11   type=HA        charge= 0.000 excl = (HD21 HD22 HD23 HG) end
  atom HD12   type=HA        charge= 0.000 excl = (HD21 HD22 HD23 HG) end
  atom HD13   type=HA        charge= 0.000 excl = (HD21 HD22 HD23 HG) end
  atom CD2    type=CH3E     charge= 0.000 end
  atom HD21   type=HA        charge= 0.000 excl = (HD11 HD12 HD13 HG) end
  atom HD22   type=HA        charge= 0.000 excl = (HD11 HD12 HD13 HG) end
  atom HD23   type=HA        charge= 0.000 excl = (HD11 HD12 HD13 HG) end
  atom C      type=C        charge= 0.500 end
  atom O      type=O        charge=-0.500 end

bond N  HN
bond N  CB      bond CB  HB
bond CB  CG      bond CG  HG
bond CG  CD1     bond CD1 HD11     bond CD1 HD12     bond CD1 HD13
bond CG  CD2     bond CD2 HD21     bond CD2 HD22     bond CD2 HD23
bond CB  CA      bond CA  HA1     bond CA  HA2
bond CA  C
bond C  O

improper HB  N    CA  CG      !chirality CB
improper HG  CB  CD1 CD2     !stereo CG
improper HA1 HA2  C   CB      !stereo CB
improper HD11 HD12 CG  HD13   !methyl CD1
improper HD21 HD22 CG  HD23   !methyl CD2

```

```

dihedral CD1 CG CB N
dihedral HD11 CD1 CG CB ! UCL methyl stagger 12-MAR-00
dihedral HD21 CD2 CG CB ! UCL methyl stagger 12-MAR-00

DONO HN N
ACCE O C
end
!-----

residue B2Y

group
atom N type=NH1 charge=-0.600 end
atom HN type=H charge= 0.400 end
atom CA type=CH1E charge= 0.000 end
atom HA type=HA charge= 0.000 end
atom CB type=CH2E charge= 0.000 end
atom HB1 type=HA charge= 0.000 end
atom HB2 type=HA charge= 0.000 end
atom CG type=CH2E charge= 0.000 end
atom HG1 type=HA charge= 0.000 end
atom HG2 type=HA charge= 0.000 end
atom CD type=CY charge= 0.000 exclude=(CH) end
atom CE1 type=CR1E charge= 0.000 exclude=(CZ2) end
atom HE1 type=HA charge= 0.000 end
atom CE2 type=CR1E charge= 0.000 exclude=(CZ1) end
atom HE2 type=HA charge= 0.000 end
atom CZ1 type=CR1E charge= 0.000 exclude=(CE2) end
atom HZ1 type=HA charge= 0.000 end
atom CZ2 type=CR1E charge= 0.000 exclude=(CE1) end
atom HZ2 type=HA charge= 0.000 end
atom CH type=CY2 charge= 0.265 exclude=(CD) end
atom OT type=OH1 charge=-0.700 end
atom HT type=H charge= 0.435 end
atom C type=C charge= 0.500 end
atom O type=O charge=-0.500 end

bond N HN
bond N CB bond CB HB1 bond CB HB2
bond CB CA bond CA HA
bond CA CG bond CG HG1 bond CG HG2
bond CG CD
bond CD CE1 bond CE1 HE1 bond CE1 CZ1
bond CD CE2 bond CE2 HE2 bond CE2 CZ2
bond CZ1 HZ1 bond CZ1 CH
bond CZ2 HZ2 bond CZ2 CH
bond CH OT bond OT HT
bond CA C
bond C O

! chirality

```

```
improper HA  CB  C  CG  !chirality CA
improper HG1 HG2 CA CD  !stereo CG
```

```
! Hs, OT, and CG around the ring
```

```
improper HE2 CE2 CZ2 CH
improper HZ2 CZ2 CH  CZ1
improper OT  CH  CZ1 CE1
improper HZ1 CZ1 CE1 CD
improper HE1 CE1 CD  CE2
improper CG  CD  CE2 CZ2
```

```
! around the ring
```

```
improper CD  CE1 CZ1 CH
improper CE1 CZ1 CH  CZ2
improper CZ1 CH  CZ2 CE2
improper CH  CZ2 CE2 CD
improper CZ2 CE2 CD  CE1
improper CE2 CD  CE1 CZ1
```

```
dihedral CD  CG  CA  CB
dihedral CE1 CD  CG  CA
dihedral CZ2 CH  OT  HT  ! UCL Added 12-MAR-00
```

```
DONO HN  N
DONO HT  OT
ACCE OT  "  "
ACCE O   C
```

```
end
```

```
!-----
```

```
residue BAY
```

```
group
```

```
atom N      type=NH1      charge=-0.600 end
atom HN     type=H       charge= 0.400 end
atom CA     type=CH1E    charge= 0.000 end
atom HA     type=HA      charge= 0.000 end
atom CB     type=CH1E    charge= 0.000 end
atom HB     type=HA      charge= 0.000 end
atom CG     type=CH2E    charge= 0.000 end
atom HG1    type=HA      charge= 0.000 end
atom HG2    type=HA      charge= 0.000 end
atom CD     type=CY      charge= 0.000 exclude=(CH) end
atom CE1    type=CR1E    charge= 0.000 exclude=(CZ2) end
atom HE1    type=HA      charge= 0.000 end
atom CE2    type=CR1E    charge= 0.000 exclude=(CZ1) end
atom HE2    type=HA      charge= 0.000 end
atom CZ1    type=CR1E    charge= 0.000 exclude=(CE2) end
atom HZ1    type=HA      charge= 0.000 end
atom CZ2    type=CR1E    charge= 0.000 exclude=(CE1) end
atom HZ2    type=HA      charge= 0.000 end
atom CH     type=CY2     charge= 0.265 exclude=(CD) end
```

```

atom OT    type=OH1    charge=-0.700 end
atom HT    type=H      charge= 0.435 end
atom CI    type=CH3E   charge= 0.000 end
atom HI1   type=HA     charge= 0.000 end
atom HI2   type=HA     charge= 0.000 end
atom HI3   type=HA     charge= 0.000 end
atom C     type=C      charge= 0.500 end
atom O     type=O      charge=-0.500 end

bond N     HN
bond N     CB          bond CB  HB          bond CB  CI
bond CB    CA          bond CA  HA
bond CA    CG          bond CG  HG1         bond CG  HG2
bond CG    CD
bond CD    CE1         bond CE1 HE1         bond CE1 CZ1
bond CD    CE2         bond CE2 HE2         bond CE2 CZ2
bond CZ1   HZ1         bond CZ1 CH
bond CZ2   HZ2         bond CZ2 CH
bond CH    OT          bond OT  HT
bond CI    HI1         bond CI  HI2         bond CI  HI3
bond CA    C
bond C     O

! Hs, OT, and CG around the ring
improper HE2 CE2 CZ2 CH
improper HZ2 CZ2 CH  CZ1
improper OT  CH  CZ1 CE1
improper HZ1 CZ1 CE1 CD
improper HE1 CE1 CD  CE2
improper CG  CD  CE2 CZ2

! around the ring
improper CD  CE1 CZ1 CH
improper CE1 CZ1 CH  CZ2
improper CZ1 CH  CZ2 CE2
improper CH  CZ2 CE2 CD
improper CZ2 CE2 CD  CE1
improper CE2 CD  CE1 CZ1

improper HB  N  CA  CI  !chirality CB
improper HA  CG  C  CB  !chirality CA
improper HI1 HI2 CA  HI3 !methyl CI
improper HG1 HG2 CA  CD  !stereo CG

dihedral  CG  CA  CB  N

DONO HN  N
DONO HT  OT
ACCE OT  "  "
ACCE O   C
end
!-----

```

residue BFA  
group

```
atom N      type=NH1      charge=-0.600 end
atom HN     type=H        charge= 0.400 end
atom CA     type=CH1E     charge= 0.000 end
atom HA     type=HA        charge= 0.000 end
atom CB     type=CH1E     charge= 0.000 end
atom HB     type=HA        charge= 0.000 end
atom CG     type=CH3E     charge= 0.000 end
atom HG1    type=HA        charge= 0.000 end
atom HG2    type=HA        charge= 0.000 end
atom HG3    type=HA        charge= 0.000 end
atom CD     type=CH2E     charge= 0.000 end
atom HD1    type=HA        charge= 0.000 end
atom HD2    type=HA        charge= 0.000 end
atom CE     type=CF        charge= 0.000 exclude=(CT) end
atom CZ1    type=CR1E     charge= 0.000 exclude=(CH2) end
atom HZ1    type=HA        charge= 0.000 end
atom CZ2    type=CR1E     charge= 0.000 exclude=(CH1) end
atom HZ2    type=HA        charge= 0.000 end
atom CH1    type=CR1E     charge= 0.000 exclude=(CZ2) end
atom HH1    type=HA        charge= 0.000 end
atom CH2    type=CR1E     charge= 0.000 exclude=(CZ1) end
atom HH2    type=HA        charge= 0.000 end
atom CT     type=CR1E     charge= 0.000 exclude=(CE) end
atom HT     type=HA        charge= 0.000 end
atom C      type=C         charge= 0.500 end
atom O      type=O         charge=-0.500 end
```

```
bond N      HN
bond N      CB      bond CB      HB
bond CA     CG      bond CG     HG1      bond CG     HG2      bond CG     HG3
bond CB     CD      bond CD     HD1      bond CD     HD2      bond CD     CE
bond CE     CZ1     bond CZ1    HZ1
bond CE     CZ2     bond CZ2    HZ2
bond CZ1    CH1     bond CH1    HH1
bond CH1    CT
bond CH2    CT
bond CZ2    CH2     bond CH2    HH2
bond CT     HT
bond CB     CA      bond CA     HA
bond CA     C
bond C      O
```

```
! Hs and CG around the ring
improper HZ2 CZ2 CH2 CT
improper HH2 CH2 CT CH1
improper HT CT CH1 CZ1
improper HH1 CH1 CZ1 CE
improper HZ1 CZ1 CE CZ2
improper CD CE CZ2 CH2
```

```
! around the ring
```

```

improper CE CZ1 CH1 CT
improper CZ1 CH1 CT CH2
improper CH1 CT CH2 CZ2
improper CT CH2 CZ2 CE
improper CH2 CZ2 CE CZ1
improper CZ2 CE CZ1 CH1

improper HB N CA CD !chirality CB
improper HA CG C CB !chirality CA
improper HD1 HD2 CB CE !stereo CD
improper HG1 HG2 CA HG3 !methyl CE

dihedral CE CD CB N

DONO HN N
ACCE O C
end
!-----

residue BVA
group
atom N type=NH1 charge=-0.600 end
atom HN type=H charge= 0.400 end
atom CA type=CH1E charge= 0.000 end
atom HA type=HA charge= 0.000 end
atom CB type=CH1E charge= 0.000 end
atom HB type=HA charge= 0.000 end
atom CG type=CH1E charge= 0.000 end
atom HG type=HA charge= 0.000 end
atom CD1 type=CH3E charge= 0.000 end
atom HD11 type=HA charge= 0.000 excl = (HD21 HD22 HD23 HG) end
atom HD12 type=HA charge= 0.000 excl = (HD21 HD22 HD23 HG) end
atom HD13 type=HA charge= 0.000 excl = (HD21 HD22 HD23 HG) end
atom CD2 type=CH3E charge= 0.000 end
atom HD21 type=HA charge= 0.000 excl = (HD11 HD12 HD13 HG) end
atom HD22 type=HA charge= 0.000 excl = (HD11 HD12 HD13 HG) end
atom HD23 type=HA charge= 0.000 excl = (HD11 HD12 HD13 HG) end
atom CE type=CH3E charge= 0.000 end
atom HE1 type=HA charge= 0.000 end
atom HE2 type=HA charge= 0.000 end
atom HE3 type=HA charge= 0.000 end
atom C type=C charge= 0.500 end
atom O type=O charge=-0.500 end

bond N HN
bond N CB bond CB HB
bond CB CG bond CG HG
bond CG CD1 bond CD1 HD11 bond CD1 HD12 bond CD1 HD13
bond CG CD2 bond CD2 HD21 bond CD2 HD22 bond CD2 HD23
bond CB CA bond CA HA
bond CA CE bond CE HE1 bond CE HE2 bond CE HE3
bond CA C
bond C O

```

```

improper HB N CA CG !chirality CB
improper HA CE C CB !chirality CA
improper HG CB CD1 CD2 !stereo CG
improper HD11 HD12 CG HD13 !methyl CD1
improper HD21 HD22 CG HD23 !methyl CD2
improper HE1 HE2 CA HE3 !methyl CE

dihedral CD1 CG CB N
dihedral HD11 CD1 CG CB ! UCL methyl stagger 12-MAR-00
dihedral HD21 CD2 CG CB ! UCL methyl stagger 12-MAR-00
dihedral HE1 CE CA CB ! UCL methyl stagger 12-MAR-00

DONO HN N
ACCE O C
end
!-----

residue MABA
group
atom N type=NH1 charge=-0.600 end
atom HN type=H charge= 0.400 end
atom CA type=CF charge= 0.000 end
atom CB type=CR1E charge= 0.000 end
atom HB type=HA charge= 0.000 end
atom CG type=CF charge= 0.000 end
atom CD type=CR1E charge= 0.000 end
atom HD type=HA charge= 0.000 end
atom CE type=CR1E charge= 0.000 end
atom HE type=HA charge= 0.000 end
atom CZ type=CR1E charge= 0.000 end
atom HZ type=HA charge= 0.000 end
atom C type=C charge= 0.500 end
atom O type=O charge= -0.500 end

bond N HN bond N CG
bond CA CB bond CA C
bond CB CG bond CB HB
bond CG CD
bond CD CE bond CD HD
bond CE CZ bond CE HE
bond CZ CA bond CZ HZ
bond C O

! Hs around the ring
improper HB CB CG CD
improper HD CD CE CZ
improper HE CE CZ CA
improper HZ CZ CA CB

! around the ring
improper CA CB CG CD
improper CB CG CD CE
improper CG CD CE CZ
improper CD CE CZ CA

```

```

improper CE CZ CA CB
improper CZ CA CB CG

DONO HN N
ACCE O C
end
!-----

residue G4A
group
atom N type=NH1 charge=-0.600 end
atom HN type=H charge= 0.400 end
atom CA type=CD1E charge= 0.000 end
atom HA type=HA charge= 0.000 end
atom CB type=CD1E charge= 0.000 end
atom HB type=HA charge= 0.000 end
atom CG type=CH1E charge= 0.000 end
atom HG type=HA charge= 0.000 end
atom CD type=CH3E charge= 0.000 end
atom HD1 type=HA charge= 0.000 end
atom HD2 type=HA charge= 0.000 end
atom HD3 type=HA charge= 0.000 end
atom C type=C charge= 0.500 end
atom O type=O charge=-0.500 end

bond N HN
bond N CG bond CG HG bond CG CB bond CG CD
bond CD HD1 bond CD HD2 bond CD HD3
bond CB CA bond CB HB
bond CA C bond CA HA
bond C O

! chirality
improper HA CB C CG !chirality CA
improper HG1 HG2 CA HG3 !stereo CG

dihedral HG1 CG CA C ! methyl stagger UCL 12-MAR-00

DONO HN N
ACCE O C
end
!-----

```

```
residue ATOB      ! PEPTide bond link alpha-to-beta, for all except PRO
```

```
  add bond -C +N
  add angle -CA -C +N
  add angle -O  -C +N
  add angle -C  +N +CB
  add angle -C  +N +HN
  add improper -C -CA +N -O          ! planar -C
  add improper +N -C +CB +HN        ! planar +N
  add improper -CA -C  +N  +CB      ! angle across peptide plane
end
!-----
```

```
residue BTOA      ! PEPTide bond link beta-to-alpha, for all except PRO
```

```
  add bond -C +N
  add angle -CA -C +N
  add angle -O  -C +N
  add angle -C  +N +CA
  add angle -C  +N +HN
  add improper -C -CA +N -O          ! planar -C
  add improper +N -C +CA +HN        ! planar +N
  add improper -CA -C  +N  +CA      ! angle across peptide plane
end
!-----
```

```
residue ATOG      ! PEPTide bond link alpha-to-gamma, for all except PRO
```

```
  add bond -C +N

  add angle -CA -C +N
  add angle -O  -C +N
  add angle -C  +N +CG
  add angle -C  +N +HN

  add improper -C -CA +N -O          ! planar -C
  add improper +N -C +CG +HN        ! planar +N
  add improper -CA -C  +N  +CG      ! angle across peptide plane
end
!-----
```

```

presidue GTOA      ! PEPTide bond link gamma-to-alpha, for all except PRO

  add bond -C +N

  add angle -CA -C +N
  add angle -O  -C +N
  add angle -C  +N +CA
  add angle -C  +N +HN

  add improper -C -CA +N -O          ! planar -C
  add improper +N -C +CA +HN        ! planar +N
  add improper -CA -C  +N  +CA      ! angle across peptide plane

end
!-----

presidue ATOG      ! PEPTide bond link alpha-to-gamma cyclic

  add bond -C +N
  add angle -CA -C +N
  add angle -O  -C +N
  add angle -C  +N +CRG
  add angle -C  +N +HN
  improper -O -C +N +HN
  improper -CA -C +N +CRG

end
!-----

presidue GTOA      ! PEPTide bond link cyclic gamma-to-alpha

  add bond -C +N
  add angle -CRA -C +N
  add angle -O  -C +N
  add angle -C  +N +CA
  add angle -C  +N +HN
  improper -O -C +N +HN
  improper -O -C +N +CA

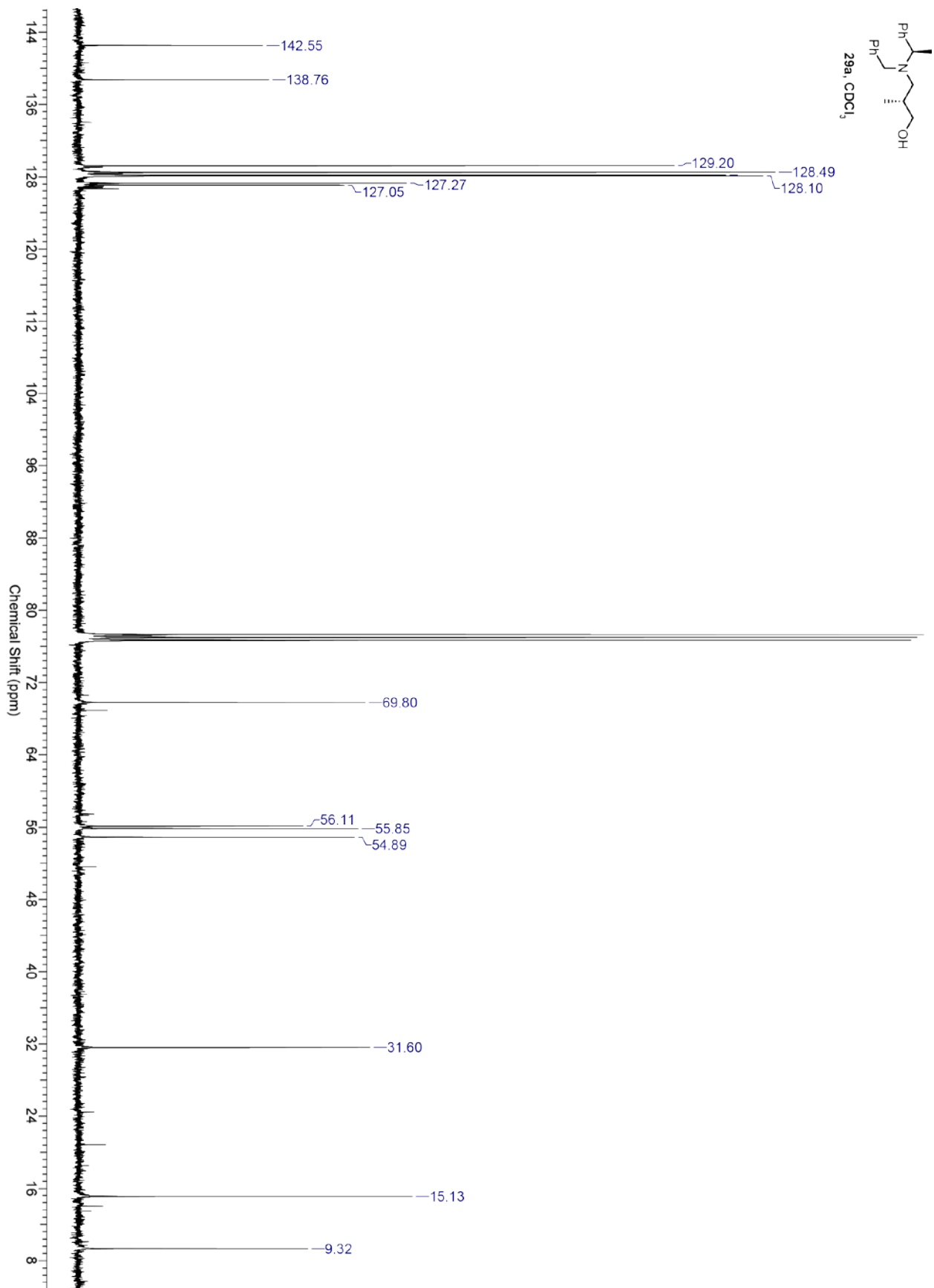
end
!-----

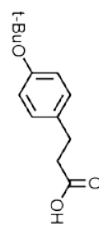
```

## APPENDIX D

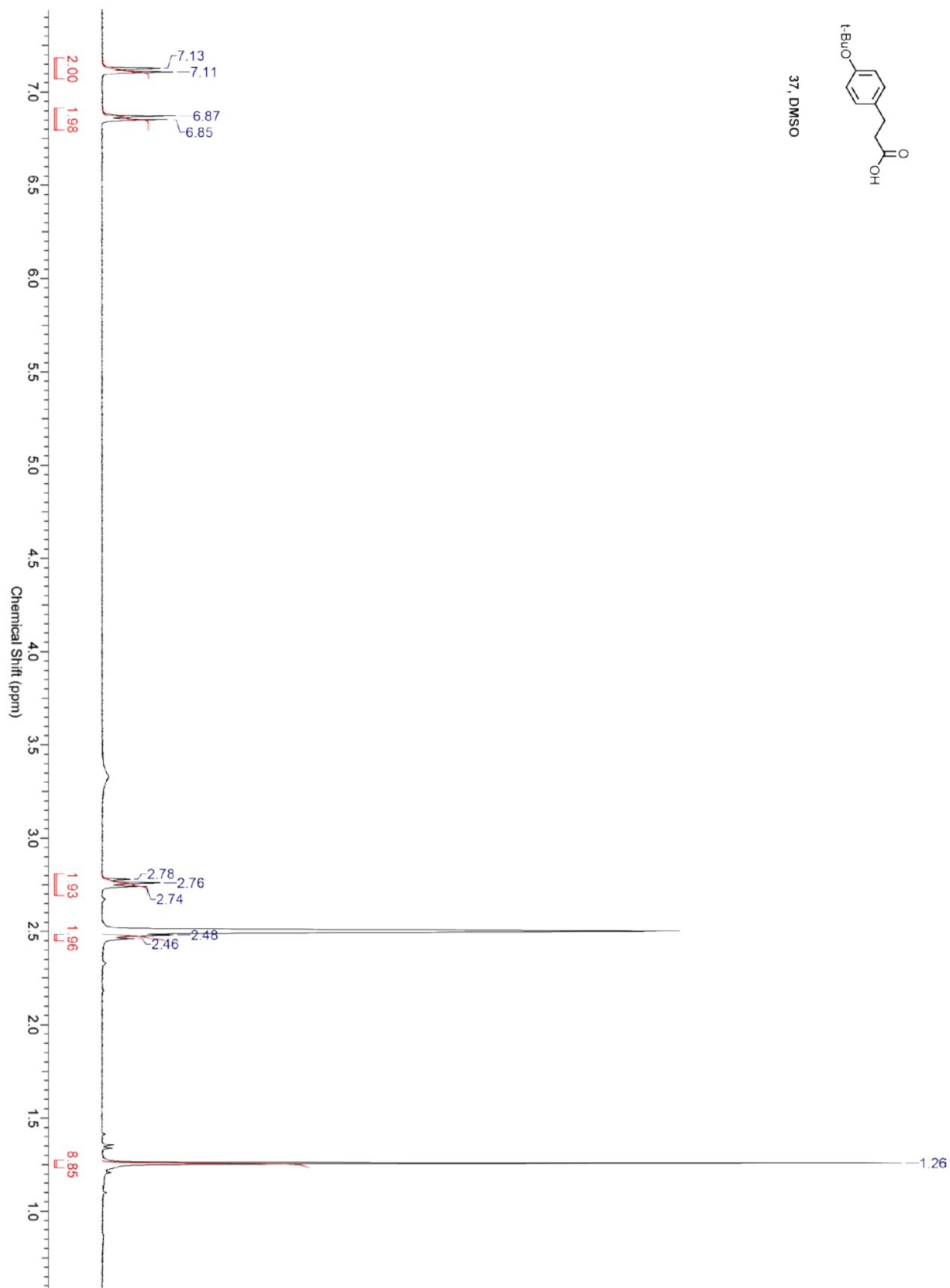
### $^1\text{H}$ AND $^{13}\text{C}$ NMR DATA FOR SYNTHETICALLY PREPARED SMALL MOLECULES

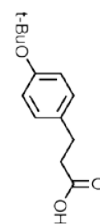




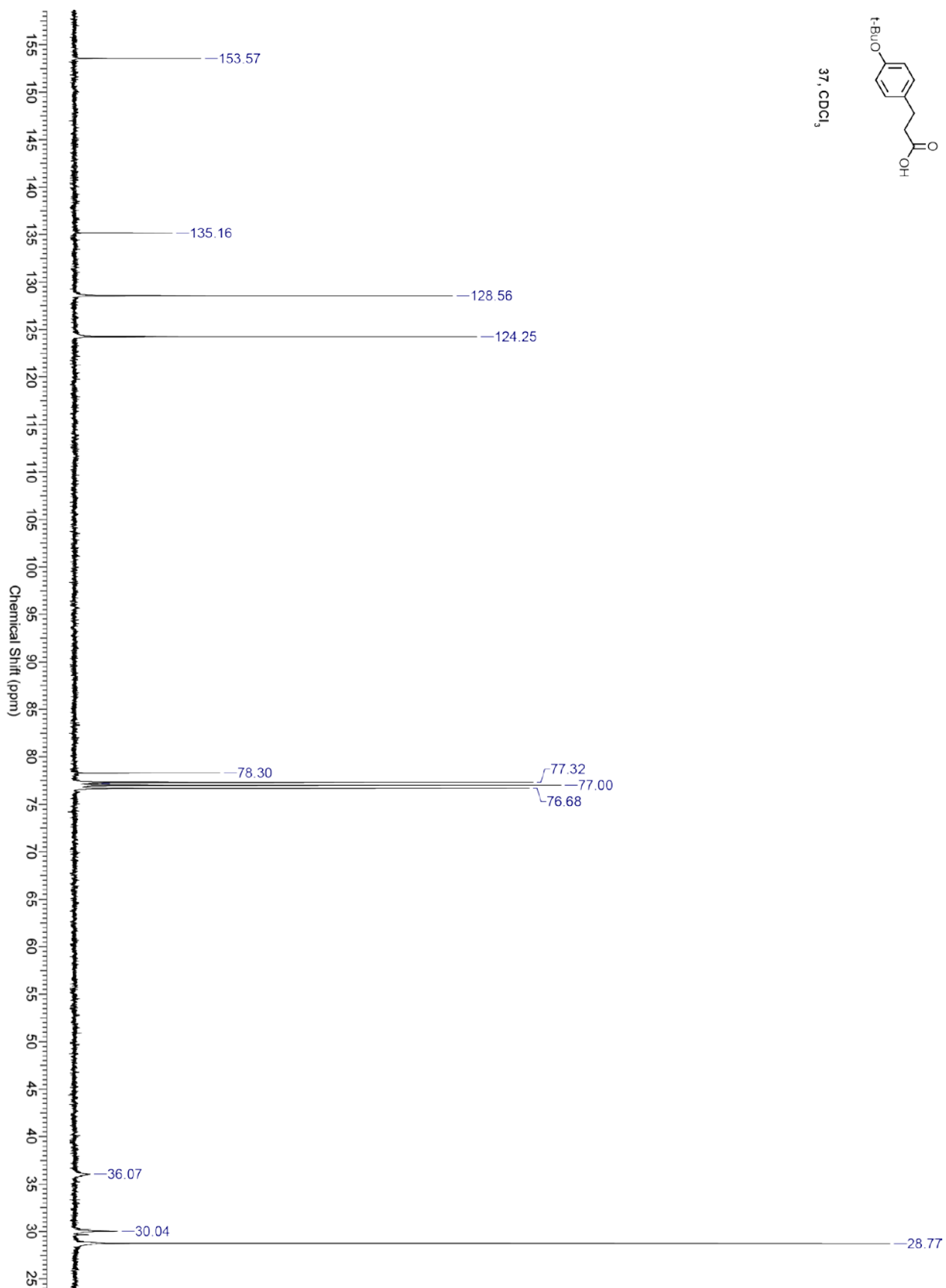


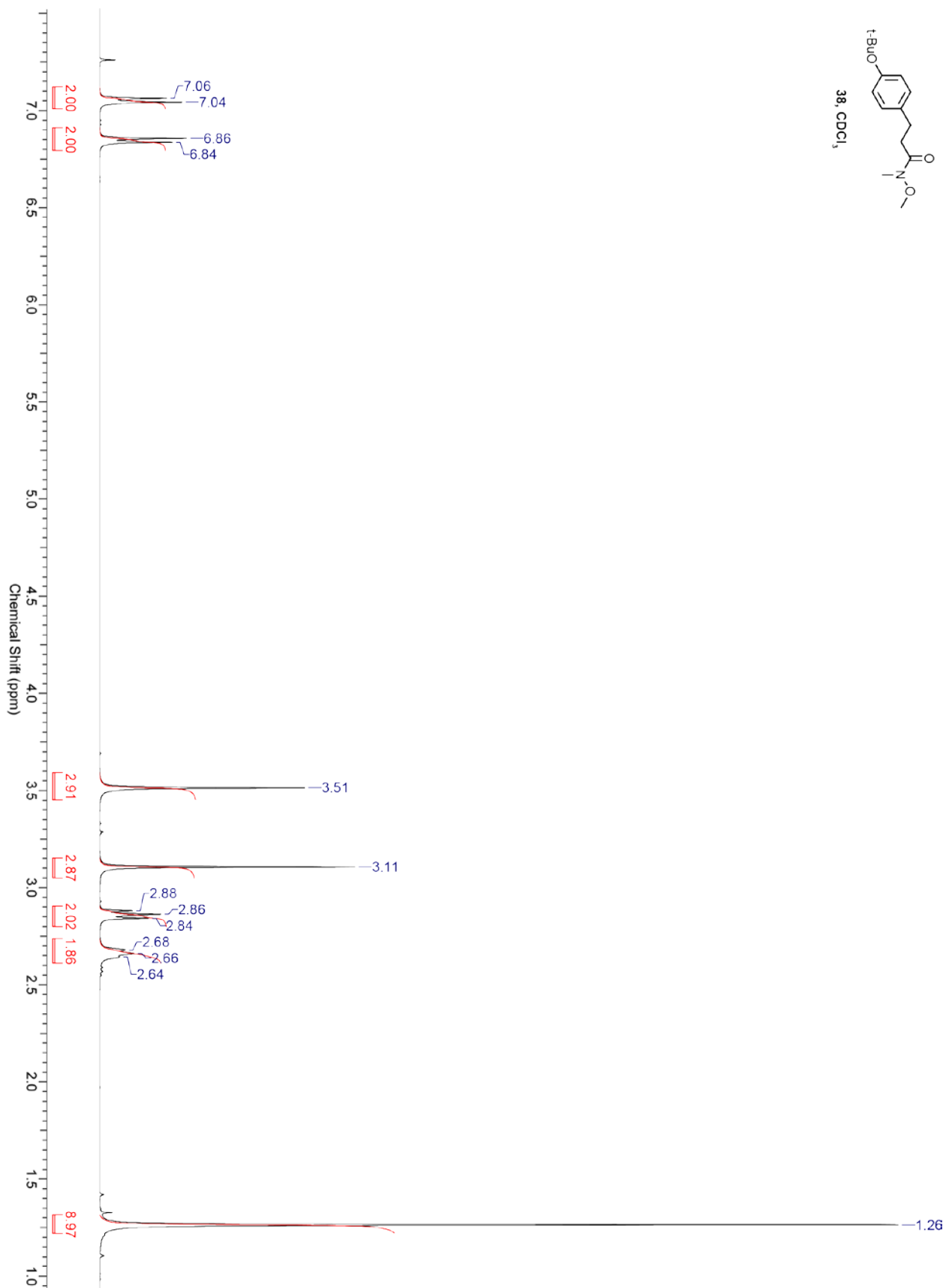
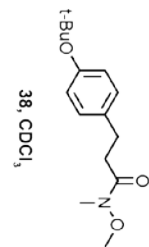
37, DMSO

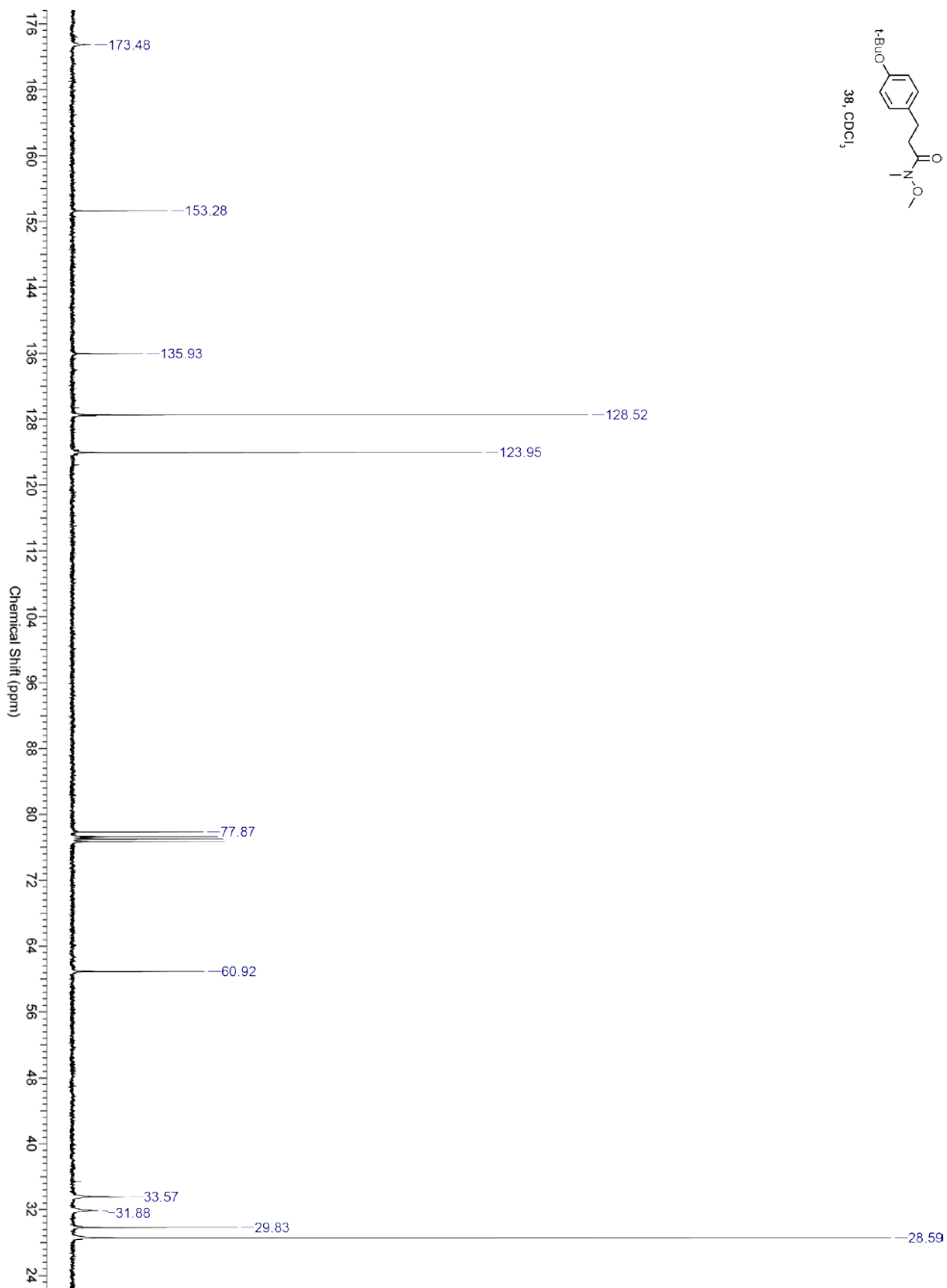
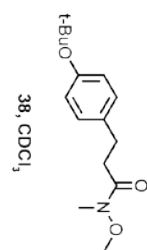


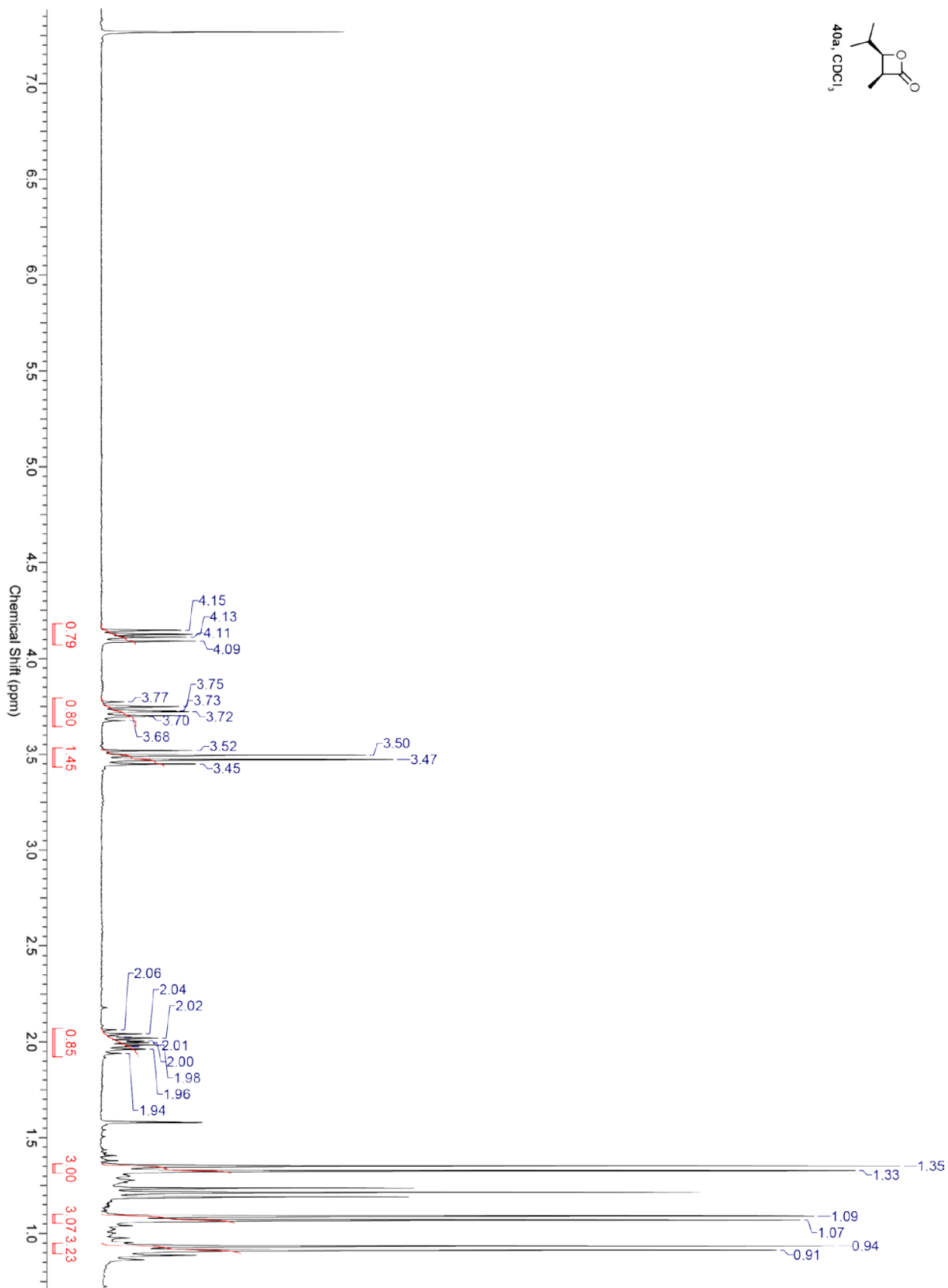
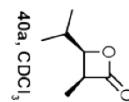


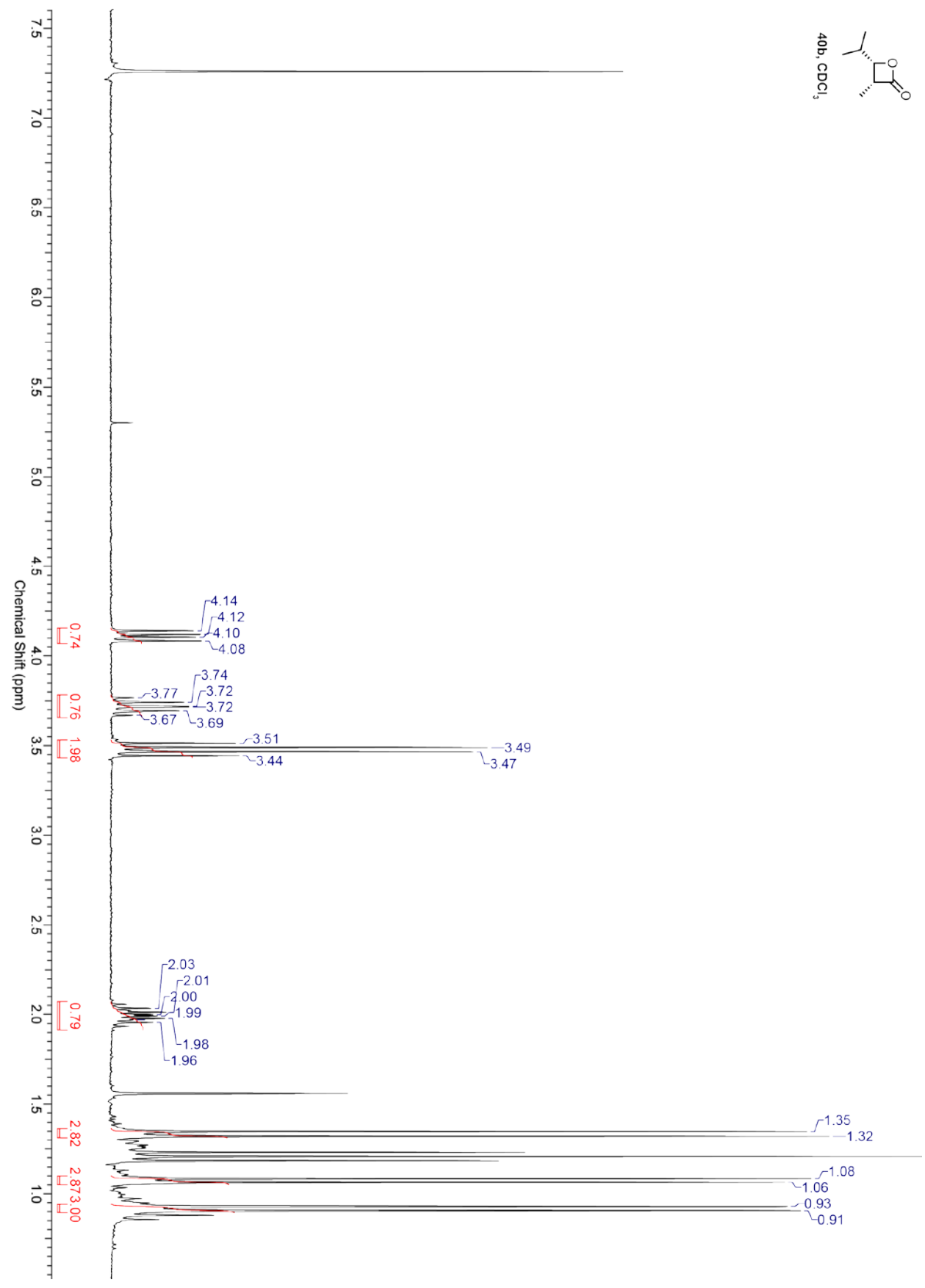
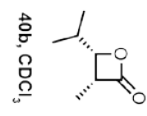
37, CDCl<sub>3</sub>

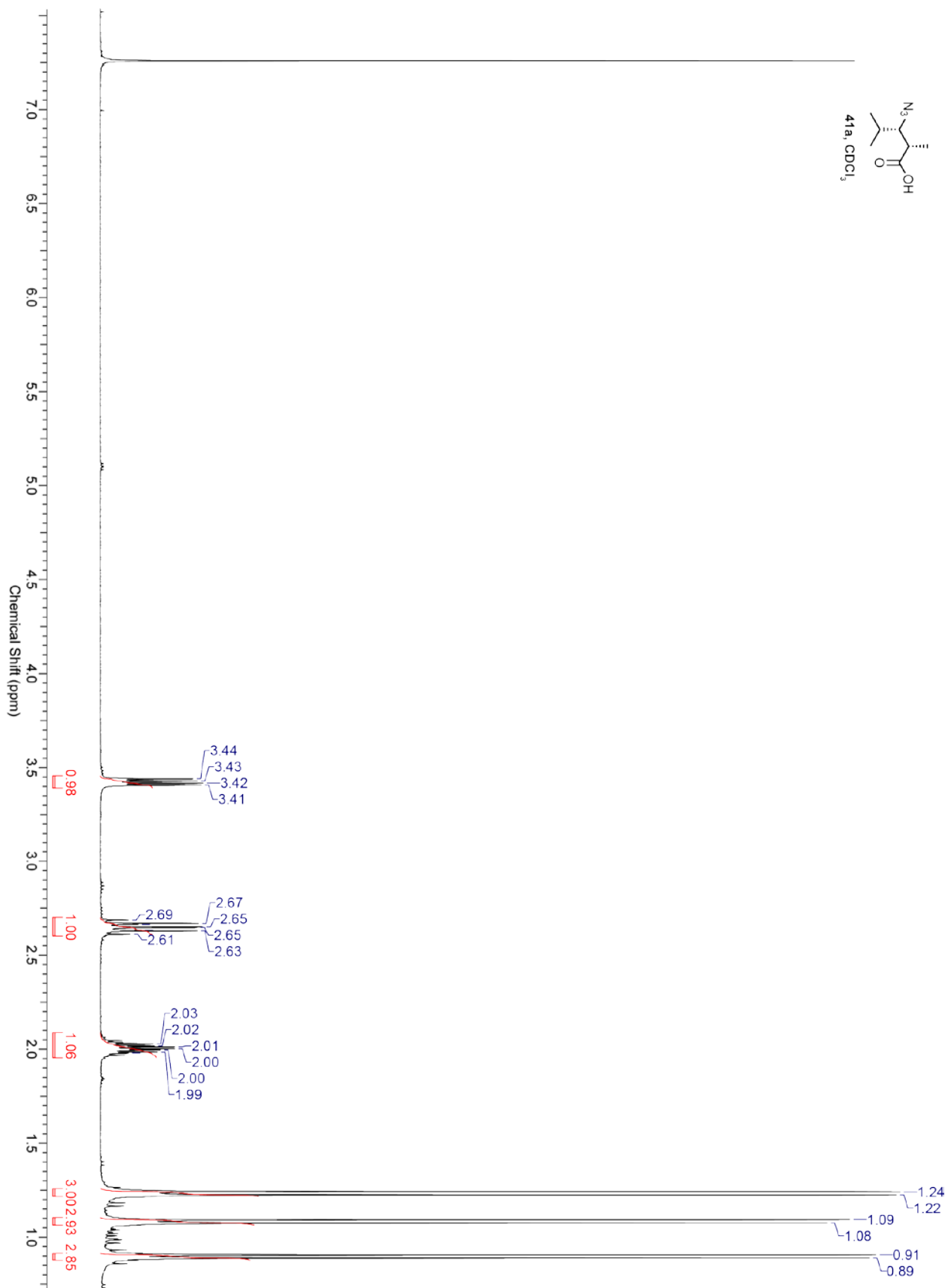
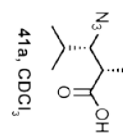


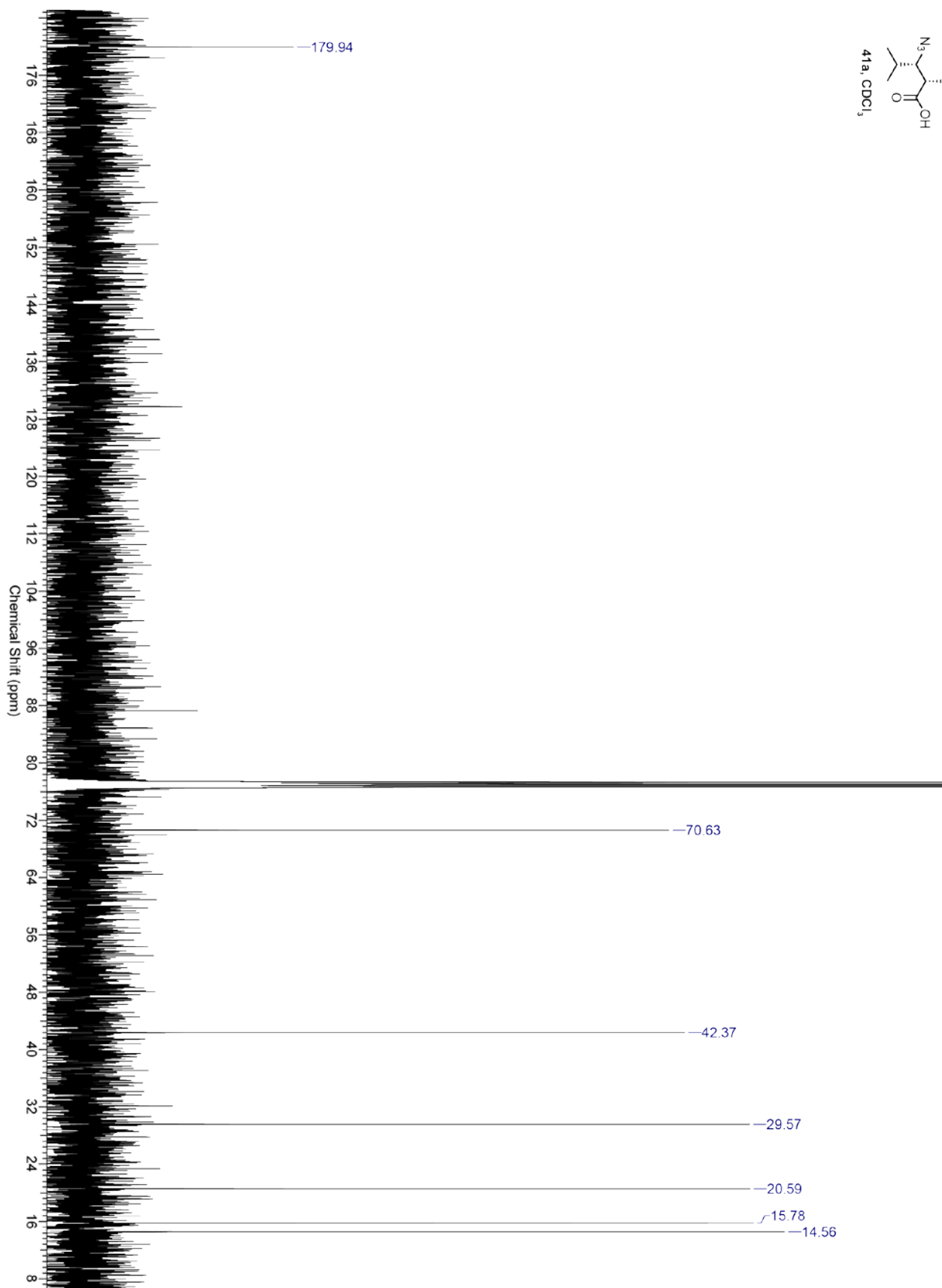
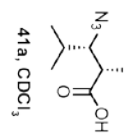


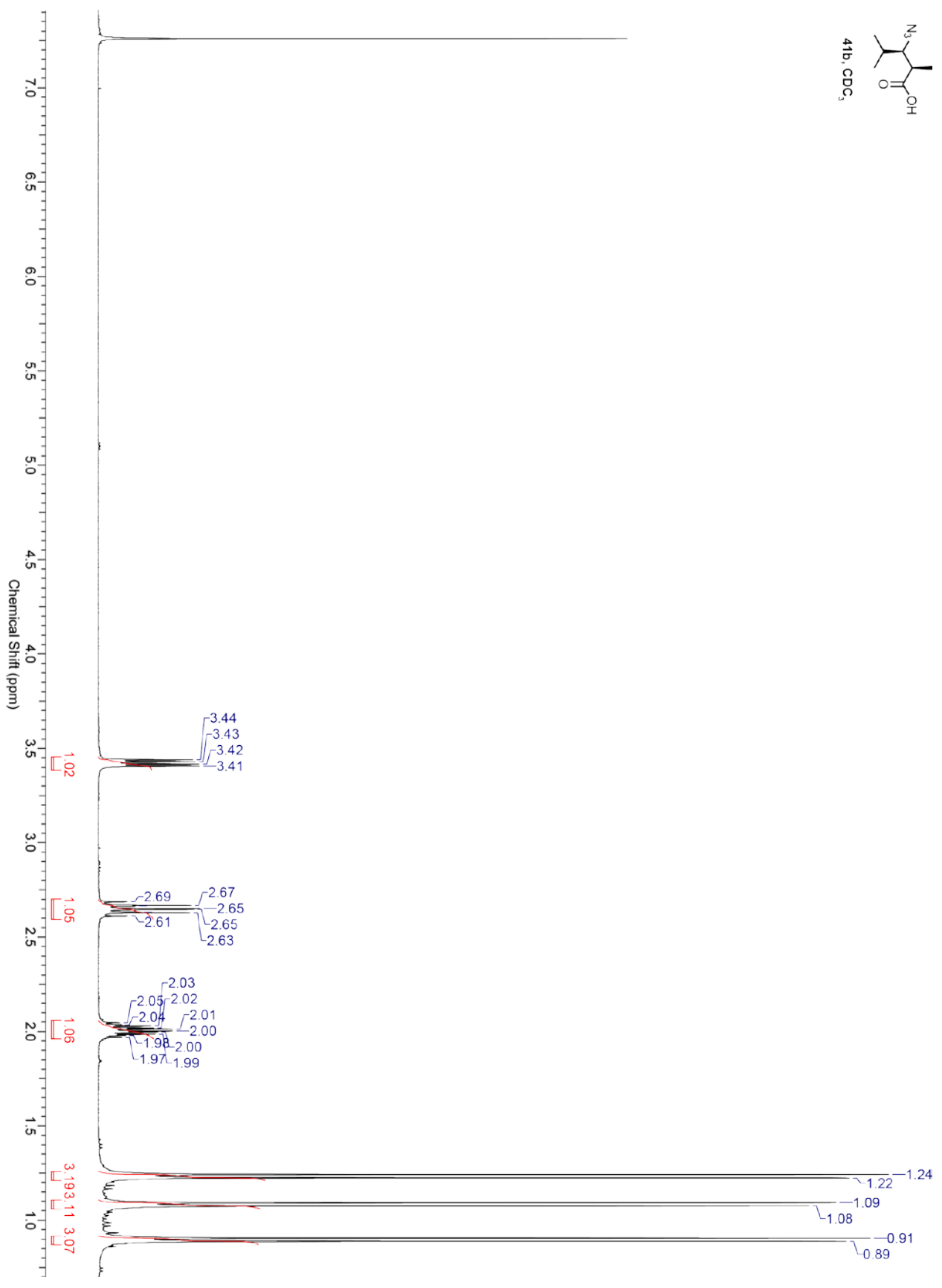
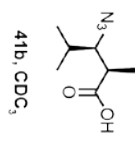


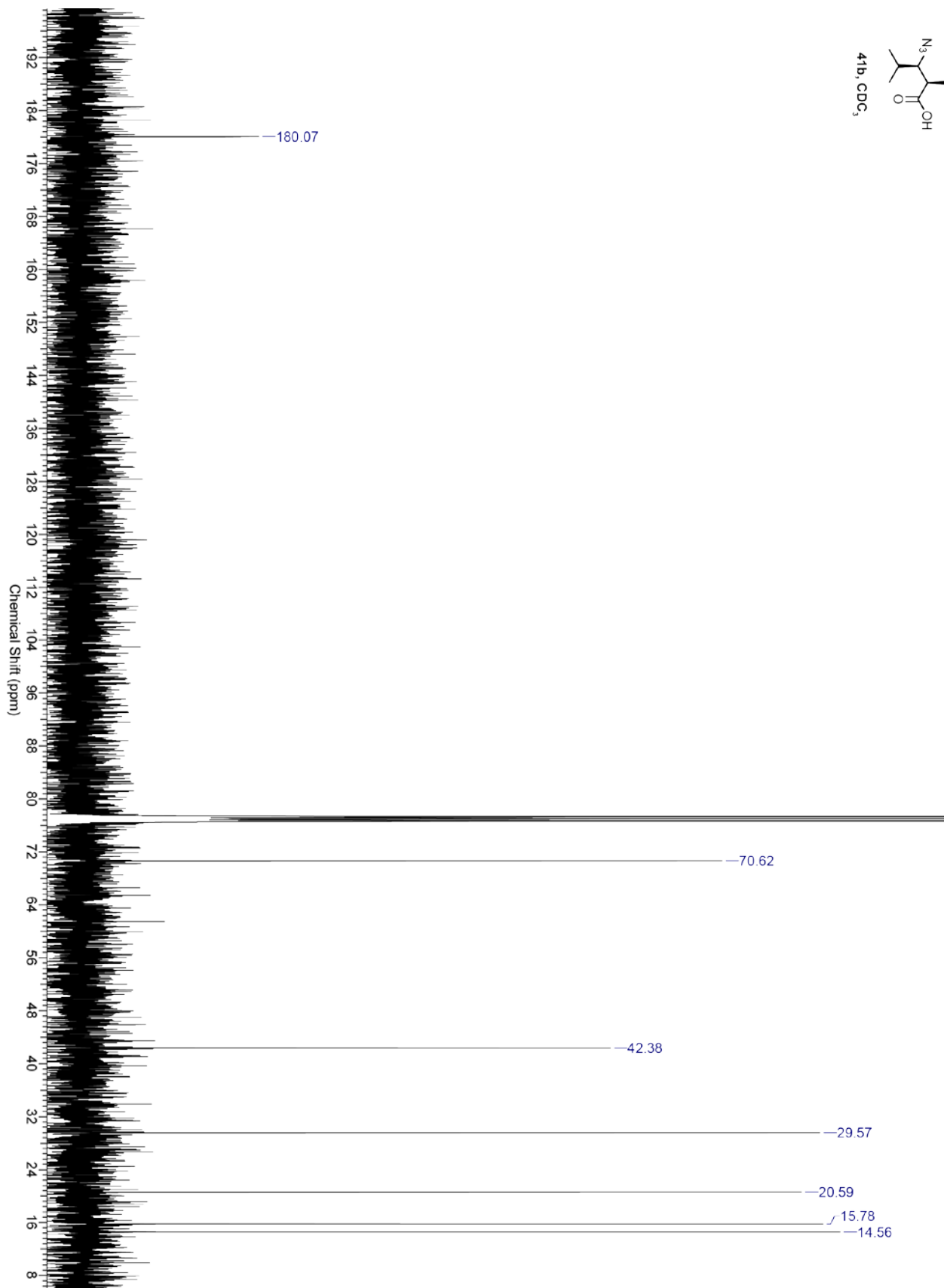
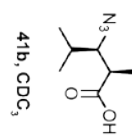


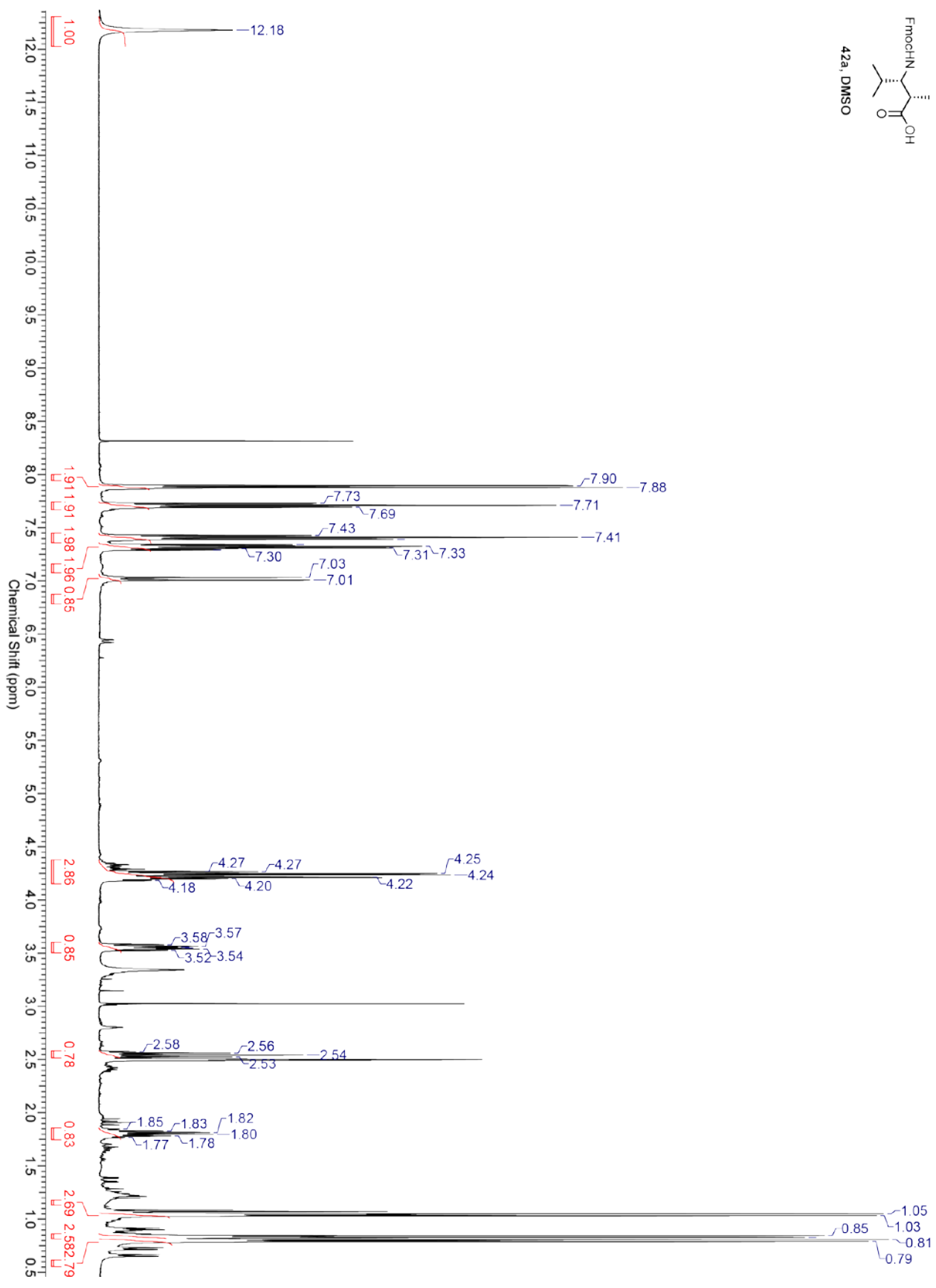
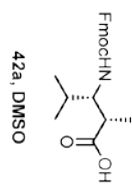


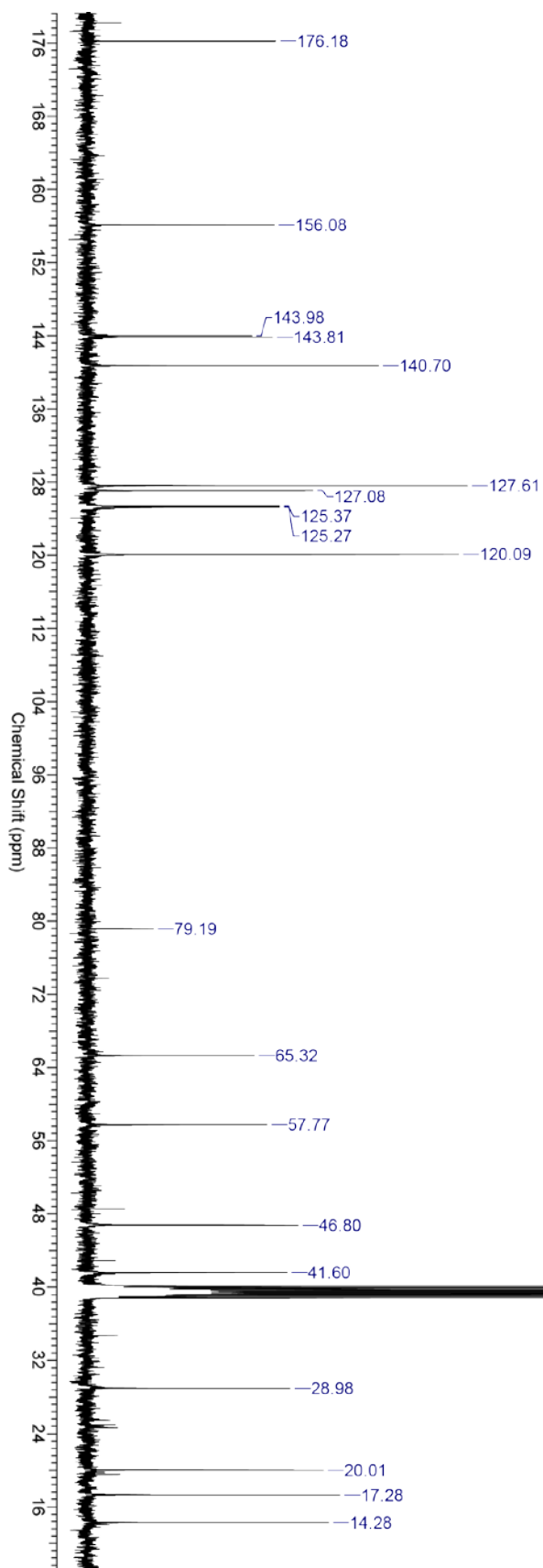
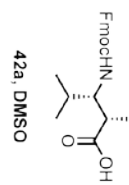


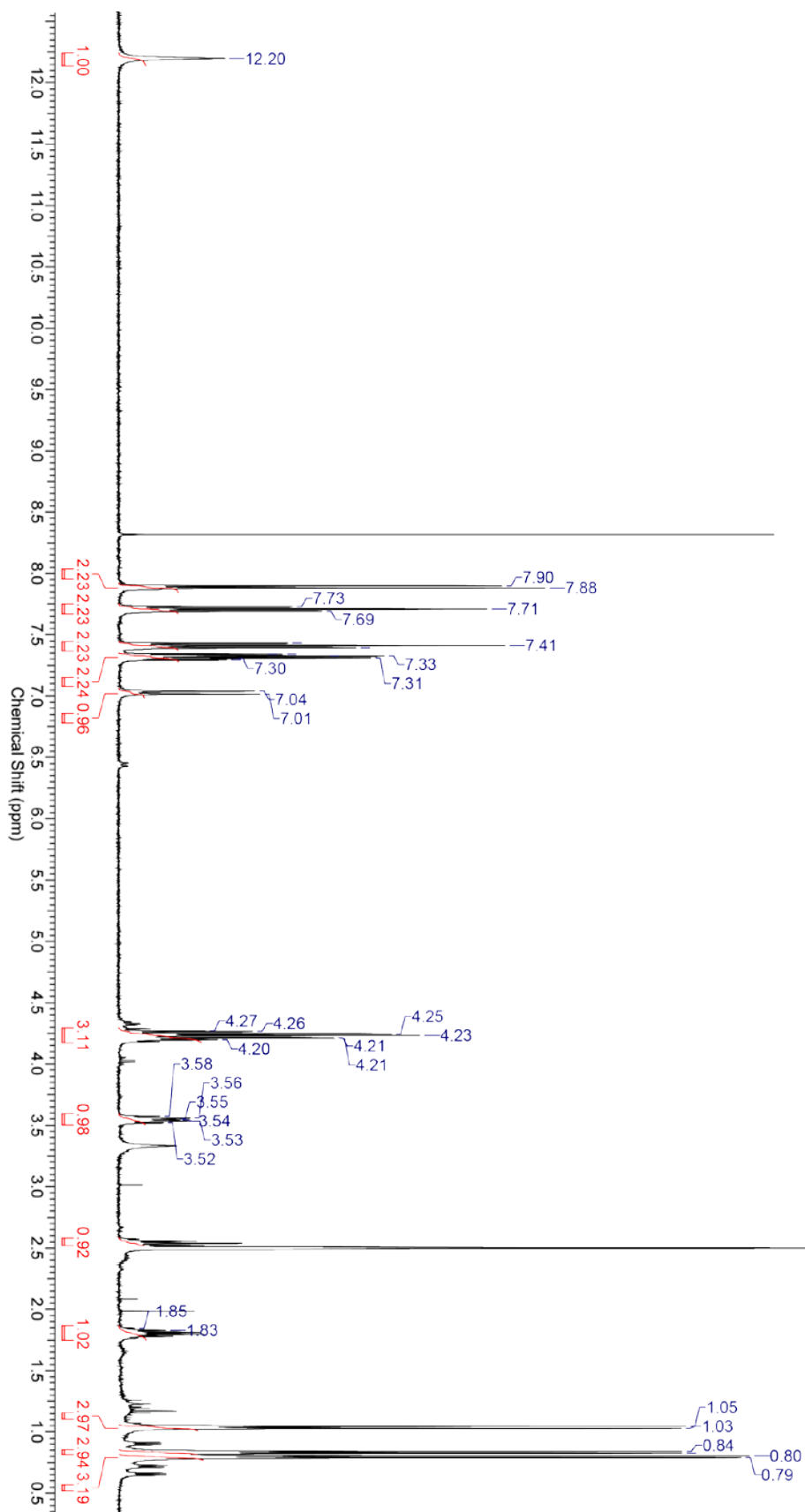
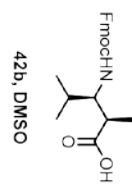


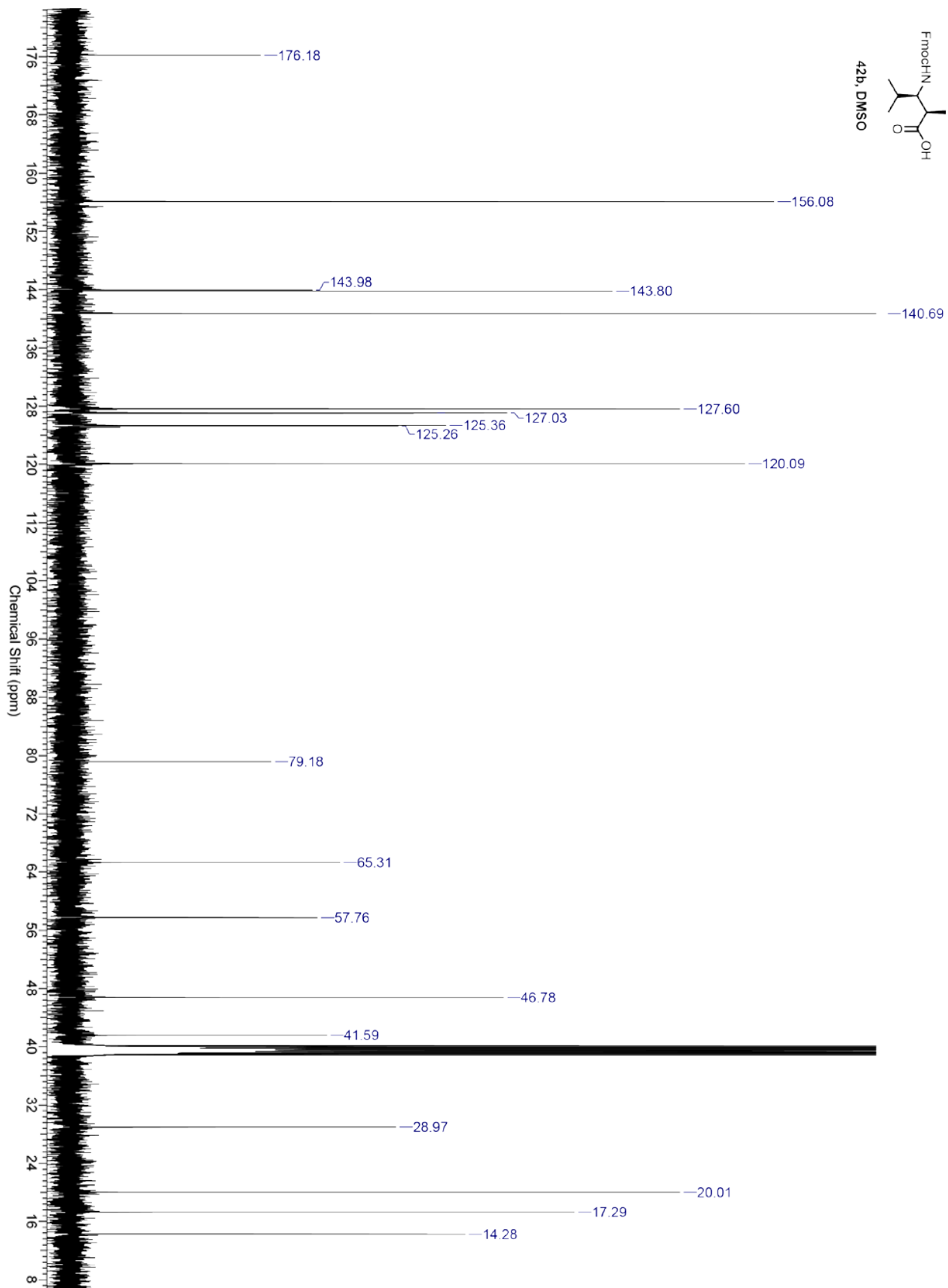


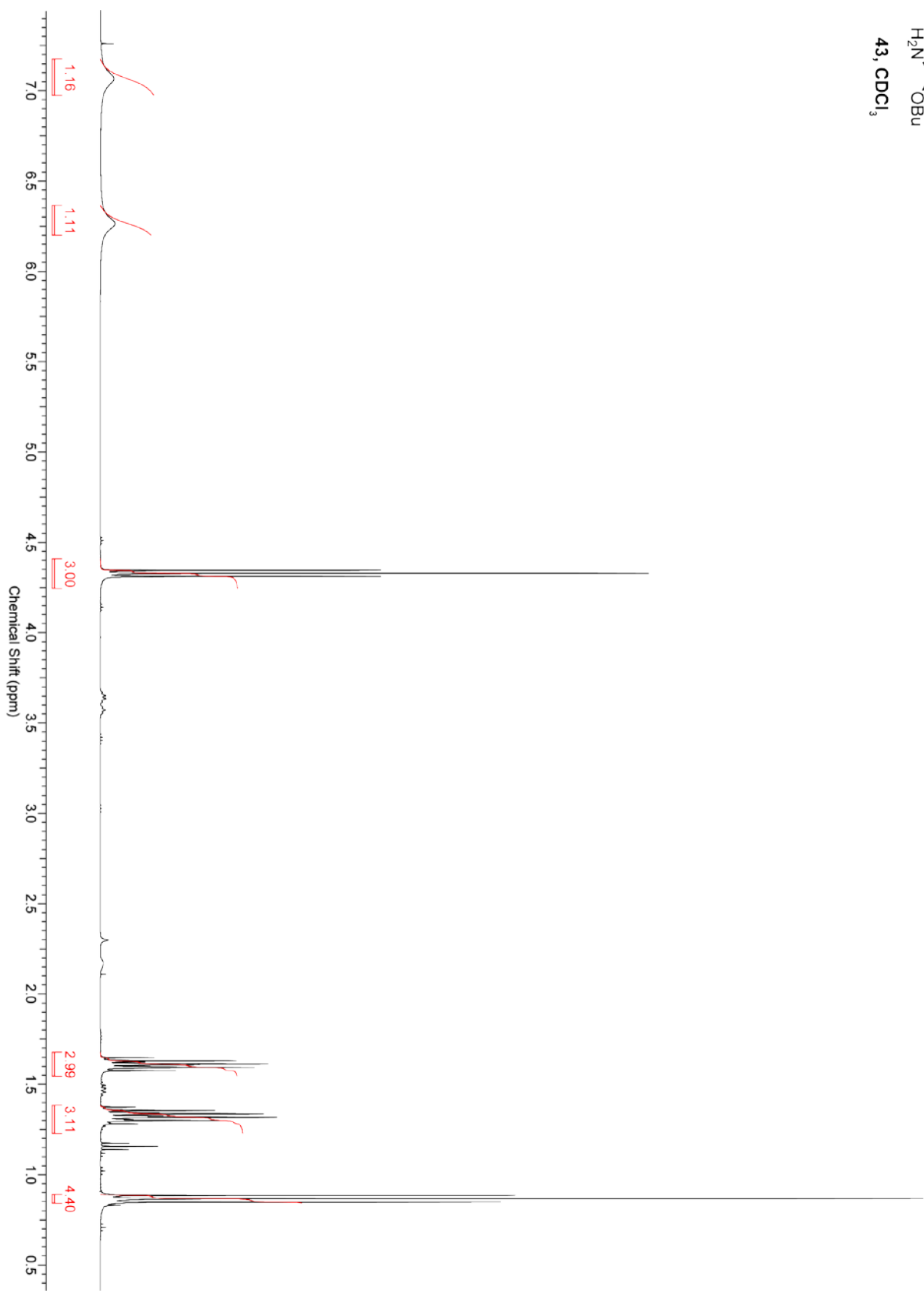
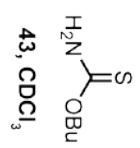


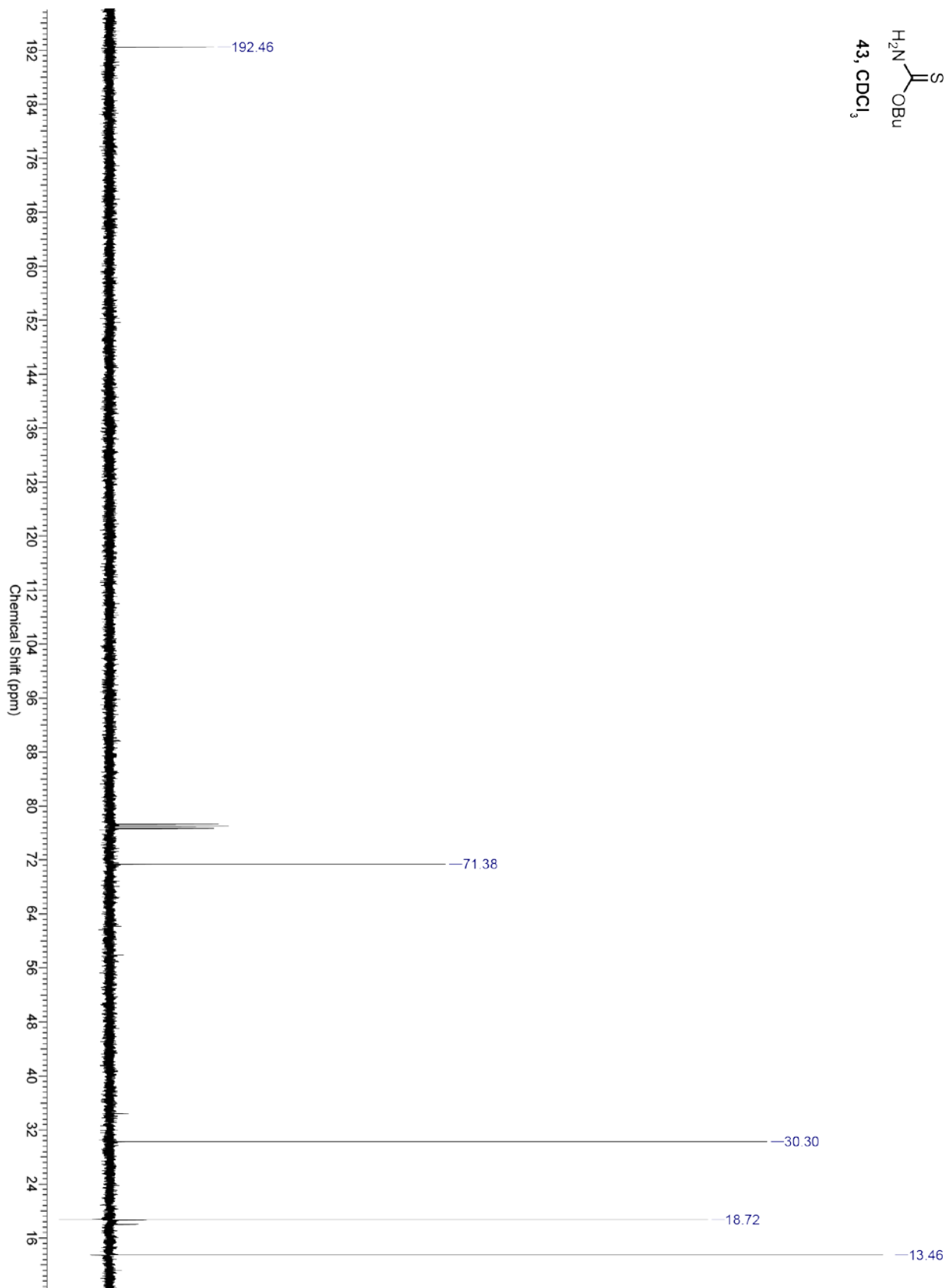
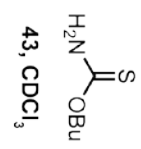


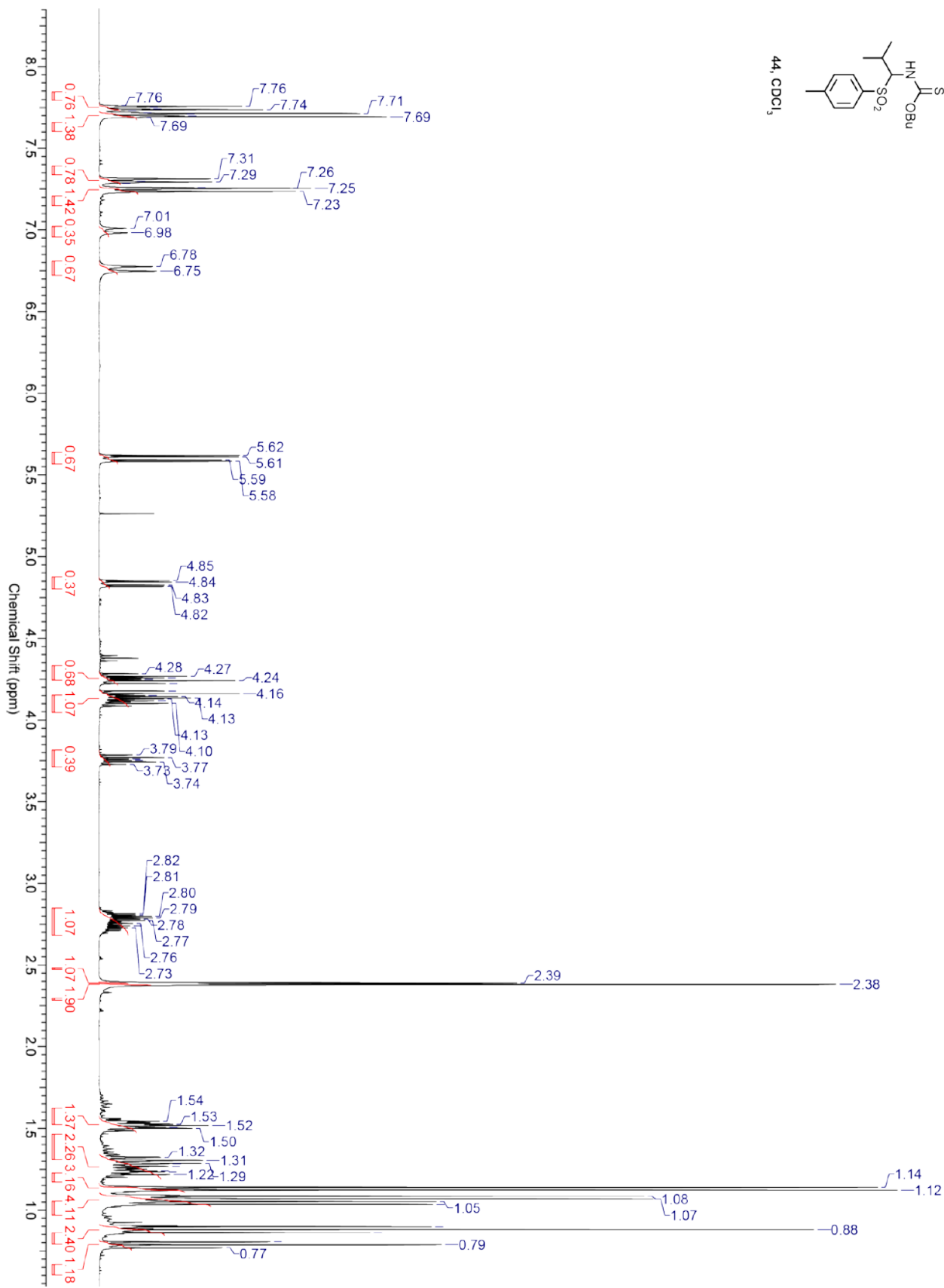


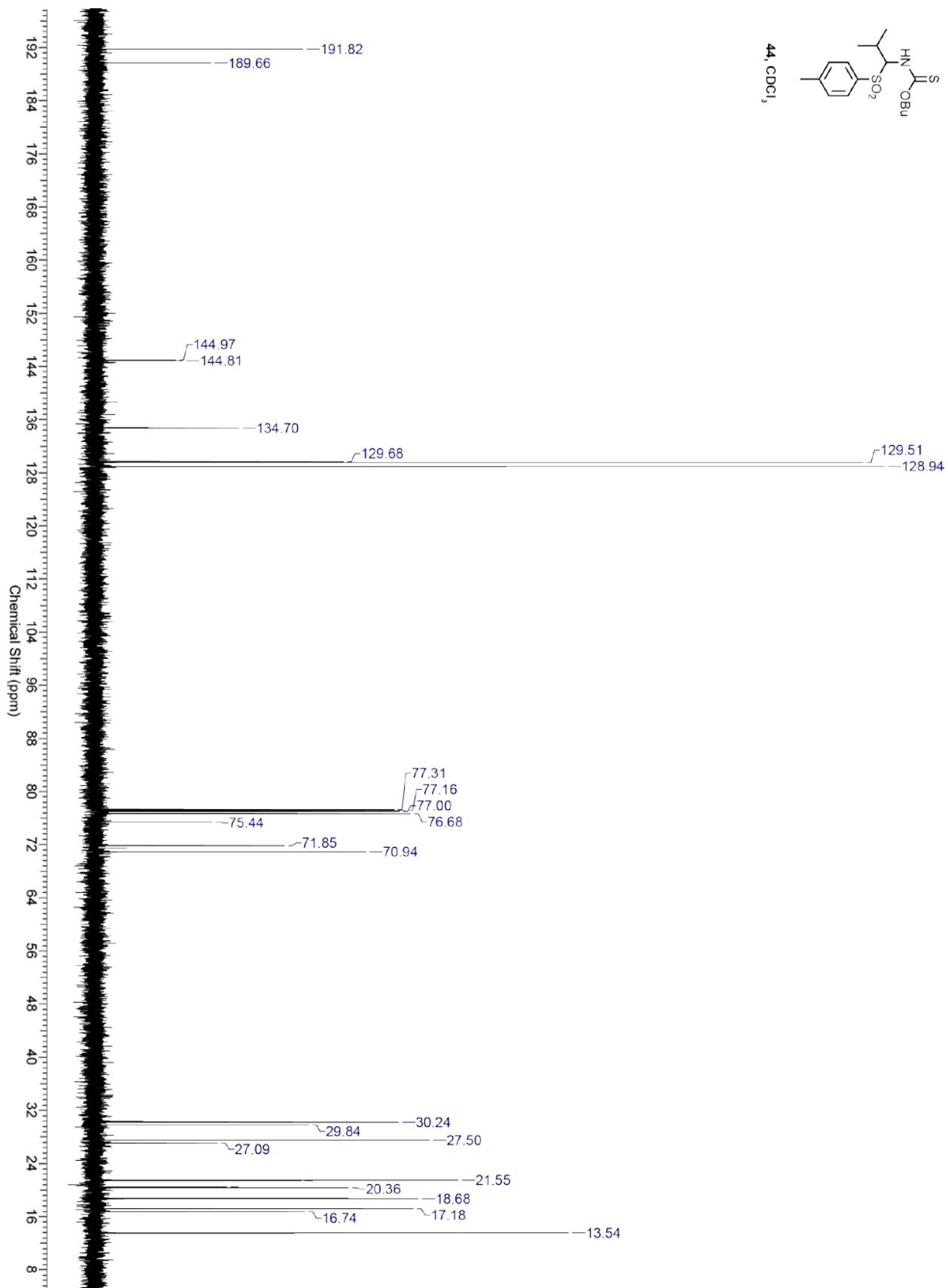
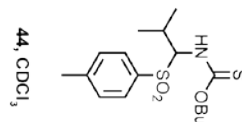


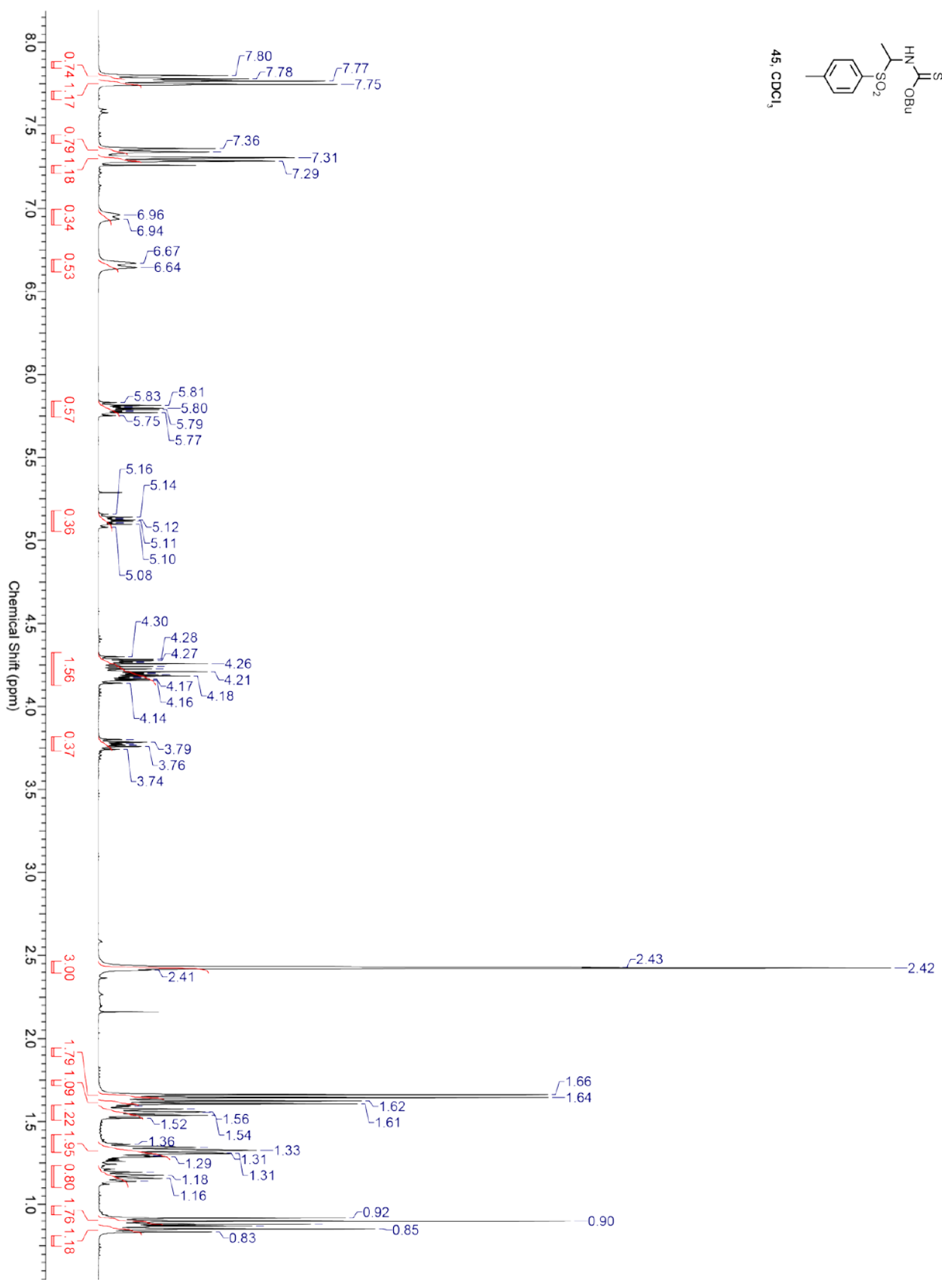
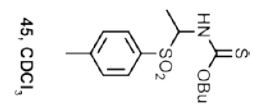


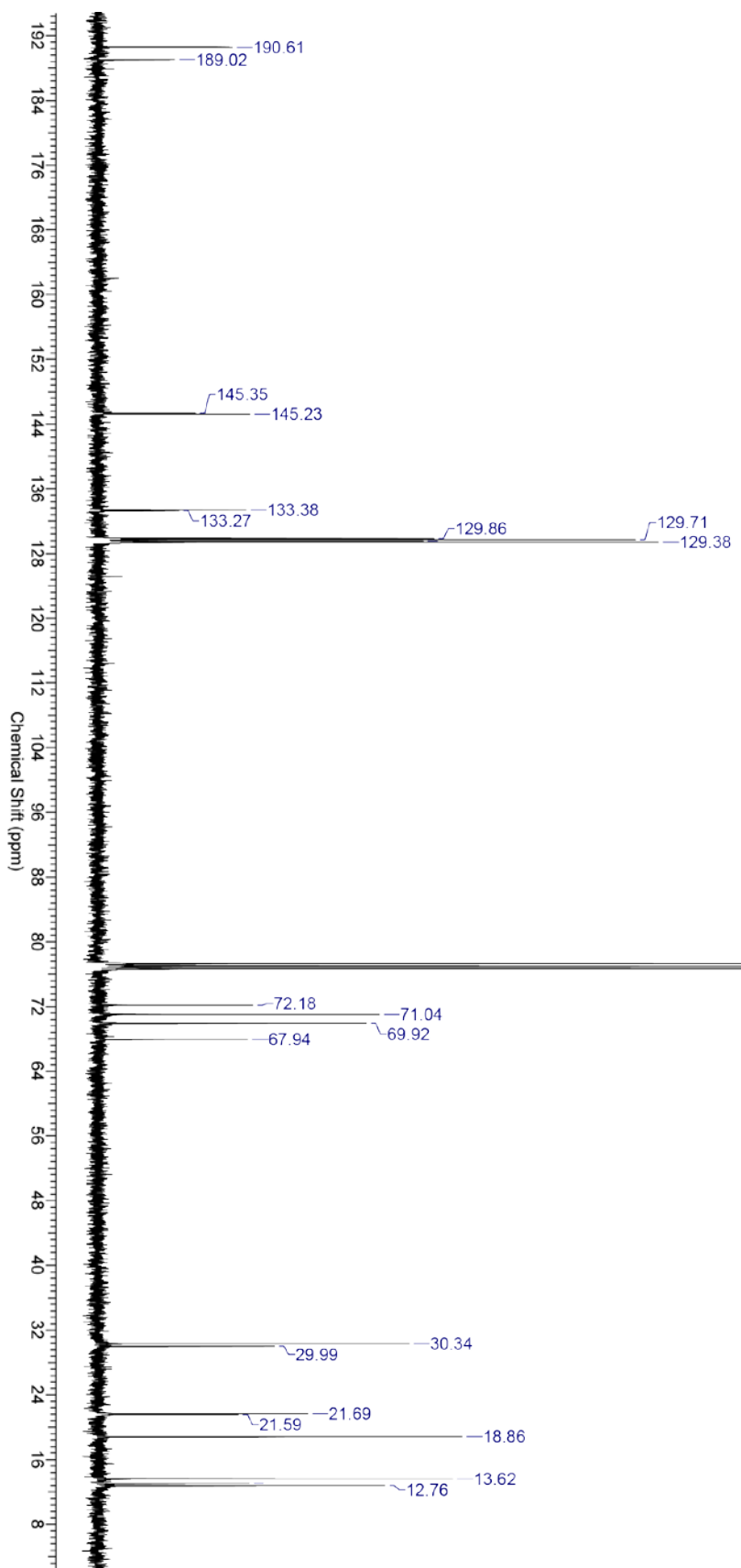
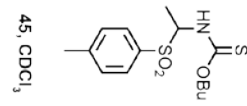


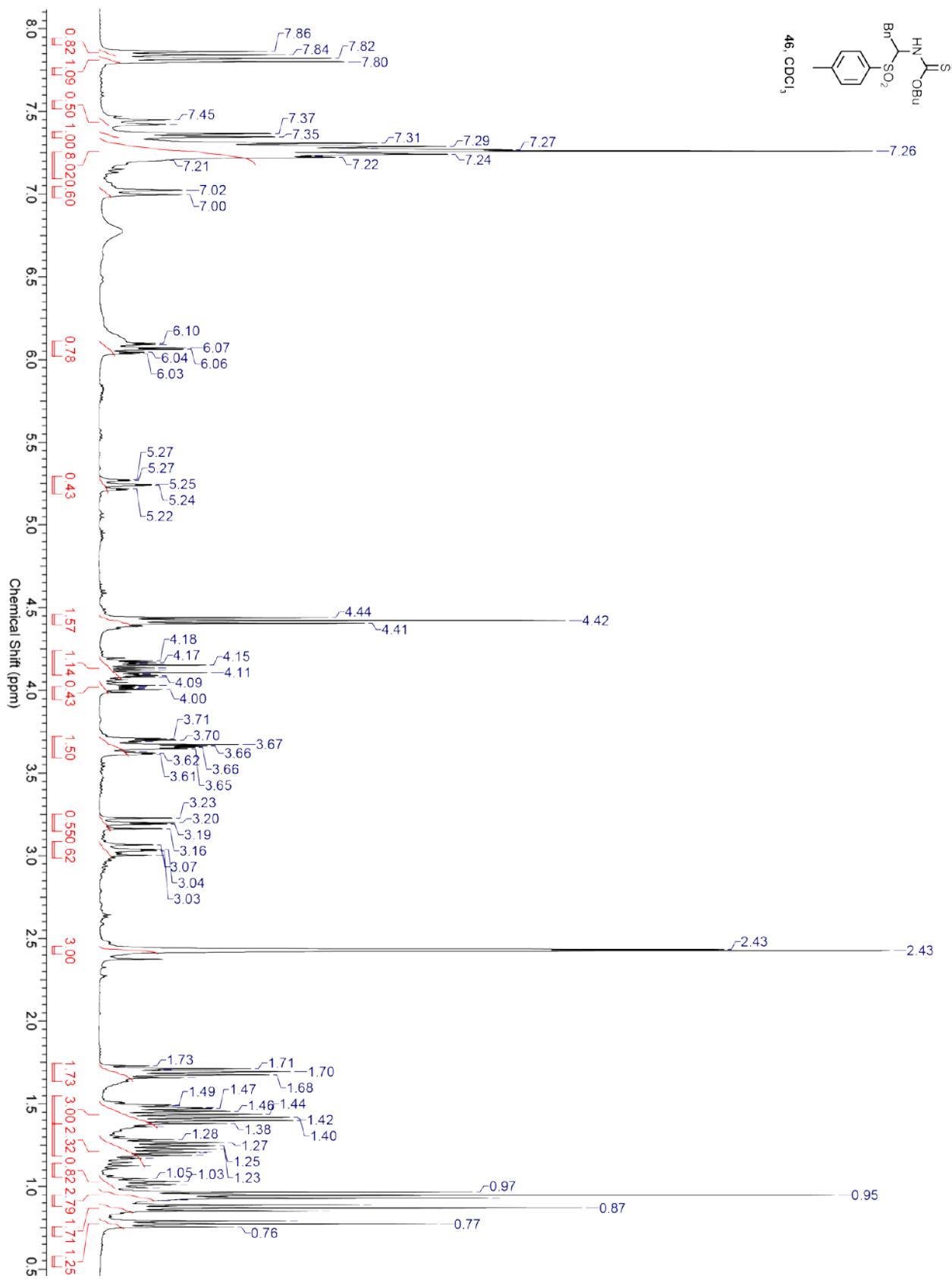


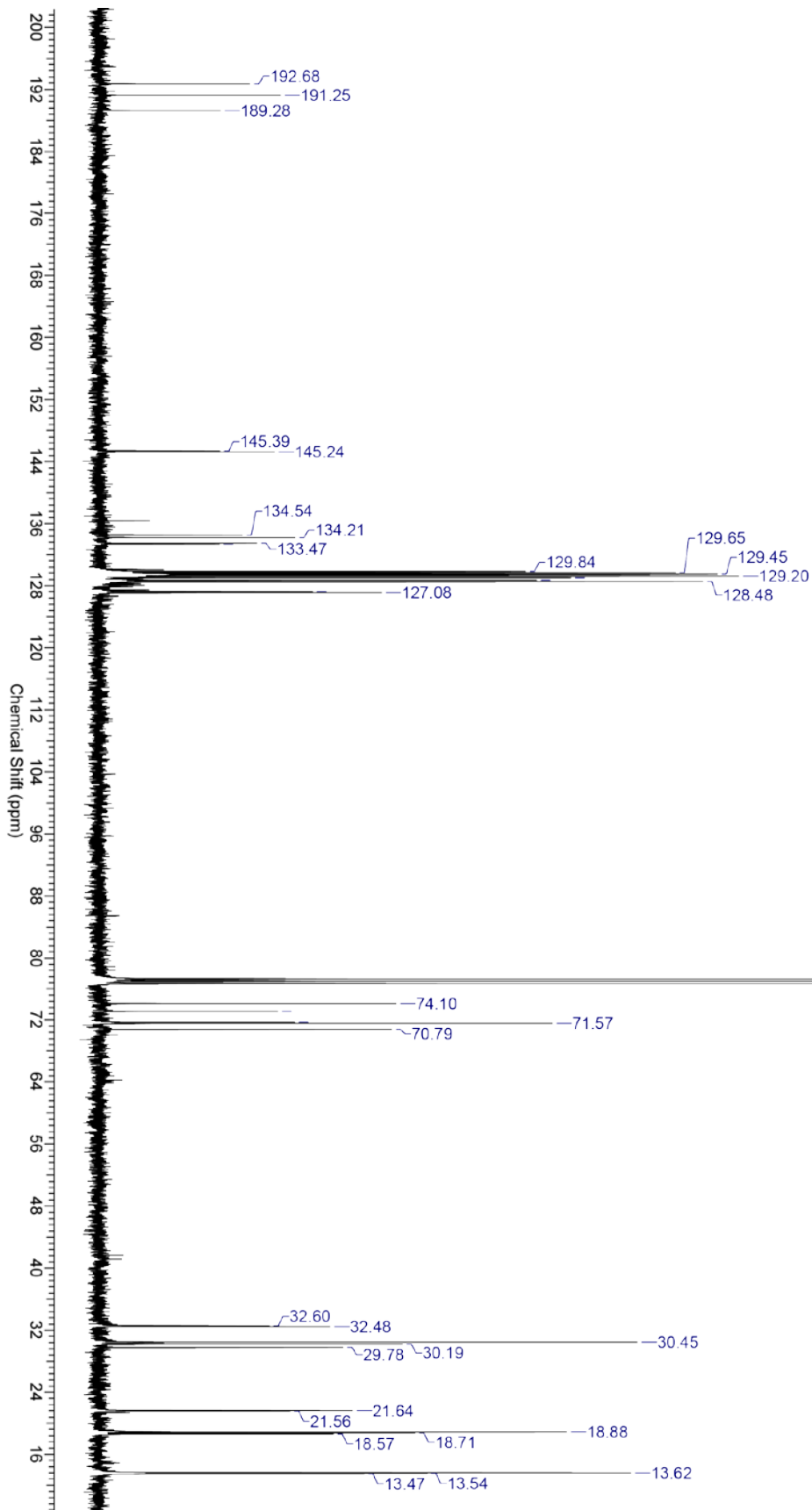
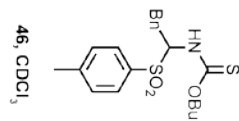


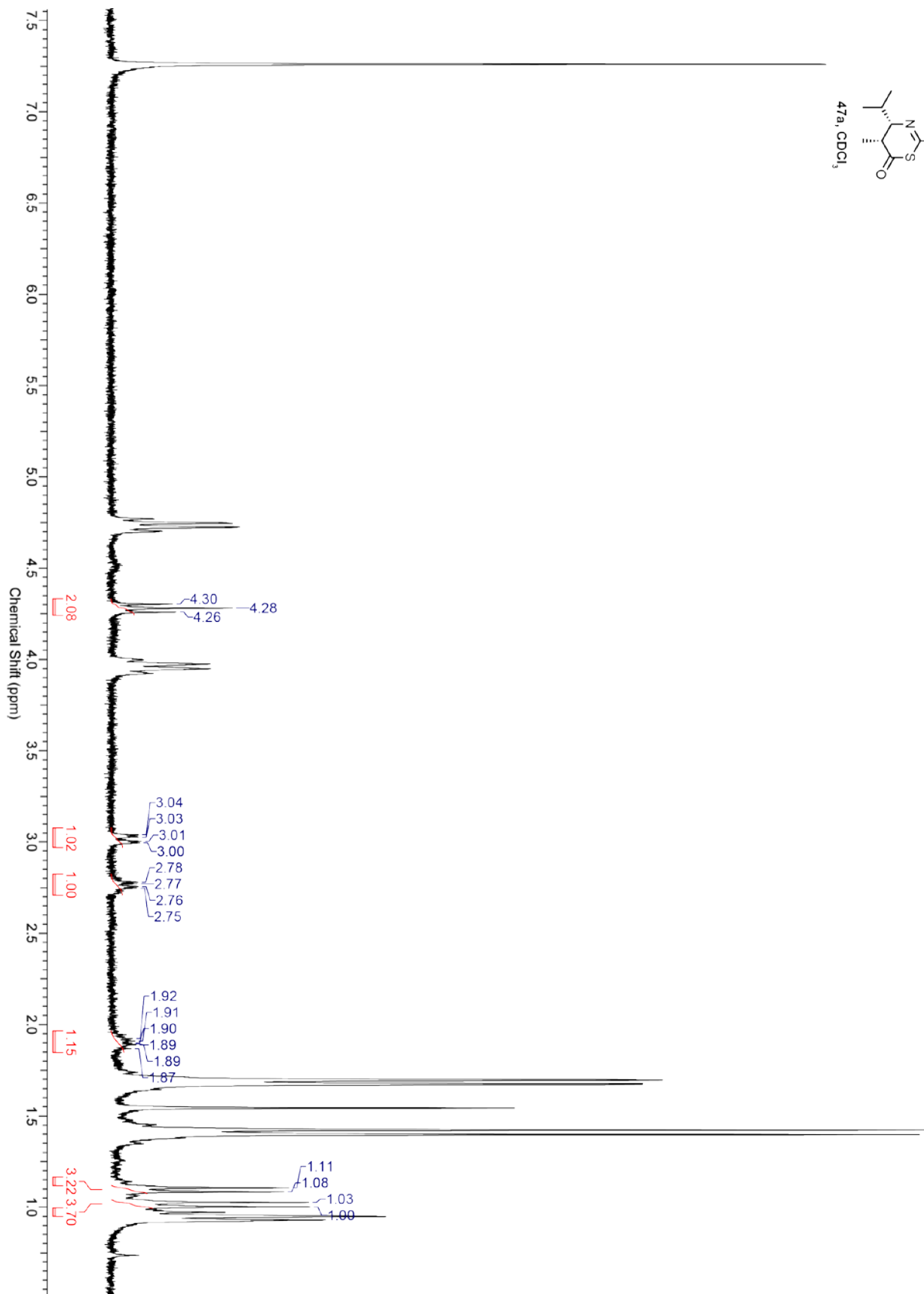
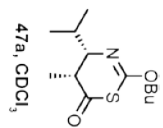


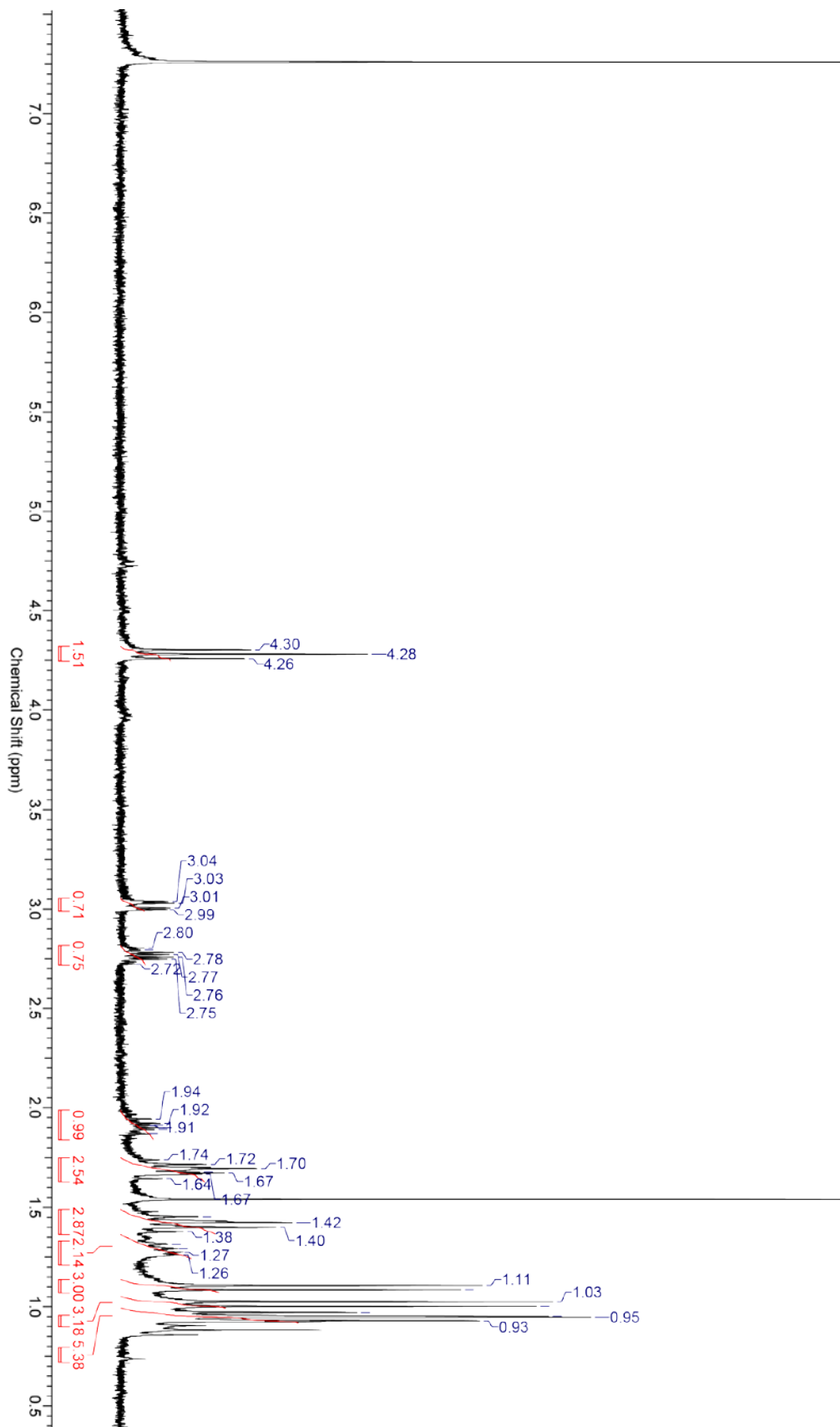
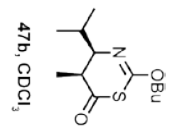


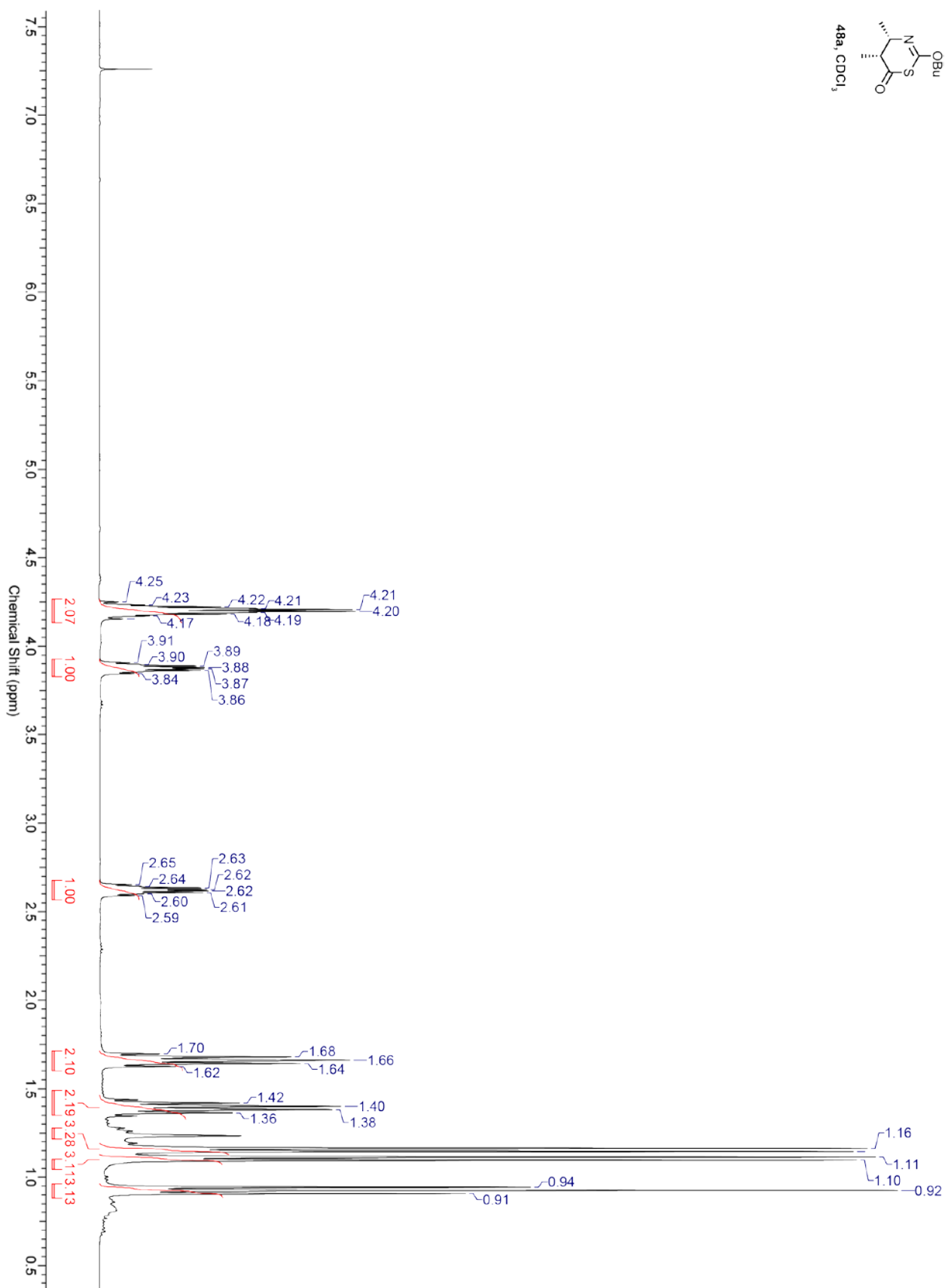
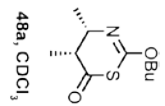


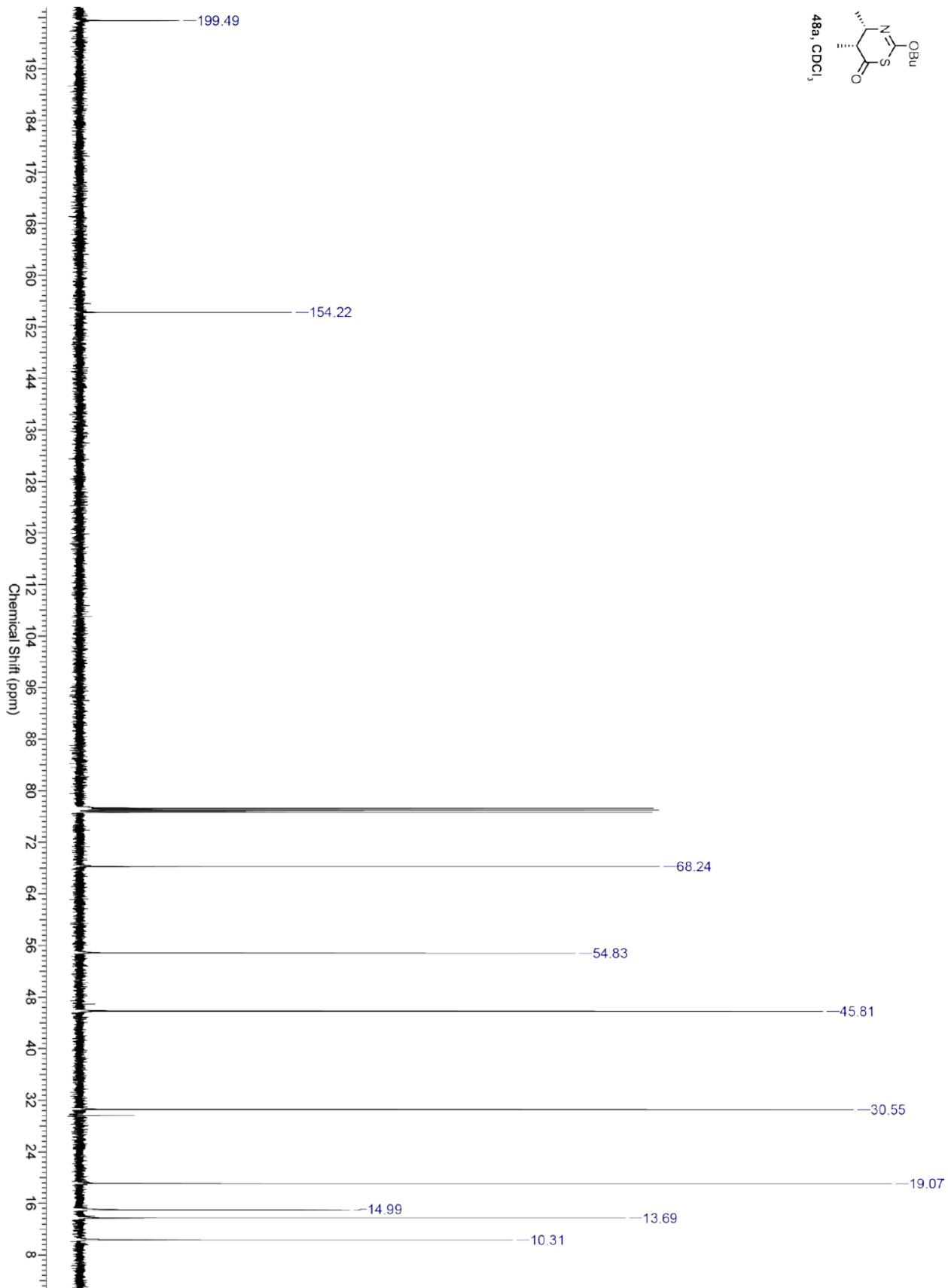
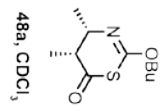


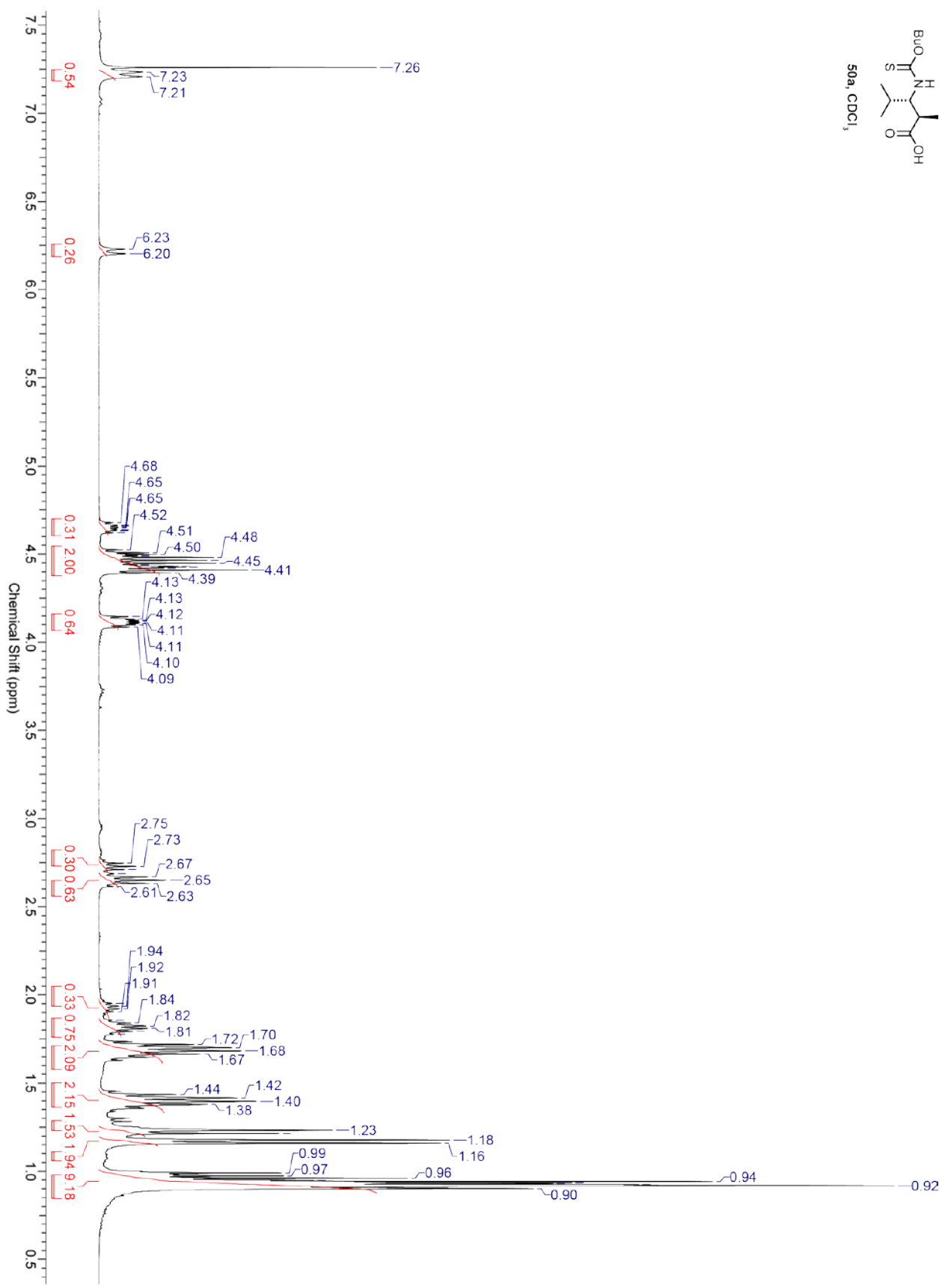
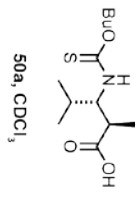


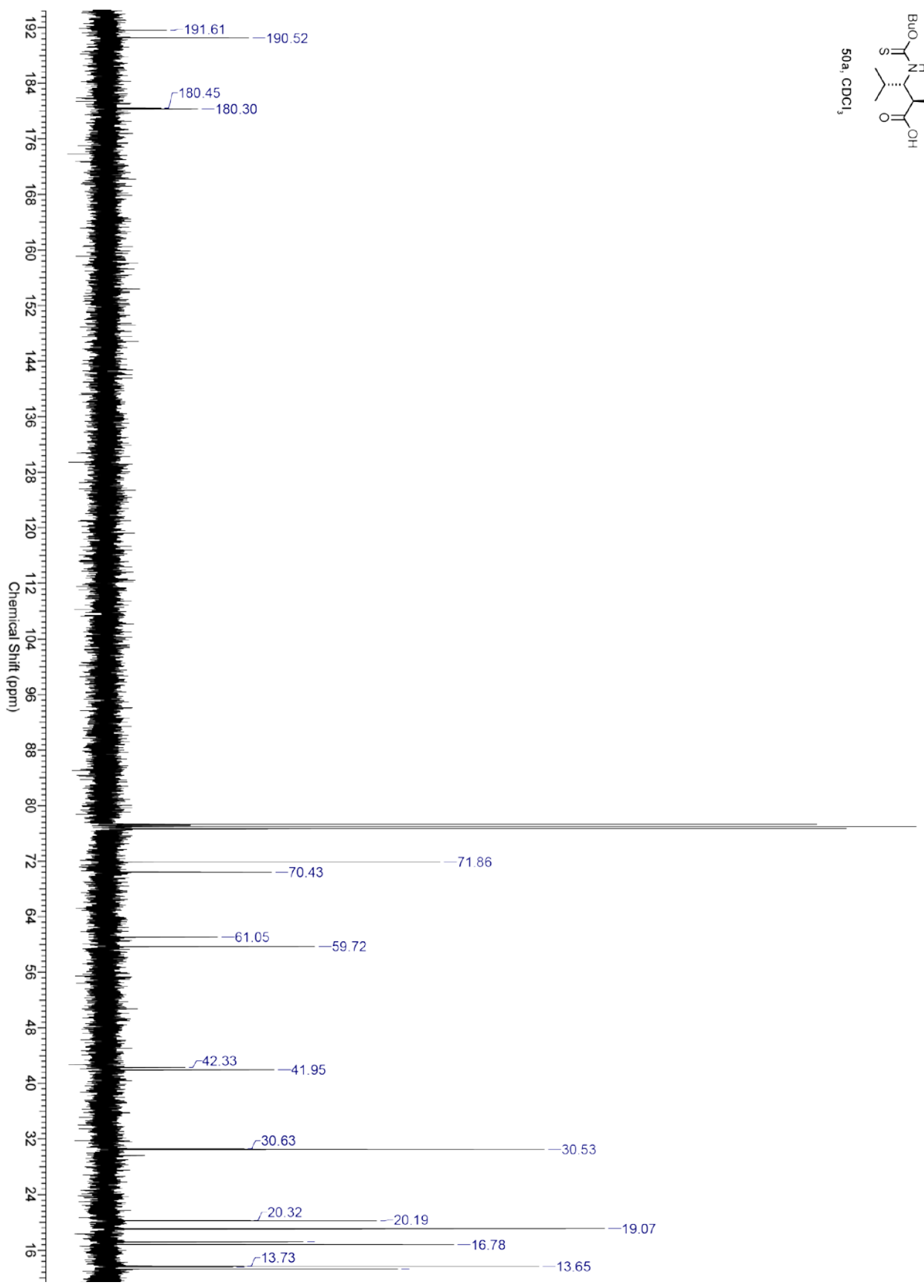
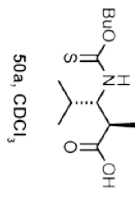


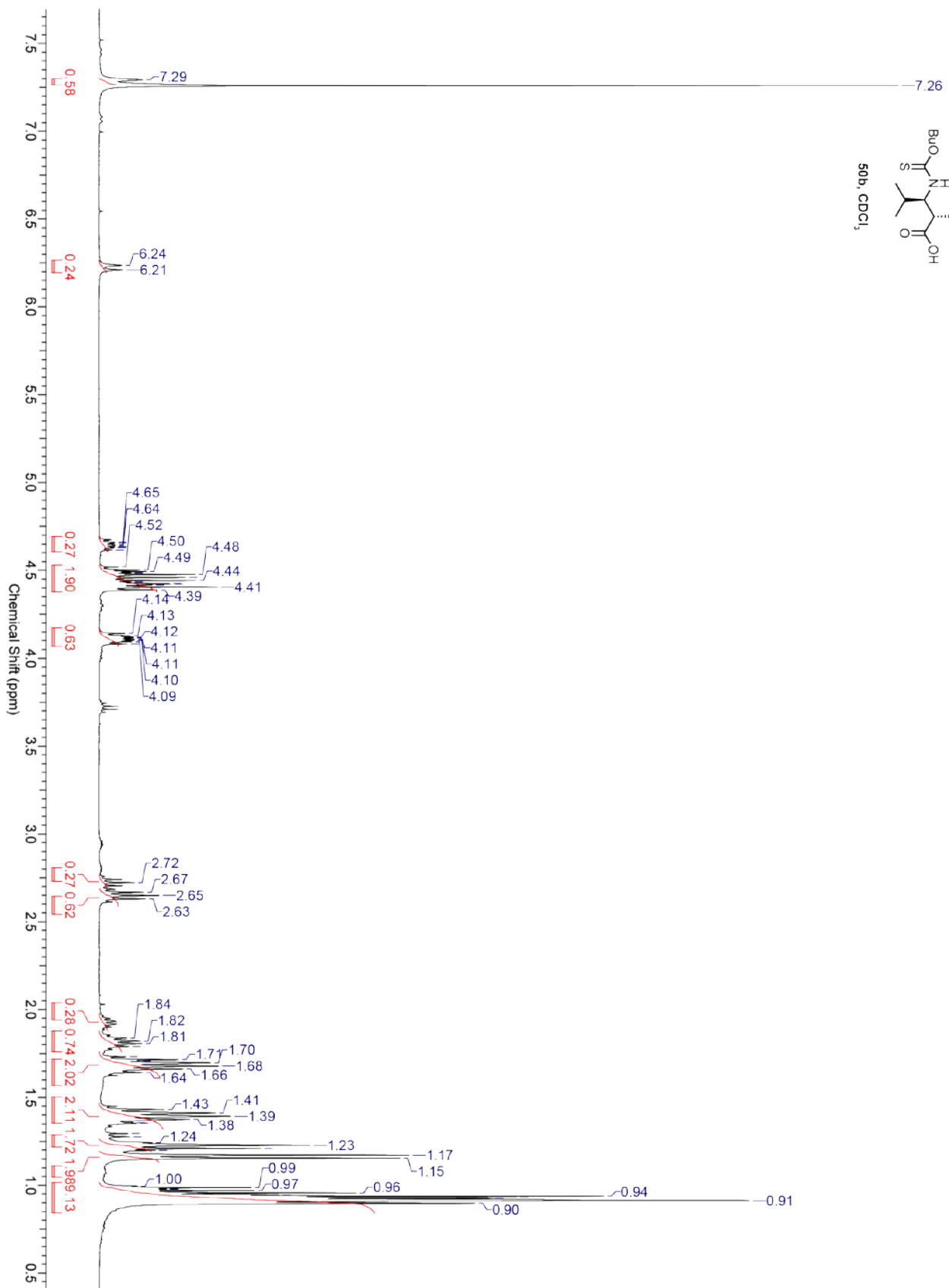


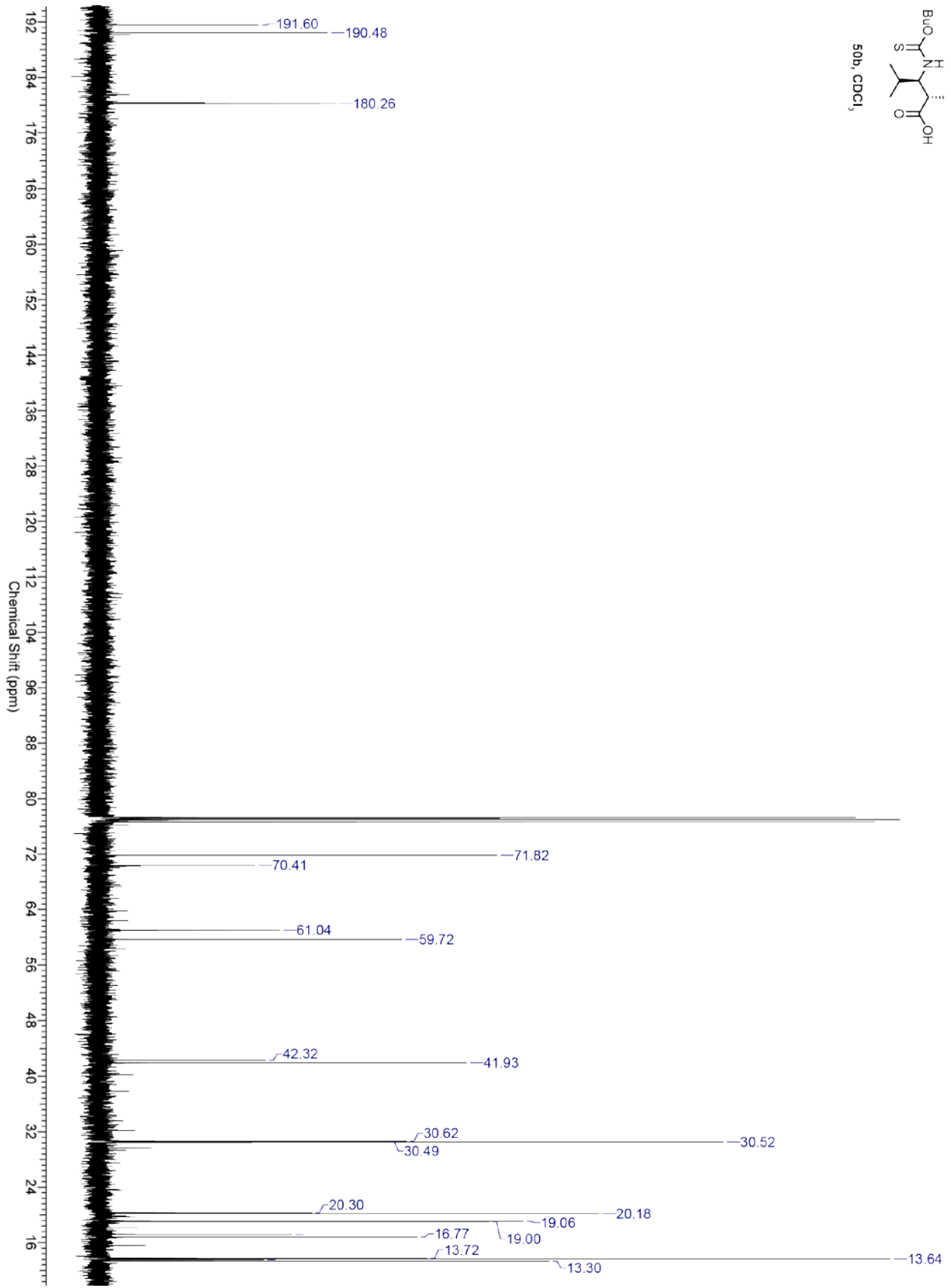
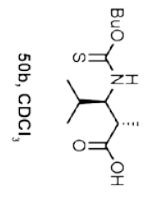


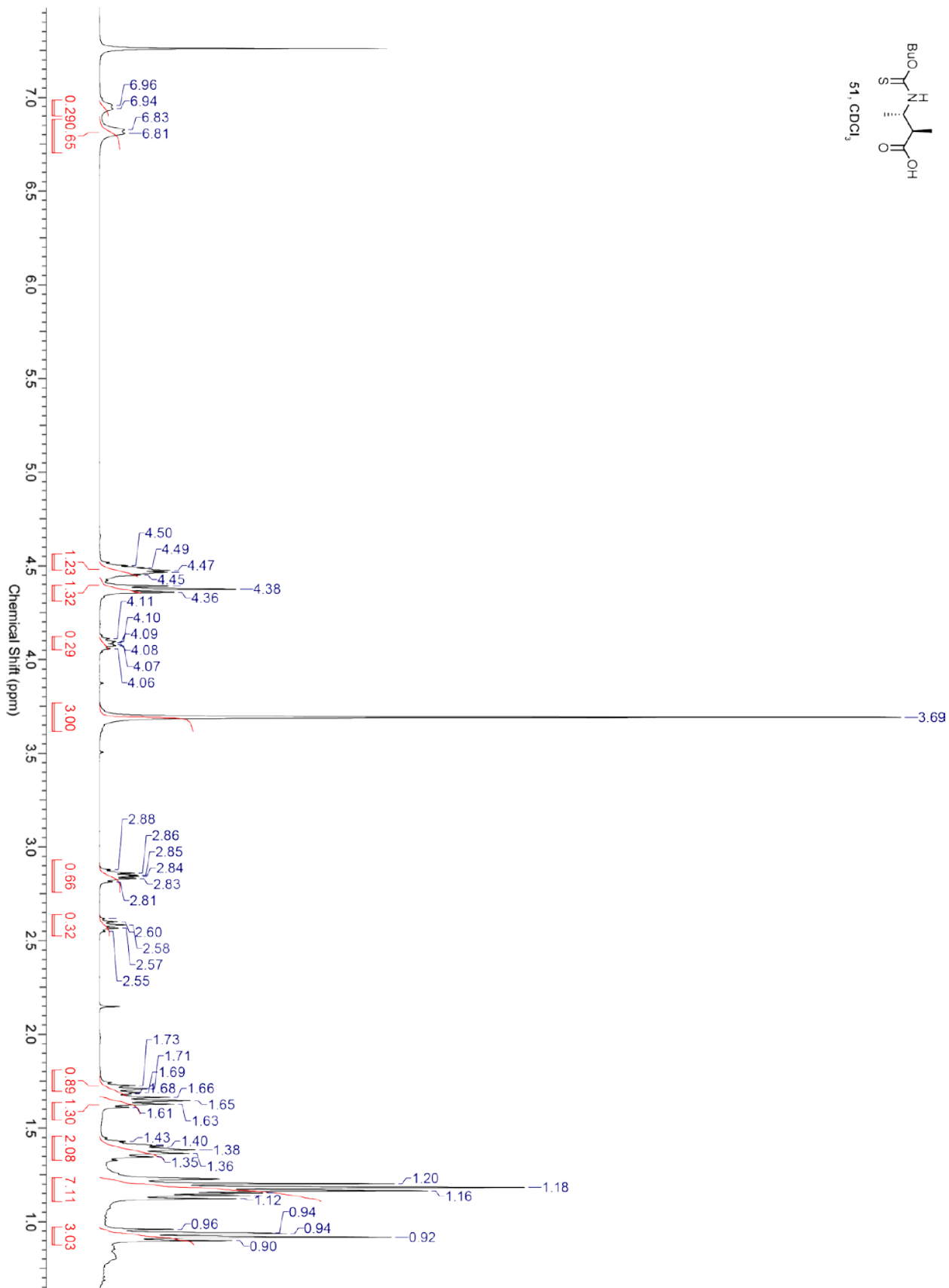
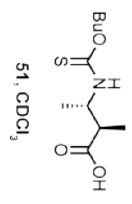


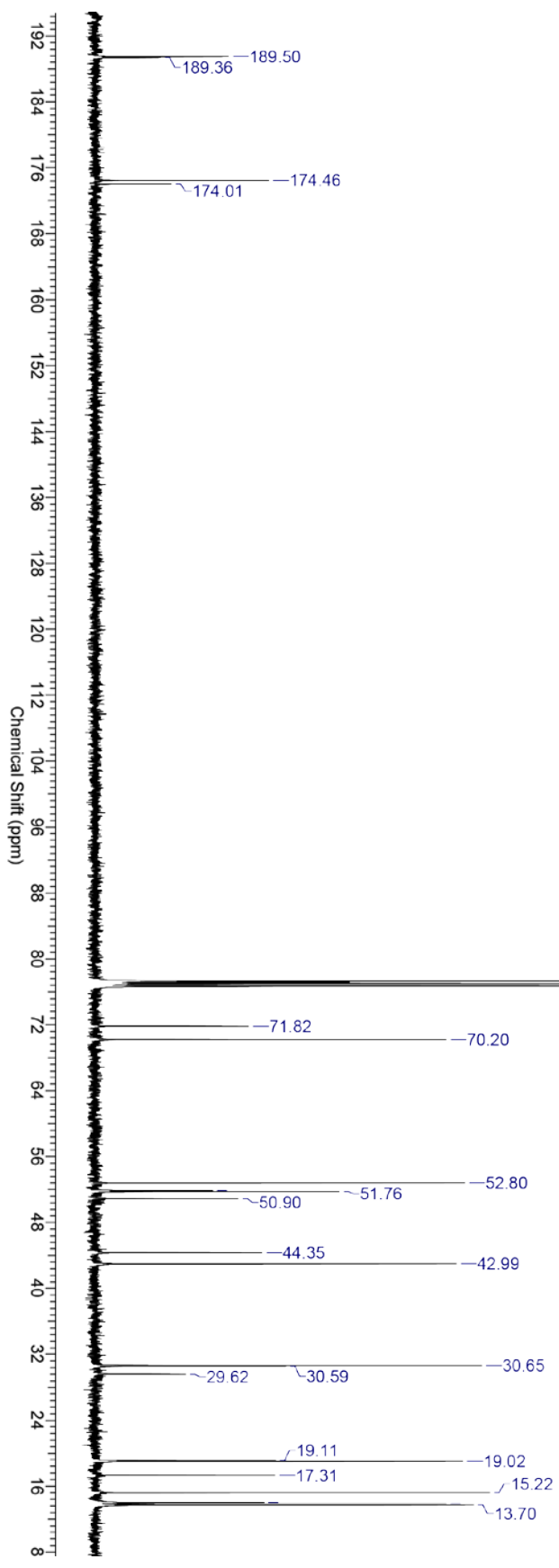
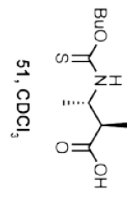


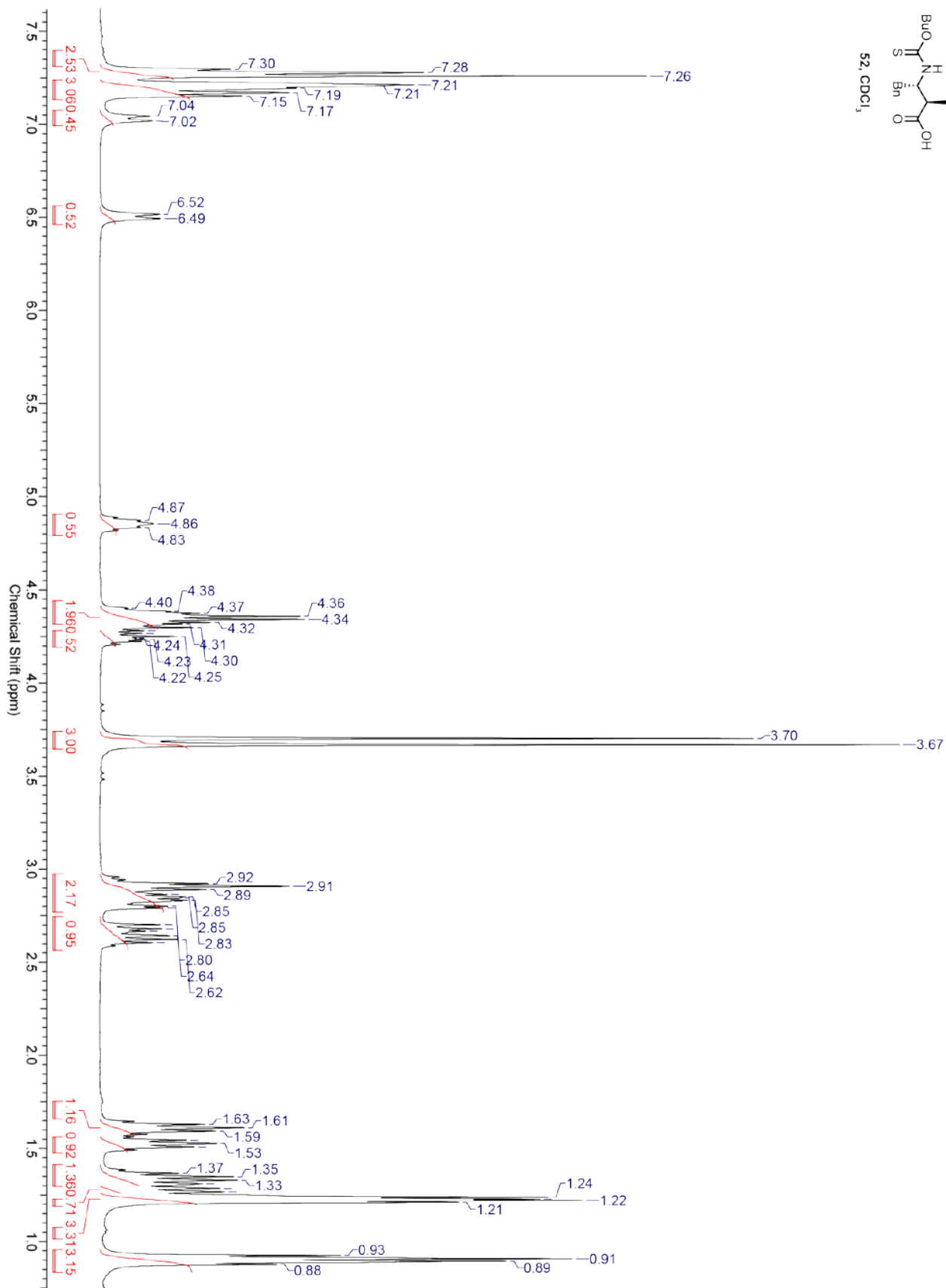
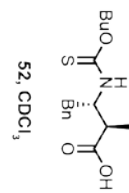


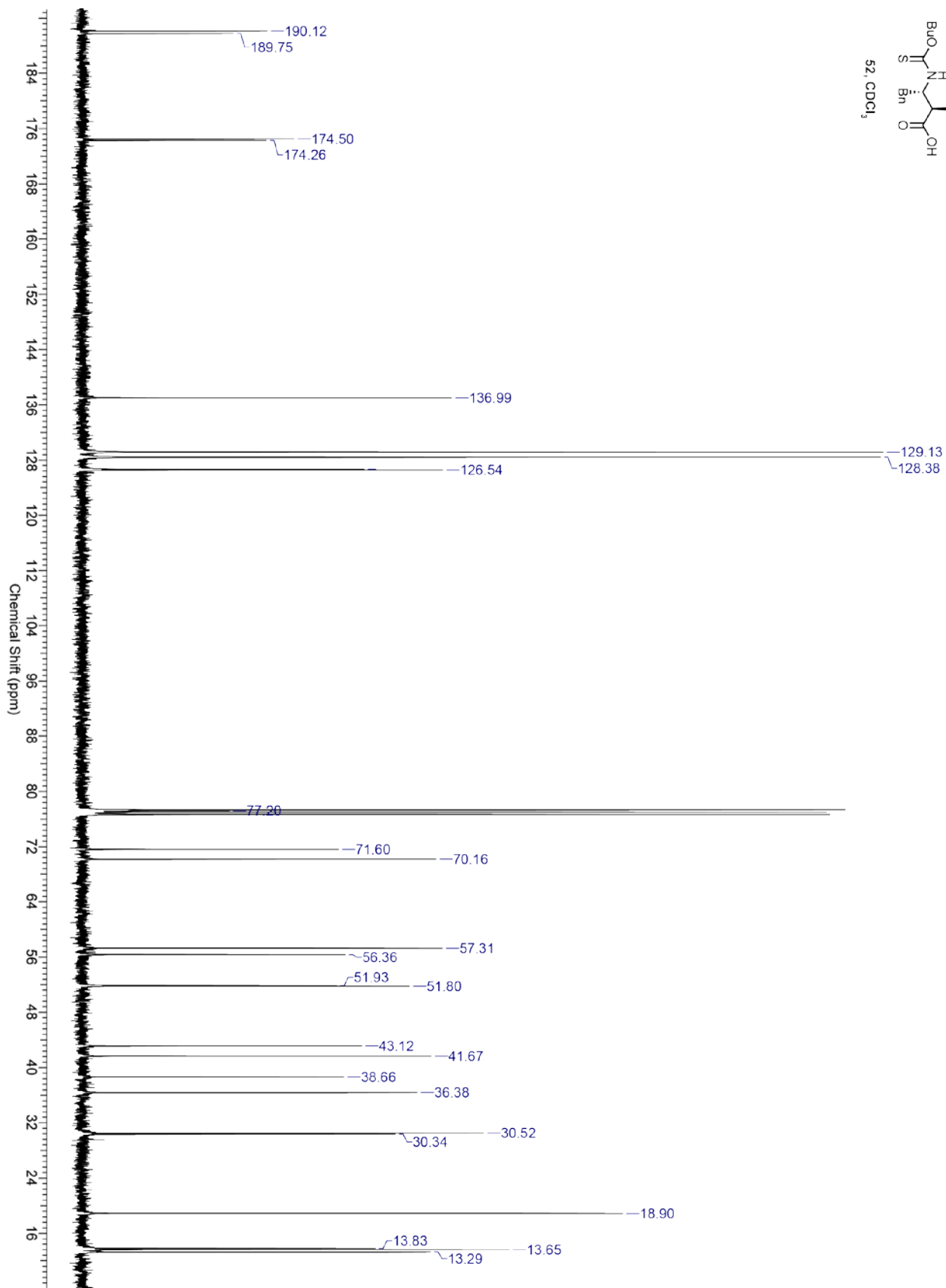
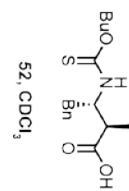


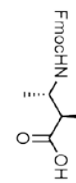




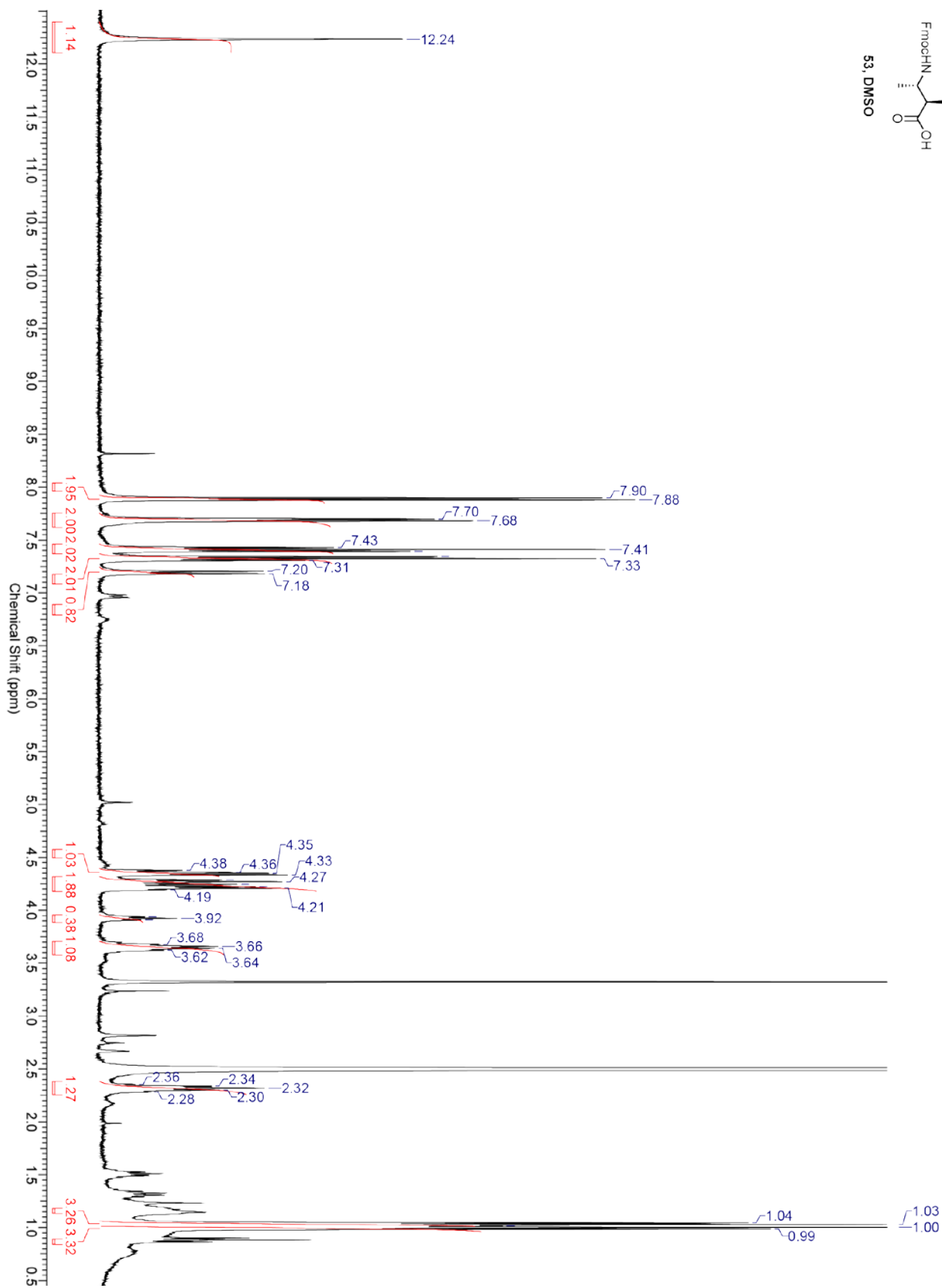


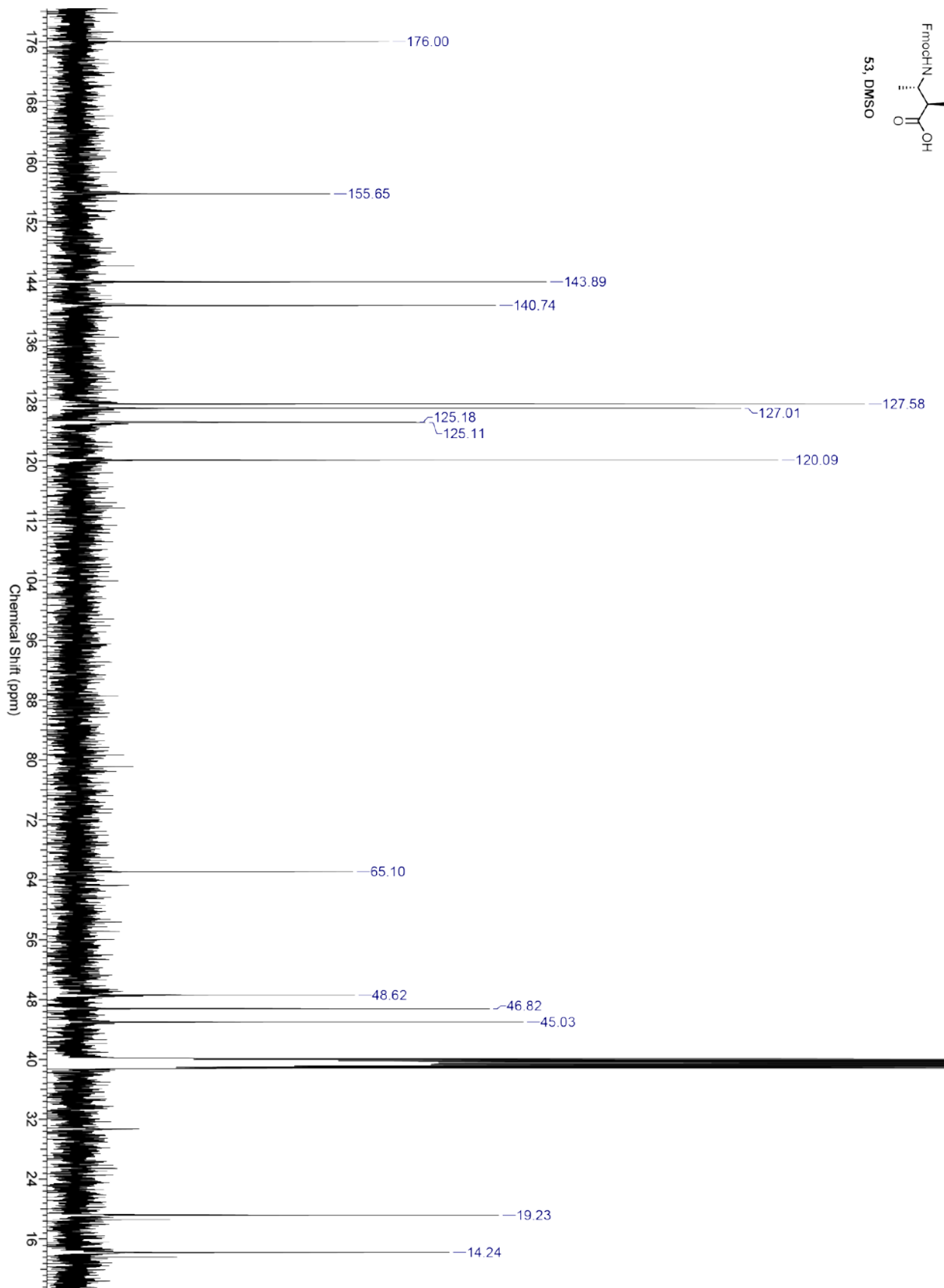
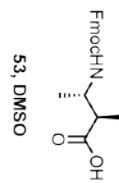


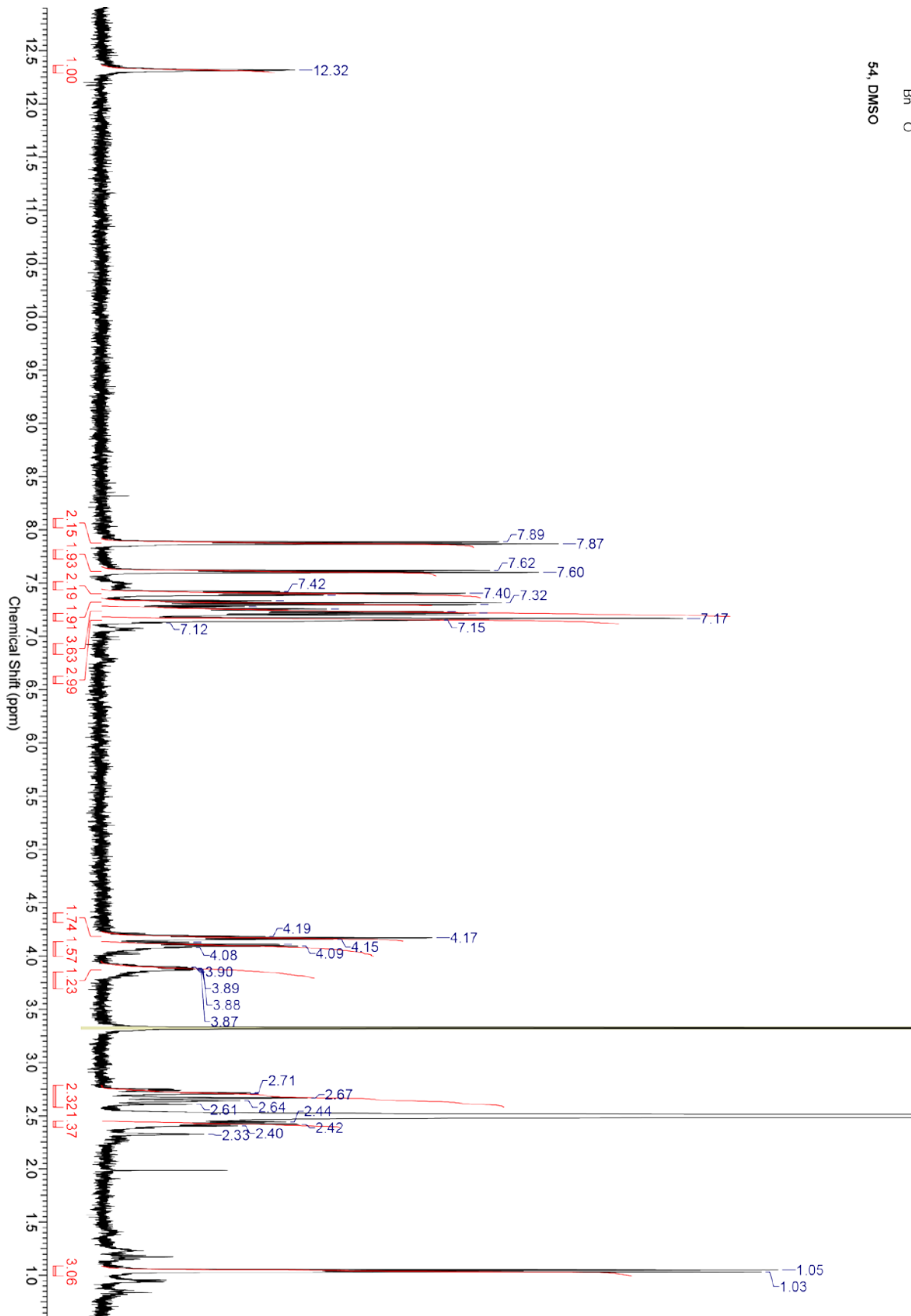
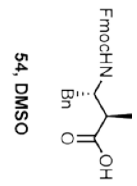


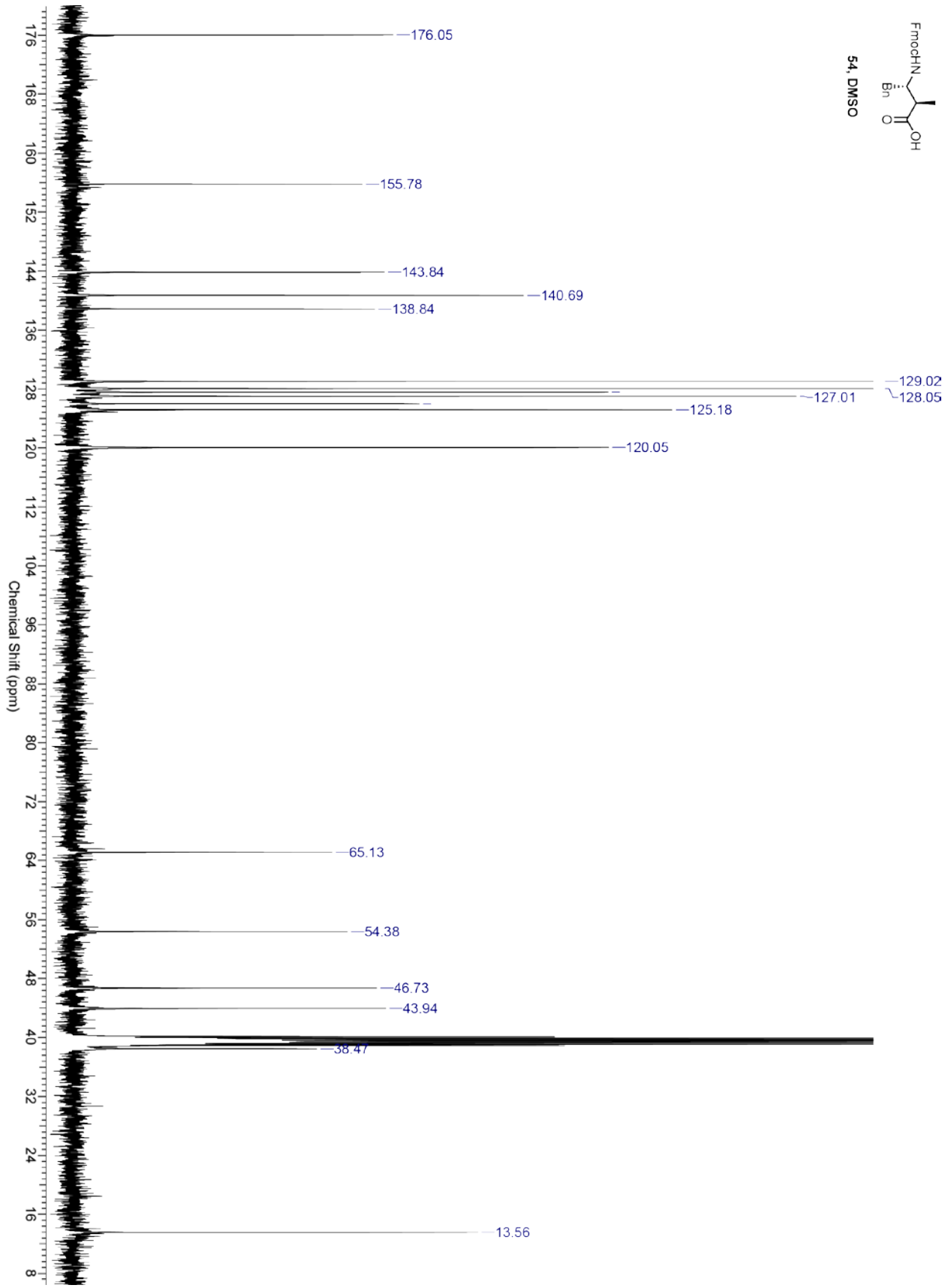
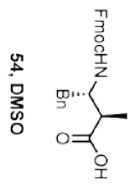


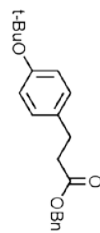
53. DMSO



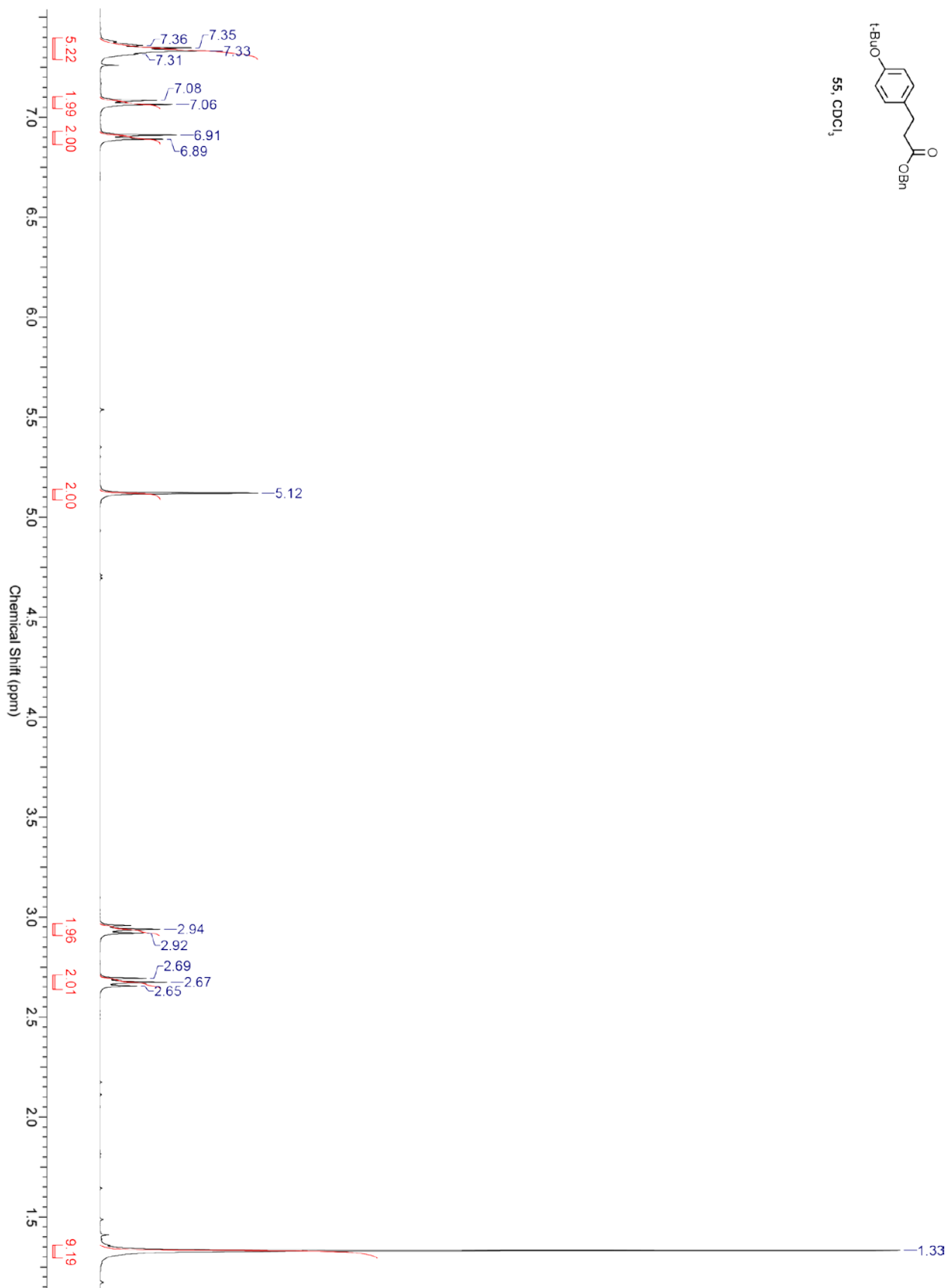


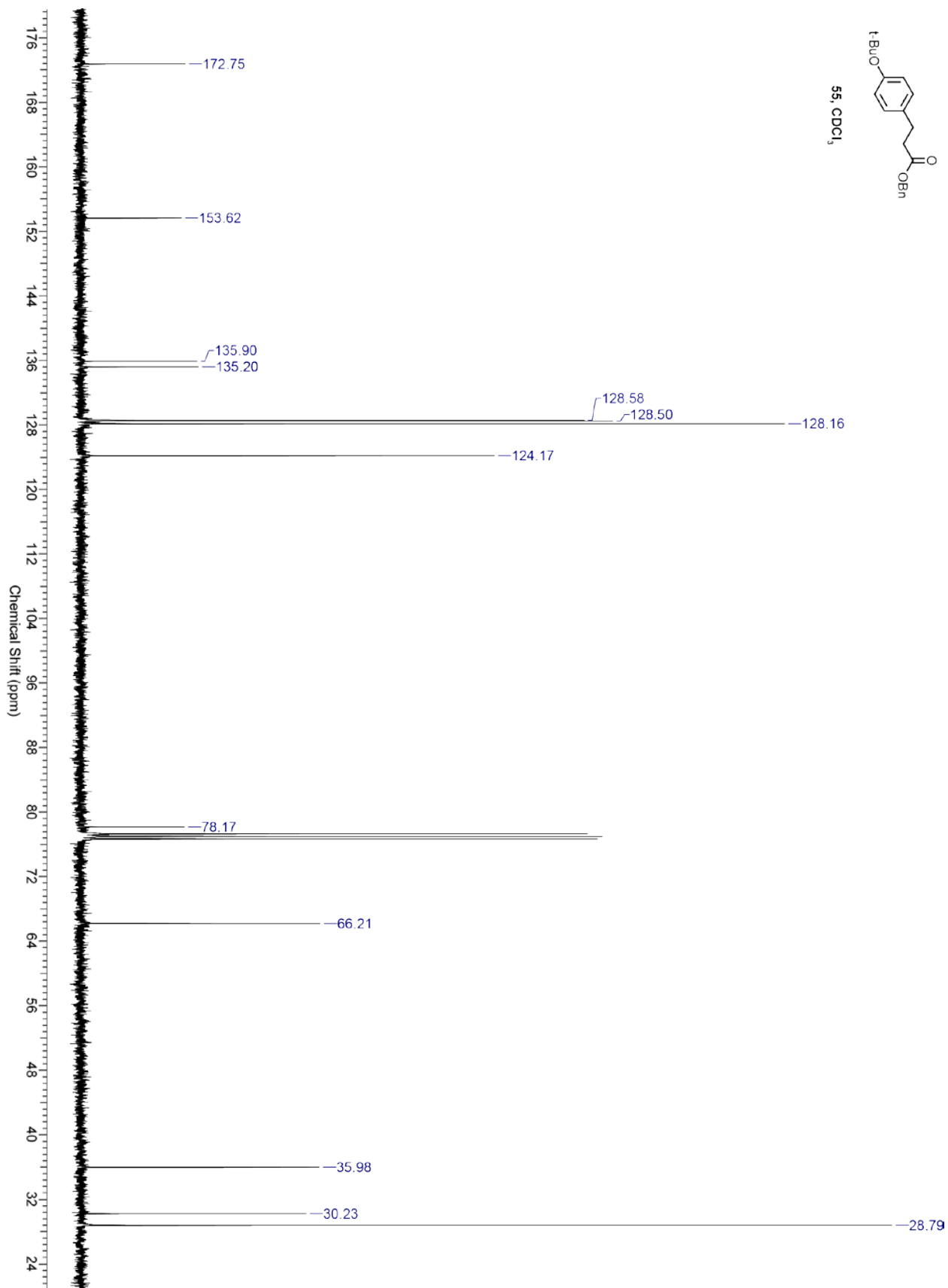


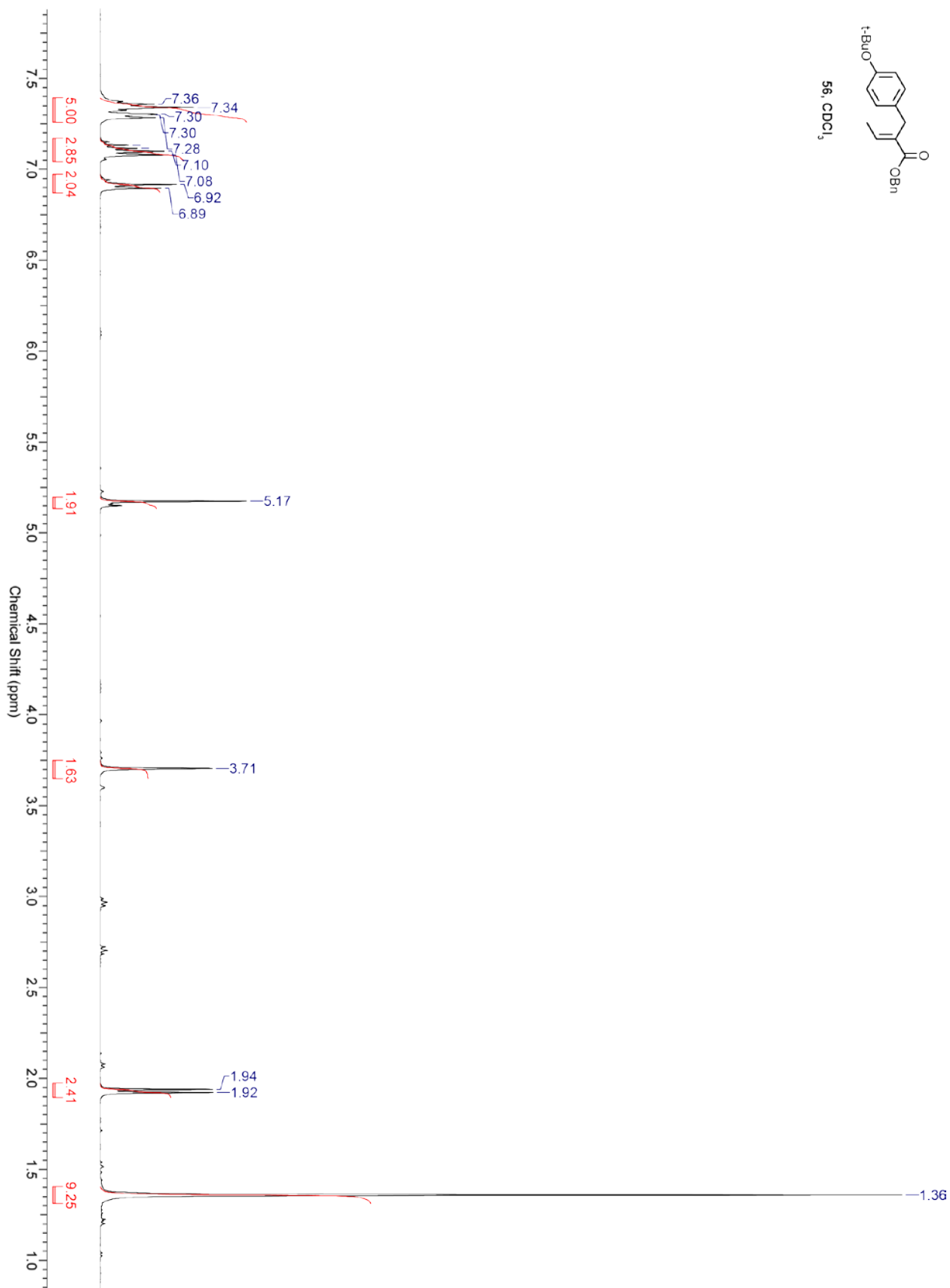
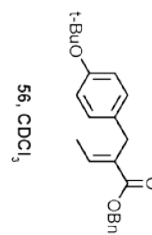


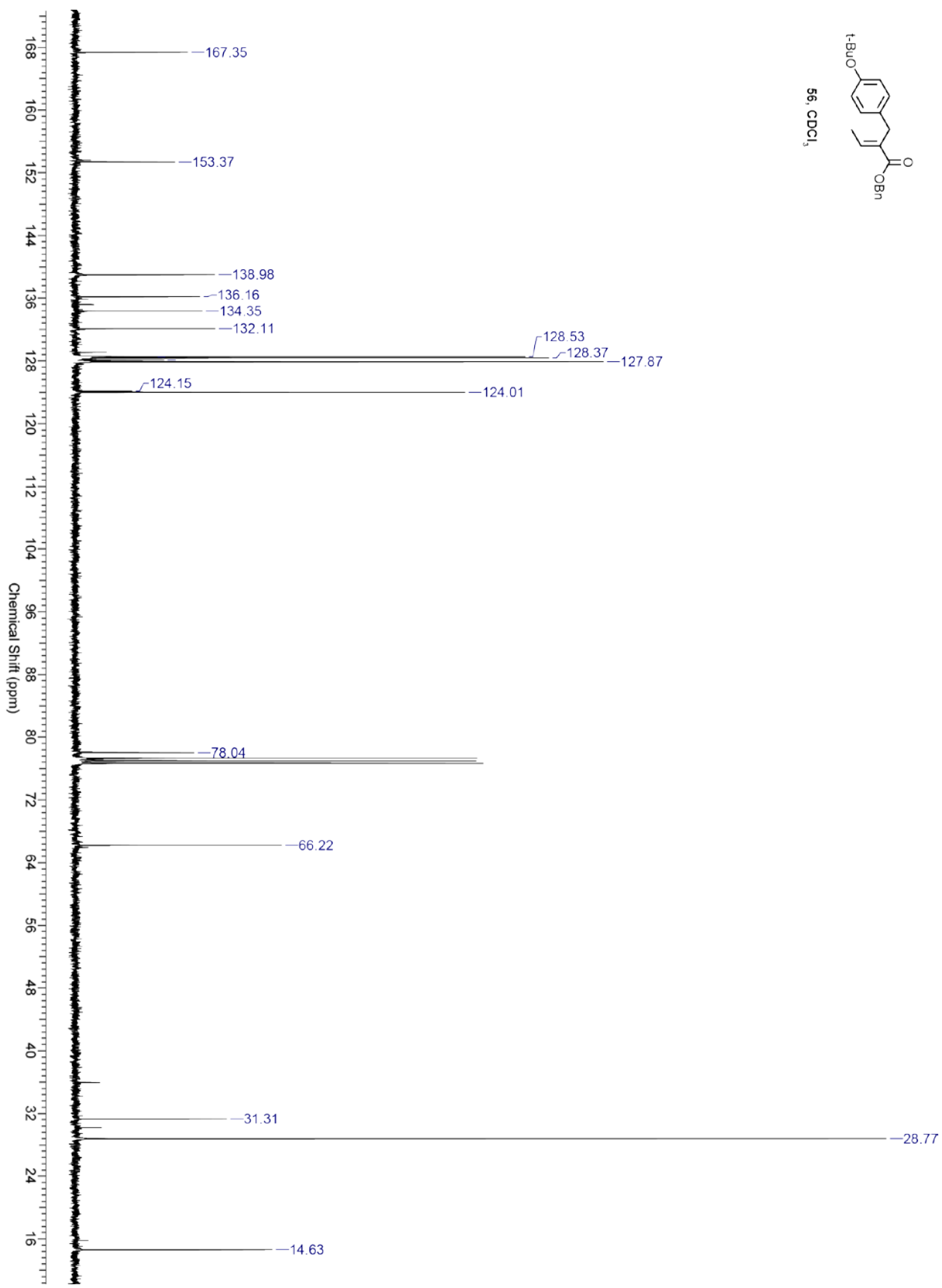
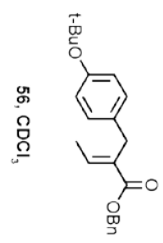


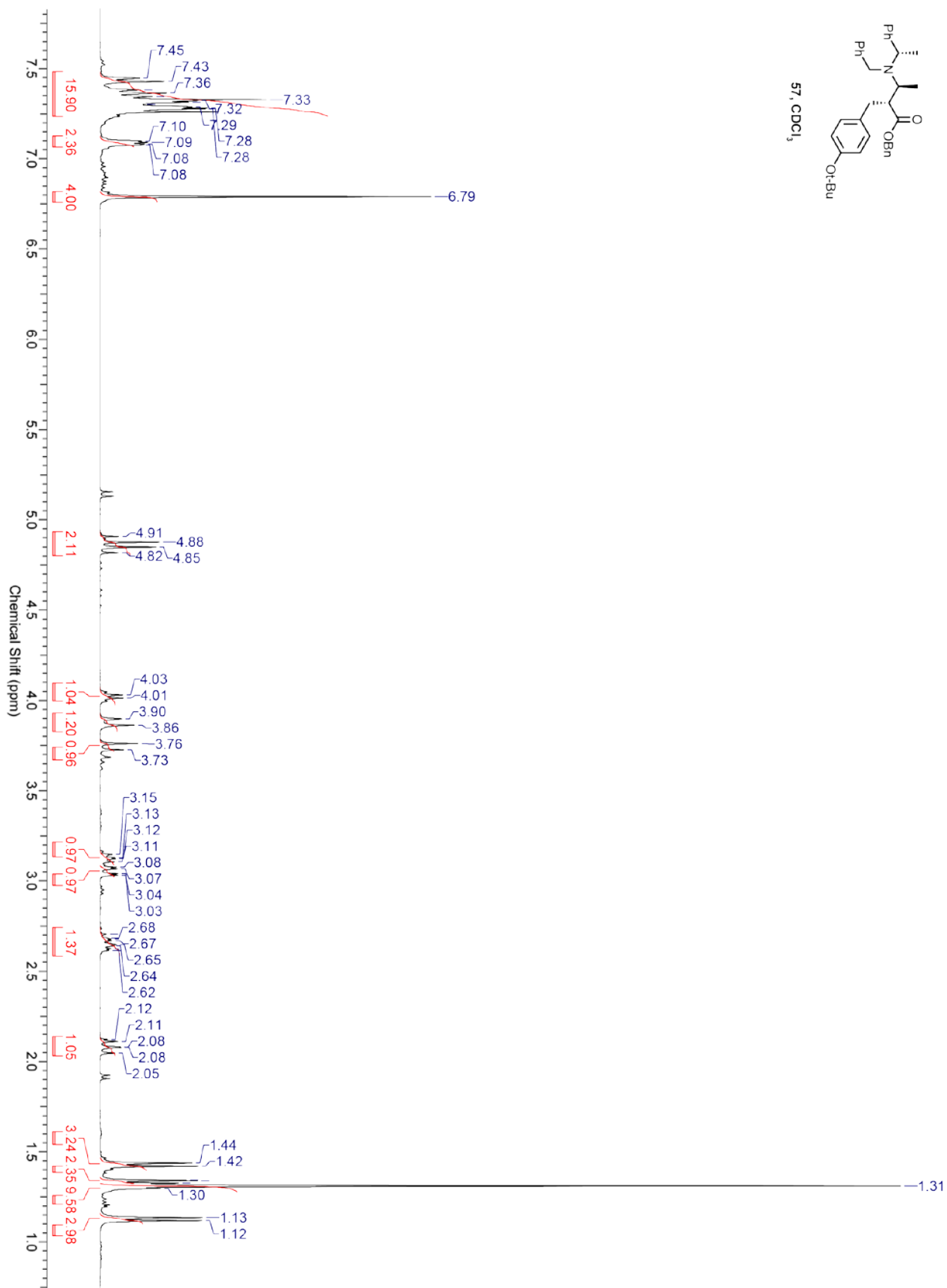
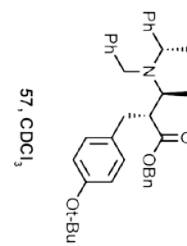
55, CDCl<sub>3</sub>

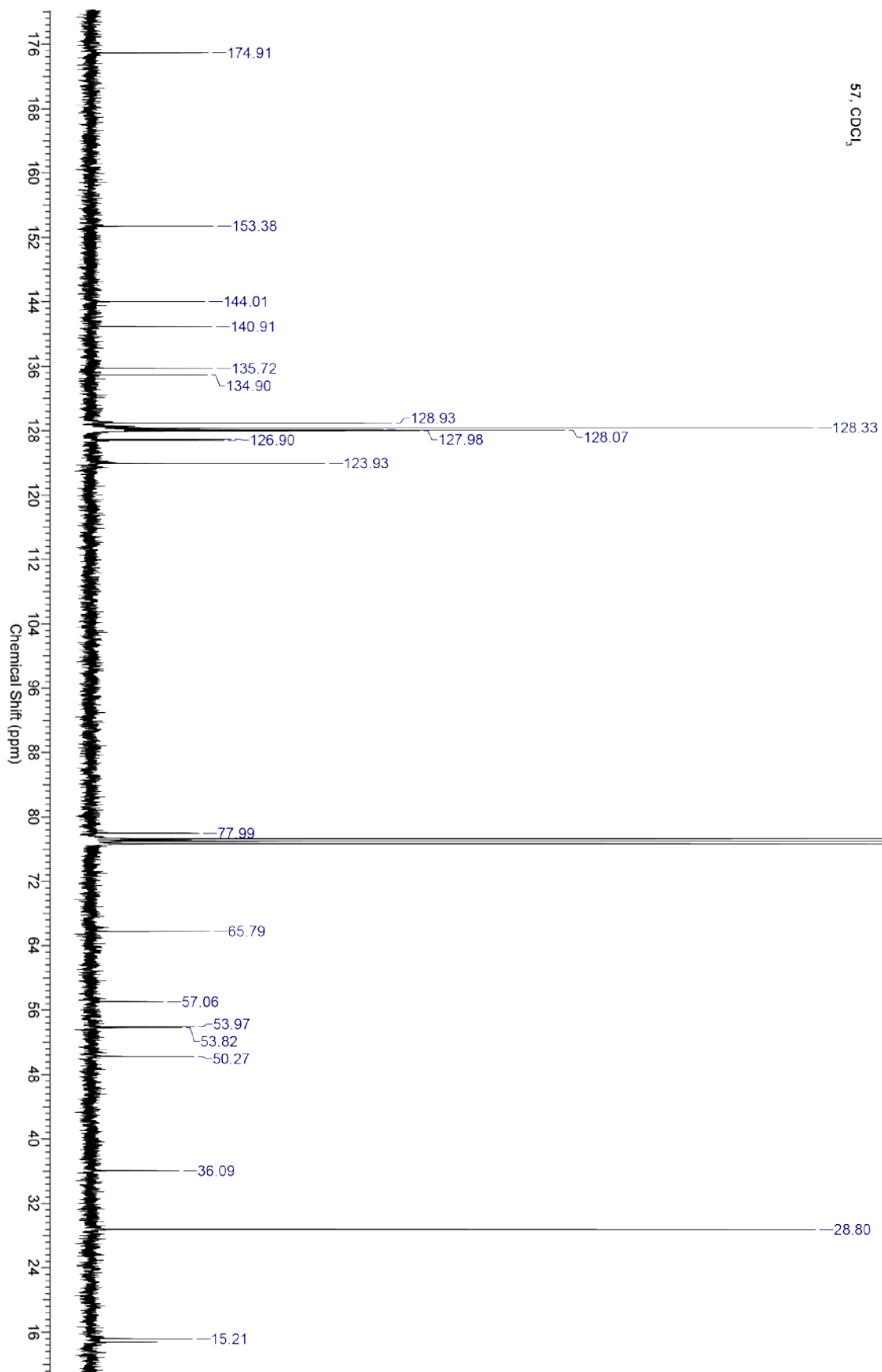
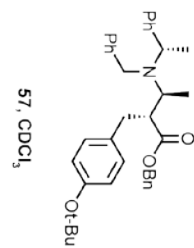


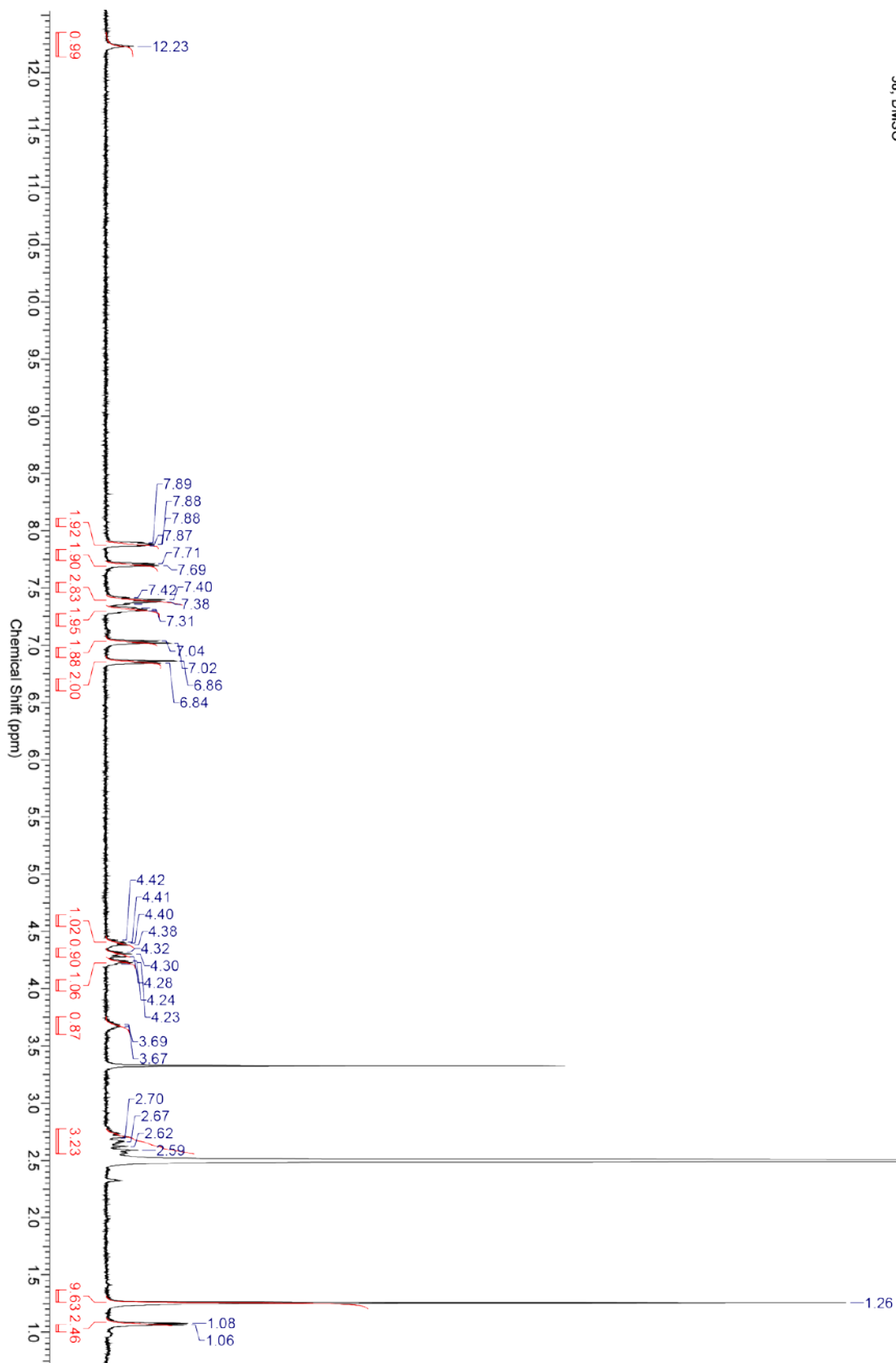
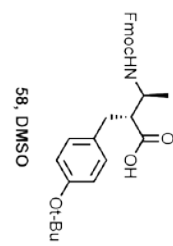


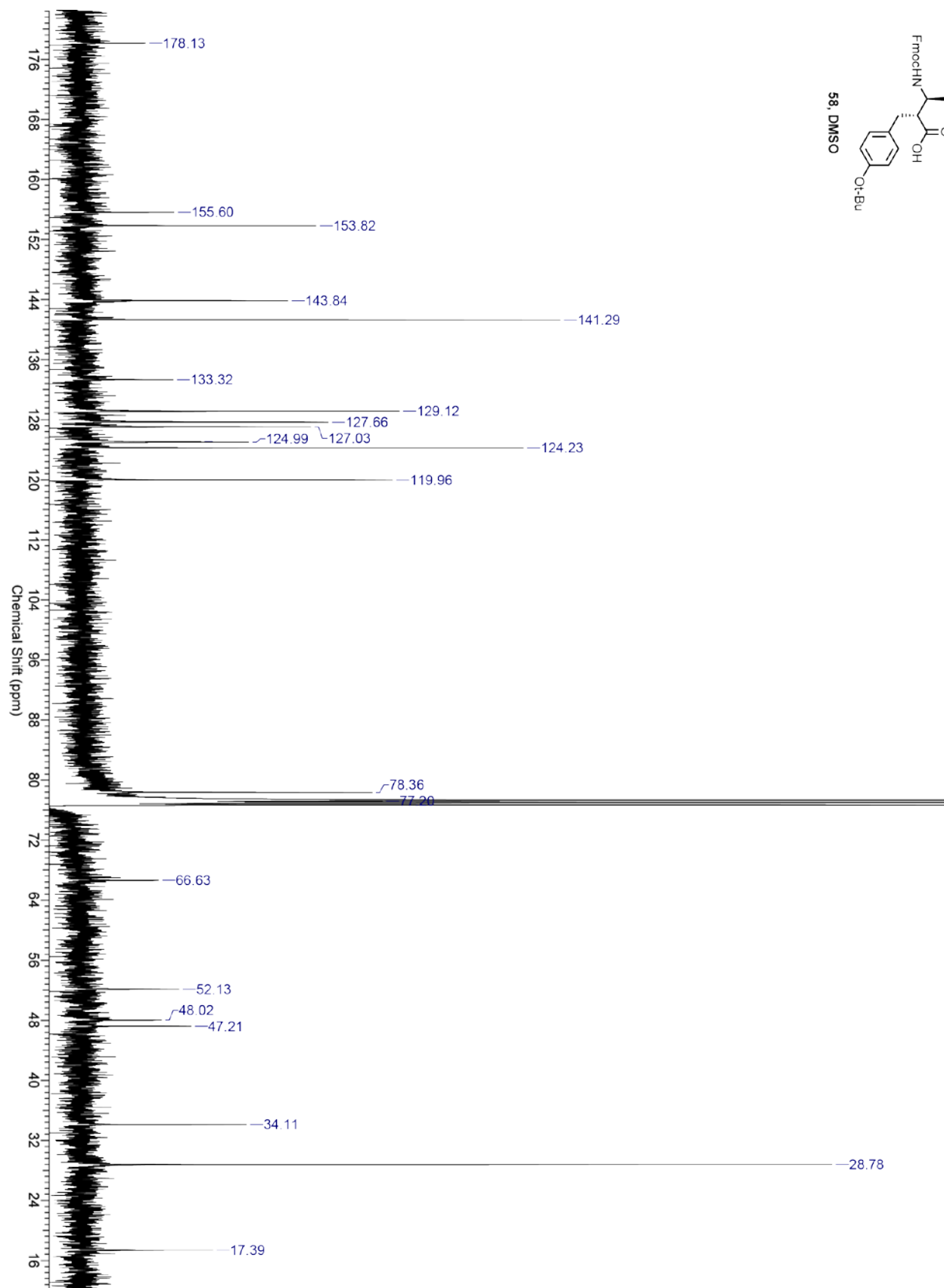


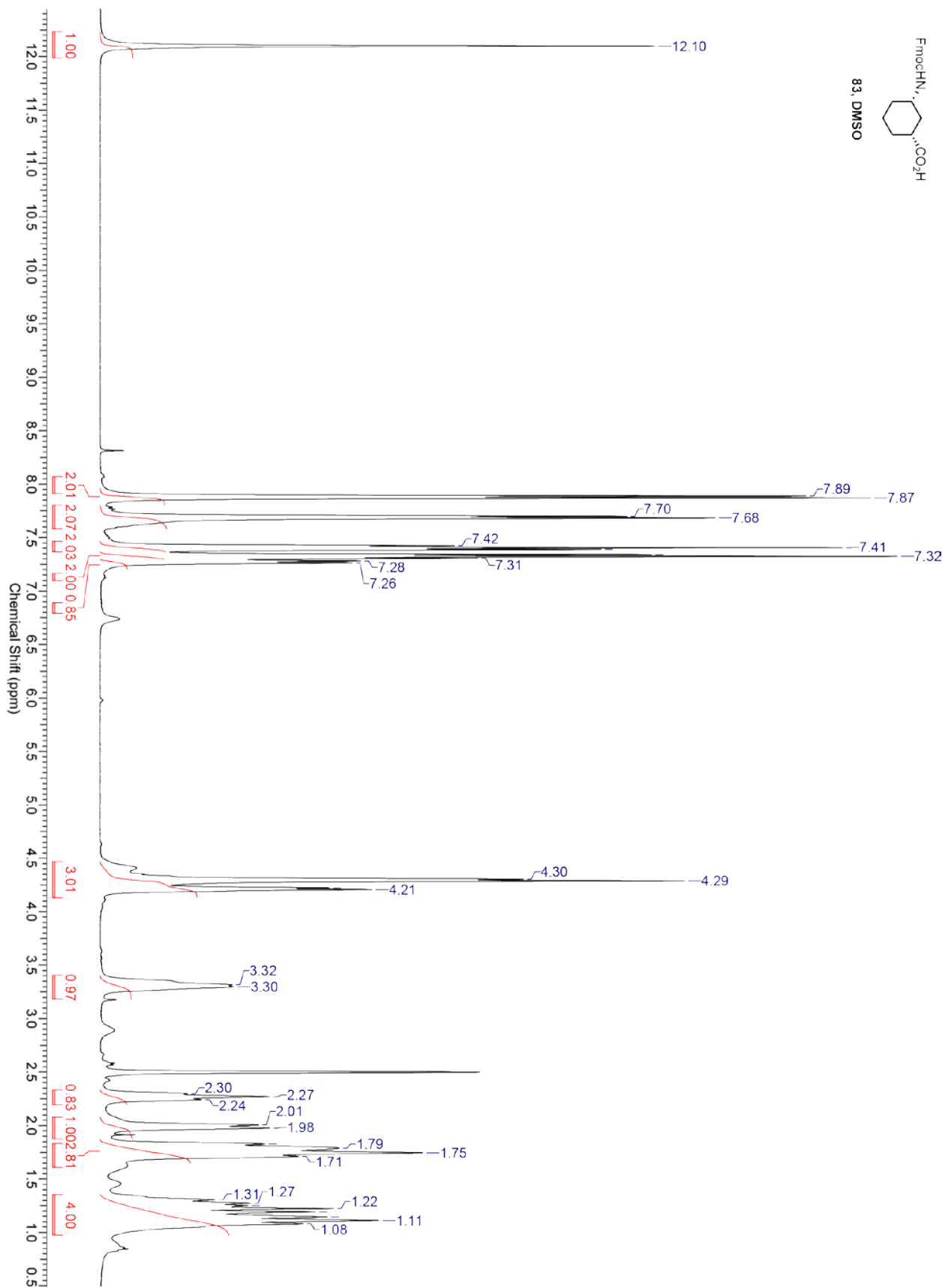
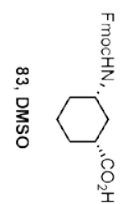


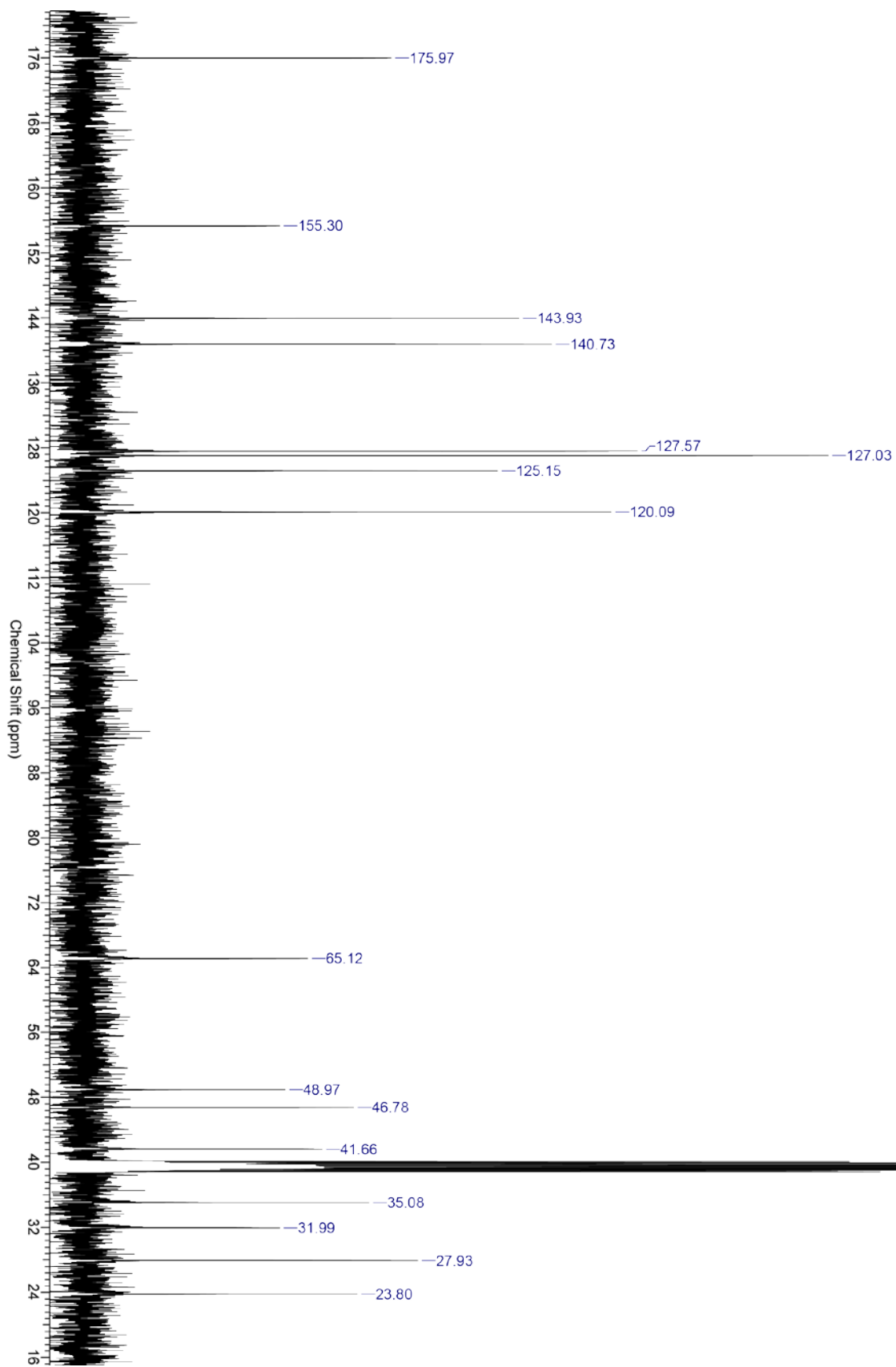
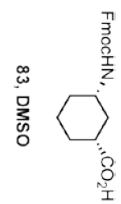


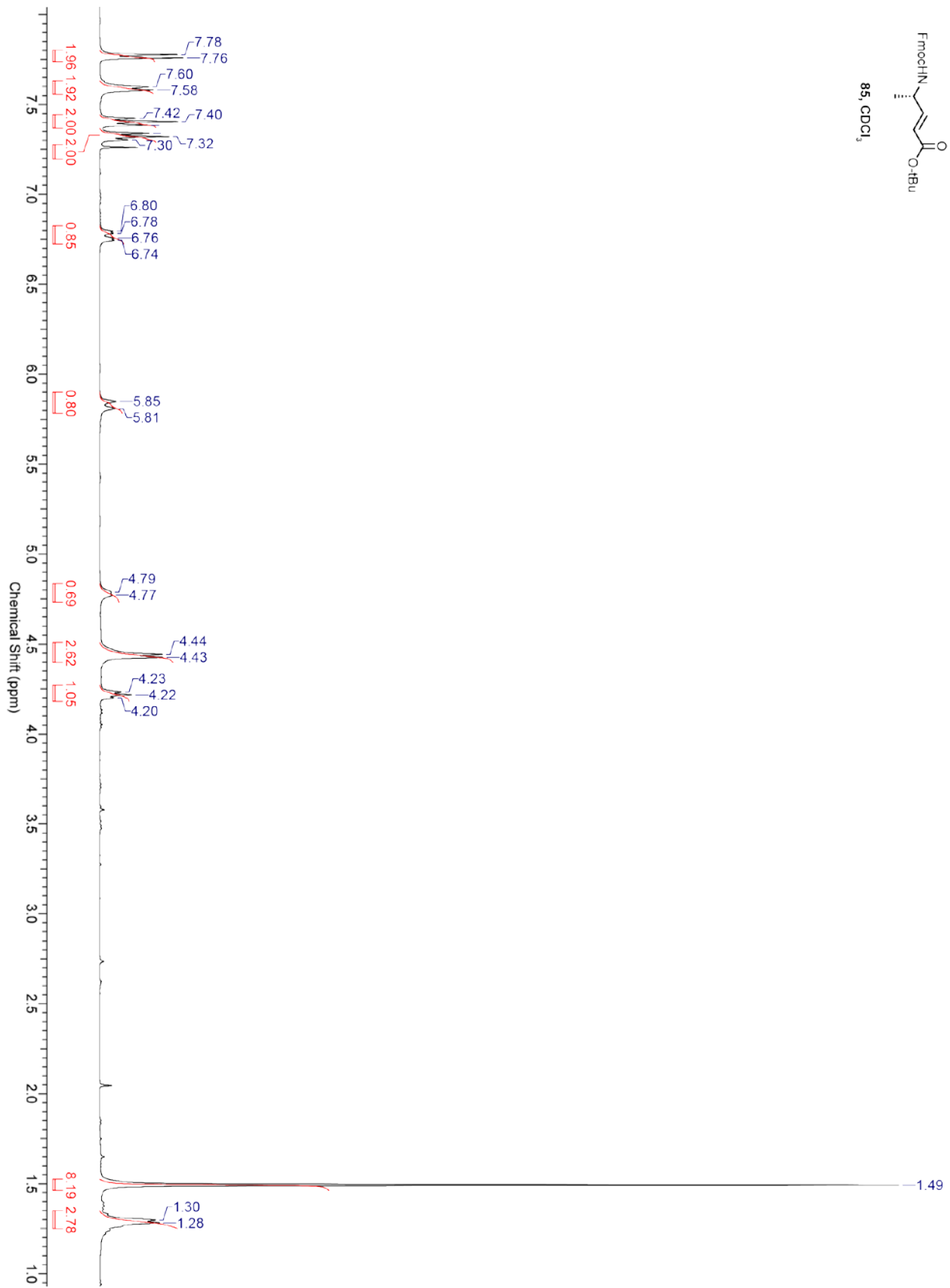
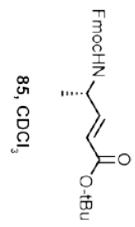


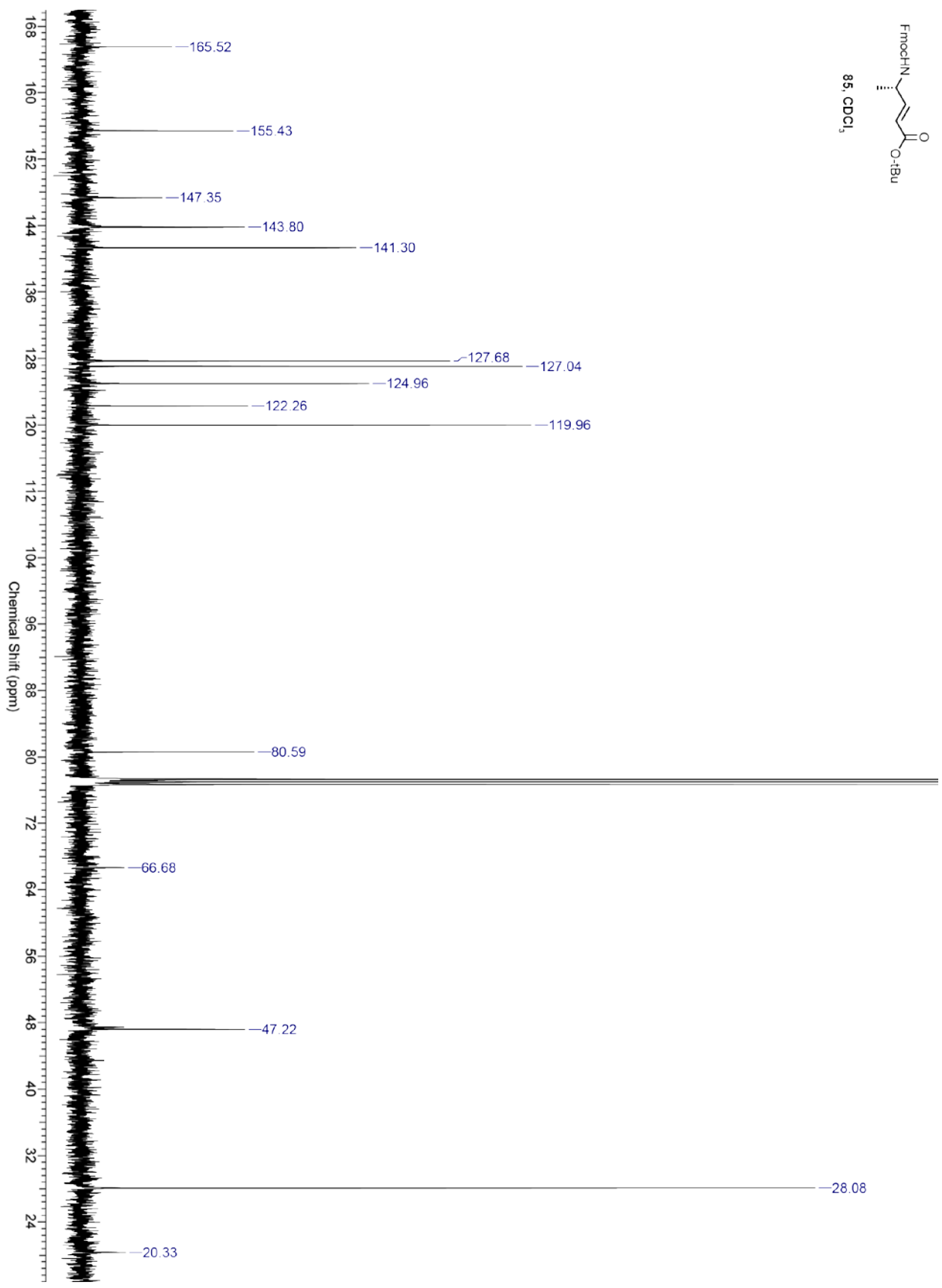
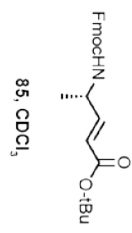


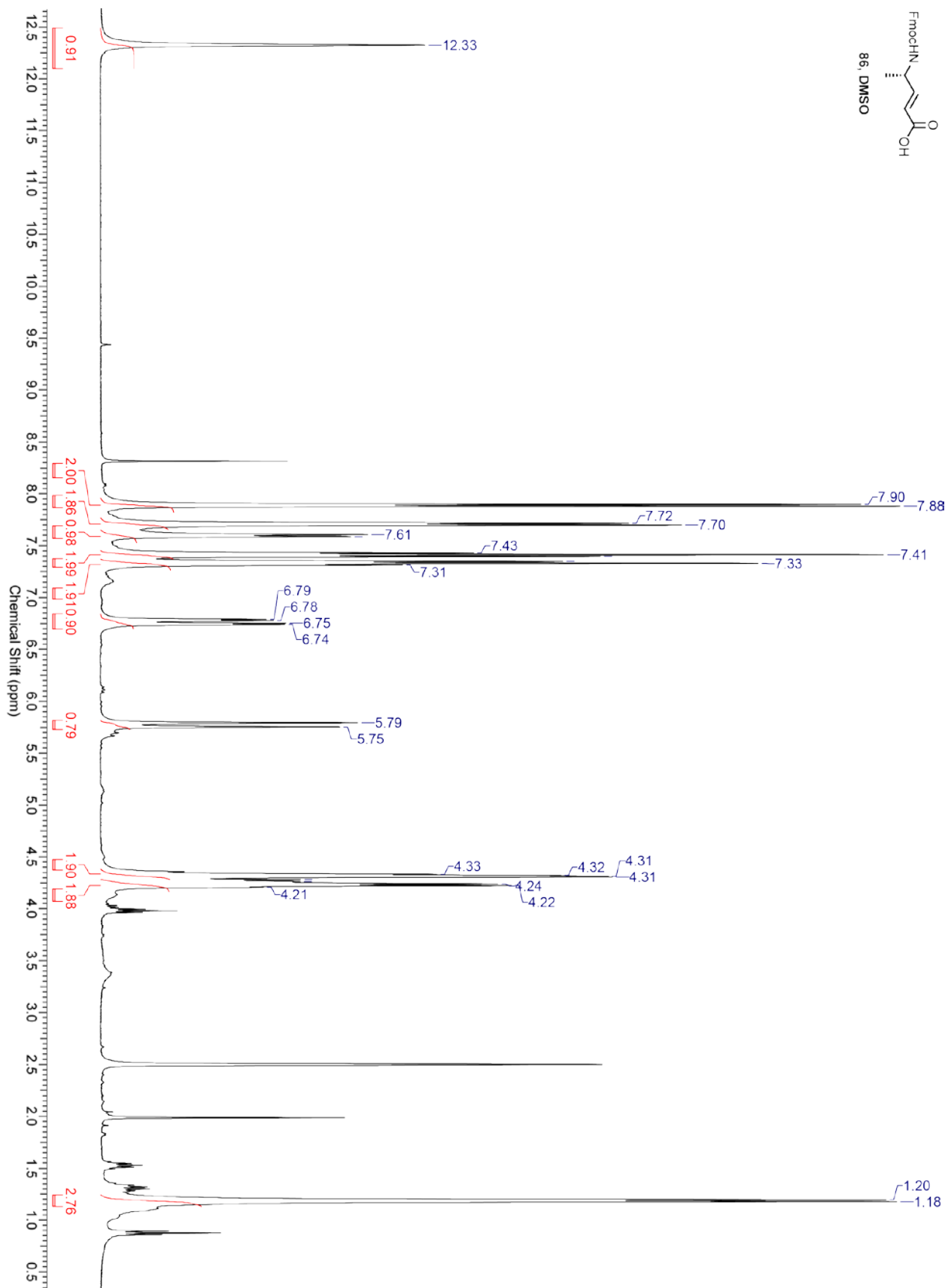
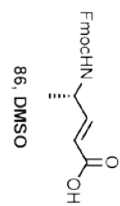


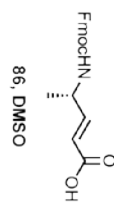
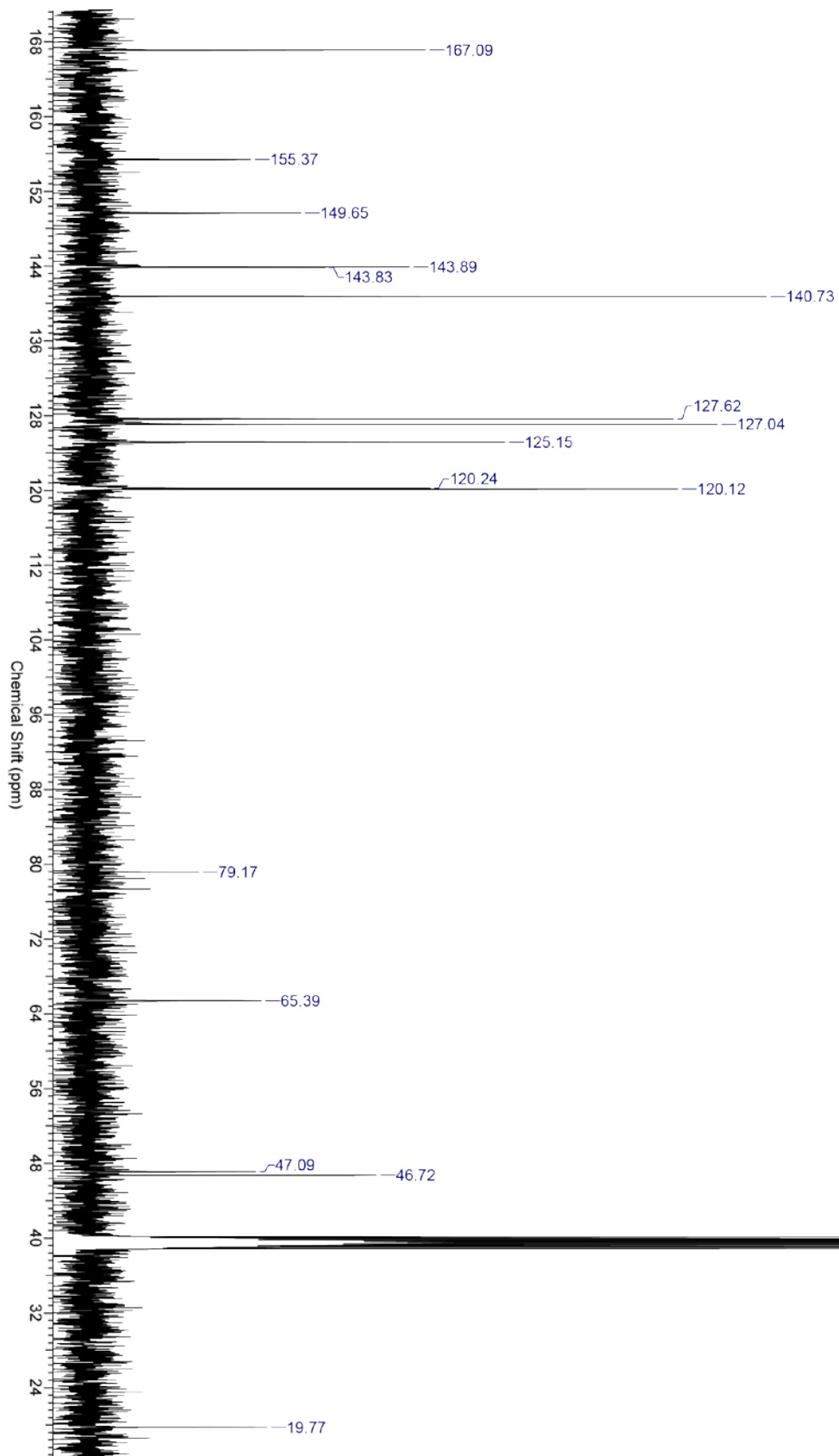


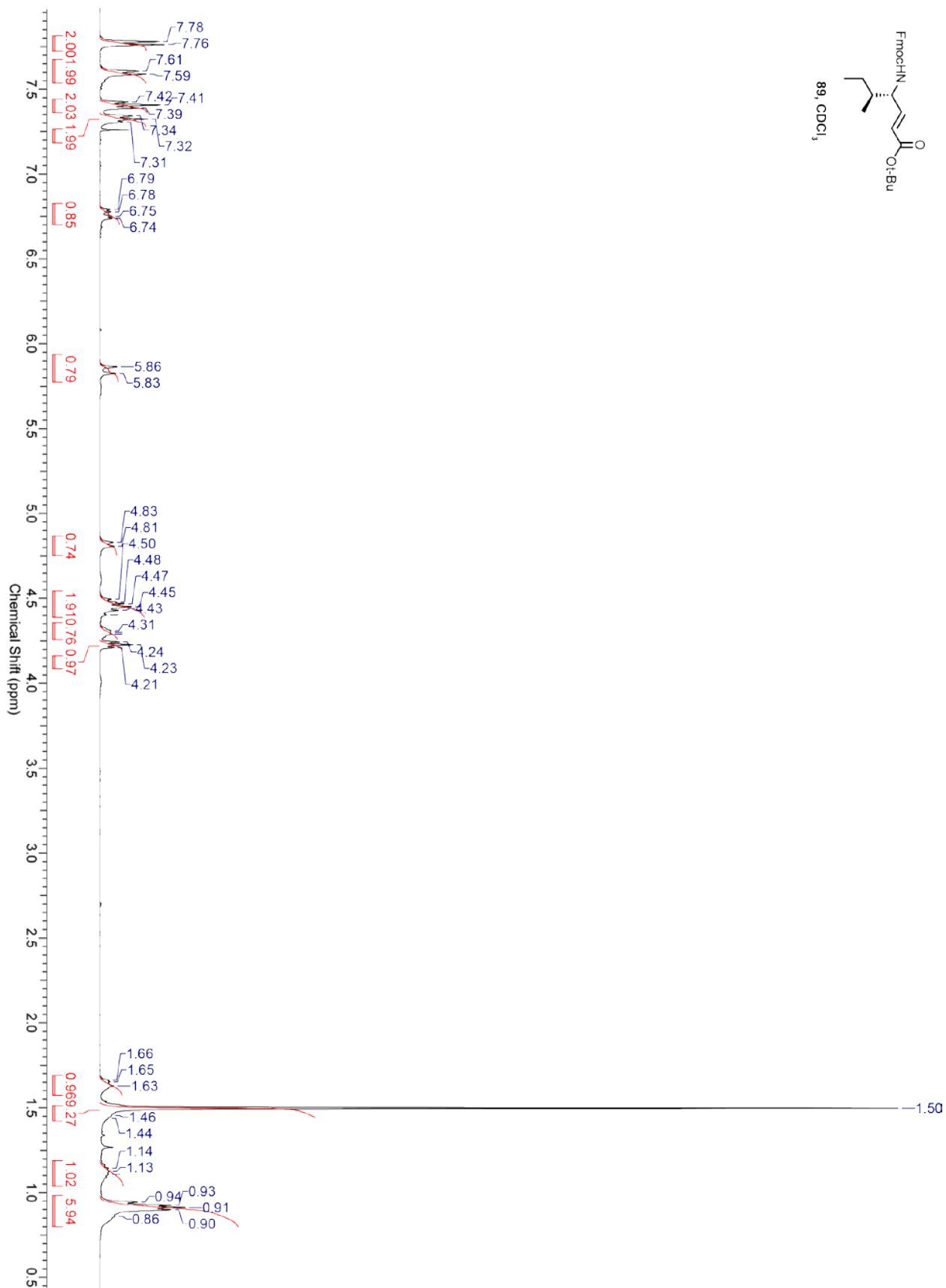
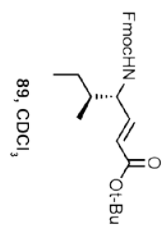


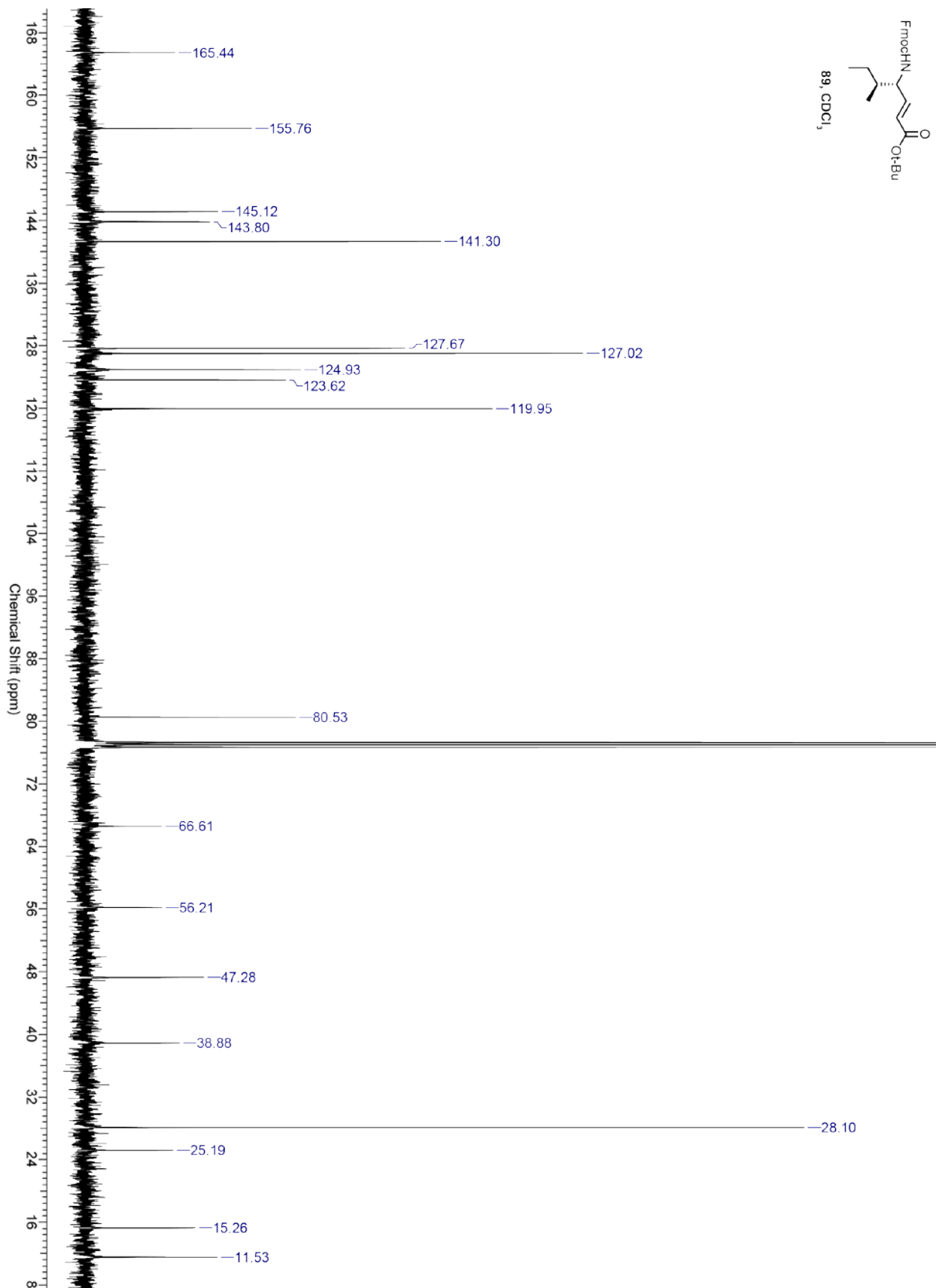


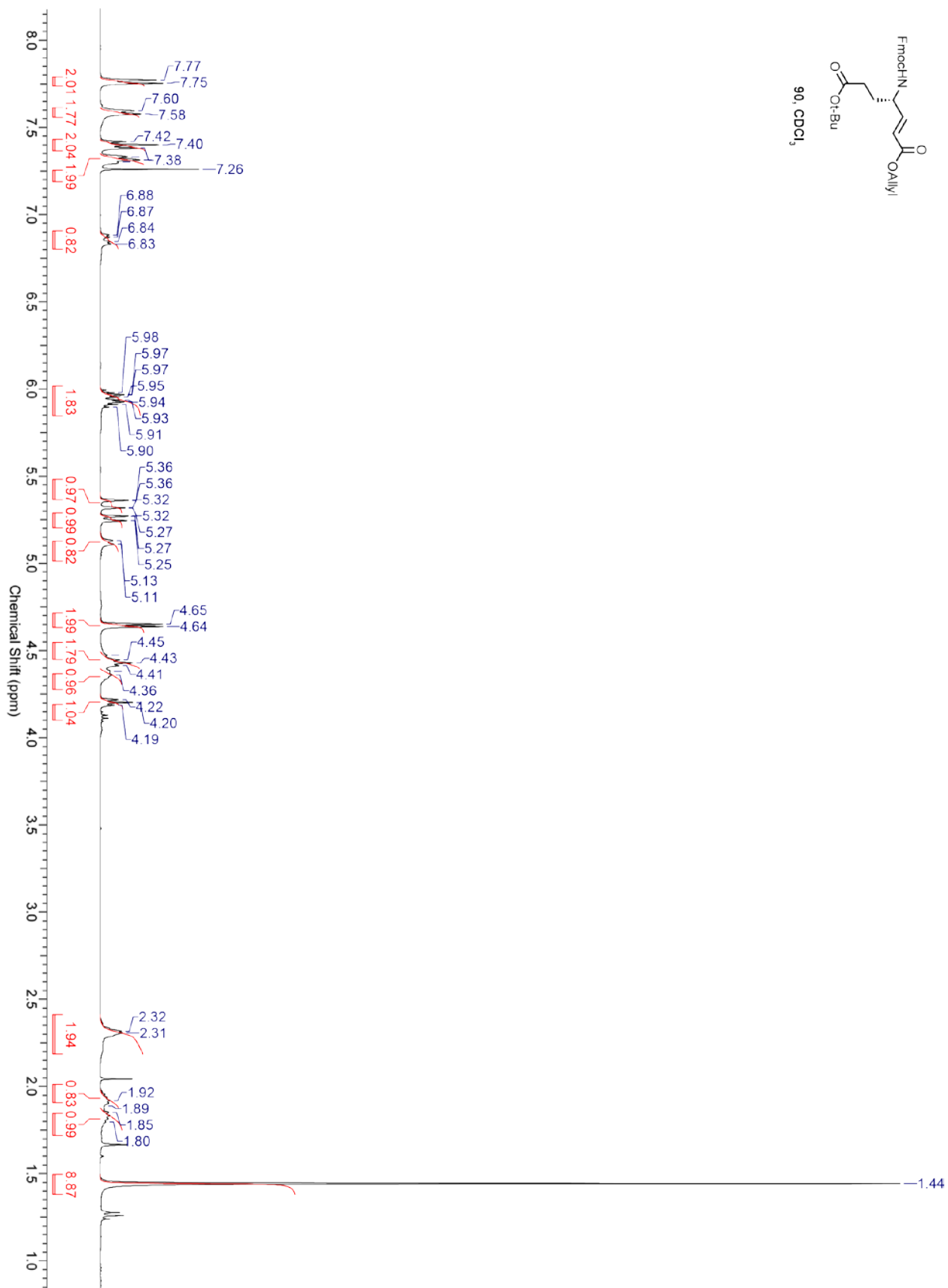
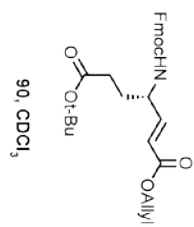


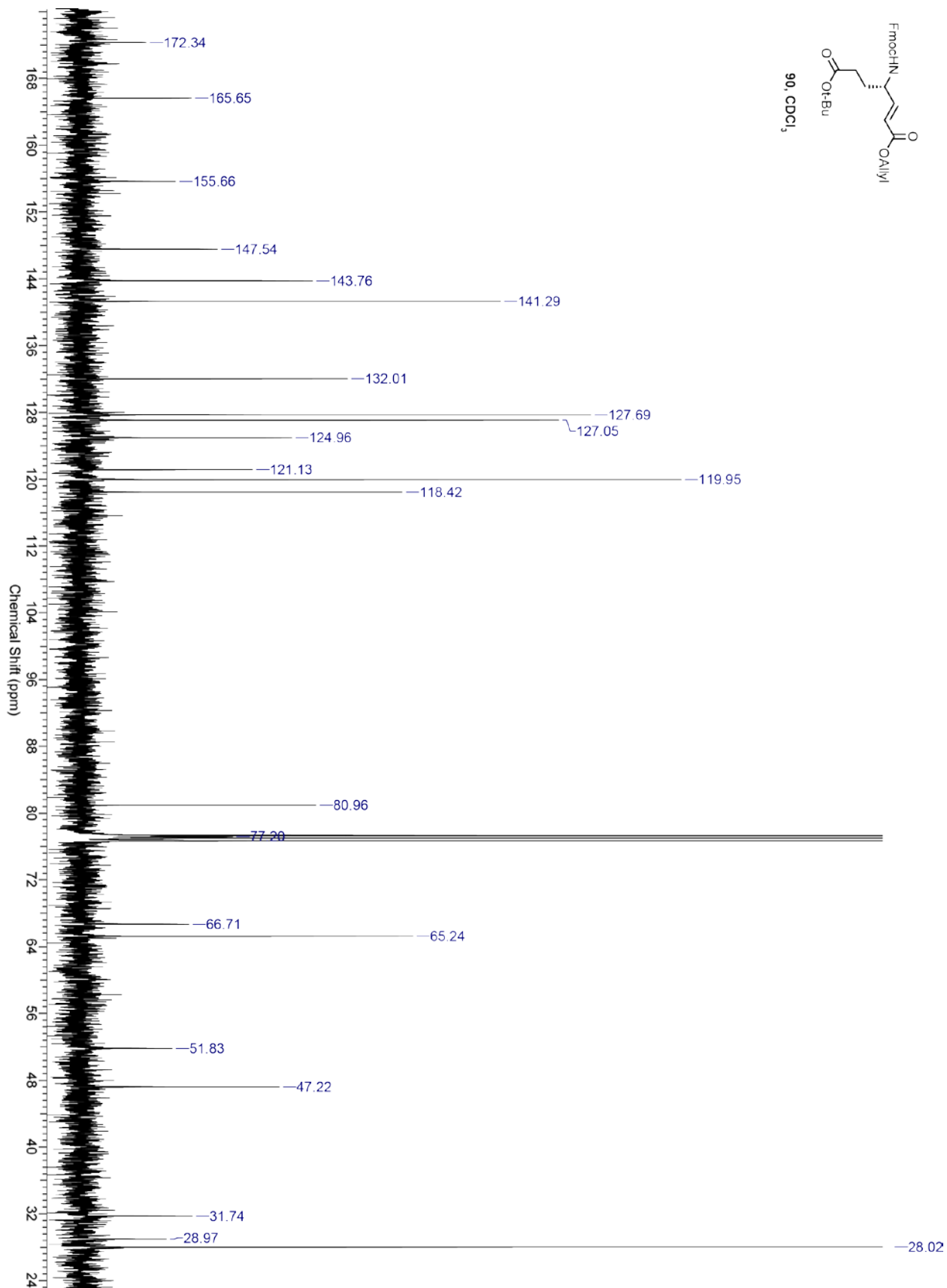


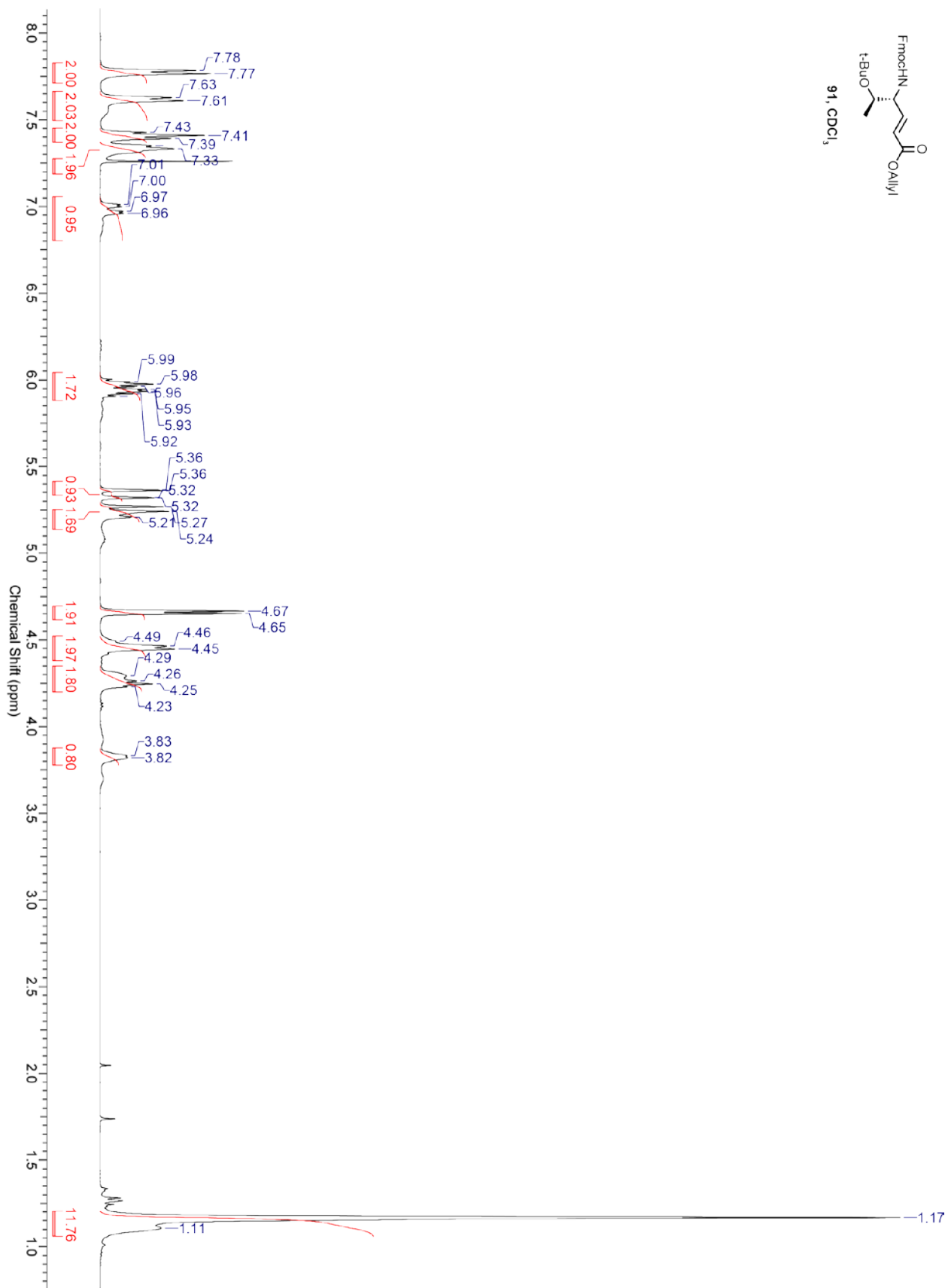
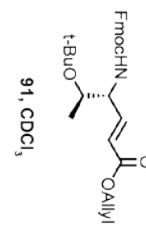


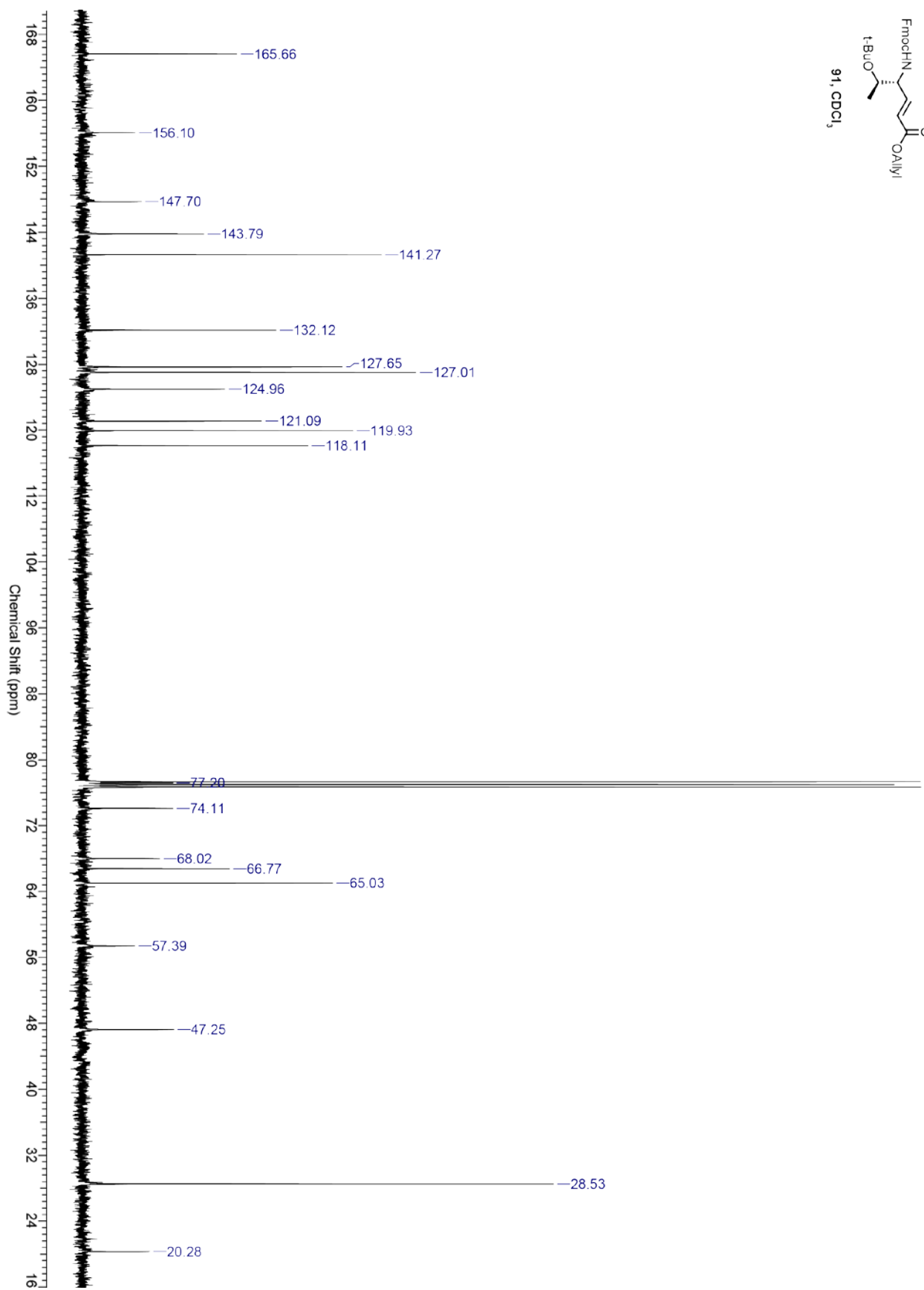
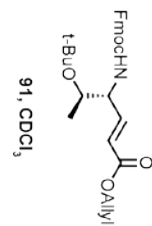


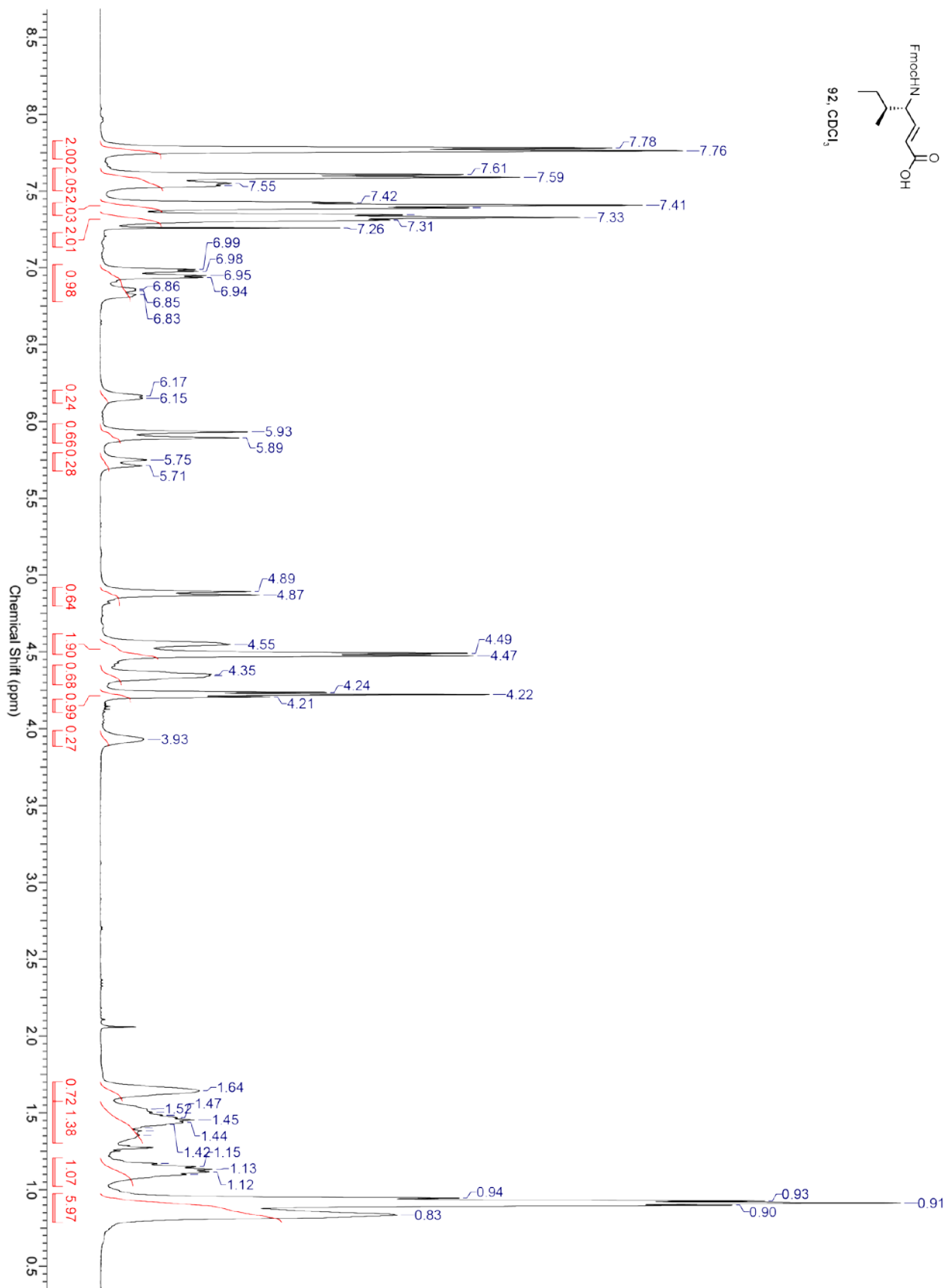


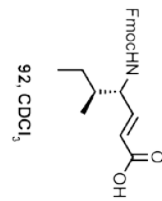
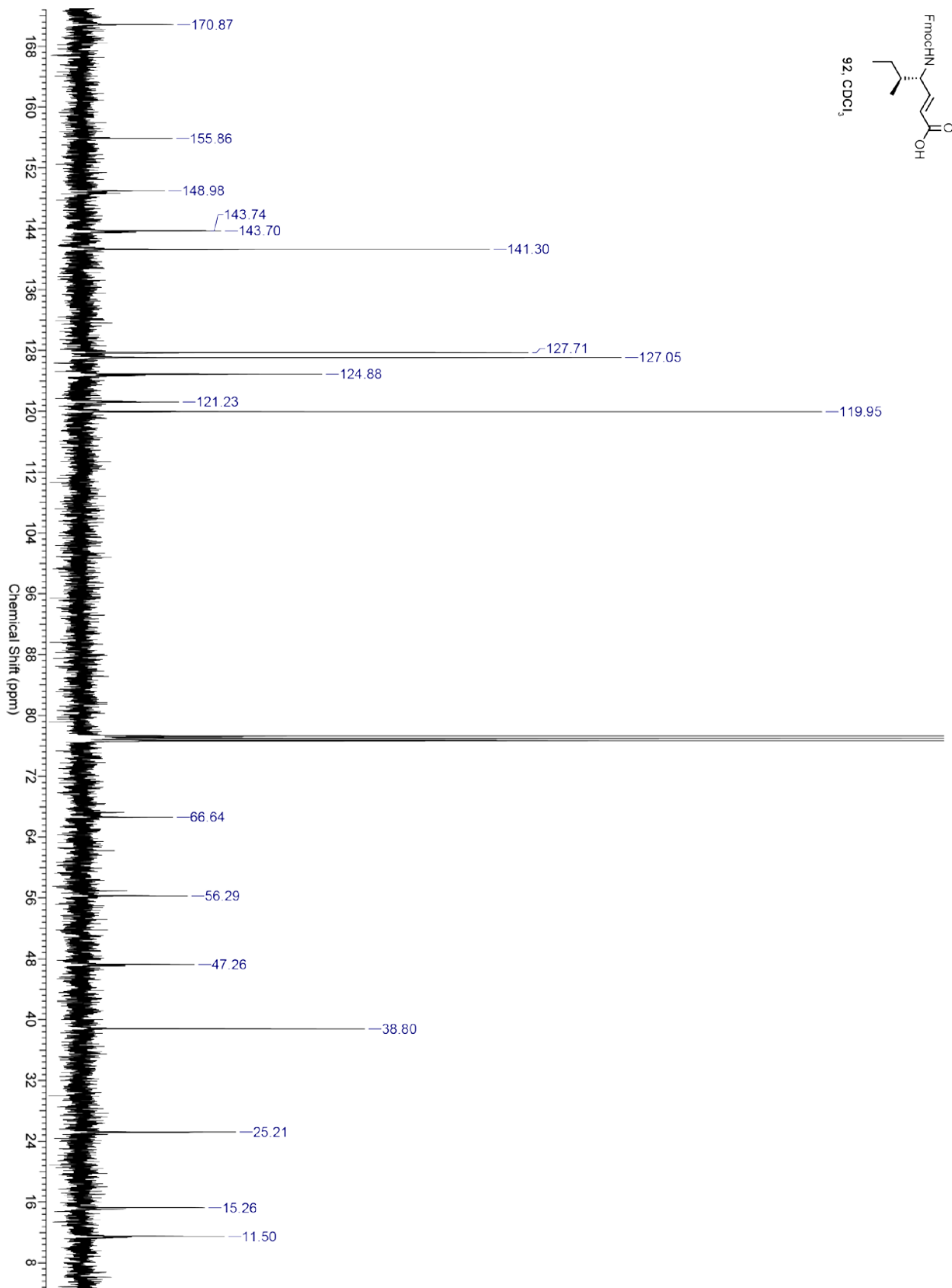


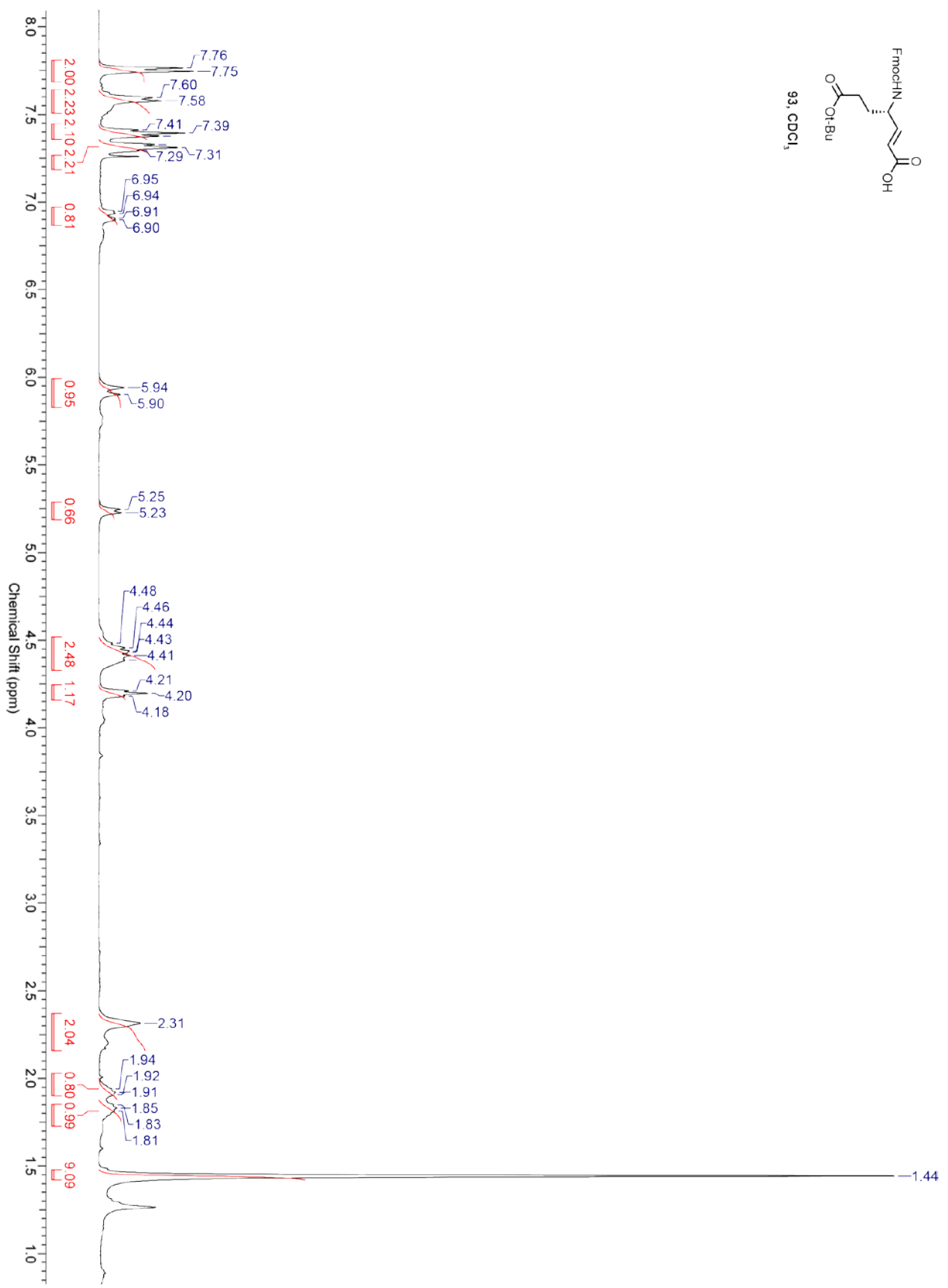
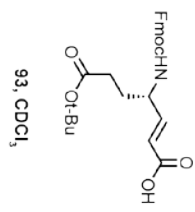


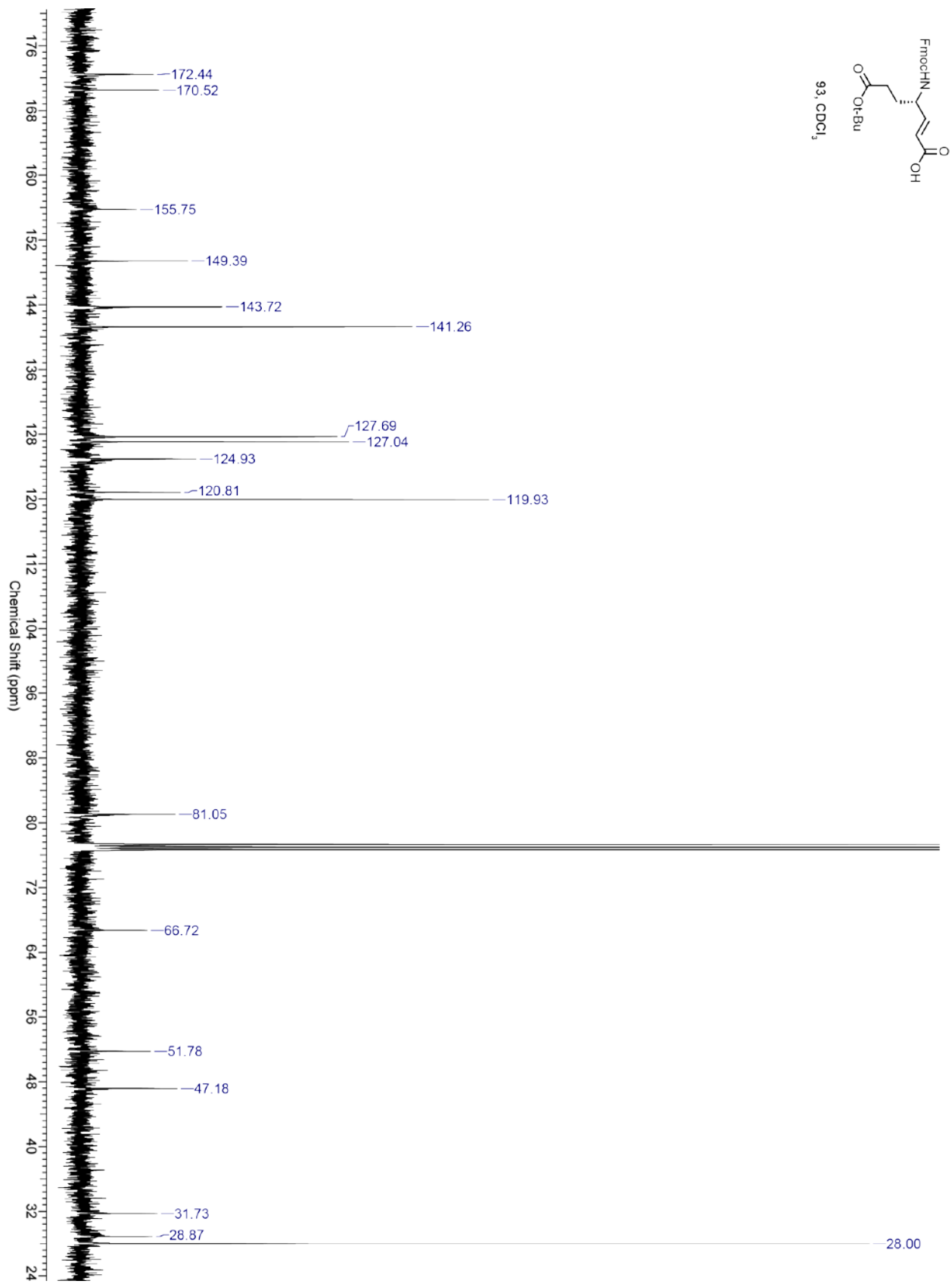


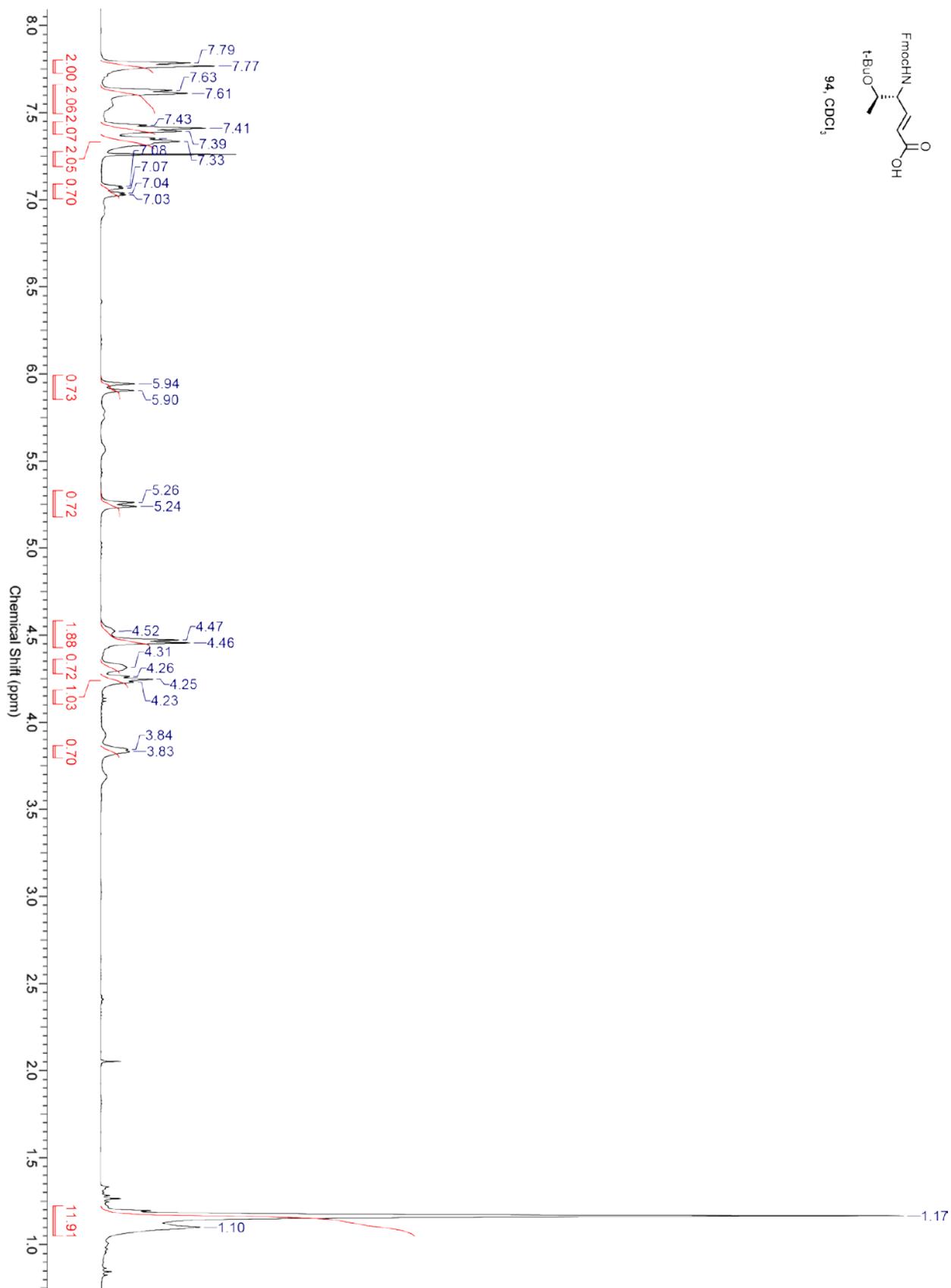
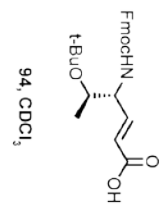


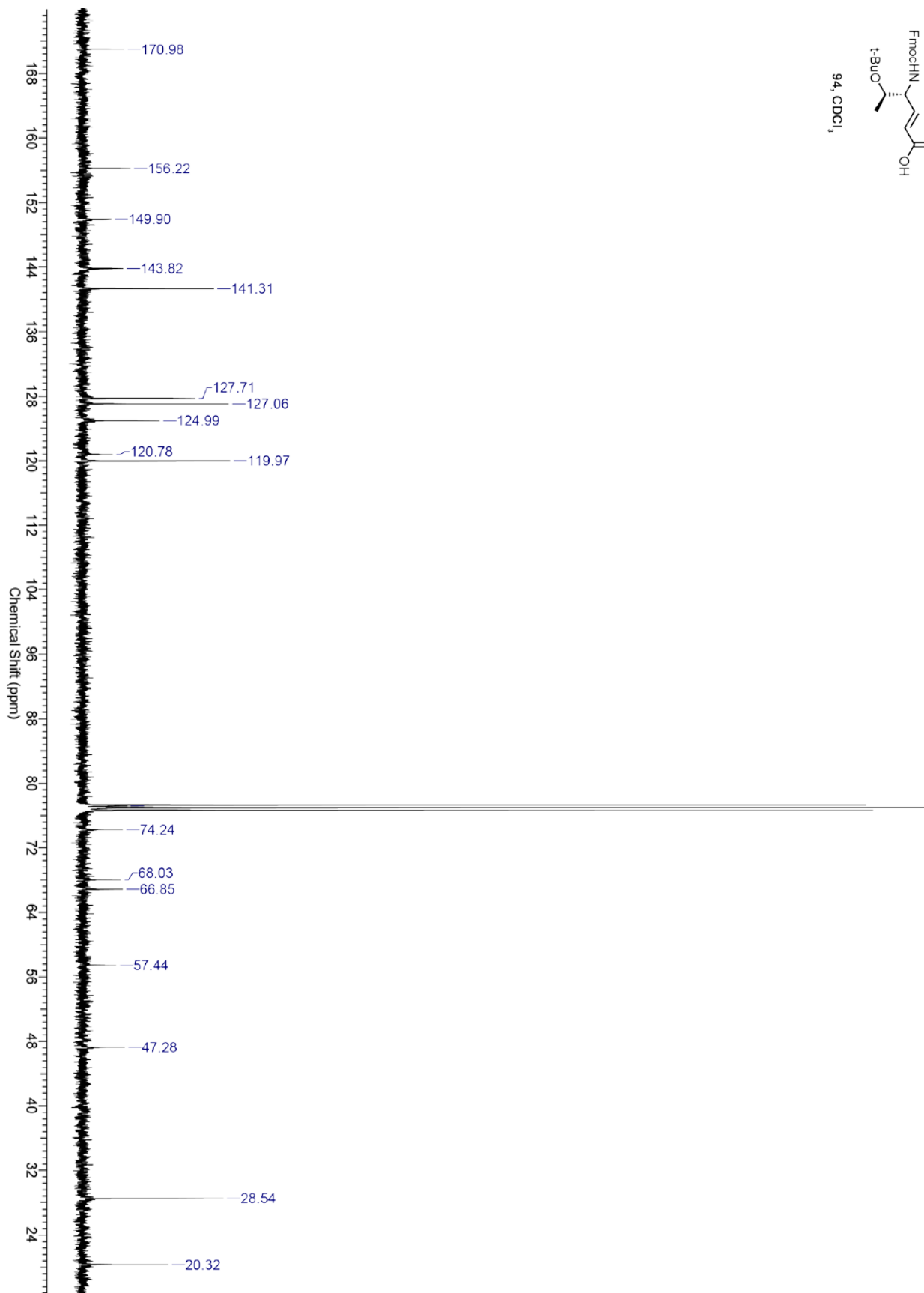
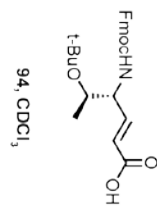












## BIBLIOGRAPHY

1. Ryan, D. P.; Matthews, J. M., "Protein–protein interactions in human disease," *Curr. Opin. Struct. Biol.* **2005**, *15*, 441.
2. Cochran, A. G., "Antagonists of protein–protein interactions," *Chem. Biol.* **2000**, *7*, R85.
3. Leader, B.; Baca, Q. J.; Golan, D. E., "Protein therapeutics: a summary and pharmacological classification," *Nat. Rev. Drug Discovery* **2008**, *7*, 21.
4. Navia, M. A.; Fitzgerald, P. M. D.; McKeever, B. M.; Leu, C.-T.; Heimbach, J. C.; Herber, W. K.; Sigal, I. S.; Darke, P. L.; Springer, J. P., "Three-dimensional structure of aspartyl protease from human immunodeficiency virus HIV-1," *Nature* **1989**, *337*, 615.
5. Kohl, N. E.; Emini, E. A.; Schleif, W. A.; Davis, L. J.; Heimbach, J. C.; Dixon, R. A.; Scolnick, E. M.; Sigal, I. S., "Active human immunodeficiency virus protease is required for viral infectivity," *Proc. Natl. Acad. Sci. USA* **1988**, *85*, 4686.
6. Zhang, Z. Y.; Poorman, R. A.; Maggiora, L. L.; Heinrikson, R. L.; Kézdy, F. J., "Dissociative inhibition of dimeric enzymes. Kinetic characterization of the inhibition of HIV-1 protease by its COOH-terminal tetrapeptide," *J. Biol. Chem.* **1991**, *266*, 15591.
7. Wild, C.; Greenwell, T.; Matthews, T., "A Synthetic Peptide from HIV-1 gp41 Is a Potent Inhibitor of Virus-Mediated Cell-Cell Fusion," *AIDS Res Hum Retroviruses* **1993**, *9*, 1051.
8. Chan, D. C.; Fass, D.; Berger, J. M.; Kim, P. S., "Core Structure of gp41 from the HIV Envelope Glycoprotein," *Cell* **1997**, *89*, 263.

9. Matthews, T.; Salgo, M.; Greenberg, M.; Chung, J.; DeMasi, R.; Bolognesi, D., "Enfuvirtide: the first therapy to inhibit the entry of HIV-1 into host CD4 lymphocytes," *Nat. Rev. Drug Discovery* **2004**, *3*, 215.
10. Weckbecker, G.; Lewis, I.; Albert, R.; Schmid, H. A.; Hoyer, D.; Bruns, C., "Opportunities in somatostatin research: biological, chemical and therapeutic aspects," *Nat. Rev. Drug Discovery* **2003**, *2*, 999.
11. Patel, Y. C.; Wheatley, T., "In Vivo and in Vitro Plasma Disappearance and Metabolism of Somatostatin-28 and Somatostatin-14 in the Rat," *Endocrinology* **1983**, *112*, 220.
12. Werle, M.; Bernkop-Schnürch, A., "Strategies to improve plasma half life time of peptide and protein drugs," *Amino Acids* **2006**, *30*, 351.
13. Gellman, S. H., "Foldamers: A manifesto," *Acc. Chem. Res.* **1998**, *31*, 173.
14. Frackenhohl, J.; Arvidsson, P. I.; Schreiber, J. V.; Seebach, D., "The Outstanding Biological Stability of  $\beta$ - and  $\gamma$ -Peptides toward Proteolytic Enzymes: An In Vitro Investigation with Fifteen Peptidases," *ChemBioChem* **2001**, *2*, 445.
15. Horne, W. S., "Peptide and peptoid foldamers in medicinal chemistry," *Expert Opin. Drug Discovery* **2011**, *6*, 1247.
16. Hook, D. F.; Bindschädler, P.; Mahajan, Y. R.; Šebesta, R.; Kast, P.; Seebach, D., "The Proteolytic Stability of 'Designed'  $\beta$ -Peptides Containing  $\alpha$ -Peptide-Bond Mimics and of Mixed  $\alpha,\beta$ -Peptides: Application to the Construction of MHC-Binding Peptides," *Chem. Biodiversity* **2005**, *2*, 591.
17. Hook, D. F.; Gessier, F.; Noti, C.; Kast, P.; Seebach, D., "Probing the Proteolytic Stability of  $\beta$ -Peptides Containing  $\alpha$ -Fluoro- and  $\alpha$ -Hydroxy- $\beta$ -Amino Acids," *ChemBioChem* **2004**, *5*, 691.
18. Sagan, S.; Karoyan, P.; Lequin, O.; Chassaing, G.; Lavielle, S., "N- and C-<sup>945</sup>-Methylation in Biologically Active Peptides: Synthesis, Structural and Functional Aspects," *Curr. Med. Chem.* **2004**, *11*, 2799.
19. Cline, L. L.; Waters, M. L., "The structure of well-folded  $\beta$ -hairpin peptides promotes resistance to peptidase degradation," *Peptide Science* **2009**, *92*, 502.

20. Tyndall, J. D. A.; Nall, T.; Fairlie, D. P., "Proteases Universally Recognize Beta Strands In Their Active Sites," *Chem. Rev.* **2005**, *105*, 973.
21. Hill, D. J.; Mio, M. J.; Prince, R. B.; Hughes, T. S.; Moore, J. S., "A Field Guide to Foldamers," *Chem. Rev.* **2001**, *101*, 3893.
22. Goodman, C. M.; Choi, S.; Shandler, S.; DeGrado, W. F., "Foldamers as versatile frameworks for the design and evolution of function," *Nat. Chem. Biol.* **2007**, *3*, 252.
23. Bautista, A. D.; Craig, C. J.; Harker, E. A.; Schepartz, A., "Sophistication of foldamer form and function in vitro and in vivo," *Curr. Opin. Chem. Biol.* **2007**, *11*, 685.
24. Horne, W. S.; Gellman, S. H., "Foldamers with Heterogeneous Backbones," *Acc. Chem. Res.* **2008**, *41*, 1399.
25. Horne, W. S.; Price, J. L.; Keck, J. L.; Gellman, S. H., "Helix Bundle Quaternary Structure from  $\alpha/\beta$ -Peptide Foldamers," *J. Am. Chem. Soc.* **2007**, *129*, 4178.
26. Horne, W. S.; Boersma, M. D.; Windsor, M. A.; Gellman, S. H., "Sequence-Based Design of  $\alpha/\beta$ -Peptide Foldamers That Mimic BH3 Domains," *Angew. Chem. Int. Ed.* **2008**, *47*, 2853.
27. Horne, W. S.; Price, J. L.; Gellman, S. H., "Interplay among side chain sequence, backbone composition, and residue rigidification in polypeptide folding and assembly," *Proc. Natl. Acad. Sci. USA* **2008**, *105*, 9151.
28. Horne, W. S.; Johnson, L. M.; Ketas, T. J.; Klasse, P. J.; Lu, M.; Moore, J. P.; Gellman, S. H., "Structural and biological mimicry of protein surface recognition by  $\alpha/\beta$ -peptide foldamers," *Proc. Natl. Acad. Sci. USA* **2009**, *106*, 14751.
29. Cox, J. P. L.; Evans, P. A.; Packman, L. C.; Williams, D. H.; Woolfson, D. N., "Dissecting the Structure of a Partially Folded Protein: Circular Dichroism and Nuclear Magnetic Resonance Studies of Peptides from Ubiquitin," *J. Mol. Biol.* **1993**, *234*, 483.
30. Searle, M. S.; Williams, D. H.; Packman, L. C., "A short linear peptide derived from the N-terminal sequence of ubiquitin folds into a water-stable non-native  $\beta$ -hairpin," *Nat. Struct. Mol. Biol.* **1995**, *2*, 999.

31. Blanco, F. J.; Jimenez, M. A.; Herranz, J.; Rico, M.; Santoro, J.; Nieto, J. L., "NMR evidence of a short linear peptide that folds into a  $\beta$ -hairpin in aqueous solution," *J. Am. Chem. Soc.* **1993**, *115*, 5887.
32. Blanco, F. J.; Rivas, G.; Serrano, L., "A Short Linear Peptide That Folds into a Native Stable  $\beta$ -Hairpin in Aqueous-Solution," *Nat. Struct. Biol.* **1994**, *1*, 584.
33. Kim, C. A.; Berg, J. M., "Thermodynamic [ $\beta$ ] -sheet propensities measured using a zinc-finger host peptide," *Nature* **1993**, *362*, 267.
34. Minor, D. L.; Kim, P. S., "Measurement of the  $\beta$ -sheet-forming propensities of amino acids," *Nature* **1994**, *367*, 660.
35. Cochran, A. G.; Skelton, N. J.; Starovasnik, M. A., "Tryptophan zippers: Stable, monomeric  $\beta$ -hairpins," *Proc. Natl. Acad. Sci. USA* **2001**, *98*, 5578.
36. Kobayashi, N.; Honda, S.; Yoshii, H.; Munekata, E., "Role of Side-chains in the Cooperative  $\beta$ -Hairpin Folding of the Short C-Terminal Fragment Derived from Streptococcal Protein G," *Biochemistry* **2000**, *39*, 6564.
37. Huyghues-Despointes, B. M. P.; Qu, X.; Tsai, J.; Scholtz, J. M., "Terminal ion pairs stabilize the second  $\beta$ -hairpin of the B1 domain of protein G," *Proteins: Struct., Funct., Bioinf.* **2006**, *63*, 1005.
38. Kier, B. L.; Shu, I.; Eidenschink, L. A.; Andersen, N. H., "Stabilizing capping motif for  $\beta$ -hairpins and sheets," *Proc. Natl. Acad. Sci. USA* **2010**, *107*, 10466.
39. Riemen, A. J.; Waters, M. L., "Design of Highly Stabilized  $\beta$ -Hairpin Peptides through Cation- $\pi$  Interactions of Lysine and N-Methyllysine with an Aromatic Pocket," *Biochemistry* **2009**, *48*, 1525.
40. Haque, T. S.; Gellman, S. H., "Insights on  $\beta$ -Hairpin Stability in Aqueous Solution from Peptides with Enforced Type I' and Type II'  $\beta$ -Turns," *J. Am. Chem. Soc.* **1997**, *119*, 2303.
41. Fesinmeyer, R. M.; Hudson, F. M.; Andersen, N. H., "Enhanced Hairpin Stability through Loop Design: The Case of the Protein G B1 Domain Hairpin," *J. Am. Chem. Soc.* **2004**, *126*, 7238.

42. Masterson, L. R.; Etienne, M. A.; Porcelli, F.; Barany, G.; Hammer, R. P.; Veglia, G., "Nonstereogenic  $\alpha$ -aminoisobutyryl-glycyl dipeptidyl unit nucleates type I'  $\beta$ -turn in linear peptides in aqueous solution," *Peptide Science* **2007**, *88*, 746.
43. Rúa, F.; Boussert, S.; Parella, T.; Díez-Pérez, I.; Branchadell, V.; Giralt, E.; Ortuño, R. M., "Self-Assembly of a Cyclobutane  $\beta$ -Tetrapeptide To Form Nanosized Structures," *Org. Lett.* **2007**, *9*, 3643.
44. Martinek, T. A.; Tóth, G. K.; Vass, E.; Hollósi, M.; Fülöp, F., "cis-2-Aminocyclopentanecarboxylic Acid Oligomers Adopt a Sheetlike Structure: Switch from Helix to Nonpolar Strand," *Angew. Chem. Int. Ed.* **2002**, *41*, 1718.
45. Martinek, T. A.; Mándity, I. M.; Fülöp, L.; Tóth, G. K.; Vass, E.; Hollósi, M.; Forró, E.; Fülöp, F., "Effects of the Alternating Backbone Configuration on the Secondary Structure and Self-Assembly of  $\beta$ -Peptides," *J. Am. Chem. Soc.* **2006**, *128*, 13539.
46. Smith, A. B.; Guzman, M. C.; Sprengeler, P. A.; Keenan, T. P.; Holcomb, R. C.; Wood, J. L.; Carroll, P. J.; Hirschmann, R., "De Novo Design, Synthesis, and X-ray Crystal Structures of Pyrrolinone-Based  $\beta$ -Strand Peptidomimetics," *J. Am. Chem. Soc.* **1994**, *116*, 9947.
47. Smith III, A. B.; Benowitz, A. B.; Favor, D. A.; Sprengeler, P. A.; Hirschmann, R., "A second-generation synthesis of scalemic 3,5,5-trisubstituted pyrrolin-4-ones: Incorporation of functionalized amino acid side-chains," *Tetrahedron Lett.* **1997**, *38*, 3809.
48. Smith III, A. B.; Favor, D. A.; Sprengeler, P. A.; Guzman, M. C.; Carroll, P. J.; Furst, G. T.; Hirschmann, R., "Molecular modeling, synthesis, and structures of N-methylated 3,5-linked pyrrolin-4-ones toward the creation of a privileged nonpeptide scaffold," *Bioorg. Med. Chem.* **1999**, *7*, 9.
49. Smith, A. B.; Hirschmann, R.; Pasternak, A.; Guzman, M. C.; Yokoyama, A.; Sprengeler, P. A.; Darke, P. L.; Emini, E. A.; Schleif, W. A., "Pyrrolinone-Based HIV Protease Inhibitors. Design, Synthesis, and Antiviral Activity: Evidence for Improved Transport," *J. Am. Chem. Soc.* **1995**, *117*, 11113.
50. Lee, K. H.; Olson, G. L.; Bolin, D. R.; Benowitz, A. B.; Sprengeler, P. A.; Smith, A. B.; Hirschmann, R. F.; Wiley, D. C., "The Crystal Structure of a Pyrrolinone–Peptide Hybrid Ligand Bound to the Human Class II MHC Protein HLA-DR1," *J. Am. Chem. Soc.* **2000**, *122*, 8370.

51. Nowick, J. S.; Powell, N. A.; Martinez, E. J.; Smith, E. M.; Noronha, G., "Molecular scaffolds. I. Intramolecular hydrogen bonding in a family of di- and triureas," *J. Org. Chem.* **1992**, *57*, 3763.
52. Nowick, J. S.; Mahrus, S.; Smith, E. M.; Ziller, J. W., "Triurea Derivatives of Diethylenetriamine as Potential Templates for the Formation of Artificial  $\beta$ -Sheets," *J. Am. Chem. Soc.* **1996**, *118*, 1066.
53. Nowick, J. S.; Holmes, D. L.; Mackin, G.; Noronha, G.; Shaka, A. J.; Smith, E. M., "An Artificial  $\beta$ -Sheet Comprising a Molecular Scaffold, a  $\beta$ -Strand Mimic, and a Peptide Strand," *J. Am. Chem. Soc.* **1996**, *118*, 2764.
54. Nowick, J. S.; Pairish, M.; Lee, I. Q.; Holmes, D. L.; Ziller, J. W., "An Extended  $\beta$ -Strand Mimic for a Larger Artificial  $\beta$ -Sheet," *J. Am. Chem. Soc.* **1997**, *119*, 5413.
55. Nowick, J. S.; Tsai, J. H.; Bui, Q.-C. D.; Maitra, S., "A Chemical Model of a Protein  $\beta$ -Sheet Dimer," *J. Am. Chem. Soc.* **1999**, *121*, 8409.
56. Nowick, J. S.; Chung, D. M.; Maitra, K.; Maitra, S.; Stigers, K. D.; Sun, Y., "An Unnatural Amino Acid that Mimics a Tripeptide  $\beta$ -Strand and Forms  $\beta$ -Sheetlike Hydrogen-Bonded Dimers," *J. Am. Chem. Soc.* **2000**, *122*, 7654.
57. Nowick, J. S.; Lam, K. S.; Khasanova, T. V.; Kemnitzer, W. E.; Maitra, S.; Mee, H. T.; Liu, R., "An Unnatural Amino Acid that Induces  $\beta$ -Sheet Folding and Interaction in Peptides," *J. Am. Chem. Soc.* **2002**, *124*, 4972.
58. Nowick, J. S., "Exploring  $\beta$ -Sheet Structure and Interactions with Chemical Model Systems," *Acc. Chem. Res.* **2008**, *41*, 1319.
59. Khakshoor, O.; Lin, A. J.; Korman, T. P.; Sawaya, M. R.; Tsai, S.-C.; Eisenberg, D.; Nowick, J. S., "X-ray Crystallographic Structure of an Artificial  $\beta$ -Sheet Dimer," *J. Am. Chem. Soc.* **2010**, *132*, 11622.
60. Reinelt, S.; Marti, M.; Dédier, S.; Reitingger, T.; Folkers, G.; de Castro, J. A. L.; Rognan, D., " $\beta$ -Amino Acid Scan of a Class I Major Histocompatibility Complex-restricted Alloreactive T-cell Epitope," *J. Biol. Chem.* **2001**, *276*, 24525.

61. Krauthäuser, S.; Christianson, L. A.; Powell, D. R.; Gellman, S. H., "Antiparallel Sheet Formation in  $\beta$ -Peptide Foldamers: Effects of  $\beta$ -Amino Acid Substitution on Conformational Preference<sup>1</sup>," *J. Am. Chem. Soc.* **1997**, *119*, 11719.
62. Langenhan, J. M.; Guzei, I. A.; Gellman, S. H., "Parallel Sheet Secondary Structure in  $\beta$ -Peptides," *Angew. Chem.* **2003**, *115*, 2504.
63. Seebach, D.; Abele, S.; Gademann, K.; Jaun, B., "Pleated Sheets and Turns of  $\beta$ -Peptides with Proteinogenic Side Chains," *Angew. Chem. Int. Ed.* **1999**, *38*, 1595.
64. Daura, X.; Gademann, K.; Schäfer, H.; Jaun, B.; Seebach, D.; van Gunsteren, W. F., "The  $\beta$ -Peptide Hairpin in Solution: Conformational Study of a  $\beta$ -Hexapeptide in Methanol by NMR Spectroscopy and MD Simulation," *J. Am. Chem. Soc.* **2001**, *123*, 2393.
65. Karle, I.; Gopi, H. N.; Balaram, P., "Infinite pleated  $\beta$ -sheet formed by the  $\beta$ -hairpin Boc- $\beta$ -Phe- $\beta$ -Phe-d-Pro-Gly- $\beta$ -Phe- $\beta$ -Phe-OMe," *Proc. Natl. Acad. Sci. USA* **2002**, *99*, 5160.
66. Karle, I. L.; Gopi, H. N.; Balaram, P., "Peptide hybrids containing  $\alpha$ - and  $\beta$ -amino acids: Structure of a decapeptide  $\beta$ -hairpin with two facing  $\beta$ -phenylalanine residues," *Proc. Natl. Acad. Sci. USA* **2001**, *98*, 3716.
67. Gopi, H. N.; Roy, R. S.; Raghothama, S. R.; Karle, I. L.; Balaram, P., " $\beta$ -Hairpins Generated from Hybrid Peptide Sequences Containing both  $\alpha$ - and  $\beta$ -Amino Acids," *Helv. Chim. Acta* **2002**, *85*, 3313.
68. Roy, R. S.; Gopi, H. N.; Raghothama, S.; Gilardi, R. D.; Karle, I. L.; Balaram, P., "Peptide hairpins with strand segments containing  $\alpha$ - and  $\beta$ -amino acid residues: Cross-strand aromatic interactions of facing Phe residues," *Peptide Science* **2005**, *80*, 787.
69. Hagihara, M.; Anthony, N. J.; Stout, T. J.; Clardy, J.; Schreiber, S. L., "Vinyllogous polypeptides: an alternative peptide backbone," *J. Am. Chem. Soc.* **1992**, *114*, 6568.
70. Bandyopadhyay, A.; Mali, S. M.; Lunawat, P.; Raja, K. M. P.; Gopi, H. N., "Synthesis and Structural Investigations of Functionalizable Hybrid  $\beta$ -Hairpin," *Org. Lett.* **2011**, *13*, 4482.
71. Srinivasulu, G.; Rao, M. H. V. R.; Kumar, S. K.; Kunwar, A. C., " $\beta$ -Hairpin peptides containing 3-amino benzoic acid, a constrained  $\gamma$ -amino acid," *ARKIVOC* **2004**, 69.

72. Hartgerink, J. D.; Granja, J. R.; Milligan, R. A.; Ghadiri, M. R., "Self-Assembling Peptide Nanotubes," *J. Am. Chem. Soc.* **1996**, *118*, 43.
73. Amorín, M.; Castedo, L.; Granja, J. R., "New Cyclic Peptide Assemblies with Hydrophobic Cavities: The Structural and Thermodynamic Basis of a New Class of Peptide Nanotubes," *J. Am. Chem. Soc.* **2003**, *125*, 2844.
74. Brea, R. J.; Amorín, M.; Castedo, L.; Granja, J. R., "Methyl-Blocked Dimeric  $\alpha,\gamma$ -Peptide Nanotube Segments: Formation of a Peptide Heterodimer through Backbone–Backbone Interactions," *Angew. Chem. Int. Ed.* **2005**, *44*, 5710.
75. Garcia-Fandino, R.; Amorin, M.; Castedo, L.; Granja, J. R., "Transmembrane ion transport by self-assembling  $\alpha,\gamma$ -peptide nanotubes," *Chem. Sci.* **2012**, *3*, 3280.
76. Yancey, P. H.; Somero, G. N., "Counteraction of urea destabilization of protein structure by methylamine osmoregulatory compounds of elasmobranch fishes," *Biochem. J.* **1979**, *183*, 317.
77. Zou, Q.; Bennion, B. J.; Daggett, V.; Murphy, K. P., "The Molecular Mechanism of Stabilization of Proteins by TMAO and Its Ability to Counteract the Effects of Urea," *J. Am. Chem. Soc.* **2002**, *124*, 1192.
78. Roccatano, D.; Colombo, G.; Fioroni, M.; Mark, A. E., "Mechanism by which 2,2,2-trifluoroethanol/water mixtures stabilize secondary-structure formation in peptides: A molecular dynamics study," *Proc. Natl. Acad. Sci. USA* **2002**, *99*, 12179.
79. Hua, L.; Zhou, R.; Thirumalai, D.; Berne, B. J., "Urea denaturation by stronger dispersion interactions with proteins than water implies a 2-stage unfolding," *Proc. Natl. Acad. Sci. USA* **2008**, *105*, 16928.
80. Bolen, D. W.; Rose, G. D., "Structure and Energetics of the Hydrogen-Bonded Backbone in Protein Folding," *Annu. Rev. Biochem.* **2008**, *77*, 339.
81. Sjöbring, U.; Björck, L.; Kastern, W., "Streptococcal protein G. Gene structure and protein binding properties," *J. Biol. Chem.* **1991**, *266*, 399.
82. Gronenborn, A. M.; Filpula, D. R.; Essig, N. Z.; Achari, A.; Whitlow, M.; Wingfield, P. T.; Clore, G. M., "A Novel, Highly Stable Fold of the Immunoglobulin Binding Domain of Streptococcal Protein-G," *Science* **1991**, *253*, 657.

83. Gallagher, T.; Alexander, P.; Bryan, P.; Gilliland, G. L., "Two Crystal Structures of the B1 Immunoglobulin-Binding Domain of Streptococcal Protein G and Comparison with NMR," *Biochemistry* **1994**, *33*, 4721.
84. Frericks Schmidt, H. L.; Sperling, L. J.; Gao, Y. G.; Wylie, B. J.; Boettcher, J. M.; Wilson, S. R.; Rienstra, C. M., "Crystal Polymorphism of Protein GB1 Examined by Solid-State NMR Spectroscopy and X-ray Diffraction," *J. Phys. Chem. B* **2007**, *111*, 14362.
85. Espinosa, J. F.; Gellman, S. H., "A Designed  $\beta$ -Hairpin Containing a Natural Hydrophobic Cluster," *Angew. Chem. Int. Ed.* **2000**, *39*, 2330.
86. Haque, T. S.; Little, J. C.; Gellman, S. H., "Stereochemical requirements for beta-hairpin formation: Model studies with four-residue peptides and depsipeptides," *J. Am. Chem. Soc.* **1996**, *118*, 6975.
87. Stanger, H. E.; Gellman, S. H., "Rules for Antiparallel  $\beta$ -Sheet Design: d-Pro-Gly Is Superior to l-Asn-Gly for  $\beta$ -Hairpin Nucleation," *J. Am. Chem. Soc.* **1998**, *120*, 4236.
88. LePlae, P. R.; Umezawa, N.; Lee, H.-S.; Gellman, S. H., "An Efficient Route to Either Enantiomer of trans-2-Aminocyclopentanecarboxylic Acid," *J. Org. Chem.* **2001**, *66*, 5629.
89. Schinnerl, M.; Murray, Justin K.; Langenhan, Joseph M.; Gellman, Samuel H., "Asymmetric Synthesis of a New Helix-Forming  $\beta$ -Amino Acid: trans-4-Aminopiperidine-3-carboxylic Acid," *Eur. J. Org. Chem.* **2003**, *2003*, 721.
90. Calter, M. A., "Catalytic, Asymmetric Dimerization of Methylketene," *J. Org. Chem.* **1996**, *61*, 8006.
91. Chi, Y.; Gellman, S. H., "Enantioselective Organocatalytic Aminomethylation of Aldehydes: A Role for Ionic Interactions and Efficient Access to  $\beta$ 2-Amino Acids," *J. Am. Chem. Soc.* **2006**, *128*, 6804.
92. Chi, Y.; English, E. P.; Pomerantz, W. C.; Horne, W. S.; Joyce, L. A.; Alexander, L. R.; Fleming, W. S.; Hopkins, E. A.; Gellman, S. H., "Practical Synthesis of Enantiomerically Pure  $\beta$ 2-Amino Acids via Proline-Catalyzed Diastereoselective Aminomethylation of Aldehydes," *J. Am. Chem. Soc.* **2007**, *129*, 6050.

93. Danner, P.; Bauer, M.; Phukan, P.; Maier, Martin E., "Total Synthesis of Cryptophycin 3," *Eur. J. Org. Chem.* **2005**, 2005, 317.
94. Guichard, G.; Abele, S.; Seebach, D., "Preparation of N-Fmoc-Protected  $\beta$ 2- and  $\beta$ 3-Amino Acids and their use as building blocks for the solid-phase synthesis of  $\beta$ -peptides," *Helv. Chim. Acta* **1998**, 81, 187.
95. Ghosh, A. K.; Gong, G., "Enantioselective Total Synthesis of Macrolide Antitumor Agent (-)-Lasonolide A," *Org. Lett.* **2007**, 9, 1437.
96. Diness, F.; Beyer, J.; Meldal, M., "Synthesis of 3-Boc-(1,3)-oxazinane-Protected Amino Aldehydes from Amino Acids and Their Conversion into Urea Precursors. Novel Building Blocks for Combinatorial Synthesis," *QSAR Comb. Sci.* **2004**, 23, 130.
97. Zhu, C.; Shen, X.; Nelson, S. G., "Cinchona Alkaloid-Lewis Acid Catalyst Systems for Enantioselective Ketene-Aldehyde Cycloadditions," *J. Am. Chem. Soc.* **2004**, 126, 5352.
98. Wang, X.; Nelson, S. G.; Curran, D. P., "The azido acid approach to  $\beta$ -peptides: parallel synthesis of a tri- $\beta$ -peptide library by fluorous tagging," *Tetrahedron* **2007**, 63, 6141.
99. Dener, J. M.; Fantauzzi, P. P.; Kshirsagar, T. A.; Kelly, D. E.; Wolfe, A. B., "Large-Scale Syntheses of Fmoc-Protected Non-Proteogenic Amino Acids: Useful Building Blocks for Combinatorial Libraries," *Org. Process Res. Dev.* **2001**, 5, 445.
100. Davies, W.; Maclaren, J. A., "The reaction of  $\alpha$ -bromobenzyl cyanide with ethyl xanthamidate (thioncarbamate)," *J. Chem. Soc.* **1951**, 1434.
101. Xu, X.; Wang, K.; Nelson, S. G., "Catalytic Asymmetric [4 + 2] Cycloadditions of Ketenes and N-Thioacyl Imines: Alternatives for Direct Mannich Reactions of Enolizable Imines," *J. Am. Chem. Soc.* **2007**, 129, 11690.
102. Fanjul, S.; Hulme, A. N.; White, J. W., "Achieving High Selectivity and Facile Displacement with a New Thiol Auxiliary for Boron-Mediated Aldol Reactions," *Org. Lett.* **2006**, 8, 4219.
103. Langenhan, J. M.; Gellman, S. H., "Preparation of Protected syn- $\alpha,\beta$ -Dialkyl  $\beta$ -Amino Acids That Contain Polar Side Chain Functionality," *J. Org. Chem.* **2003**, 68, 6440.

104. Csomós, P.; Kanerva, L. T.; Bernáth, G.; Fülöp, F., "Biocatalysis for the preparation of optically active  $\beta$ -lactam precursors of amino acids," *Tetrahedron: Asymmetry* **1996**, *7*, 1789.
105. Kámán, J.; Forró, E.; Fülöp, F., "Enzymatic resolution of alicyclic  $\beta$ -lactams," *Tetrahedron: Asymmetry* **2000**, *11*, 1593.
106. Forró, E.; Fülöp, F., "Lipase-Catalyzed Enantioselective Ring Opening of Unactivated Alicyclic-Fused  $\beta$ -Lactams in an Organic Solvent," *Org. Lett.* **2003**, *5*, 1209.
107. Searle, M. S.; Griffiths-Jones, S. R.; Skinner-Smith, H., "Energetics of Weak Interactions in a  $\beta$ -hairpin Peptide: Electrostatic and Hydrophobic Contributions to Stability from Lysine Salt Bridges," *J. Am. Chem. Soc.* **1999**, *121*, 11615.
108. Griffiths-Jones, S. R.; Searle, M. S., "Structure, Folding, and Energetics of Cooperative Interactions between the  $\beta$ -Strands of a de Novo Designed Three-Stranded Antiparallel  $\beta$ -Sheet Peptide," *J. Am. Chem. Soc.* **2000**, *122*, 8350.
109. Kiehna, S. E.; Waters, M. L., "Sequence dependence of beta-hairpin structure: Comparison of a salt bridge and an aromatic interaction," *Protein Sci.* **2003**, *12*, 2657.
110. Fesinmeyer, R. M.; Hudson, F. M.; Olsen, K.; White, G. N.; Euser, A.; Andersen, N., "Chemical Shifts Provide Fold Populations and Register of  $\beta$  Hairpins and  $\beta$  Sheets," *J. Biomol. NMR* **2005**, *33*, 213.
111. Maynard, A. J.; Sharman, G. J.; Searle, M. S., "Origin of  $\beta$ -Hairpin Stability in Solution: Structural and Thermodynamic Analysis of the Folding of a Model Peptide Supports Hydrophobic Stabilization in Water," *J. Am. Chem. Soc.* **1998**, *120*, 1996.
112. Syud, F. A.; Espinosa, J. F.; Gellman, S. H., "NMR-Based Quantification of  $\beta$ -Sheet Populations in Aqueous Solution through Use of Reference Peptides for the Folded and Unfolded States," *J. Am. Chem. Soc.* **1999**, *121*, 11577.
113. Ramirez-Alvarado, M.; Blanco, F. J.; Serrano, L., "De novo design and structural analysis of a model  $\beta$ -hairpin peptide system," *Nat. Struct. Mol. Biol.* **1996**, *3*, 604.
114. Kessler, H.; Bats, J.-W.; Wagner, K.; Will, M., "Conformational analysis of cyclic peptides in solution," *Biopolymers* **1989**, *28*, 385.

115. Krause, E.; Beyermann, M.; Fabian, H.; Dathe, M.; Rothmund, S.; Bienert, M., "Conformation of a water-soluble  $\beta$ -sheet model peptide. A circular dichroism and Fourier-transform infrared spectroscopy study of double D-amino acid replacements," *Int. J. Pept. Protein Res.* **1996**, *48*, 559.
116. Deechongkit, S.; Nguyen, H.; Powers, E. T.; Dawson, P. E.; Gruebele, M.; Kelly, J. W., "Context-dependent contributions of backbone hydrogen bonding to  $\beta$ -sheet folding energetics," *Nature* **2004**, *430*, 101.
117. Wüthrich, K. *NMR in structural biology : a collection of papers by Kurt Wüthrich*; World Scientific: Singapore ; River Edge, NJ, 1995.
118. Brünger, A. T.; Adams, P. D.; Clore, G. M.; DeLano, W. L.; Gros, P.; Grosse-Kunstleve, R. W.; Jiang, J.-S.; Kuszewski, J.; Nilges, M.; Pannu, N. S.; Read, R. J.; Rice, L. M.; Simonson, T.; Warren, G. L., "Crystallography & NMR System: A New Software Suite for Macromolecular Structure Determination," *Acta Crystallogr., Sect D* **1998**, *54*, 905.
119. Brunger, A. T., "Version 1.2 of the Crystallography and NMR system," *Nat. Protocols* **2007**, *2*, 2728.
120. Roy, R. S.; Gopi, H. N.; Raghothama, S.; Karle, I. L.; Balaram, P., "Hybrid Peptide Hairpins Containing  $\alpha$ - and  $\omega$ -Amino Acids: Conformational Analysis of Decapeptides with Unsubstituted  $\beta$ -,  $\gamma$ -, and  $\delta$ -Residues at Positions 3 and 8," *Chem. Eur. J.* **2006**, *12*, 3295.
121. Cody, W. L.; He, J. X.; Reily, M. D.; Haleen, S. J.; Walker, D. M.; Reyner, E. L.; Stewart, B. H.; Doherty, A. M., "Design of a Potent Combined Pseudopeptide Endothelin-A/Endothelin-B Receptor Antagonist, Ac-dBhg16-Leu-Asp-Ile-[NMe]Ile-Trp21 (PD 156252): Examination of Its Pharmacokinetic and Spectral Properties," *J. Med. Chem.* **1997**, *40*, 2228.
122. Chatterjee, J.; Rechenmacher, F.; Kessler, H., "N-Methylation of Peptides and Proteins: An Important Element for Modulating Biological Functions," *Angew. Chem. Int. Ed.* **2013**, *52*, 254.
123. Spencer, R.; Chen, K. H.; Manuel, G.; Nowick, J. S., "Recipe for  $\beta$ -Sheets: Foldamers Containing Amyloidogenic Peptide Sequences," *Eur. J. Org. Chem.* **2013**, *2013*, 3523.
124. Laufer, B.; Frank, A. O.; Chatterjee, J.; Neubauer, T.; Mas-Moruno, C.; Kummerlöwe, G.; Kessler, H., "The Impact of Amino Acid Side Chain Mutations in Conformational Design of Peptides and Proteins," *Chem. Eur. J.* **2010**, *16*, 5385.

125. Manavalan, P.; Momany, F. A., "Conformational energy studies on N-methylated analogs of thyrotropin releasing hormone, enkephalin, and luteinizing hormone-releasing hormone," *Biopolymers* **1980**, *19*, 1943.
126. Hovmöller, S.; Zhou, T.; Ohlson, T., "Conformations of amino acids in proteins," *Acta Crystallogr., Sect D* **2002**, *58*, 768.
127. Badland, M.; Bains, C. A.; Howard, R.; Laity, D.; Newman, S. D., "An improved synthesis of (1R,3S)-3-[(tert-butoxycarbonyl)amino]cyclohexanecarboxylic acid," *Tetrahedron: Asymmetry* **2010**, *21*, 864.
128. Wang, G.; Mahesh, U.; Chen, G. Y. J.; Yao, S. Q., "Solid-Phase Synthesis of Peptide Vinyl Sulfones as Potential Inhibitors and Activity-Based Probes of Cysteine Proteases," *Org. Lett.* **2003**, *5*, 737.
129. Kranich, R.; Aydt, E. M.; Busemann, A. S., "Novel multi-cyclic compounds comprising dihydroxy- or dimethoxyphenyl subunits and their use as selectin antagonists," EP 2005-20511, 2007.
130. Mali, S. M.; Bandyopadhyay, A.; Jadhav, S. V.; Kumar, M. G.; Gopi, H. N., "Synthesis of  $\alpha,\beta$ -unsaturated  $\gamma$ -amino esters with unprecedented high (E)-stereoselectivity and their conformational analysis in peptides," *Org. Biomol. Chem.* **2011**, *9*, 6566.
131. Cregut, D.; Serrano, L., "Molecular dynamics as a tool to detect protein foldability. A mutant of domain B1 of protein G with non-native secondary structure propensities," *Protein Sci.* **1999**, *8*, 271.
132. Reinert, Z. E.; Musselman, E. D.; Elcock, A. H.; Horne, W. S., "A PEG-Based Oligomer as a Backbone Replacement for Surface-Exposed Loops in a Protein Tertiary Structure," *ChemBioChem* **2012**, *13*, 1107.
133. Reinert, Z. E.; Lengyel, G. A.; Horne, W. S., "Protein-like Tertiary Folding Behavior from Heterogeneous Backbones," *J. Am. Chem. Soc.* **2013**, *135*, 12528.
134. Greenfield, N. J., "Applications of circular dichroism in protein and peptide analysis," *TrAC, Trends Anal. Chem.* **1999**, *18*, 236.

135. Johnson, W. C., "Secondary Structure of Proteins Through Circular Dichroism Spectroscopy," *Annu. Rev. Biophys. Biophys. Chem.* **1988**, *17*, 145.
136. Shortle, D.; Meeker, A. K.; Freire, E., "Stability mutants of staphylococcal nuclease: large compensating enthalpy-entropy changes for the reversible denaturation reaction," *Biochemistry* **1988**, *27*, 4761.
137. Alexander, P.; Fahnestock, S.; Lee, T.; Orban, J.; Bryan, P., "Thermodynamic analysis of the folding of the streptococcal protein G IgG-binding domains B1 and B2: why small proteins tend to have high denaturation temperatures," *Biochemistry* **1992**, *31*, 3597.
138. Bechtel, W. J.; Schellman, J. A., "Protein stability curves," *Biopolymers* **1987**, *26*, 1859.
139. Debaene, F.; Mejias, L.; Harris, J. L.; Winssinger, N., "Synthesis of a PNA-encoded cysteine protease inhibitor library," *Tetrahedron* **2004**, *60*, 8677.